Chromosome organisation and segregation during sporulation in *Bacillus subtilis*

David Michael Roberts

Thesis submitted in partial fulfilment of the requirements of the regulation for the degree of Doctor of Philosophy

Newcastle University

Faculty of Medical Sciences

Institute for Cell and Molecular Biosciences

September 2017

Abstract

In times of nutrient scarcity, *Bacillus subtilis* can form highly resistant spores. Sporulation is a complex differentiation process requiring the coordinated differential expression of hundreds of genes in the smaller prespore and larger mother cell. The critical morphological events in sporulation include a conformational change of the chromosomes and polar anchoring of the chromosome origins that are normally located at quarter cell positions. This is followed by asymmetric cell division that bisects the prespore chromosome, and the subsequent transfer of this chromosome into the spore (Lewis *et al.*, 1994; Wu and Errington, 1998; Ben-Yehuda and Losick, 2002; Ben-Yehuda *et al.*, 2003b; Wu and Errington, 2003). Since these events are critical, there are dedicated systems to ensure their success. This work explores aspects of these processes.

In this thesis, I began by attempting to map the precise chromosomal boundaries at the site of the asymmetric septum. For this I performed chromatin-affinity-purification and also developed a methylase-based method. Next, I examined several novel proteins involved in capturing the DNA at the cell pole. This included deciphering the genetic hierarchy and localisation patterns of the newly implicated proteins (MinD and ComN), and confirmed the reported functional redundancy between chromosome capture machineries. Finally my work explored the role played by Soj (ParA) in chromosome movement and origin capture at the cell pole using high resolution microscopy. Soj is a member of the chromosomally encoded *B. subtilis* ParABS system, and has been long implicated in controlling chromosome segregation and DNA replication initiation (Ireton *et al.,* 1994; Wu and Errington, 2003; Murray and Errington, 2008). My work has demonstrated that the ATPase function of Soj is not necessary for origin capture, but simply the Soj-ATP monomer is proficient. Based on these data, I propose two models for Soj function in polar origin capture during sporulation.

Acknowledgements

Publications

Kloosterman, T.G., Lenecic, R., Willis, C.R., **Roberts, D.M.,** Hamoen, L.W., Errington, J., Wu, L.J. (2016) 'Complex polar machinery required for proper chromosome segregation in vegetative and sporulating cells of *Bacillus subtilis*', *Molecular Microbiology* **101**, pp. 333-350.

Santos-Beneit, F., **Roberts, D.M.,** Cantlay, S., McCormick, J.R., Errington, J. (2017) 'A mechanism for FtsZ-independent proliferation in *Streptomyces*', *Nature Communications.* **8**, 1378.

Table of Figures

Table of Tables

List of Abbreviations

Å	Angström
ADP	Adenosine diphosphate
ATP	Adenosine triphosphate
BMOE	Bismaleimidoethane crosslinker
CAA	Casamino acids
$CaCl_2$	Calcium chloride
CH	Casein hydrolysate
ChAP	Chromatin affinity purification
CiP	Calf intestinal phosphatase
CoIP	Co-immunoprecipitation
C-terminal	Carboxy-terminal
DAPI	4',6-Diamidino-2-phenylindole
dNTP	Dexoyribonucleoside 5'-triphosphate
DSP	Dithiobis(succinimidyl propionate)) crosslinker
DTT	Dithiothreitol
ECL	Enhanched chemiluminesence
EDTA	Ethylenediaminetetraacetic acid
$FeCl_3.6H_2O$	Iron(III) chloride hexahydrate
FM5-95	*N*-(3-trimethylammoniumpropyl)-4-(6-(4-(Diethylamino)phenyl) hexatrienyl)Pyridinium Dibromide
g	Gram(s)
g/l	Grams per litre

GFP	Green fluorescent protein
h	Hours
H_2O	Water
HCl	Hydrochloric acid
HEPES	4-(2-hydroxyethyl)-1-piperazineethanesulfonic acid)
HRP	Horseradish peroxidase
IPTG	Isopropyl β-D-1-thiogalactopyranoside
Kb	Kilobase
kDa	Kilodalton
KH_2PO_4	Potassium dihydrogen phosphate
LB	Luria-Bertani medium
M	Molar
mM	Millimolar
mGFP	Monomeric green fluorescent protein
min	Minutes
mNG	Monomeric Neon Green
ml	Millilitre
$MgCl_2$	Magnesium chloride
$MgCl_2 \cdot 6H_2O$	Magnesium chloride hexahydrate
$MnCl_2 \cdot 4H_2O$	Manganese(II) chloride tetrahydrate
NaCl	Sodium chloride
Na_2SO_4	Sodium sulphate
ng	Nanogram

ng/μl	Nanogram per microliter
NH_4Cl	Ammonium chloride
NH_4NO_3	Ammonium nitrate
N-terminal	Amino-terminal
NO	Nucleoid occlusion
OD_{600}	Optical Density at 600 nm
PAGE	Polyacrylamide gel electrophoresis
PacBio	Pacific Biosciences
PBS	Phosphate buffered saline
PCR	Polymerase chain reaction
qPCR	Quantitative polymerase chain reaction
pmole	Picomole
PTM	Pre-transformation medium
PVDF	Polyvinylidene fluoride
rpm	Revolutions per minute
SDS	Sodium dodecyl sulphate
SDS-PAGE	Sodium dodecyl sulphate polyacrylamide gel electrophoresis
sec	Seconds
SMM	Standard minimal medium
SMRT	Single molecule real time
SSC	Salt sodium citrate medium
SSC-L	Salt sodium citrate lysozyme medium
TBE	Tris-borate-EDTA
TM	Transformation medium

T_m	DNA 'melting' temperature
Tris	Tris (hydroxylmethyl) aminomethane
Triton X-100	*Iso*-octylphenoxypolyethoxethanol
Tween 20	Polyoxyethylenesorbitan monolaurate
U	Units
UT	Urea-Triton buffer
UT-EB	Urea-Triton elution buffer
UV	Ultraviolet
v/v	Volume per volume
w/v	Weight per volume
X-gal	5-bromo-4-chloro-3-indolyl-β-D-galactopyranoside
^{o}C	Degrees celcius
μg	Micrograms
μl	Microlitre
μm	Micrometre
μM	Micromolar
μg/ml	Micrograms per millilitre
%	Percent

Table of Contents

Chapter 1

Introduction

All bacteria must readily adapt to ever changing environmental conditions in order to survive. In the soil, the natural environment for *Bacillus subtilis* (*B. subtilis*), nutrient scarcity is common. As a consequence, *B. subtilis* has evolved a range of survival strategies, including the formation of endospores (herein termed spores) (Errington, 2003; Rao *et al.*, 2008; Burton and Dubnau, 2010; Vlamakis *et al.*, 2013; Tan and Ramamurthi, 2014). On committing to sporulation, a *B. subtilis* cell deviates from symmetrical cell division and undergoes a highly asymmetric division event that bisects the nucleoid and defines the small prespore and much larger mother cell (Tan and Ramamurthi, 2014). Upon completion of asymmetric septation, the prespore and mother cell sequentially activate distinct gene expression programmes that drive their alternate cell fates. Following engulfment of the developing prespore by the mother cell, in a phagocytic-like process, the prespore dehydrates and extensive coat and cortex layers are developed that protect the spore from extreme chemical, physical and environmental stresses (McKenney *et al.*, 2013). The final stage of sporulation involves the release of the mature spore upon lysis of the mother cell. Clearly, sporulation encompasses many critical events involved in cellular differentiation in higher organisms (e.g. generation of asymmetry, engulfment, differential gene expression, programmed cell death and different cell fates). An outline of the main stages of spore formation as described by (Ryter, 1965) are given in Figure 1.1.
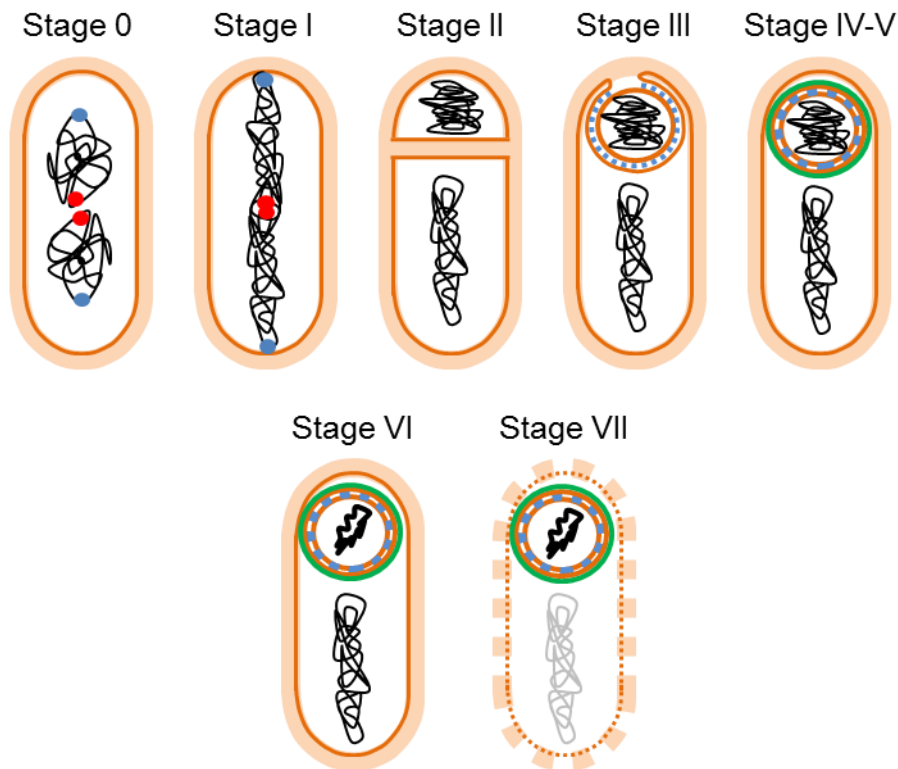
Figure 1.1 Schematic overview of the main stages of sporulation in *B. subtilis*.
From many studies, spore formation was characterised as a series of morphogenic stages: initiation (0); axial filament formation (I); asymmetric division (II); engulfment (III); cortex and coat development (IV and V); maturation (VI) and release (VII). Origins are labelled in blue; termini in red. Cell membranes are indicated as thin orange lines; the cell wall is represented thick light orange. Spore cortex, coat and peptidoglycan layers are labelled in blue and green. Information adapted from Ryter, 1965; Errington, 2010 and Tan and Ramamuthri, 2014.

This thesis describes studies that fall within the early stages (I and II) of sporulation, when asymmetry, nucleoid re-distribution and alternate cell fates are generated. Figure 1.2 schematically summarises known events in these early stages of sporulation that were elucidated from the mid-1980s onwards (Errington, 1993; Wu and Errington, 1994; Wu and Errington, 1998; Bath *et al.*, 2000; Ben-Yehuda and Losick, 2002; Wu and Errington, 2002; Ben-Yehuda *et al.*, 2003b; Wu and Errington, 2003). Key to understanding these processes was the exploitation of mutants for asymmetric cell division (Errington, 2010). Not only did this provide a means to understand these processes in sporulating cells, but the developed models could readily be applied to vegetatively growing cells of *B. subtilis*.
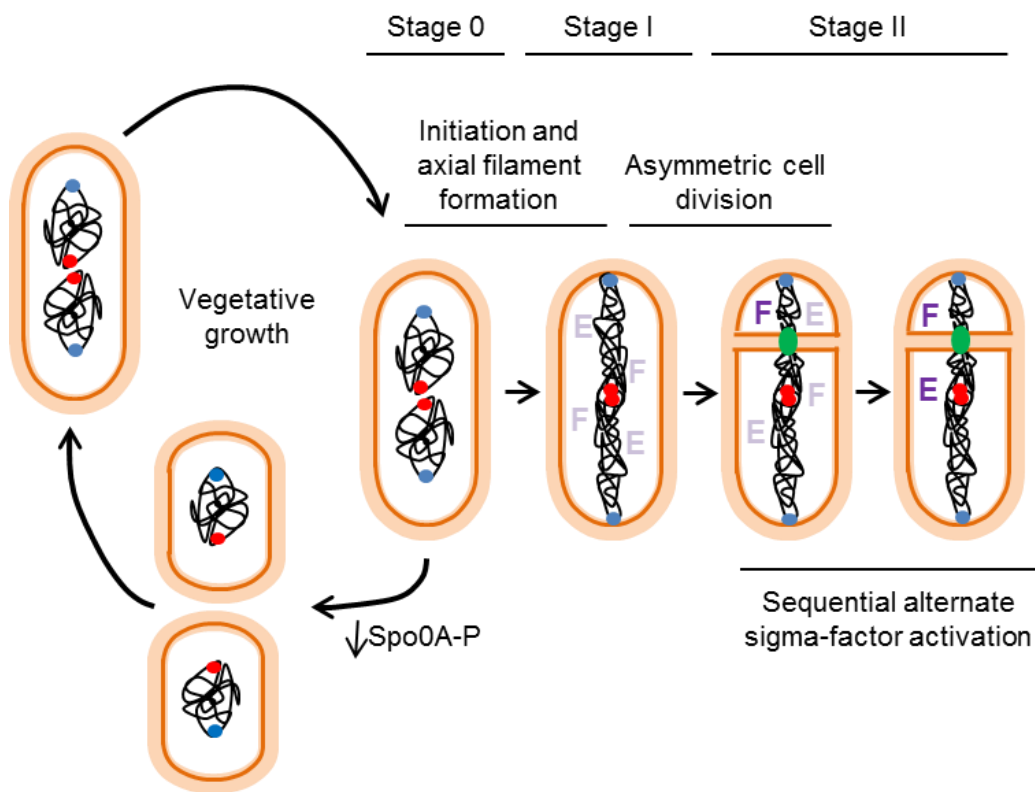
Figure 1.2 Key events in the initial stages of sporulation.

Upon initiation of sporulation, cells leave the vegetative growth cycle and axial filaments form as chromosome origins (blue) become anchored at opposite cell poles. Both σ^F and σ^E are expressed and present in this cell but are held in an inactive state (light purple letters). Next, asymmetric cell division determines the small prespore and large mother cell, leading to the specific prespore activation of σ^F (dark purple letters). Following the activation of σ^F, σ^E becomes specifically activated in the mother cell (dark purple letters). Origins are labelled in blue; termini are labelled in red. Thin dark orange lines represent cell membranes; thick light orange lines represent the cell wall. The SpoIIIE translocase (green) binds the bisected DNA.

Although many molecular details of these early events in sporulation have been established, several pertinent questions remain. These include:

1. What is the precision of asymmetric bisection of the prespore chromosome at the DNA level, and how is this affected in chromosome organisation mutants?
2. What is the full repertoire of players involved in, and the molecular mechanisms pertaining to, chromosome segregation and origin retention at cells poles during axial filament formation?
3. How is asymmetric cell division site placement regulated, and in particular, how are the vegetative control mechanisms that exist to prevent polar division overcome?
4. How are chromosome terminus regions segregated and distributed?

Experiments have been conducted herein to address aspects of questions 1 and 2. In the following sections of the Introduction, a review of stages I-III of sporulation (the reader is directed to reviews (McKenney *et al.*, 2013; Tan and Ramamurthi, 2014) for details of Stages IV-VI) and then the factors and processes implicated in chromosome replication, organisation, movement (segregation) and division site placement, will be described in both sporulating and, where appropriate, vegetatively dividing cells. Finally, a list of the specific aims addressed in this thesis will be provided.

1.1 *B. subtilis* as a model organism

In addition to being a model for sporulation, *B. subtilis* is one of the most well characterised and widely studied bacteria. There are several reasons for this. Firstly, *B. subtilis* grows rapidly under standard laboratory conditions. Secondly, since being identified as naturally competent and transformable in the late 1950s (Spizizen, 1958; Anagnostopoulos and Spizizen, 1961), genetic manipulation and the isolation and characterisation of genetic mutants is relatively straightforward in this organism. These processes have enabled mutants of virtually all critical processes to be isolated and studied *in vivo*. Thirdly, being non-pathogenic and readily able to secrete fully folded proteins, this organism has been widely exploited in biotechnology for production of commercially valuable biologics (Schallmey *et al.*, 2004; Pohl and Harwood, 2010).

1.2 Sporulation in *B. subtilis*

Spores are dehydrated structures, highly resistant to a wide range of environmental and chemical insults including UV radiation, temperature, detergents, hydrolytic enzymes and chemical solvents (Nicholson *et al.*, 2000). They can persist in the environment for decades, but upon sensing the return of favourable conditions, will initiate germination (Cano and Borucki, 1995; Nicholson *et al.*, 2000; Vreeland *et al.*, 2000). Many spore forming bacteria are of particular interest because they are major pathogens (e.g. *Bacillus anthracis, Clostridium botulinum, Clostridium difficile* and *Clostridium tetani*), with sporulation being critical to their pathogenesis (Swick *et al.*, 2016; Girinathan *et al.*, 2017). Therapeutic targeting of sporulation is therefore subject to intensive research effort (Deakin *et al.*, 2012; Durre, 2014; Girinathan *et al.*, 2017; Soutourina, 2017).

1.2.1 Commitment to sporulation

Since sporulation is an irreversible cellular differentiation event that takes many hours and requires the coordinated differential expression of hundreds of genes, the commitment to sporulation is a highly regulated process. Although no single trigger for sporulation has been identified, the critical stimulus is nutrient limitation in a dense population of cells. This also appears to be general starvation, since limiting any particular individual nutrient does not appear to trigger sporulation, and because the wide variety of sensor proteins can each integrate multiple signals (LeDeaux *et al.*, 1995). Furthermore, it has been noted that sporulation is a heterogeneous process, with subpopulations of cells committing in a series of stages (or not at all). It has been postulated that this bet-hedging strategy enables cells to "confirm" the need for the irreversible and lengthy process of sporulation (Veening *et al.*, 2008).

The master initiator is Spo0A. Transcriptomics and microarray data has demonstrated that Spo0A is a transcriptional regulator, and that up to 10% of all *B. subtilis* genes are differentially regulated by it, either directly or indirectly. These genes are collectively known as the Spo0A regulon (Molle *et al.*, 2003). The activity of Spo0A is regulated by phosphorylation (Spo0A~P), with this protein forming the base of an expanded two component signalling complex known as the phospho-relay system (Jiang *et al.*, 2000). The phosphor-relay includes two further phosphotransfer proteins, Spo0F and Spo0B, and five autophosphorylating histidine kinases (KinA-E), that collectively integrate a wide range of internal and external stimuli to control the critical decision for activating sporulation (Figure 1.3).

Diminished
respiration

↓e⁻ transport   NAD⁺

DNA replication
DNA damage

↑GTP

Sda

CodY-GTP———⊣ KinB   KinA   KinC   KinD   KinE

PhrA, C, E ———⊣ RapA, B, E ———⊣ Spo0F

↑Cell density

Spo0B

Spo0A ⊢———Spo0E
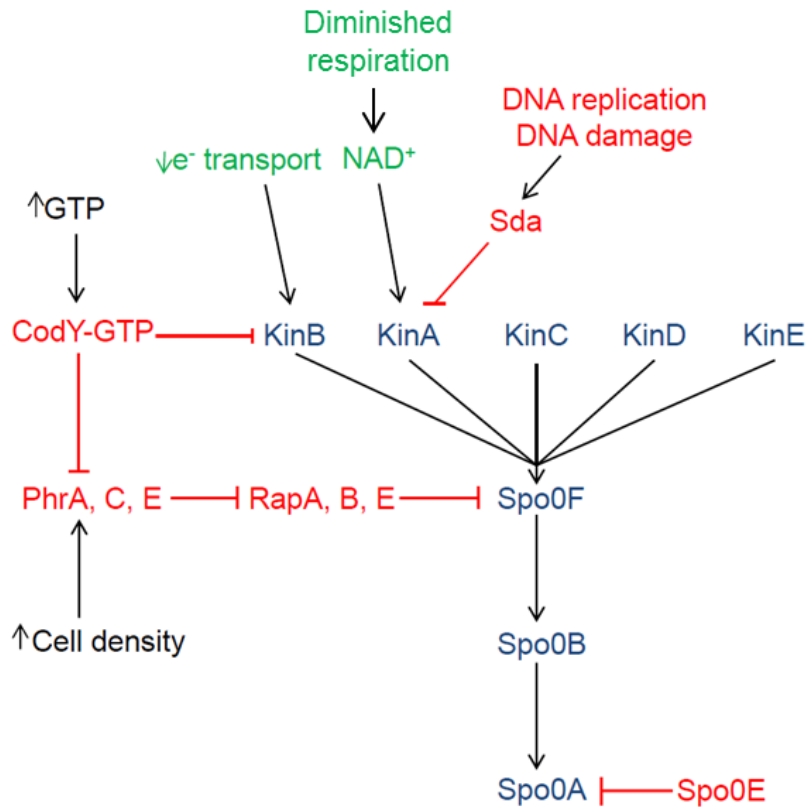
Figure 1.3 Regulation of sporulation initiation.

The autophosphorylating Kin kinases and Spo0F-B-A phosphorelay and are shown in blue. A wide variety of internal and external stimuli are sensed by the latter system to ensure sporulation only initiates under appropriate cellular and environmental conditions. Molecules and processes that inhibit the phosphorelay are shown in red. By contrast, cellular signals that promote phosphorylation and activation of the pathway are shown in green. Information adapted from Piggot & Hilbert., 2004.

As mentioned, high cell density is critical for sporulation initiation, because at low cell density, the Rap-family of aspartyl phosphate phosphatases, RapA, RapB and RapE, acts to inhibit Spo0F phosphorylation (Figure 1.3) (Ishikawa *et al.*, 2002; Piggot and Hilbert, 2004). The Rap proteins are, in turn, controlled by a complex export/import pathway of the 39-57 amino acid residue Phr oligopeptides (Perego, 2013). PhrA, PhrC and PhrE peptides are secreted from the cell in a Sec-dependent manner and upon accumulating to a critical level at high cell density, they are processed into pentapeptides and re-imported where they then bind and inhibit the Rap phosphatases (Pottathil and Lazazzera, 2003; Mirouze *et al.*, 2011; Parashar *et al.*, 2011; Gallego del Sol and Marina, 2013). This permits the prolonged phosphorylation of Spo0F (Figure 1.3). Phosphorylation of Spo0F, and subsequent

de-phosphorylation by RapA, has been proposed to contribute to the heterogeneity of sporulation (Veening *et al.*, 2005).

Whilst high Spo0A~P levels drive cells to initiate sporulation, *B. subtilis* also possesses other survival strategies that are called upon prior to the irreversible and extreme survival tactic of making a metabolically dormant spore. Relevant here are biofilm formation and cannibalism, that dominate at low levels of Spo0A~P (presumably at the early stages of phosphorelay activation). The control of these differential cell fates is dependent upon the activities of SinR (a transcriptional repressor), and the SinR antagonist - SinI, an activator of matrix production in biofilm formation (Chai *et al.*, 2011; Newman *et al.*, 2013). There are numerous operators upstream of *sinI* that have different affinities for Spo0A~P. When levels of Spo0A~P are low, the Spo0A~P only recognises and binds the high affinity *sinI* operators, leading to the expression of SinI with the consequential inhibition of SinR, therefore promoting matrix production and cannibalism (with concomitant inhibition of sporulation) (Newman *et al.*, 2013) (Figure 1.4). However, when Spo0A~P levels accumulate after prolonged phosphorelay activation, lower affinity Spo0A~P operators are also bound such that these occlude the transcription of *sinI* but activate the genes for sporulation (Fujita *et al.*, 2005; Fujita and Losick, 2005; Kearns *et al.*, 2005; Chai *et al.*, 2011).
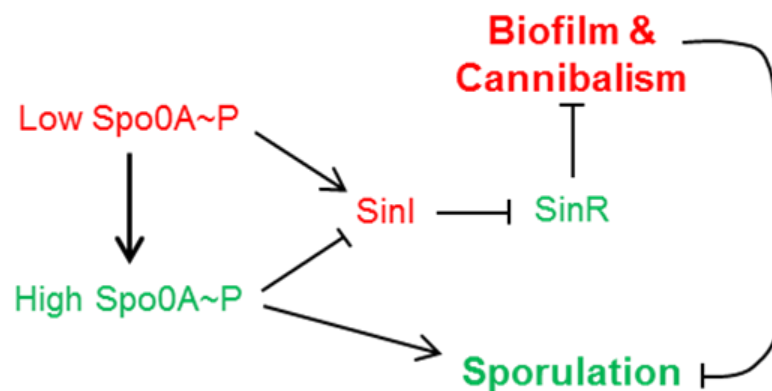
Figure 1.4 High and low levels of Spo0A~P drive alternate survival strategies
Low levels of Spo0A~P activate SinI and drive biofilm and cannibalism. Upon reaching a high level, Spo0A~P stimulates entry into sporulation. See text for details. Molecules and processes in green stimulate sporulation, whereas those in red inhibit the process. Arrow heads indicate activation, blocked lines indicate repression.

For sporulation to initiate, the pre-asymmetric divisional cell must contain two completely replicated chromosomes, so the final round of DNA replication must be coordinated with the subsequent formation of an axial filament and asymmetric cell division (Jameson and Wilkinson, 2017). Indeed, sporulation is robustly blocked in any cell that has ongoing replication, irrespective of other signals, to preclude the formation of poorly viable di/polyploid spores (Veening *et al.*, 2009) (see section 1.3.2).

Once committed to sporulation, the two chromosomes form a structure known as an axial filament, marking morphological Stage I (Figure 1.1). This arises as a result of nucleoid elongation, and the replication origin regions, which are normally located at about ¼ and ¾ quarters of cell length, now migrate to the cell poles where they become anchored, with the termini remaining at mid-cell (Bylund *et al.*, 1993; Glaser *et al.*, 1997) (Figure 1.5).
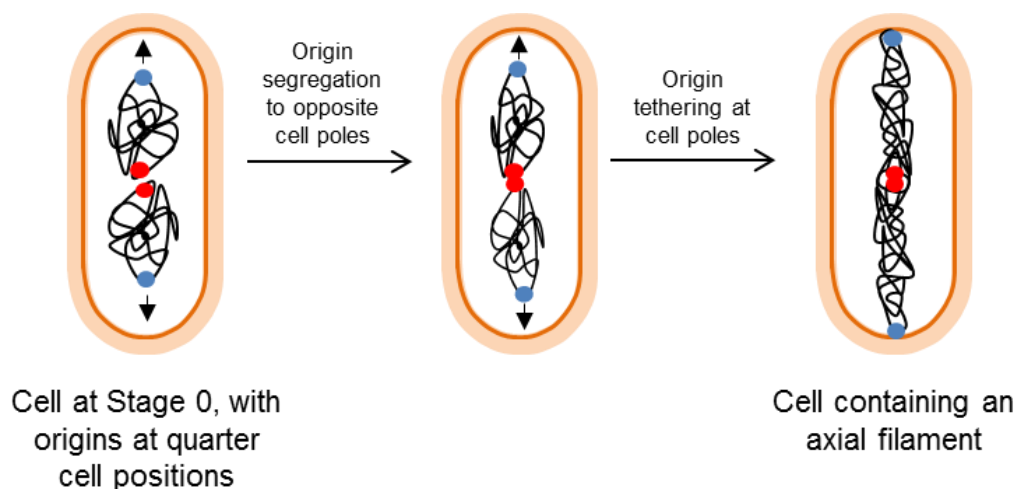
Figure 1.5 Axial filament formation
Following activation of Spo0A~P, the normally quarter cell origins (blue) are segregated to the cell poles where they become anchored. Termini (red) remain at mid-cell. Black arrows indicated chromosome movement.

Early genetic studies (Sharpe and Errington, 1996) revealed that Spo0J (known as ParB in other organisms) protein was required for proper chromosome orientation during sporulation. Imaging studies (Glaser *et al.*, 1997) then showed that Spo0J is tightly associated with the origin chromosome region and that this protein migrates to the extreme cell poles early in sporulation. Subsequently, DivIVA protein,

which had earlier been identified as a polar localized protein required for division site selection (Edwards and Errington, 1997) was shown to have an additional role in prespore chromosome capture (Thomaides *et al.*, 2001). RacA was subsequently discovered as a sporulation-specific protein (regulated as part of the Spo0A and σ^H regulons) critical for origin anchoring to the cell pole. It recognises specific inverted GC-rich sequences (known as RacA binding motif or *ram* sites) that are located on the origin-proximal arm region left of *oriC* (Wu and Errington, 2002; Ben-Yehuda *et al.*, 2003b; Wu and Errington, 2003; Ben-Yehuda *et al.*, 2005). RacA may also bind DNA non-specifically, with adjacent DNA-RacA interactions promoting DNA compaction into the axial filament (Ben-Yehuda *et al.*, 2005; Schumacher *et al.*, 2016). Further details of the mechanisms underlying axial filament formation are described in Chapters 4 and 5.

1.2.3 Asymmetric cell division and establishment of alternative gene expression

Following axial filament formation, the second morphological step (Stage II) of sporulation occurs – asymmetric cell division (Lewis *et al.*, 1994; Levin and Losick, 1996). This is a crucial event, defining the small prespore and larger mother cell, which is critical for the establishment of genetic asymmetry. In normal vegetatively growing cells, the tubulin homologue FtsZ (the major component of the divisome) specifically accumulates at mid-cell such that daughter cells are equal in size (Errington and Wu, 2017). The two systems that function to restrict the accumulation of FtsZ to mid-cell (and the subsequent divisome that forms) are the Min system and nucleoid occlusion (NO) (see section 1.5).

At least three factors have been recognised as important for establishing asymmetric division during sporulation: Spo0A~P mediated expression of the serine phosphatase SpoIIE, an increase in the amount of FtsZ protein, (Molle et al., 2003; Carniol et al., 2005) and RefZ (Wagner-Herman et al., 2012). The first of these, SpoIIE, has three domains and two functions (see later) (Barak and Youngman, 1996; Feucht *et al.*, 1996). In asymmetric cell division, specific amino acid substitutions in regions II and III were found to abolish polar localisation of the division machinery (Carniol *et al.*, 2005). The second factor, FtsZ, begins to accumulate at mid-cell but then becomes re-deployed towards each cell pole involving the formation of spiral intermediates (Ben-Yehuda and Losick, 2002). Once there, the two redeployed divisomes mature at different rates. A signal transduction

system recognises completion of the first septum and triggers inhibition of the second developing septum, ensuring that only one prespore persists. Mutants in sigma factor signalling (e.g. *spoIIGA*) prevent this inhibition resulting in the formation of diasporic cells (Lewis *et al.*, 1994; Pogliano *et al.*, 1997; Wu *et al.*, 1998). RefZ (the third factor) has been shown to facilitate this re-distribution (Wagner-Herman *et al.*, 2012), and can bind *refZ*-binding motifs (*rbm*) located on the chromosome proximal to the point where asymmetric division bisects the axial filament (Miller *et al.*, 2015). However, it remains unclear whether RefZ is a direct inhibitor or activator of asymmetric division. It has been proposed that RefZ acts to fine-tune this process to ensure that the relevant region of the chromosome is consistently trapped in the prespore (Miller *et al.*, 2015). Although the precise mechanism for asymmetric division site placement is unclear, it does appear to be a non-random process. This is because, in developing spores, ~30% of the prespore chromosome is initially captured in the small compartment upon septum bisection (Wu and Errington, 1994; Wu *et al.*, 1995; Wu and Errington, 1998). Following asymmetric cell division and bisection of the prespore-destined chromosome, a membrane translocase termed SpoIIIE pumps the remaining two thirds of the DNA into the prespore (see section 1.4.3).

The temporary asymmetry generated by bisecting the prespore chromosome near the origin is important for establishing compartmentalised gene expression, a process critical for generating the two alternative cell fates. Central to this are the prespore and mother cell sigma factors (σ^F, encoded by *spoIIA* (*sigF*) and σ^E, encoded by *spoIIGB*) that are synthesised, again dependent on phosphorylated Spo0A, long before asymmetric division occurs (Errington and Illing, 1992; Fujita and Losick, 2002; Molle *et al.*, 2003). They are initially held in an inactive state by the anti-sigma factor SpoIIAB (for σ^F) or as an inactive pro-σ^E (Errington and Illing, 1992; Tan and Ramamurthi, 2014). As well as binding and inactivating σ^F, SpoIIAB also phosphorylates the anti-anti sigma factor, SpoIIAA, inactivating it (Magnin *et al.*, 1996). Then, following asymmetric cell division the serine phosphatase SpoIIE, which preferentially localises as a ring at the membrane on the prespore side of the septum, performs a second key function (after its role in asymmetric division) to dephosphorylate SpoIIAA (Duncan *et al.*, 1995; Wu *et al.*, 1998; Feucht *et al.*, 2002; Errington, 2003). Once dephosphorylated, now active SpoIIAA sequesters SpoIIAB, enabling σ^F activation and expression of critical prespore genes.

As well as being critical in the activation of σ^F, the asymmetry generated by asymmetric division also restricts gene expression to only those genes present in each compartment. For example, the genes for *de novo* lipid synthesis are not within the 30% of the chromosome that is initially captured within the prespore (Wu and Errington, 1998). Therefore, the prespore is initially unable to synthesise lipid (Pedrido *et al.*, 2013), which is important for activation of σ^E. Asymmetry is also critical in the activation of mother cell gene expression. The pro- σ^E protein is activated by cleavage by the aspartic protease, SpoIIGA (Jonas *et al.*, 1988; Stragier *et al.*, 1988; Errington and Illing, 1992; Imamura *et al.*, 2008; Imamura *et al.*, 2011) in a process summarised in Figure 1.6 (Errington and Illing, 1992; Hofmeister *et al.*, 1995; Imamura *et al.*, 2008; Diez *et al.*, 2012) .
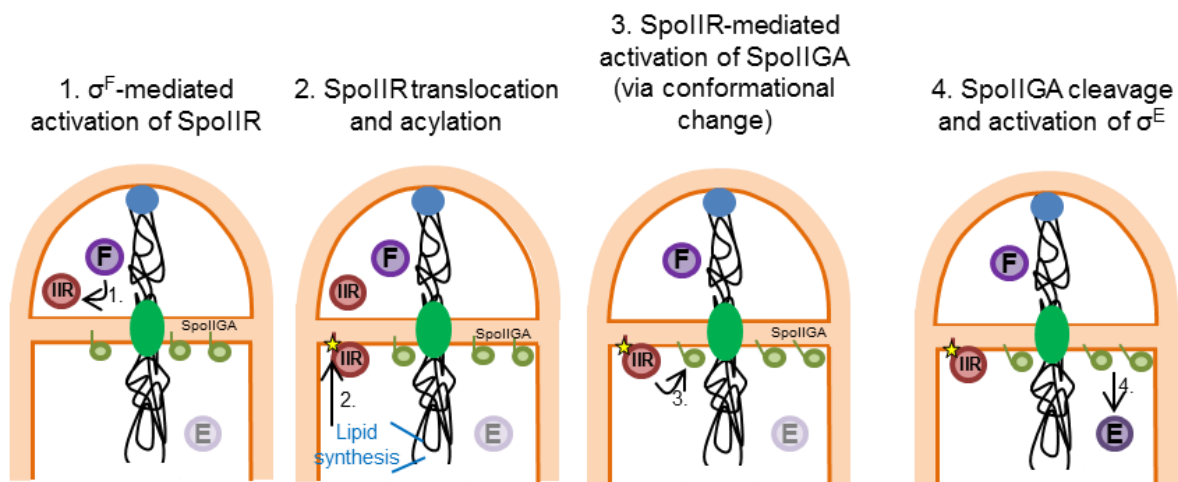
Figure 1.6 Activation of the mother cell sigma factor, σ^E

σ^F (F)-mediated activation of the prespore protein, SpoIIR (IIR, 1) leads to translocation of the latter across the prespore membrane (2) where it is specifically acylated (yellow star). Since lipid synthesis is confined to the mother cell (blue), only translocated SpoIIR is modified. Acylated-SpoIIR in turn stimulates an activating conformational change in SpoIIGA (3). Finally, the activated aspartate protease SpoIIGA cleaves the pro- σ^E (E) into mature σ^E (indicated by transition from light to dark purple). Information taken from Errington and Illing, 1992; Hofmeister *et al.*, 1995; Imamura *et al.*, 2008; Diez *et al.*, 2012; Pedrido *et* al.,2013 and Tan and Ramamuthri, 2014.

1.2.4 Prespore engulfment

Following asymmetric cell division and the activation of prespore and mother cell sigma-factors, the prespore becomes engulfed by the mother cell in a phagocytic-like process (although this process and phagocytosis in eukaryotes utilise

completely distinct cellular machineries) (Tan and Ramamurthi, 2014). As a result, the prespore becomes bound by a double membrane in the mother cell cytoplasm. Due to high internal osmotic pressure, extensive membrane and cell wall re-modelling is required to ensure the continued viability of both the mother cell and prespore during engulfment (Ojkic *et al.*, 2016). A complex of three proteins, SpoIID, SpoIIM and SpoIIP localise to the leading edge of the engulfing mother cell membrane, where SpoIIP removes stem peptides from the peptidoglycan (PG), and SpoIID degrades residual PG (Abanes-De Mello *et al.*, 2002; Chastanet and Losick, 2007; Gutierrez *et al.*, 2010; Morlot *et al.*, 2010). Furthermore, membrane-localised SpoIIQ (prespore) and SpoIIIAH (mother cell) interact (in a process similar to a "zipper") to prevent backward movement of the progressing engulfment machinery, even in the absence of any cell wall following lysozyme treatment (Blaylock *et al.*, 2004; Broder and Pogliano, 2006; Ojkic *et al.*, 2016). Cryo-electron microscopy revealed that the re-modelled cell wall in between the engulfing prespore and mother cell membranes is thinner than that in the lateral cell wall (Tocheva *et al.*, 2013). The deposition of new PG is essential during engulfment, since the addition of cell wall inhibitors to cells led to blocks in engulfment. How PG synthesis is coordinated with SpoIIDMP mediated PG degradation and re-modelling of existing material is unknown (Meyer *et al.*, 2010). It has been hypothesised that the new PG may provide a track required for engulfment, similarly to actin in eukaryotic phagocytosis (Ojkic *et al.*, 2016).

1.3 DNA replication

The faithful replication of genetic material is a central event in the cell cycle in all organisms. Unlike in eukaryotes, where DNA replication and chromosome segregation occur in distinct cell cycle phases (S-phase and mitosis, respectively), these processes occur concomitantly in bacteria (Kuzminov, 2014). In all cells, DNA replication can be split into three main stages: initiation, elongation and termination. Following the assembly of the DNA replication machinery at a single origin of replication site (*oriC*), replication elongation occurs in a bi-directional manner along each arm of the circular bacterial genome. Upon reaching the replication terminus (*Ter*), located 180° from *oriC*, termination of DNA replication occurs, where the replisomes are disassembled.

1.3.1 DNA replication initiation and control in vegetatively growing cells of *Bacillus subtilis*

DNA replication initiation begins upon the binding of a critical initiator protein, DnaA, to specific sequences called DnaA-boxes located within the origin (Bramhill and Kornberg, 1988b; Fujikawa *et al*., 2003). The DnaA boxes have various binding affinities for DnaA, and in *B. subtilis* are organised in a bipartite manner, with DnaA-box clusters separated by the *dnaA* gene (as compared to a continuous origin in *E. coli*) (Mott and Berger, 2007) (Figure 1.7A). The bipartite organisation is critical for replication initiation in *B. subtilis*, but how origin architecture affects replication in various organisms is unknown (Jameson and Wilkinson, 2017). DnaA is an AAA+ ATPase and contains four key domains (Messer *et al*., 1999) (Figure 1.7B).
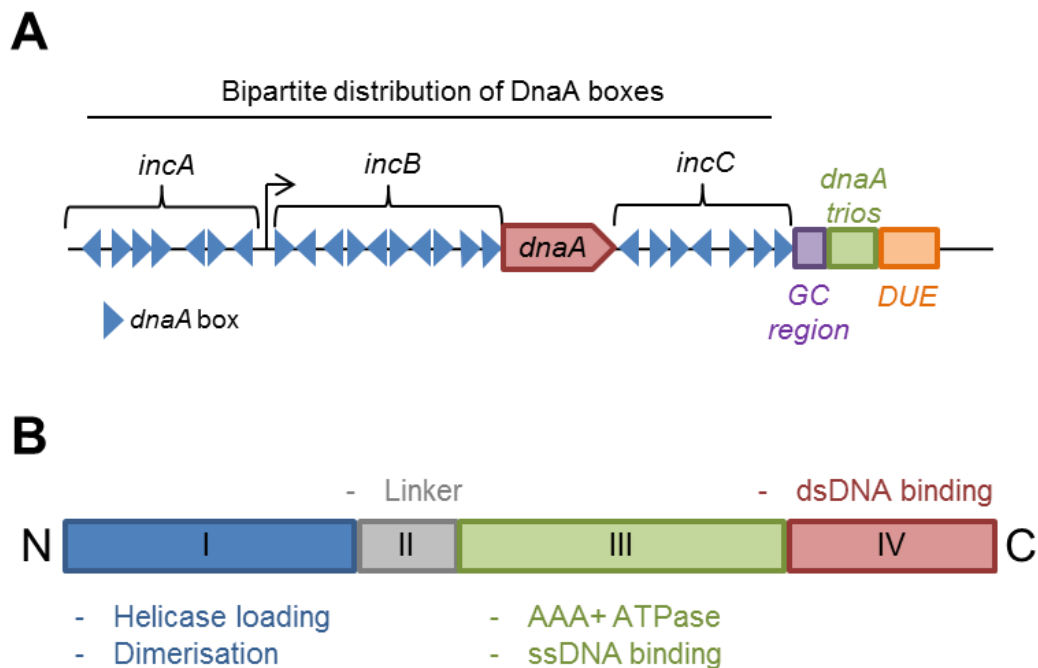
Figure 1.7 Replication origin organisation and DnaA domain structure
Schematic diagram showing the organisation and orientation of the DnaA-boxes (blue arrows) in the origin (A). There are three main DnaA-box regions: *incA*, *incB* and *incC*. The *incAB* and *incC* are separated by the *dnaA* gene (promoter indicated by black arrow). Downstream of the final DnaA-box resides a GC-rich region (purple), DnaA-trio sequences (green) and the DUE element (orange). Schematic shows the four domains of DnaA, with the key functions highlighted (B). Figure adapted from Richardson *et al*., 2016 and Jameson and Wilkinson, 2017.

DNA binding triggers the oligomerisation of ATP-bound DnaA and formation of a right-handed helix that extends along the DNA, leading to stretching of one strand, which causes unwinding within an AT-rich DNA unwinding element (DUE) (Fuller *et al.*, 1984; Sekimizu *et al.*, 1987; Bramhill and Kornberg, 1988a; Kowalski and Eddy, 1989; Nishida *et al.*, 2002; Erzberger *et al.*, 2006; Zorman *et al.*, 2012). The melting of the DNA is aided by a DNA modifying protein, DnaD (Zhang *et al.*, 2005). Unwinding of the DNA leads to positive supercoiling, which has been proposed to be compensated by negative writhe in the DUE, where stabilisation of the ssDNA is mediated through the ssDNA-binding function within domain III of DnaA (Erzberger *et al.*, 2006; Mott and Berger, 2007). Furthermore, novel trinucleotide sequences (of the consensus 3'-G/AAT-5', separated from the DnaA-boxes by a GC-rich region) have been recently identified within the origin, where they play a critical role in specifying DNA unwinding and ssDNA binding (Richardson *et al.*, 2016).

Following unwinding, DnaA recruits further members of the replication initiation machinery: DnaC (the DNA helicase, a process facilitated by the helicase loader DnaI and DnaB), the primase (DnaG) and polymerase β-clamp (DnaN), along with other non-essential factors (Bruand *et al.*, 1995; Fang *et al.*, 1999; Zhang *et al.*, 2005; Jameson and Wilkinson, 2017). Once the replication machinery has been assembled, the DNA is processively synthesised by the replisome complex, which contains two DNA polymerases in *B. subtilis*: PolC and DnaE (Dervyn *et al.*, 2001). Synthesis of each DNA arm occurs concurrently, and upon reaching the *Ter*, replication is terminated in a not fully understood mechanism that appears to be centred on the replication termination protein (RPT) binding to specific sites on the DNA (Vivian *et al.*, 2007).

Since DNA replication is a critical event during the cell cycle, the process is highly regulated to prevent unwanted, potentially harmful, replication events. Most of the regulatory mechanisms are exerted at the level of initiation. There are three main proteins involved in controlling DNA replication initiation: YabA, DnaD and Soj (a protein that is a focus of this thesis, albeit in its non-DNA replication role).

YabA functions as an inhibitor of DNA replication, affecting both the timing and frequency of initiation. Indeed, *ΔyabA* cells display growth and over-replication defects (Hayashi *et al.*, 2005; Noirot-Gross *et al.*, 2006). The negative regulatory mechanism of YabA is mediated through two processes. The first is direct interaction

of YabA with DnaA, which prevents the oligomerisation and helix assembly of DnaA necessary for DNA strand unwinding (Cho *et al.*, 2008; Scholefield and Murray, 2013). The second process is where YabA causes DnaA to associate with DnaN (the sliding clamp that accumulates behind the moving replication forks), sequestering DnaA away from *oriC* (Noirot-Gross *et al.*, 2002; Noirot-Gross *et al.*, 2006; Soufo *et al.*, 2008; Merrikh and Grossman, 2011). In turn, this reduces the concentration of DnaA in the origin region.

A second negative regulator of DNA replication is DnaD. Similarly to YabA, *in vitro* studies have suggested that DnaD inhibits ATP-dependent oligomerisation of DnaA, which in turn prevents the formation of the extended helix required for DNA strand unwinding (Bonilla and Grossman, 2012; Scholefield and Murray, 2013).

Finally, DNA replication initiation can be controlled by Soj (ParA in other organisms) (Murray and Errington, 2008). Soj is a Walker-type ATPase, containing a P-loop required for ATP binding (Leonard *et al.*, 2005). Soj ATP status is a critical determinant of its role in regulating DNA replication, where it can either activate or inhibit replication, while a *Δsoj* mutant over-initiates (Murray and Errington, 2008).

When not bound by ATP, Soj can reside as a monomer in the cytoplasm. In this state, Soj inhibits the initiation of replication by binding to domain III of DnaA and preventing the formation of the DnaA-helix (Scholefield *et al.*, 2012). Upon binding ATP, Soj forms a homodimer, which through specific arginine residues enables non-specific binding to DNA. This ATP-dimeric form of Soj can in turn activate DnaA, possibly by maintaining DnaA in a replication competent state (Ogura *et al.*, 2003; Lee and Grossman, 2006; Murray and Errington, 2008; Scholefield *et al.*, 2012). A second protein, Spo0J, is the regulator of Soj. As mentioned above, Spo0J associates with the origin region. This occurs by binding to specific sequences in the *oriC* region called *parS* sites through a classical helix-turn-helix motif (Lin and Grossman, 1998; Leonard *et al.*, 2004). DNA binding triggers many lateral and bridging interactions in Spo0J, resulting in the formation of a large nucleoprotein complex (Murray *et al.*, 2006; Graham *et al.*, 2014). Origin bound Spo0J molecules can interact with Soj at the Soj-homodimer interface, stabilising the ATPase domain of Soj and driving ATP hydrolysis (Zhang and Schumacher, 2017). Therefore, Spo0J acts as the molecular switch, controlling Soj DNA replication activation and inhibition activities (Scholefield *et al.*, 2011).

Together, Soj-Spo0J-*parS* constitute the chromosomally encoded ParABS system. As well as playing critical roles in controlling DNA replication initiation in *B. subtilis*, ParABS systems have been widely implicated in controlling the segregation of both chromosomal DNA and plasmids in a variety of bacterial species (see section 1.4).

1.3.2 Regulation of DNA replication during sporulation

As highlighted in section 1.2.2, replication must be controlled during sporulation to maintain diploidy – resulting in one chromosomal copy for the prespore and one for the mother cell. Polyploidy during sporulation can lead to reduced spore viability, failure to activate gene expression properly and defects in spore germination. Similarly to vegetative growth, the control of DNA replication during sporulation is controlled by several coordinated regulatory mechanisms.

Studies in the 1970's revealed that during nutrient starvation there was a specific period, termed the 'sensitive period', in which cells can initiate sporulation (Mandelstam and Higgs, 1974; Dunn *et al.*, 1978). Any cell that fails to enter sporulation during this period must complete at least one more vegetative cell cycle before potentially entering the sporulation pathway. It was later realised that central to establishment of the 'sensitive period' was the cellular concentration of Spo0A~P. Spo0A~P levels, which were found to fluctuate throughout the cell cycle, are highest upon the completion of a round of DNA replication (Veening *et al.*, 2009; Narula *et al.*, 2015). This observation suggested the existence of a cell cycle dependent regulator of Spo0A~P levels. Sda is an allosteric inhibitor of KinA and KinB, and so leads to inhibition of the phosphorelay (through the decreased phosphorylation of the KinA/B target, Spo0F) (Burkholder *et al.*, 2001; Veening *et al.*, 2009; Jameson *et al.*, 2014). The *sda* gene is activated by the replication proficient form of DnaA in its role as a transcription factor (Veening *et al.*, 2009; Washington *et al.*, 2017). As a result, there is a sharp increase in Sda expression upon (or just after) the activation of DNA replication, consequently leading to inhibition of sporulation (Veening *et al.*, 2009). Sda is then degraded during the vegetative cell cycle, 're-setting' the system (Ruvolo *et al.*, 2006).

As well as Sda, the chromosomal location of phosphorelay members also helps to ensure that the cell contains the correct genetic complement upon entry into

sporulation (Veening *et al.*, 2009). The *spo0F* gene is located near the origin. By contrast, its activator, *kinA*, is located near the terminus. Deliberately altering the locations of these genes (e.g. by expressing *spo0F* at an ectopic site) can affect the ratios of these proteins. Since a high Spo0F to KinA concentration inhibits sporulation (Chapman and Piggot, 1987; Grimshaw *et al.*, 1998), changing the location of these genes can affect their cellular ratios (and KinA phosphorylation) (Narula *et al.*, 2015). In a vegetative cell undergoing active DNA replication, there will be two copies of *spo0F* but only one of *kinA* for much of the cell cycle, ensuring the higher ratio of Spo0F:KinA to prevent sporulation initiation in these partially polyploid cells (Narula *et al.*, 2015).

Once a cell enters sporulation, no new rounds of DNA replication occur. Furthermore, even cells artificially forced into sporulation during the rapid growth did not over-initiate DNA replication (Rahn-Lee *et al.*, 2009). This is because of the action of the Spo0A dependent protein, SirA. Once expressed, SirA causes displacement of DnaA from the DnaA-boxes at the origin, thereby inhibiting replication (Wagner *et al.*, 2009). SirA accomplishes this through interactions with a patch of residues within domain I of DnaA (Rahn-Lee *et al.*, 2011; Jameson *et al.*, 2014). Spo0A~P has also been implicated in directly controlling chromosome copy number. The presence of Spo0A-binding sites in the origin region allows direct Spo0A~P binding to the *oriC* region, thus compounding inhibition of DNA replication (Boonstra *et al.*, 2013).

1.4 Chromosome segregation in bacteria

1.4.1 Plasmid partitioning

Much of our understanding of DNA partitioning is derived from studies on the segregation of low copy number plasmids. Low copy number plasmids frequently encode a specific partitioning (Par) system, which contains three elements: a specific DNA sequence (or *par* site) that constitutes a bacterial centromere, a *par* site specific DNA binding protein, and an NTPase (Figure 1.8) (Gerdes *et al.*, 2010; Baxter and Funnell, 2014; Brooks and Hwang, 2017).
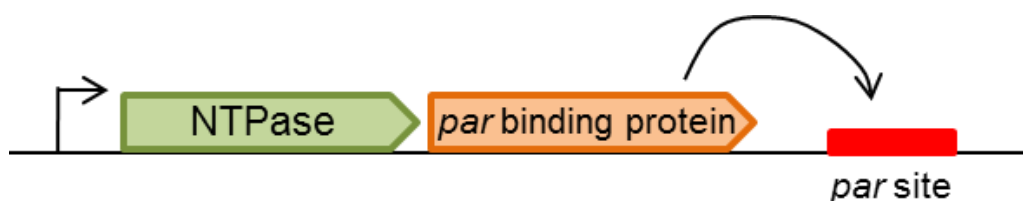
Figure 1.8 Typical genetic organisation of plasmid Par systems

The NTPase (green) and *par* binding protein (orange) reside in the same operon. The *parS* site (red) is bound by *par* binding protein dimers, usually resulting in spreading of the *par* binding protein and the formation of a nucleoprotein complex. Black arrow indicates site specific binding of the gene product. Information taken from Gerdes *et al.*, 2010.

The *par* loci have been characterised based upon the properties of the NTPase (Gerdes *et al.*, 2000; Hayes, 2000; Larsen *et al.*, 2007): a P-loop ATPase with a deviant Walker A motif (Type I); an actin derived ATPase (Type II) and a tubulin-based GTPase (Type III). Table 1.1 summarises key examples from each type of system (Jensen *et al.*, 1998; Radnedge *et al.*, 1998; Ebersbach and Gerdes, 2001; Ravin *et al.*, 2003; Becker *et al.*, 2006; Larsen *et al.*, 2007; Schumacher *et al.*, 2007; Derman *et al.*, 2009; Ni *et al.*, 2010; Tanaka, 2010; Wu *et al.*, 2011; Derman *et al.*, 2012).

Plasmid	Host	NTPase	*par* binding protein	*par* site	Reference
Type I (ATPase system)					
P1, P7	*E. coli*	ParA	ParB	*parS*	Radnedge *et al.,* 1998
F	*E. coli*	SopA	SopB	*sopC*	Ravin *et al.*, 2003
pB171	*E. coli*	ParA	ParB	*parC*	Ebersbach & Gerdes, 2001
Type II (ATPase system)					
R1	*E. coli*	ParM	ParR	*parC*	Ebersbach & Gerdes, 2001; Jensen *et al.,* 1998; Schumacher *et al.*, 2007
pLS20	*B. subtilis*	Alp7a	Alp7R	*alp7C*	Derman *et al.*, 2009, 2012
pLS32	*B. subtilis*	AlfA	AlfB	*parN*	Tanaka, 2010; Becker *et al.*, 2006
Type III (GTPase system)					
pXO1	*B. anthracis, B. thuringiensis*	TubZ	TubR	*tubC*	Larsen *et al.*, 2007; Ni *et al.*, 2010

Table 1.1 Plasmid partition systems in bacteria

Nomenclature and Type are given in the Table. References in the table are limited to the discovery and characterisation of the given systems. See Gerdes *et al.*, 2010 and Baxter and Funnell, 2014 for an extensive review of the systems.

The Type I plasmid partitioning system is the most common (Baxter and Funnell, 2014; Brooks and Hwang, 2017). Furthermore, it closely resembles the ParABS system that has been implicated in chromosome segregation in a variety of species (described in sections 1.4.2 and 1.4.4). In the Type I systems, ParB/SopB binds to the *parS/sopC* site and spreads to form large nucleoprotein complex. In turn, ParB/SopB binding to ParA/SopA drives the ATPase of the latter, promoting plasmid segregation. Initial studies on Type I systems led to the development of a filament-based mechanism for plasmid partitioning. *In vivo* imaging experiments suggested that ParA forms cloud-like helical structures over the nucleoid that appeared to oscillate (Ebersbach and Gerdes, 2001; Ebersbach and Gerdes, 2004; Hatano *et al.*, 2007). Furthermore, ParA formed extended linear and helical polymers upon ATP binding *in vitro* (Barilla *et al.*, 2005; Ebersbach *et al.*, 2006). An influential *in vivo* study of the pB171 plasmid of *E. coli* (Table 1.1) suggested that ParA actively filamented until the ParB-*parC* nucleoprotein complex of the plasmid was bound. Upon this interaction, ParA ATPase activity was stimulated, driving filament disassembly to actively pull the plasmid in a particular direction (Ringgaard *et al.*, 2009) (Figure 1.9A). Constant polymerisation/depolymerisation ensures movement of plasmids over generations.

More recently, extensive *in vitro* reconstitutions of ParABS systems have proposed an alternate, ratchet-based model for Type I-mediated plasmid segregation. These models propose that upon ATP binding, ParA does not form a filament, but instead undergoes a slow conformational switch to an ATP dimer that enables non-specific binding across the nucleoid (Vecchiarelli *et al.*, 2010). In the absence of ParB, the ParA-ATP dimers bind uniformly across the DNA. However, once ParB/*parS* associates, the high local concentration of ParB at the site of binding drives rapid ParA-ATP hydrolysis and subsequent release from the DNA. This in turn depletes the ParA-ATP dimers in the vicinity of the plasmid ParB/*parS*, and coupled with the slow re-binding kinetics of ParA-ATP dimers creates a gradient of ParA on the nucleoid. This gradient, on the surface of the nucleoid drives movement of the ParB/*parS* complex (Figure 1.9B) (Hwang *et al.*, 2013; Vecchiarelli *et al.*, 2013; Vecchiarelli *et al.*, 2014).
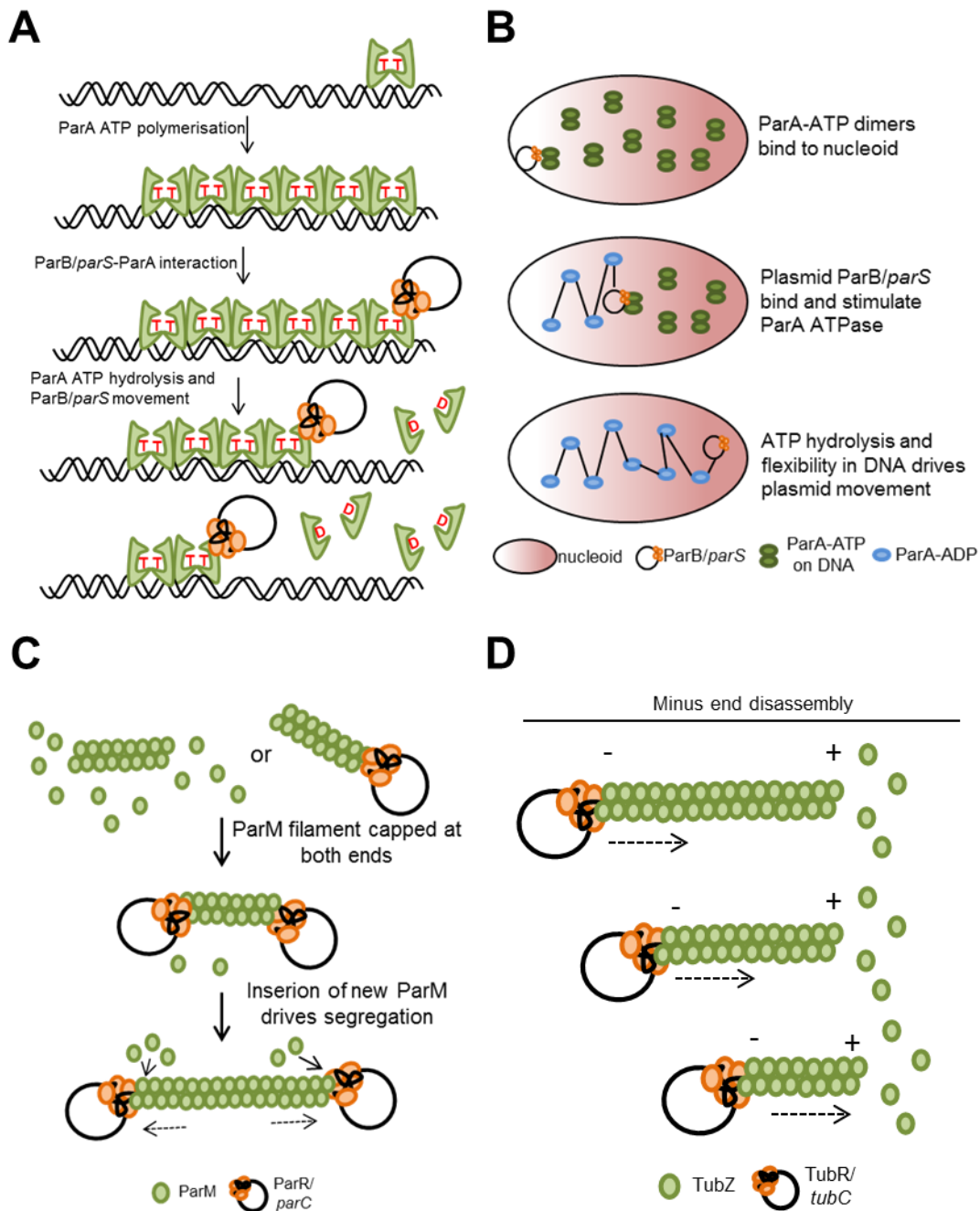
Figure 1.9 Plasmid partitioning systems in bacteria

There are two proposed Type I segregation mechanisms. The first filament-based model (A) suggests that ParB/*parS* drives disassembly of ParA filaments, driving segregation. The alternate ratchet model (B) suggests ParA is bound non-specifically over the DNA (no filaments), where sequential ParB/*parS* interactions drive a gradient of ParA and movement of the DNA. In the Type II system (C), the insertion of new ParM monomers drives plasmids in opposite directions. Minus end disassembly of treadmilling TubZ drives plasmid (TubR/*tubC*) movement towards cell poles in the Type III system (D). See text for details. Information adapted from Brooks and Hwang, 2017 and Gerdes *et al*., 2010.

The *E. coli* Type II ParMRC actin-based system of the R1 plasmid (Table 1.1) is probably the best characterised plasmid partitioning system. ParM is an actin homologue that forms a two stranded helical filament in the presence of nucleotide triphosphate, which are intrinsically unstable and rapidly depolymerise unless stabilised by the capping (van den Ent *et al.*, 2002; Garner *et al.*, 2004; Garner *et al.*, 2007; Popp *et al.*, 2008; Galkin *et al.*, 2009; Rivera *et al.*, 2011). End capping occurs upon interaction of ParM filament with the ParR/*parC* nucleoprotein complex of plasmids (Schumacher *et al.*, 2007). Only when ParM filaments are capped at *both* ends is the filament fully stabilised. The subsequent insertion of new ParM monomers into capped filaments actively pushes the two plasmids in opposite directions (Figure 1.9C) (Møller-Jensen *et al.*, 2003; Campbell and Mullins, 2007; Garner *et al.*, 2007).

In the mid-2000s, a novel type of Par system was discovered (the Type III system) to facilitate plasmid segregation in *Bacilli* (e.g. *B. anthracis* and *B. thuringiensis*) (Tang *et al.*, 2006; Tinsley and Khan, 2006; Larsen *et al.*, 2007). Structural studies revealed that the NTPase, TubZ, is a tubulin-like GTPase, and contains the classic Rossman fold seen in many tubulins, including FtsZ (Aylett *et al.*, 2010; Ni *et al.*, 2010). The *par*-binding TubR and *tubS* site constitute the rest of the system. Upon GTP binding, TubZ forms a polar parallel double helix structure, which treadmills by monomer assembly and disassembly at the plus and minus end, respectively (Larsen *et al.*, 2007; Aylett *et al.*, 2010). Recent *in vitro* reconstitution of the TubZRC system suggested that the plasmid binds to the minus end of the TubZ filament (Fink and Löwe, 2015) and that the filament treadmilling exerts a pulling force on the plasmid until the plasmid reaches the cell pole (Figure 1.9D) (Fink and Löwe, 2015).

1.4.2 Chromosome segregation during vegetative growth in *Bacillus subtilis*

Accurate segregation of the chromosomes is an essential step of the cell cycle. In bacteria, the segregation of the chromosome occurs concomitantly with DNA replication, where the newly replicated chromosome origins partition soon after replication behind the progressing bi-directional replication machinery (Viollier *et al.*, 2004). The simultaneous coordination of these two processes ensures that the cell cycle can keep pace with the rapid growth rate of bacteria. As a result, chromosome

segregation must be robustly and accurately regulated and coordinated to prevent non-productive, potentially lethal, entanglements of the large DNA macromolecules.

After placing fluorescent markers at various chromosome locations, imaging experiments revealed a series of sequential events involved in chromosome segregation in vegetatively growing *B. subtilis.* Following the initiation of DNA replication, chromosome origins re-locate to mid-cell, transitioning from an *ori-ter-ori* to arm-*ori*/*ter*-arm organisation. This is followed by the segregation of sister origins towards opposite cell poles, re-establishing the *ori-ter-ori* organisation (Figure 1.10) (Wang *et al.*, 2014a).
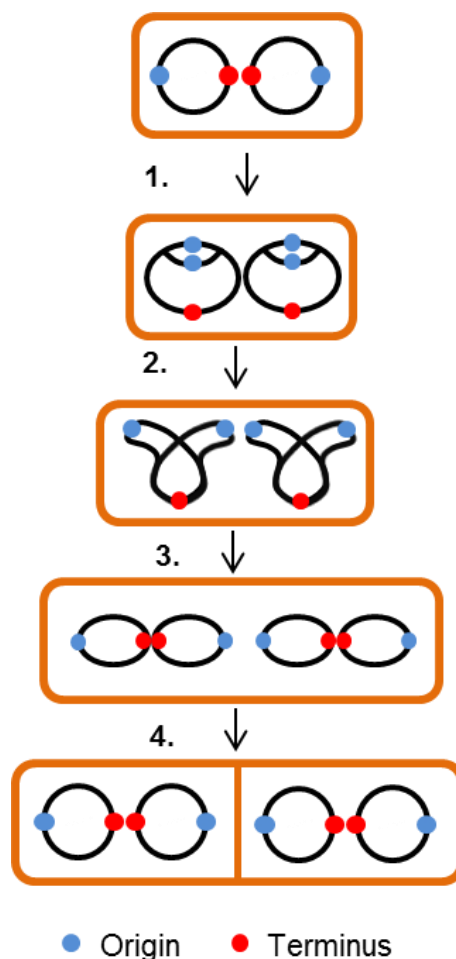
Figure 1.10 Model for chromosome segregation during vegetative growth

Following DNA replication, chromosome origins re-localise leading to a *ori-ter-ori* to arm-*ori/ter*-arm organisation of the chromosome (1). Due to ongoing segregation of the chromosome arms towards opposite ends of the cell (2), the *ori-ter-ori* organisation is re-established (3). Once at quarter cell positions, the terminus regions segregate prior to cell division (4). Adapted from Wang *et al.,* 2014a.

Two key proteins that have long been implicated in chromosome segregation are Soj/ParA and Spo0J/ParB (Lin and Grossman, 1998; Wu and Errington, 2003; Wang *et al.*, 2013). These proteins, along with *parS* sites, constitute the chromosomally encoded ParABS system (or bacterial centromere), which is analogous to the plasmid equivalents (section 1.4.1) and have been identified in more than 65% of sequenced bacterial chromosomes (Livny *et al.*, 2007). *B. subtilis* contains 10 *parS* sequences, 8 of which are located within the origin region (Lin and Grossman, 1998). Upon binding of Spo0J to *parS*, an array of lateral and bridging interactions drives the formation of a large nucleoprotein complex at the origin (Murray *et al.*, 2006; Graham *et al.*, 2014). Biochemical and structural analyses have revealed that Soj forms a homodimer when bound to ATP (Leonard *et al.*, 2005),

while in the absence of nucleotide, or when bound by ADP, Soj is monomeric (Scholefield *et al.*, 2011). Upon dimerisation of Soj-ATP monomers, key arginine residues allow the protein to bind non-specifically to DNA (Leonard *et al.*, 2005; Hester and Lutkenhaus, 2007). Through the presence of critical N-terminal residues, Spo0J is able to stimulate the ATPase of Soj-ATP homodimers (Scholefield *et al.*, 2011). Since Soj and Spo0J have established roles in DNA replication control (Section 1.3), their redundant role in chromosome segregation may be central to the coordination of these two critical processes *in vivo*. Studies have shown that Δ*spo0J* mutants have an origin segregation defect leading to an increase in anucleate cells (Ireton *et al.*, 1994), whilst deletion of *soj* had no major segregation defect alone in vegetatively growing cells, although slight origin segregation defects have been reported (Ireton *et al.*, 1994; Lee and Grossman, 2006; Wang *et al.*, 2014a). Significant chromosome segregation defects were observed when Δ*soj* cells were deleted for the *smc* gene (Lee and Grossman, 2006). It has therefore been proposed that the ParABS system ensures the localisation of origin at the leading edge of the nucleoid (Lin *et al.*, 1997; Wang *et al.*, 2013)

Structural maintenance of chromosome (SMC) complexes, also known as condensin (with homologues cohesin and condensin in eukaryotes), are major determinants of chromosome organisation and segregation in bacteria (Gruber, 2017). SMC complexes comprisethree proteins in *B. subtilis*: SMC, ScpA and ScpB (Figure 1.11A) (Hirano, 2016). The SMC head domain contains the ATP-binding sites, and binding of nucleotide concomitantly with DNA drives the opening of the SMC rod, forming a ring structure that promotes loading onto the chromosome (Gruber *et al.*, 2003; Soh *et al.*, 2015; Wilhelm *et al.*, 2015; Kamada *et al.*, 2017).
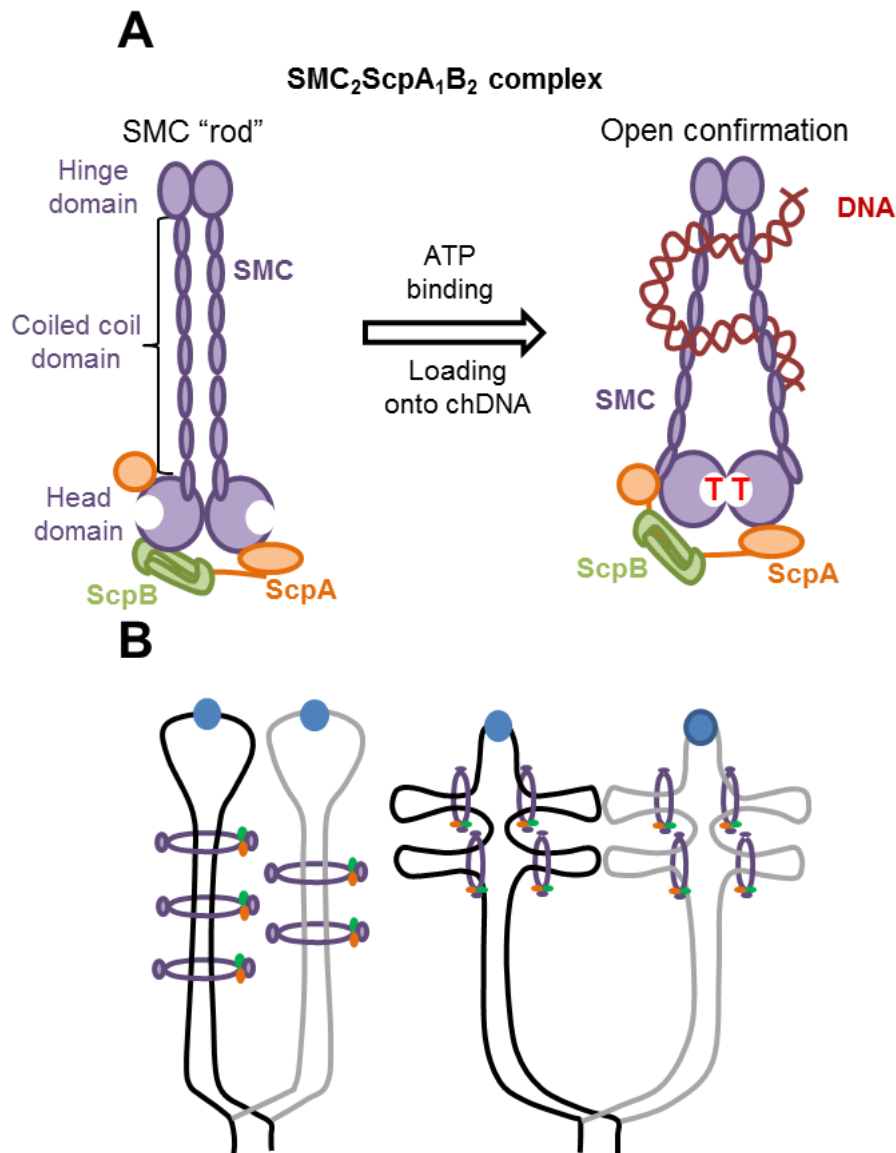
Figure 1.11 SMC complexes in bacteria

SMC complexes are composed of three proteins: SMC, ScpA and ScpB, and exist as a non-DNA, non-ATP bound rod, or as a chromosome binding open ring structure (A). SMC complexes restrict and condense the chromosome arms (black and grey), driving separation (B). Internal arm restriction also creates topological loops in the DNA structure (B, right). Origins are highlighted by blue circles.

SMC complexes are recruited to the *B. subtilis* chromosome by Spo0J bound to *parS* sites, uponwhich it is loaded onto the DNA (Gruber and Errington, 2009; Sullivan *et al.*, 2009). The loading of SMC complexes is critical for ordered segregation of the origins since *Δsmc* strains of *B. subtilis* grown in rich medium (rapid growth) exhibited impaired chromosome segregation. However, when these mutants were grown in minimal medium (slow growth) this segregation defect was

repressed (Gruber *et al.*, 2014; Wang *et al.*, 2014b). Indeed, by artificially reducing replication fork velocity using hydroxyurea, Gruber *et al* 2014 were able to demonstrate that chromosome segregation could occur in *Δsmc* cells. This led to a model in which SMC promotes condensation of newly replicated DNA, reducing sister DNA inter-tangling as well as movement of sister *oriC* regions towards opposite poles (Figure 1.11B) (Gruber *et al.*, 2014; Wang *et al.*, 2014b). More recently, SMC has been implicated in driving bulk chromosome segregation more generally. Following loading at the origin, SMC complexes hydrolyse ATP, transitioning back to the rod structure, although the complex remains bound to DNA. This ATP hydrolysis has been proposed to stimulate active sliding of SMC along the chromosome in an origin-to-terminus direction (Minnen *et al.*, 2016), leading to the juxtaposition of replicated chromosome arms that minimises the chances of DNA tangling, promoting segregation (Figure 1.11B) (Wang *et al.*, 2015; Wang *et al.*, 2017). It is therefore thought that SMC complexes are major determinants of chromosome segregation in vegetatively growing *B. subtilis*, with Soj and Spo0J playing a supporting role, although the precise molecular details of this remain unclear.

1.4.3 Chromosome segregation during sporulation in *Bacillus subtilis*

Chromosome segregation during sporulation can be classified into two key stages. The first is the movement of the normally quarter cell origins to opposite cell poles, at which they become anchored. Although the precise mechanism pertaining to this polar movement is unknown, mutagenesis studies have implicated a number of proteins: Soj, Spo0J and RacA. From analysing the chromosome organisation in mutants of these proteins, it has been postulated that Soj and Spo0J are key in bulk chromosome movement towards the cell pole, where RacA then binds arm localised *ram* sites in the *oriC* region (Wu and Errington, 2002; Ben-Yehuda *et al.*, 2003b; Wu and Errington, 2003; Ben-Yehuda *et al.*, 2005).

The second stage occurs upon asymmetric cell division. SpoIIIE protein localises to the leading edge of the closing septum whereupon it conducts two key functions (Wu and Errington, 1997; Ben-Yehuda *et al.*, 2003a; Liu *et al.*, 2006; Fleming *et al.*, 2010). First, upon DNA binding, SpoIIIE translocates (and therefore segregates) the mother cell localised two thirds of the bisected chromosome into the prespore in an ATP dependent manner (Wu and Errington, 1994; Wu *et al.*, 1995;

Bath *et al.*, 2000; Becker and Pogliano, 2007). Secondly, it has been implicated in controlling membrane dynamics during chromosome translocation (Liu *et al.*, 2006; Fleming *et al.*, 2010).

Considerable work has gone into establishing how SpoIIIE (and the homologue in *E. coli*, FtsK) translocates the bisected chromosome. Structural studies and bioinformatics have revealed that SpoIIIE consists of three domains: an N-terminal transmembrane domain containing four membrane spanning helices, a flexible linker and a globular C-terminal motor domain (Figure 1.12.A) (Massey *et al.*, 2006). The C-terminal domain contains a further 3 sub-domains termed α (SpoIIIE specific domain), β (ATPase domain) and γ (the DNA binding domain) (Massey *et al.*, 2006; Besprozvannaya *et al.*, 2013; Besprozvannaya *et al.*, 2014). Furthermore, SpoIIIE/FtsK forms a hexameric structure upon binding of each chromosome arm (Figure 1.12B), with each hexamer containing a 30Å internal diameter that accommodates double stranded DNA (Figure 1.12C) (Massey *et al.*, 2006; Lowe *et al.*, 2008).
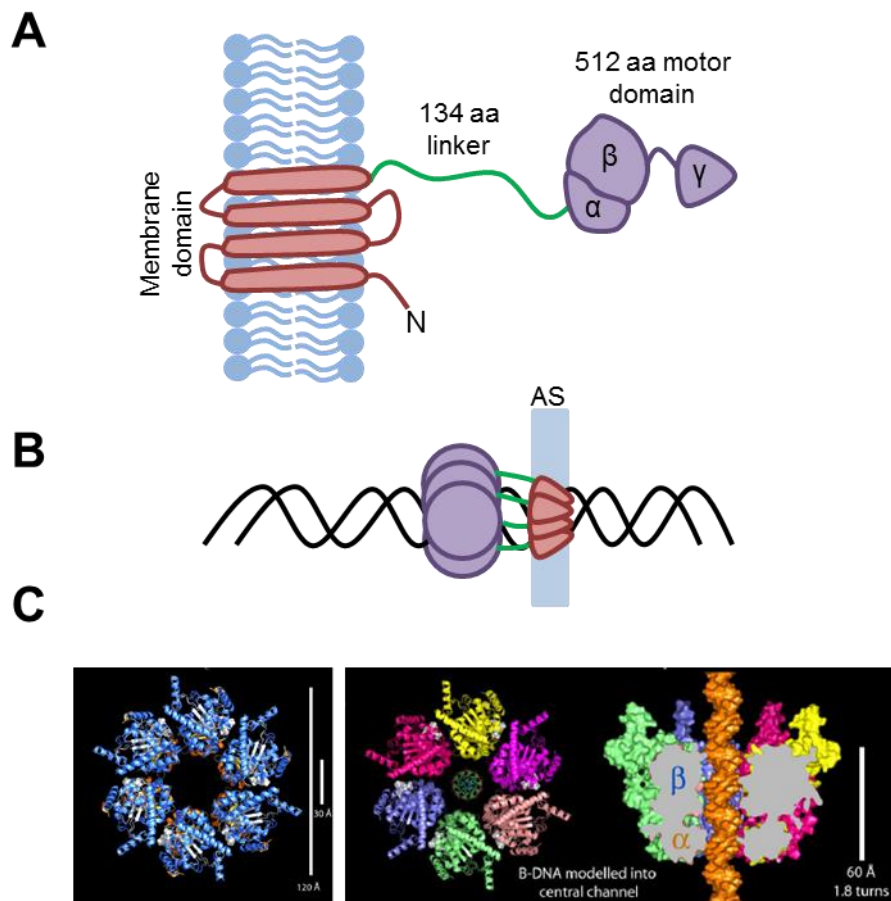
Figure 1.12 Structure and localisation of SpoIIIE

SpoIIIE contains three main domains: transmembrane, linker and motor domains (A), and the protein localises to the leading edge of the asymmetric septum (AS) (B). Structural studies using the SpoIIIE homologue in *E. coli* (FtsK), demonstrated that each hexamer binds one double stranded chromosome arm (C). Adapted from Massey *et al.*, 2006 and Cattoni *et al.*, 2014.

During asymmetric division, SpoIIIE appears to be recruited to the leading edge of the closing septum which bisects the chromosome (Wu and Errington, 1997; Sharp and Pogliano, 1999). Based on *in vitro* studies it is assumed that SpoIIIE hexamers initially bind the DNA non-specifically. This SpoIIIE-DNA interaction has been termed the 'open and inactive' form. In this state, SpoIIIE scans along the DNA in a ATP-independent manner until it reaches a specific activating sequence, known as a sequence recognition site (SRS) (Cattoni *et al.*, 2013; Cattoni *et al.*, 2014). SRS sequences are highly asymmetric and are scattered throughout the genome (Pease *et al.*, 2005; Ptacin *et al.*, 2008; Cattoni *et al.*, 2013). Upon binding and recognition of the SRS, SpoIIIE hexamers form a 'closed and active' state that pumps the DNA in an ATP-dependent manner (Besprozvannaya *et al.*, 2013; Cattoni *et al.*, 2013;

Cattoni *et al.*, 2014). The lack of symmetry in the SRS promotes directionality in the SpoIIIE-mediated pumping of DNA, ensuring that it is only the mother cell-localised 70% fraction of the chromosome that is moved through the septum (Marquis *et al.*, 2008; Besprozvannaya *et al.*, 2013; Cattoni *et al.*, 2013; Lee *et al.*, 2014). The existence of SRS sequences throughout the genome is thought to allow re-initiation of rapid active pumping if the protein encounters large roadblocks that cause complex disassembly (Cattoni *et al.*, 2014). Cell biology studies revealed that both chromosome arms are translocated simultaneously, and that SpoIIIE actively strips proteins off the chromosome (Burton *et al.*, 2007; Marquis *et al.*, 2008). The latter has been hypothesised to aid in the re-programming of prespore gene expression (Marquis *et al.*, 2008).

As mentioned earlier, SpoIIIE is also involved in membrane dynamics, and therefore extensive effort has been made to establish the precise SpoIIIE quaternary conformation and organisation in the membrane. From this work, two contrasting models have emerged (Burton *et al.*, 2007; Ptacin *et al.*, 2008; Fleming *et al.*, 2010; Fiche *et al.*, 2013; Yen Shin *et al.*, 2015) (Figure 1.13). The first model proposes that SpoIIIE localises at the leading edge of the septum, upon which it forms a protein-DNA pore (Wu and Errington, 1994; Fiche *et al.*, 2013). Furthermore, from super-resolution imaging the SpoIIIE hexamers are slightly localised to the mother cell side during translocation, which occurs upon extension of the linker upon ATP-dependent pumping by SpoIIIE (Figure 1.13A) (Fiche *et al.*, 2013). In this model, the membranes do not fuse until after translocation of the chromosome has occurred. An alternative mechanism suggests that following DNA binding and septal membrane fusion, pairs of SpoIIIE hexamers align on each chromosome arm, where upon recognition of an SRS sequence, one hexamer becomes activated to pump the DNA, with the oppositely oriented SpoIIIE molecules remaining in an inactive state (Figure 1.8B) (Liu *et al.*, 2006; Burton *et al.*, 2007; Fleming *et al.*, 2010; Yen Shin *et al.*, 2015). Although evidence for both models exists, it remains to be determined how the circular terminus region is transported across the septum, particularly if the membranes had fully fused (Figure 1.13B). There is no current evidence suggesting cleavage, membrane translocation and re-ligation of the terminus during sporulation.
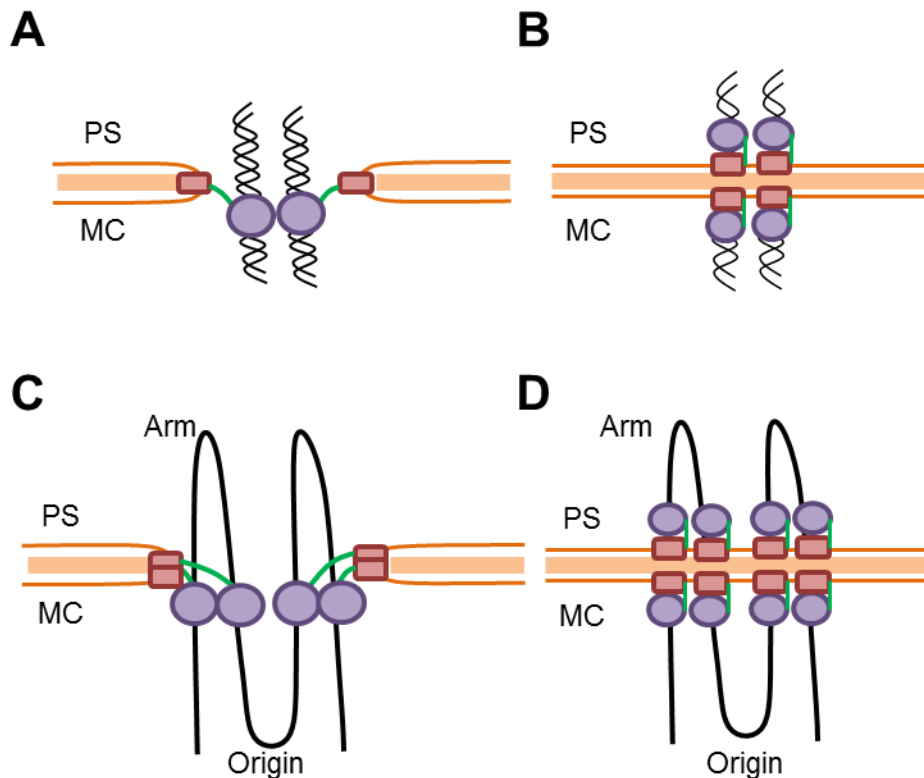
Figure 1.13 Models for SpoIIIE organisation in the asymmetric septum

It has been proposed that SpoIIIE localises to the leading edge of the closing septum, where it binds DNA and translocates prior to septum closure (A). Alternative models propose that SpoIIIE hexamers align in the prespore (PS) and mother cell (MC) membranes (B). Isolation of chromosome organisation mutants revealed that at least 4 (C) or 8 (D) hexamers would be required to bind the DNA depending on the models in A-B. Dark orange line = double membrane; light orange line = septal cell wall; Black lines = prespore chromosome; red-green and purple schematic represents the domains of SpoIIIE.

SpoIIIE is a non-abundant protein, with estimates as low as 50 (Fiche *et al.*, 2013), and up to 100 (Burton *et al.*, 2007) subunits per cell during sporulation. In the wild-type situation, only 2-4 hexamers (12-24 SpoIIIE monomers) would be necessary (Figure 1.13A-B). One possible advantage in expressing more SpoIIIE protein than strictly required was revealed through the isolation of chromosome segregation mutants that have an altered and unusual chromosome organisation structure. Knockouts of *soj racA* or *divIVA* failed to segregate the origin to the pole, but were able localise the origin proximal arm regions correctly (in the spore region; Figure 1.13C-D) (Wu and Errington, 2003; Errington *et al.*, 2005). Topologically, the DNA in these mutants would need to cross the asymmetric septum at least 4 (Figure 1.13C) or 8 (Figure 1.13D) times depending upon the precise organisation of SpoIIIE in the septum.

The identification of the chromosome organisation mutants exploited a class of point mutations in *spoIIIE* (represented usually by *spoIIIE36*) for which the protein product retained the ability to bind DNA and allow activation of compartment specific sigma factor signalling (suggesting correct compartmentalisation), but was DNA translocation deficient (Wu and Errington, 1994; Wu *et al.*, 1995). The *spoIIIE36* mutation results in a single amino acid substitution in the C-terminal ATPase domain of SpoIIIE36 (V429M), which prevents coordination between the ATPase and DNA binding domains, abolishing translocation (Besprozvannaya *et al.*, 2014). This phenotype contrasts with that of a *spoIIIE* null mutation, in which there is leakage of components and lack of compartmentalised gene expression between the prespore and mother cell.

1.4.4 Chromosome segregation in *Caulobacter crescentus*

Caulobacter crescentus (*C. crescentus*) is a dimorphic Gram-negative model organism, in which all cell division events are asymmetric, generating differentiated stalked and swarmer cell types (Thanbichler, 2009). Like *B. subtilis*, the *C. crescentus* origin region (called *cori*) contains *parS* sequences that are bound by ParB (Mohl and Gober, 1997; Livny *et al.*, 2007; Toro *et al.*, 2008). Furthermore, the ParABS system is essential (Mohl and Gober, 1997). Critical to studying chromosome and cell cycle dynamics was the ability to synchronise the *C. crescentus* population (Jensen and Shapiro, 1999). A seminal study using fluorescent *in situ* hybridisation revealed that the *cori* was localised near to the old cell pole, with the *ter* at the new pole. Following DNA replication initiation, the newly replicated origin then rapidly re-located towards the new pole and the terminus concomitantly re-localised at the mid-cell site (Jensen and Shapiro, 1999; Jensen and Shapiro, 2003). Subsequent high-resolution chromosome conformation capture experiments (Hi-C) have shown that the chromosome adopts a linear organisation, with arms positioned side by side and *cori* and *ter* regions at opposite ends of the cell, confirming these earlier findings (Figure 1.14) (Le *et al.*, 2013).
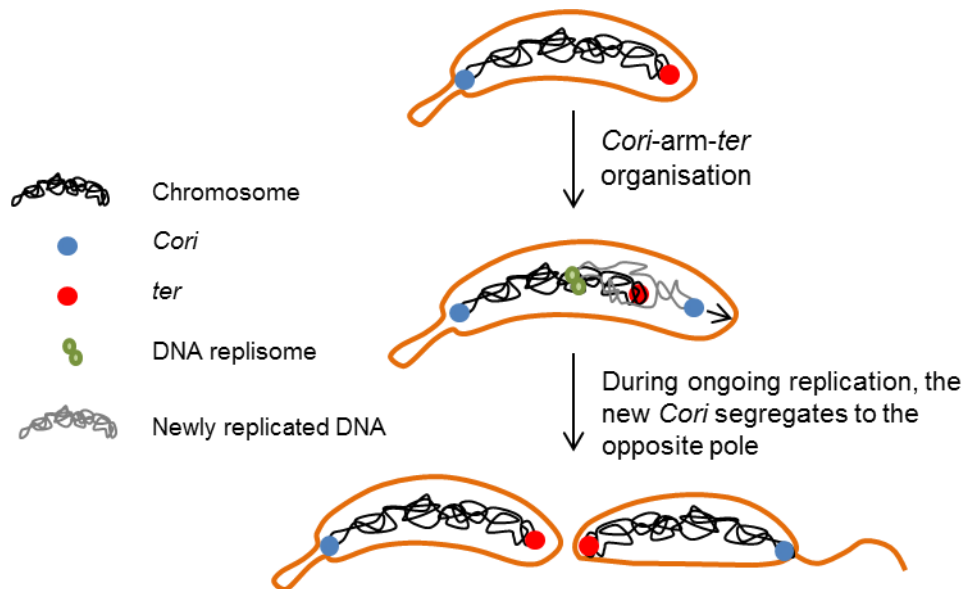
Figure 1.14. Chromosome organisation and segregation in *C. crescentus*

The chromosome adopts a *cori*-arm-*ter* organisation, with the *cori* anchored to the stalked pole. Upon the initiation of DNA replication, the newly replicated *cori* segregates to the opposite cell pole (which later becomes the flagellated pole), whilst the *ter* re-locates to mid cell. See text for details. Adapted from Wang *et al.*, 2013.

The origin *parS*-ParB region in *C. crescentus* is anchored to the old cell pole by a major polar hub protein, PopZ (Viollier *et al.*, 2004; Bowman *et al.*, 2008; Ebersbach *et al.*, 2008). Recently, it has been shown that PopZ can bind at least eight cell cycle proteins, and that the PopZ polar hub region is intrinsically disordered, where rapid binding and release interactions maintain high local concentrations of all of the interaction components (Holmes *et al.*, 2016).

Fluorescent imaging suggested that ParA ATP dimers formed a "cloud-like" pattern that co-localised over the nucleoid. It was hypothesised that this was caused by non-specific DNA binding (Ptacin *et al.*, 2010; Schofield *et al.*, 2010; Shebelut *et al.*, 2010). Following DNA replication initiation, the newly replicated origin *parS*-ParB that is not bound to the cell pole trails the receding ParA cloud, where it was proposed that the shrinking ParA structure "pulled" the second *cori* to the opposite cell pole, analogous to that of Type I plasmid partitioning (Ptacin *et al.*, 2010; Schofield *et al.*, 2010). Subsequent studies have suggested an alternative mechanism in which ParA-ATP dimers bind non-specifically along the nucleoid. Following DNA replication initiation, the second *parS*-ParB complex interacts with proximal ParA-dimers, driving ATP hydrolysis. The ParB nucleoprotein complex can

then contacts nearby ParA-ATP dimers before the release of the now monomeric ParA (whose ATPase was just stimulated). Repeated cycles of ParB-ParA binding, ParA ATP hydrolysis and release drive the movement of the *cori* along the nucleoid in a DNA-relay mechanism, where PopZ can sequester free ParA (Lim *et al.*, 2014; Ptacin *et al.*, 2014). Modelling studies suggested that a combination of the constrained ParA-ATP dimers bound to the chromosome, the rate of ParA-ATPase stimulation by ParB and a slow ParA-chromosome re-binding speed are together sufficient for the establishment of a ParA gradient along the chromosome (Surovtsev *et al.*, 2016a; Surovtsev *et al.*, 2016b). Released ParA monomers accumulate at the new cell pole via interactions with the TipN, a major determinant of the new pole (Lam *et al.*, 2006; Schofield *et al.*, 2010). ParA-TipN interactions ensure that chromosome segregation occurs unidirectionally by preventing ParA dimerisation and re-binding to the chromosome behind the progressing origin (Schofield *et al.*, 2010). Irrespective of which model drives chromosome segregation, the ParABS system, particularly the activity of ParA ATP hydrolysis, is critical for chromosome segregation (Toro *et al.*, 2008).

SMC in *C. crescentus* has largely the same structure as that in *B. subtilis*. However, imaging of SMC revealed multiple foci at various cellular locations throughout the cell cycle (Jensen and Shapiro, 2003). Deletion of *smc* causes chromosome segregation defects, and therefore it has been proposed that SMC complexes are critical for constraining chromosome arms (Schwartz and Shapiro, 2011; Le *et al.*, 2013). DnaA has also been linked to chromosome segregation (Mera *et al.*, 2014). Indeed, DnaA binding sites were found in between *parS* sites. It was proposed that in addition to promoting DNA replication, DnaA may also play an independent role in moving the *cori* along the length of the cell, potentially providing coordination between replication and segregation of the DNA (Mera *et al.*, 2014). Whether a similar process occurs in *B. subtilis* during sporulation is unknown.

1.5 Septum positioning in bacteria

1.5.1 The Min system

The Min system prevents cell division near the cell pole, and is dependent upon MinD and MinC, as well as MinE (in *E. coli*), and DivIVA and MinJ (in *B. subtilis*)

(Lutkenhaus, 2007; van Baarle and Bramkamp, 2010). MinD is an ATPase, and MinD ATP dimers associate with the cell pole via an amphipathic helix. In turn, MinD homodimers recruit MinC, the inhibitor of FtsZ ring formation. In *E. coli*, MinCD oscillates from pole to pole roughly every 40 seconds, forming a concentration gradient along the cell length that is highest at the poles (Figure 1.15A) (Bonny *et al.*, 2013). MinE drives this process by accumulating in a ring like structure at the membrane that limits the localisation of MinCD. Upon reaching the cell pole, MinE chases MinD off the membrane (and therefore MinC is released) through the activation of MinD-ATP hydrolysis. Specifically, interaction of MinE with a critical N45 residue in the switch I loop of the MinD homodimers activates the MinD ATPase, upon which the MinD monomers dissociate from the membrane and relocate to the opposite pole (Zhao *et al.*, 1995; Raskin and De Boer, 1999; Hu and Lutkenhaus, 2001; Loose *et al.*, 2008; Park *et al.*, 2012). Following this, MinE can either release from the membrane into the cytoplasm, or interact with a neighbouring MinD ATP homodimer. The high concentrations of MinD found in the cell pole region favour the latter, allowing MinE to chase along the membrane in a so-called "Tarzan of the Jungle" model (Figure 1.15B) (Park *et al.*, 2011).
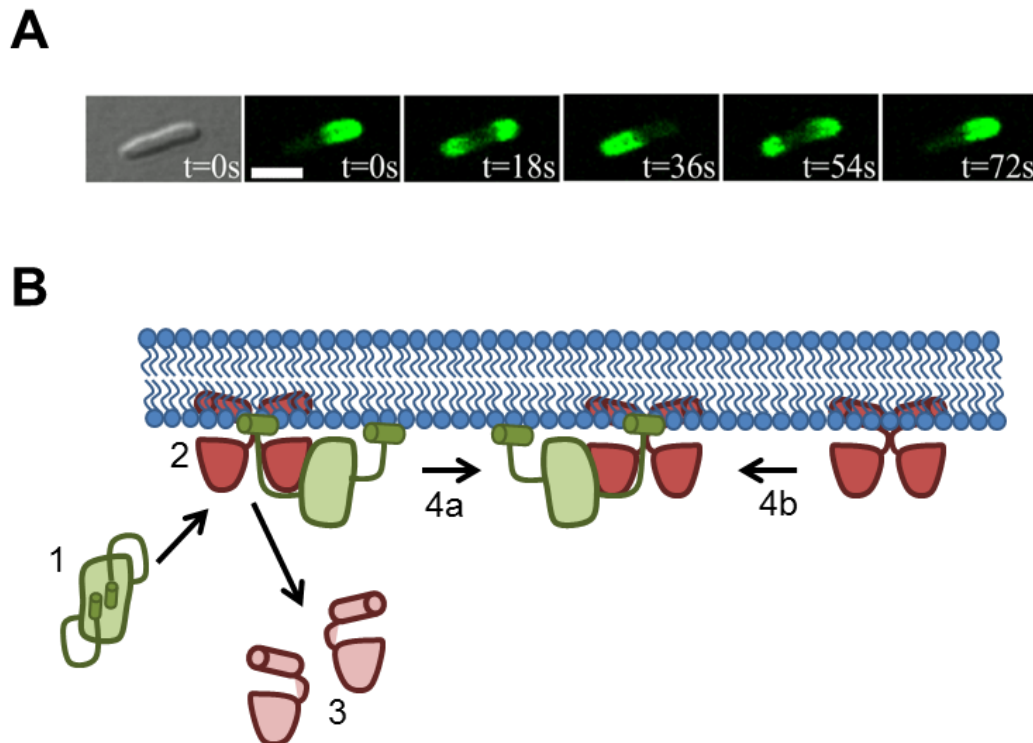
Figure 1.15 The Min system in *E. coli*

(A) The Min system oscillates from one pole to the approximately every 40 s. (B) "Tarzan of the Jungle" model for the role of MinE (green) in oscillation. Upon interaction with the membrane, two critical β-1 strands are released from the core (1) structure and in conjunction with flanking α-helix residues, interact with the membrane and MinD (red) to stabilise the structure (2). The latter interaction stimulates MinD ATPase and release from the membrane (released MinD labelled in pink) (3). If retained at the membrane, MinE is then handed to the next MinD-homodimer (red) (4a) and the process is sequentially repeated (4b), allowing MinE to glide along the membrane surface, releasing MinD in the process. Adapted from Bonny *et al.*, 2013 and Park *et al.*, 2011

In *B. subtilis* the Min system is static and is dependent upon DivIVA, which localises to areas of negative curvature – division sites and cell poles (Lenarcic *et al.*, 2009; Strahl and Hamoen, 2010). Current models suggest that upon divisome assembly at mid-cell and the initiation of cell division, areas of negative curvature are created and DivIVA accumulates at these sites. This in turn leads to the recruitment of MinJ, MinD and MinC. Since the divisome is assembled and actively undergoing constriction, the inhibitory activity of MinC is overcome. However, upon completion of division and the breakdown of the division machinery, the presence of MinC at this "new pole" prevents any re-accumulation of Z-rings proximal to the cell pole (Marston *et al.*, 1998; Bramkamp *et al.*, 2008; Gregory *et al.*, 2008).

Nucleoid occlusion (NO) describes the long-standing reports that the cells tend not to divide in the vicinity of the chromosome. Indeed, the process of nucleoid occlusion was originally described in the 1980-90s (Mulder and Woldringh, 1989; Woldringh *et al.*, 1991; Woldringh *et al.*, 1994). However, it was not until the 2000s that mechanistic details began to emerge. In *B. subtilis* NO was found to be mediated, at least in part, by the nucleoid occlusion protein, Noc (Wu and Errington, 2004). Deletion or overexpression of Noc promoted division through the nucleoid or cell elongation, respectively, implicating this protein directly in NO, combining DNA binding and cell division functions simultaneously (Wu and Errington, 2004). Noc binds to specific palindromic sequences that are located around the genome, with the notable exception of the terminus regions (Wu *et al.*, 2009), possibly because these are located closer to mid cell during vegetative growth. Through a weak amphipathic helix, Noc is able to bind the cell membrane, but this membrane association is dependent upon the formation of Noc-mediated nucleoprotein complexes that are assembled at the *noc*-binding sites (Adams *et al.*, 2015). By interacting with DNA and the membrane simultaneously, Noc inhibits the establishment of Z-rings over the nucleoid by physically preventing the assembly of the divisome at these sites (Adams *et al.*, 2015).

1.6 Specific Aims of this thesis

The main aims of this work were to investigate several remaining problems associated with chromosome dynamics and polar septation at the onset of sporulation. Several of the proteins involved, including DivIVA, MinD, Soj, Spo0J and SpoIIIE, have important widely conserved roles in cell cycle dynamics more generally. Specifically, my aims were to:

1. Precisely map the DNA captured in SpoIIIE translocation complexes upon asymmetric cell division to gain further insight into the exact organisation of the axial filament in wild type and mutant cells.
2. Visualise components of the origin capture complexes during sporulation and investigate their functions.

3. Specifically investigate the role of Soj in chromosome segregation and polar anchoring of the origins during early sporulation.

Chapter 2

Materials and Methods

2.1 Bacterial Strains and their growth and maintenance

Bacillus subtilis, Escherichia coli strains used and constructed in this thesis are listed in Table 2.1, along with their genotypes and any published references, where appropriate.

Strain	Genotype	Reference
168CA	*trpC2*	(Kunst *et al.*, 1997)
654	*trpC2 ilvB2 leuB16 (spoIIAABC::cat)*	Laboratory Stock
901	*trpC2 (spoIIGA-aph-A3)*	Laboratory Stock
BWX2006	*yycR::(tetO120 erm)* *ycgO::(P$_{ftsW}$-tetR-mcherry phleo)* *sacA::(hbs-gfp cat)*	Wang et al., 2014.
DMR004	*trpC2 spoIIIE-12xHis::erm*	This work. Transformation of 168CA with pDMR001
DMR006	*trpC2 spoIIIE36-12xHis::erm*	This work. Transformation of spoIIIE36 with pDMR001
DMR013	*trpC2 spoIIIE36::kan ywjI::(P$_{spoIIQ}$-cfp;erm)*	This work. Transformation of pKH173 (Rudner lab) into DMR064
DMR014	*trpC2 ΔspoIIIE yycR::(P$_{spoIIQ}$-yfp spc)*	This work. Transformation of pNS059 (Rudner lab) into the *ΔspoIIIE* lab stock strain
DMR023	*trpC2 spo0J-12xHis::erm*	From Ling Juan Wu. 168ED
DMR025	*trpC2 spo0J-12xHis::erm*	This work. Transformation of 168CA with DMR023
DMR045	*trpC2 ΔspoIIGA::kan*	This work. Transformation of 168CA with 901 DNA.
DMR056	*trpC2 spoIIIE36 amyE::(P$_{spoIIQ}$-dam spc)*	This work. Transformation of spoIIIE36 with pDMR011
DMR058	*trpC2 amyE::(P$_{spoIIQ}$-dam spc)*	This work. Transformation of 168CA with pDMR011
DMR060	*trpC2 ΔspoIIGA::kan amyE::(P$_{spoIIQ}$-dam spc)*	This work. Transformation of DMR045 with pDMR011

DMR062	*trpC2 ilvB2 leuB16 (spoIIAABC::cat) amyE::(P_{spoIIQ}-dam spc)*	This work. Transformation of DMR058 with 654.
DMR063	*trpC2 spoIIIE36::cat*	Laboratory Stock
DMR064	*trpC2 spoIIIE36::kan*	Laboratory Stock
DMR065	*trpC2 gfp-soj::neo*	This work. Transformation of 168CA with HM4
DMR066	*trpC2 ΔcomN::zeo amyE::(P_{comN}-comN-gfp spc)*	This work. Transformation of 168CA with TK314.
DMR067	*trpC2 minD::(gfp-minD kan)*	Kloosterman et al., 2016
DMR070	*trpC2 ΔcomN minD::(gfp-minD kan)*	Kloosterman et al., 2016
DMR075	*trpC2 ΔcomN::zeo*	Tomas Kloosterman, unpublished
DMR080	*trpC2 spo0J-gfp::neo*	Alan Koh, unpublished
DMR081	*trpC2 amyE::(P_{spoIIA}-mcherry cat)*	Veening et al., 2009
DMR109	*trpC2 Δ(soj spo0J)::tet*	This work. Transformation of 168CA with HM31
DMR108	*aprE::(P_{spac}-mcherry-comN cat)*	This work. Transformation of 168CA with TK93
DMR111	*trpC2 minD::(gfp-minD kan) aprE::(P_{spac}-mcherry-comN cat)*	Kloosterman et al., 2016.
DMR113	*trpC2 amyE::(P_{xyl} -divIVA-msfGFP spc)*	This work. Transformation of 168CA with chDNA gifted from Henrik Strahl.
DMR114	*trpC2 minCD::(minC⁺ ΔminD Ωerm)*	This work. Transformation of 168CA with 1901.
DMR115	*trpC2 ΔdivIVA::tet*	Laboratory Stock
DMR117	*trpC2 Δsoj::neo*	Alan Koh, unpublished
DMR119	*trpC2 ΔracA::erm*	From Tomas Kloosterman
DMR124	*trpC2 ΔracA::erm ΔcomN::zeo*	This work. Transformation of DMR075 with TK105
DMR131	*trpC2 amyE::(spc P_{xyl}-WALP23-gfp)*	This work. Transformation of 168CA with pDMR013.
DMR132	*trpC2 amyE::(spc P_{xyl}-WALP23-mgfp)*	This work. Transformatino of 168CA with pDMR014.
DMR133	*trpC2 amyE::(spc P_{xyl}-WALP23-gfp) yycR::(tetO120 erm)*	This work. Transformation of DMR131 with BWX2006
DMR134	*trpC2 amyE::(spc P_{xyl}-WALP23-mgfp)*	This work. Transformation

	yycR::(tetO120 erm)	of DMR132 with BWX2006.
DMR135	*trpC2 amyE::(spc P_{xyl}-WALP23-gfp)* *yycR::(tetO120 erm)* *ycgO::(P_{ftsW}-tetR-mcherry phleo)*	This work. Transformation of DMR133 with BWX2006.
DMR136	*trpC2 amyE::(spc P_{xyl}-WALP23-mgfp)* *yycR::(tetO120 erm)* *ycgO::(P_{ftsW}-tetR-mcherry phleo)*	This work. Transformation of DMR134 with BWX2006.
DMR137	*trpC2 spo0J-gfp::neo* *aprE::(P_{spac}-mcherry-comN cat)*	This work. Transformation of DMR080 with DMR108.
DMR138	*trpC2 pelB::(lacO48 kan)* *thrC::(P_{pen}-lacIΔ11 –gfpmut2 erm)* *amyE::(spc P_{xyl}-WALP23-mcherryB)*	From Seoungjun Lee
DMR139	*trpC2* *amyE::(spc P_{xyl}-WALP23-mcherryB)*	This work. Transformation of 168CA with DMR138
DMR140	*trpC2 ΔyabT::erm*	From Richard Daniel
DMR145	*trpC2 spo0J-gfp::neo* *amyE::(spc P_{xyl}-WALP23-mcherryB)*	This work. Transformation of DMR080 with DMR139
DMR146	*trpC2 spo0J-gfp::neo ΔracA::erm* *amyE::(spc P_{xyl}-WALP23-mcherryB)*	This work. Transformation of DMR145 with DMR119
DMR147	*trpC2 spo0J-gfp::neo ΔcomN::zeo* *amyE::(spc P_{xyl}-WALP23-mcherryB)*	This work. Transformation of DMR145 with DMR075
DMR148	*trpC2* *amyE::(spc P_{xyl(M9R)}-WALP23-gfpmut1_{A>K})* *ycgO::(P_{ftsW}-tetR-mcherry phleo)* *yycR::(tetO120 erm)*	Clare Willis, unpublished
DMR149	*trpC2* *amyE::(spc P_{xyl(M9R)}-WALP23-gfpmut1_{A>K})* *ycgO::(P_{ftsW}-tetR-mcherry phleo)* *dacC::(tetO240 cat)*	Clare Willis, unpublished
DMR150	*trpC2* *amyE::(spc P_{xyl(M9R)}-WALP23-gfpmut1_{A>K})* *ycgO::(P_{ftsW}-tetR-mcherry phleo)* *yycR::(tetO120 erm) dacC::(tetO240 cat)*	This work. Transformation of DMR149 with DMR148
DMR151	*trpC2 ΔspoIIGA::zeo*	Clare Willis, unpublished
DMR152	*trpC2 (soj(G12V) spo0J-gfp)::neo*	GJS79
DMR153	*trpC2 (soj(D40A) spo0J-gfp)::neo*	GJS80
DMR154	*trpC2 (Δsoj spo0J-gfp)::neo*	Heath Murray, unpublished

DMR155	*trpC2 (soj(K16A) spo0J-gfp)::neo*	HM63
DMR156	*trpC2 (soj(K16A) spo0J-gfp)::neo amyE::(spc P_{xyl}-WALP23-mcherryB)*	This work. Transformation of DMR139 with DMR155
DMR157	*trpC2 (soj(G12V) spo0J-gfp)::neo amyE::(spc P_{xyl}-WALP23-mcherryB)*	This work. Transformation of DMR139 with DMR152
DMR158	*trpC2 (soj(D40A) spo0J-gfp)::neo amyE::(spc P_{xyl}-WALP23-mcherryB)*	This work. Transformation of DMR139 with DMR153
DMR159	*trpC2 (Δsoj spo0j-gfp)::neo amyE::(spc P_{xyl}-WALP23-mcherryB)*	This work. Transformation of DMR139 with DMR154
DMR161	*trpC2 amyE::(spc P_{xyl(M9R)}-WALP23-gfpmut1_{A>K}) ycgO::(P_{ftsW}-tetR-mcherry phleo) yycR::(tetO120 erm) dacC::(tetO240 cat) ΔspoIIGA::kan*	This work. Transformation of DMR150 with DMR045
DMR167	*trpC2 amyE::(spc Pxyl-WALP23-mcherryB)ΔracA::erm*	This work. Transformation of DMR139 with DMR119
DMR171	*trpC2 ΔracA::erm amyE::(spc Pxyl-WALP23-mcherryB) (soj(G12V) spo0J-gfp)::neo*	This work. Transformation of DMR167 with DMR152
DMR172	*trpC2 ΔracA::erm amyE::(spc Pxyl-WALP23-mcherryB) (soj(D40A) spo0J-gfp)::neo*	This work. Transformation of DMR167 with DMR153
DMR173	*trpC2 ΔracA::erm amyE::(spc Pxyl-WALP23-mcherryB) (Δsoj spo0J-gfp)::neo*	This work. Transformation of DMR167 with DMR154
DMR174	*trpC2 ΔracA::erm amyE::(spc Pxyl-WALP23-mcherryB) (soj(K16A) spo0J-gfp)::neo*	This work. Transformation of DMR167 with DMR155
DMR178	*trpC2 spoIIIE36::cat yycR::(P_{spoIIQ}-yfp spc) ywjI::(P_{spoIIQ}-cfp erm)*	From Tomas Kloosterman, unpublished
DMR179	*trpC2 spoIIIE36::cat yycR::(P_{spoIIQ}-yfp spc)*	From Tomas Kloosterman,

	ywjl::(P$_{spoIIQ}$-cfp erm) (soj(G12V))::neo	unpublished
DMR181	*trpC2 spoIIIE36::cat yycR::(P$_{spoIIQ}$-yfp spc)* *ywjl::(P$_{spoIIQ}$-cfp erm) (soj(K16A))::neo*	From Tomas Kloosterman, unpublished
DMR184	*trpC2 (soj(K16A) spo0J(L5H))::neo* *spoIIIE36::cat yycR::(P$_{spoIIQ}$-yfp spc)* *ywjl::(P$_{spoIIQ}$-cfp erm)*	From Tomas Kloosterman, unpublished
DMR185	*trpC2 (soj(G12V) spo0J(L5H))::neo* *spoIIIE36::cat yycR::(P$_{spoIIQ}$-yfp spc)* *ywjl::(P$_{spoIIQ}$-cfp erm)*	From Tomas Kloosterman, unpublished
DMR190	*trpC2 spoIIIE36::cat yycR::(P$_{spoIIQ}$-yfp spc)* *ywjl::(P$_{spoIIQ}$-cfp erm) ΔracA::erm*	This work. Transformation of DMR178 with DMR119
DMR191	*trpC2 spoIIIE36::cat yycR::(P$_{spoIIQ}$-yfp spc)* *ywjl::(P$_{spoIIQ}$-cfp erm) ΔracA::erm* *(soj(G12V))::neo*	This work. Transformation of DMR179 with DMR119
DMR192	*trpC2 spoIIIE36::cat yycR::(P$_{spoIIQ}$-yfp spc)* *ywjl::(P$_{spoIIQ}$-cfp erm) ΔracA::erm* *(soj(K16A))::neo*	This work. Transformation of DMR181 with DMR119
DMR193	*trpC2 ftsA::HaloTag ftsZ-mNeonGreen*	Gifted from Seamus Holden
DMR194	*trpC2 spoIIIE36::zeo* *yycR::(P$_{spoIIQ}$-yfp spc)*	This work. Transformation of DMR014 with TK261
DMR195	*trpC2 ywjl::(P$_{spoIIQ}$-cfp erm)*	This work. Transformation of 168CA with DMR013
DMR199	*trpC2 spo0J-gfp::neo amyE::(spc P$_{xyl}$-WALP23-mcherry(B)) ΔracA::erm ΔcomN::zeo*	This work. Transformation of DMR146 with DMR075
DMR200	*trpC2 ΔminCD::cat*	This work. Transformation of 168CA with a 3-way ligation to replace *minCD* operon with cat
DMR203	*trpC2 minCD::(ΔminC minD$^+$ Ωcat)*	This work. Transformation of 168CA with a 3-way ligation to replace *minC* with cat
DMR206	*trpC2 mNG-soj::neo*	This work. Transformation

		of DMR109 with 3 way ligation to insert mNG 5' of Soj
DMR208	*trpC2 mNG-soj(G12V)::neo*	This work. Transformation of DMR109 with 3 way ligation to insert mNG 5' of Soj(G12V)
DMR210	*trpC2 mNG-soj(K16A)::neo*	This work. Transformation of DMR109 with 3 way ligation to insert mNG 5' of Soj(K16A)
DMR213	*trpC2 spoIIIE36::zeo yycR::(P$_{spoIIQ}$-yfp spc) ywjI::(P$_{spoIIQ}$-cfp erm)*	This work. Transformation of DMR178 with TK261.
DMR214	*trpC2 spoIIIE36::zeo soj(G12V)::neo yycR::(P$_{spoIIQ}$-yfp spc) ywjI::(P$_{spoIIQ}$-cfp erm)*	This work. Transformation of DMR179 with TK261
DMR215	*trpC2 spoIIIE36::zeo yycR::(P$_{spoIIQ}$-yfp spc) ywjI::(P$_{spoIIQ}$-cfp erm) ΔracA::tet*	This work. Transformation of DMR190 with TK261.
DMR216	*trpC2 spoIIIE36::zeo soj(G12V)::neo yycR::(P$_{spoIIQ}$-yfp spc) ywjI::(P$_{spoIIQ}$-cfp erm) ΔracA::tet*	This work. Transformation of DMR191 with TK261
DMR217	*trpC2 spoIIIE36::zeo yycR::(P$_{spoIIQ}$-yfp spc) ywjI::(P$_{spoIIQ}$-cfp erm) ΔminCD::cat*	This work. Transformation of DMR213 with DMR200
DMR218	*trpC2 spoIIIE36::zeo yycR::(P$_{spoIIQ}$-yfp spc) ywjI::(P$_{spoIIQ}$-cfp erm) minCD::(ΔminC minD$^+$ Ωcat)*	This work. Transformation of DMR213 with DMR203
DMR219	*trpC2 spoIIIE36::zeo soj(G12V)::neo yycR::(P$_{spoIIQ}$-yfp spc) ywjI::(P$_{spoIIQ}$-cfp erm) ΔminCD::cat*	This work. Transformation of DMR214 with DMR200
DMR220	*trpC2 spoIIIE36::zeo soj(G12V)::neo yycR::(P$_{spoIIQ}$-yfp spc) ywjI::(P$_{spoIIQ}$-cfp erm) minCD::(ΔminC minD$^+$ Ωcat)*	This work. Transformation of DMR214 with DMR203.
DMR221	*trpC2 spoIIIE36::zeo yycR::(P$_{spoIIQ}$-yfp spc) ywjI::(P$_{spoIIQ}$-cfp erm) ΔracA::tet*	This work. Transformation of DMR215 with DMR200

	ΔminCD::cat	
DMR222	*trpC2 spoIIIE36::zeo yycR::(P_spoIIQ-yfp spc) ywjI::(P_spoIIQ-cfp erm) ΔracA::tet minCD::(ΔminC minD⁺ Ωcat)*	This work. Transformation of DMR215 with DMR203
DMR223	*trpC2 spoIIIE36::zeo soj(G12V)::neo yycR::(P_spoIIQ-yfp spc) ywjI::(P_spoIIQ-cfp erm) ΔracA::tet ΔminCD::cat*	This work. Transformation of DMR216 with DMR200
DMR224	*trpC2 spoIIIE36::zeo soj(G12V)::neo yycR::(P_spoIIQ-yfp spc) ywjI::(P_spoIIQ-cfp erm) ΔracA::tet minCD::(ΔminC minD⁺ Ωcat)*	This work. Transformation of DMR216 with DMR203.
spoIIIE36	*trpC2 spoIIIE36*	(Wu & Errington, 1994)
TK244	*trpC2 spo0J(L5H) spoIIIE36::cat yycR::(P_spoIIQ-yfp spc) ywjI::(P_spoIIQ-cfp erm) Δsda::tet*	From Tomas Kloosterman
TK261	*trpC2 spoIIIE36::zeo*	Tomas Kloosterman, unpublished.
TK313	*trpC2 ΔminD::erm amyE::(P_comN-comN-gfp spc)*	Kloosterman et al., 2016
TK421	*trpC2 (soj(K16A) spo0J(L5H))::neo*	From Tomas Kloosterman, unpublished
TK422	*trpC2 (soj(G12V) spo0J(L5H))::neo*	From Tomas Kloosterman, unpublished
TK423	*trpC2 (soj(D40A) spo0J(L5H))::neo*	From Tomas Kloosterman, unpublished

Table 2.1 Strains used in this study

The compositions of various liquid growth media are shown in Table 2.2. Oxoid nutrient agar was used for growth and selection of *B. subtilis* and *E. coli* strains on plates. In all cases, antibiotics and/or other supplements were added as appropriate (see Table 2.3).

Media/Component	Composition
Solution A	0.098 % (w/v) $FeCl_3.6H_2O$ 0.83 % (w/v) $MgCl_2.6H_2O$ 1.979 % (w/v) $MnCl_2.4H_2O$
Solution B	5.35 % (w/v) NH_4Cl 1.06 % (w/v) Na_2SO_4 0.68 % (w/v) KH_2PO_4 0.97 % (w/v) NH_4NO_3
Solution C	5% (w/v) L-glutamate
Solution D	0.1 M $CaCl_2$
Solution E	40 % (w/v) glucose
Solution F	1 M $MgSO_4.7H_2O$
Solution G	1.06 % (w/v) Casein hydrolysate (Oxoid) 0.39 % (w/v) L-glutamic acid 0.13 % (w/v) L-alanine 0.147 % (w/v) L-asparagine 0.144 % (w/v) KH_2PO_4 0.011 % (w/v) Na_2SO_4 0.01 % (w/v) NH_4NO_3 0.057 % (w/v) NH_4Cl 1.04 mg/l $FeCl_3.6H_2O$ adjusted to pH 7.0. Solution G was autoclaved at 15 psi for 30 minutes
Solution H	35 % sodium lactate
Solution P	25 ml Solution F 5 ml Solution D 0.1 ml Solution H made up to 70 ml in deionised water
SMM salts	0.2 % (w/v) ammonium sulphate 1.4 % (w/v) dipotassium phosphate 0.6 % (w/v) potassium dihydrogen phosphate 0.1 % sodium citrate dehydrate 0.02 % (w/v) magnesium sulphate
SMM media	10 ml SMM salts 125 µl Solution E 100 µl Tryptophan 60 µl Solution F 10 µl Casamino acids 5 µl ferric ammonium citrate

SMM starvation media	10 ml SMM salts 125 µl Solution E 60 µl Solution F
LB media	10 g Tryptone 5 g Yeast Extract (Difco) 10 g NaCl Adjust to pH 7.0 (with NaOH) and make up to 1 L
CH media	100 ml Solution G 200 µl Solution H 100 µl Solution D 40 µl Solution F 1 ml Tryptophan
A+B sporulation salts	90 ml A+B media 4 ml Solution C 1 ml Solution D 4 ml Solution F 1 ml Tryptophan
PTM media	10 ml SMM salts (see above) 1% glucose 250 mM $MgSO_4$ 5 mM $CaCl_2$ 47 µM $MnSO_4$ 0.04% casamino acids 20 µg/ml tryptophan
TM media	10 ml SMM salts (see above) 0.6% glucose 20 mM $MgSO_4$ 0.001% CAA 20 µg/ml tryptophan

Table 2.2 Composition of media used in this study

Supplement	Final Concentration
Erythromycin	1 µg/ml
Lincomycin	25 µg/ml
Chloramphenicol	5 µg/ml
Spectinomycin	50 µg/ml
Tetracycline	6 µg/ml
Ampicillin	100 µg/ml
Kanamycin	5 µg/ml or 2 µg/ml
Zeocin	10 µg/ml
Phleomycin	0.8 µg/ml
5-bromo-4-chloro-3-indolyl-β-D-galactopyranoside (X-gal)	0.02% (w/v)
Isopropyl β-D-1-thiogalactopyranoside (IPTG)	1 mM
Xylose	1% (v/v)
Starch	1% (w/v)
Tryptophan	20 µg/ml

Table 2.3 List of media supplements

Liquid *B. subtilis* cultures were grown in either Luria-Bertani (LB) media (Table 2.2), SMM minimal media (Table 2.2), or rich CH media (as described by Nicholson & Setlow., 1990, modified by Partridge & Errington, 1993) (Table 2.2). All *B. subtilis* strains are derived from 168CA, and contained the *trpC2* mutation, so all cultures were supplemented with tryptophan (20 µg/ml) to permit growth. Unless stated otherwise, all transformations and cloning using *E. coli* was conducted using *dam-*methylase plus strain, DH5α. In all cases, antibiotics and/or other supplements were added as appropriate (see Table 2.3).

For the propagation and extraction of plasmids, *E. coli* colonies were cultured in appropriate volumes of LB media supplemented with 100 µg/ml ampicillin.

For long-term storage of all bacterial strains, 20% glycerol stocks of cultures were generated and stored at -80°C.

2.2 General Methods

2.2.1 Buffers and solutions

Table 2.4 lists the composition of solutions for many of the methods described, with the exception of those provided as part of commercial kits.

Solution	Final Concentration
DNA Loading Dye	50 % (v/v) glycerol + bromophenol blue crystals
DAPI	1 µg/ml (w/v) in deionised water
FM5-95	150 µg/ml (Invitrogen)
SSC	150 mM NaCl 10 mM Na$_3$-citrate pH 7.0
SSC-L	150 mM NaCl 10 mM Na$_3$-citrate 2 mg/ml lysozyme pH 7.0
SYBR Gold	SYBR Gold DNA Stain (Thermo Fisher) (use at 1:5000 dilution from stock)
TBE	90 mM Tris-borate, 2 mM EDTA, pH 8.0
10x T4 Ligase Buffer	300 mM Tris-HCl (pH 7.8) 100 mM MgCl$_2$ 100 mM DTT 10 mM ATP
Lysis buffer A	50 EDTA pH 8.0 300 µg/ml lysozyme (Sigma Aldrich) 300 µg/ml RNase (Thermo Fisher)
Western Blot Lysis buffer	50 mM Tris-HCl pH 8.0 1x NuPAGE Reducing Agent (Invitrogen)

	200 mM NaCl	
	5 mg/ml lyosozyme	
	10 mM $MgCl_2$	
	0.01% (w/v) Triton X-100	
	1x Roche EDTA-free protease inhibitor cocktail tablet	
UT Buffer	0.1M HEPES	
	0.5 M NaCl	
	50 mM imidazole	
	8 M urea	
	1 % Triton X-100	
	1 mM DTT	
	1x Roche EDTA-free protease inhibitor cocktail tablet	
	pH 7.5	
UT-EB	0.1 M Tris-HCl	
	0.5 M imidazole	
	1 % SDS	
	pH 7.5.	
Blotting Buffer B	0.5x MOPS (Life Technologies)	
	16% methanol	
Blocking Buffer	0.1% Tween	
	0.5x Marvel milk powder	
	in PBS	

Table 2.4 Composition of buffers and solutions

2.2.2 Synthesis of synthetic oligonucleotides

All oligonucleotides were designed using specific software (Clone Manager v8.0 or Primer3Plus) and ordered from Eurogentec (Belgium) as 100 µM pre-dissolved stocks in deionised water. Primer stocks were heat treated at 90°C for 10 min followed by cooling on ice for 15 min to prevent dimer formation, and were subsequently stored at -20°C. A full list of oligonucleotides used throughout this work is given in Table 2.5.

Name	Sequence (5 prime to 3 prime)	Comments
oDMR01	ATAGAATTCAGGTGAAGCTGTATTGGCTG	Binds 1Kb from end of SpoIIIE. Contains EcoR1 site and was for cloning with pMUTIN-His.
oDMR02	TTACTCGAGAGAAGAGAGCTCATCATATTT CTC	Binds at the end of SpoIIIE in frame with the last codon before stop to ensure that it is in frame with the His within the pMUTIN plasmid. Contains a BamH1 site for cloning.
oDMR129	ATAATTGCATGCTGGATAGGTTGTATATATT TTCAGAAAAGTGTTCAGAATGTTGCTGAGG GAGGGAGACGATTTTGATGAAGAAAAATCG CGCTTTTTTGAAGTGGGCAGGGGGCAAG	Binds at the start codon of the *dam* methylase of *E. coli*. Primer contains the P_{spoIIQ} promoter. Contains SphI site for cloning.
oDMR130	ATATTACTCGAGGTAATGCCATAGTTACGC AAGG	Binds after the stop codon of the *E. coli dam* methylase gene. Contains XhoI site for cloning.
oDMR176	ATAGCATGCATGGCCTTCTGCTTAGCTAGA GCG	To amplify the *amyE* and *spec* regions of pDR111 to reverse orient *dam*. Contains SphI site
oDMR177	ATTGTCGACCATTACCAGTTGGTCTGGTGT C	To amplify the *amyE* and *spec* regions of

		pDR111 to reverse orient *dam*. Contains SalI site.
oDMR178	GCAGGAATTCGACTCTCTAGC	Binds within pDR111 5' of MCS for sequencing of *dam* construct
oDMR179	TGACACCAGACCAACTGGTAATG	Binds within pDR111 3' of MCS for sequencing of *dam* construct
oDMR184	GTGTGGAATTGTGAGCGGATAAC	Binds 70bp upstream of the *lacZ* gene and MCS in pUC19 for cloning DpnI digested fragments
oDMR185	CATTAATGCAGCTGGCACGACAGG	Binds ~230 bp upstream of the *lacZ* gene and MCS in pUC19 for cloning DpnI digested fragments
oDMR194	TCAATTATTTCCCTTCTGATTCGG	Binds 200 bp 5' of *soj* for sequencing (G12V) and (K16A) region
oDMR195	TTCAGCTTGCAGGGGCTGAGATCG	Binds within *soj* to sequence the R189A mutation
oDMR196	GAAGGTGTATTGCTGACAATGC	Binds within *soj*, 200 bp 5' of *spo0J(L5H)* for sequencing.
oDMR197	AACCCGTTGCAAAGGCTCACTGGGC	Binds 3' of *spo0J* to amplify the operon

55

oDMR215	CGCAATACCACCTGGCCTGAGAAAGTGAT CGG	Primer to amplify upstream of *minC* to create a *minC* and *minCD* knockouts by 3-way PCR
oDMR218	CACAATTTGTCTACAGATTAATAATTATTCC TATCACATTAAGATCTTACTC	Primer to amplify end of *minC* and *minD* to generate a *minC* knockout by 3-way PCR
oDMR219	CATTTTTCGGAGTAAGATCTTAATGTGATAG GAATAATTATTAATCTGTAGAC	Binds within pAPNC::cat plasmid to amplify *cat* gene. Used to generate a *minC* knockout by 3-way PCR
oDMR220	AAAAAAACCTGACACAGCATATGCTTTGTC AGCTTATAAAGCCAGTCATTAGG	Binds within pAPNC::cat plasmid to amplify *cat* gene. Used in 3-way PCR knockouts of *minC* and *minCD*.
oDMR221	CAGATAGGCCTAATGACTGGCTTTTATAAG CTGACAAAGCATATGCTGTGTCAG	Generates downstream fragment for 3-way PCR knockouts of *minC* and *minCD*.
oDMR222	CATGGATATAGTGCCTTTGCCGATATTCC	Generates downstream fragment for 3-way PCR knockouts of *minC* and *minCD*.
oDMR223	CACAATTTGTCTACAGATTAATAATTATTCC TCAACAACATACTCATTTCGTC	Primer to knockout *minCD* by 3-way PCR

oDMR224	CTTTTTTTGACGAAATGAGTATGTTGTTGAG GAATAATTATTAATCTGTAGAC	Primer to knockout *minCD* by 3-way PCR
oDMR225	CCGCTTCTGTGGCGTTAATCG	Primer for fragment 1 in 3-way PCR to generate mNG-Soj constructs
oDMR227	CATATTATCCTCCTCTCCTTTCGAAACCATG ATGTCACCTACTTTCACATG	Primer for fragment 1 in 3-way PCR to generate mNG-Soj constructs
oDMR229	GTACATGTTCATGTGAAAGTAGGTGACATC ATGGTTTCGAAAGGAGAGGAG	Primer for fragment 2 in 3-way PCR to generate mNG-Soj constructs
oDMR231	GGTTCGTAATTGCTATGATTTTTCCCACCG TGGATCCTGAGCCGCTTCCTGA	Primer for fragment 2 in 3-way PCR to generate mNG-Soj constructs
oDMR232	TCAGGAAGCGGCTCAGGATCCACGGTGGG AAAAATCATAGCAATTAC	Primer for fragment 3 in 3-way PCR to generate mNG-Soj constructs
oDMR233	CTTGATCATGATCGAGGCAATGG	Primer for fragment 3 in 3-way PCR to generate mNG-Soj constructs

Table 2.5 List of oligonucleotides used in this study

2.2.3 Polymerase chain reaction

To amplify DNA fragments from genomic DNA or plasmid templates, a reaction mix containing 0.5 U/μl DNA polymerase (Q5, Pfu Turbo, Novogen Extreme Hot Start or Phire, as appropriate), 1x polymerase buffer as supplied with the polymerase, 200 μM of each dNTP (Promega/Novogen), 0.5 μM of each primer and 70-140 ng template DNA was prepared in a final volume of 100 μl.

Using a Techne PCR machine, a typical PCR reaction would include initial heat denaturation at 98^oC for 30 sec, followed by 35 cycles of: 98^oC for 10 sec (template denaturation), 55^oC for 10 sec (primer annealing), and 72^oC for 1 min per kb of DNA to amplify (primer extension). Following cycling, a final extension at 72^oC was conducted for 2 min. Following PCR, products would be cleaned using a Qiagen PCR Purification Kit and manufacturer's protocols.

2.2.4 Agarose gel electrophoresis

DNA samples were mixed with 1x loading dye (Table 2.4) and SYBR Gold DNA stain (ThermoFisher) (Table 2.4). To resolve the DNA fragments by size, samples were loaded into a 1-3% (as appropriate) agarose gel in a 1x TBE buffer (Table 2.4) and run at 120 V until samples had migrated through as appropriate. Following electrophoresis, DNA was visualised using a UV transluminator (Syngene). The sizes of DNA bands were approximated using 1 Kb or Quick-Load low molecular weight DNA ladders (NEB).

2.2.5 Site-directed mutagenesis

For the introduction of point mutations into Soj/Spo0J genes, primers were designed containing the appropriate point mutation. All site directed mutagenesis was conducted using the plasmid pAK82 as the starting template (Alan Koh and Heath Murray, unpublished), which contained the genetically linked s*oj-spo0J* genes and had been previously optimised for cloning through *E. coli* to reduce *soj*-mediated toxicity. The primer sequence corresponding to the point mutation was minimally changed to ensure the primers remained as homologous to the template strands as possible. The site-directed mutagenesis PCR reaction was carried out as outlined in

Table 2.6, typically starting with 50 ng/µl of DNA, mutagenic primers at a final concentration of 10 µM, 1 U of DNA polymerase (Novogen) and Novogen 2x reaction buffer:

Cycle stage	Temperature/Time	Number of cycles
Initial denaturation	94°C/2 min	-
Sample denaturation Primer annealing Primer extension	98°C/10 sec 55-65°C/30 sec 72°C/1 min per kbp	8 cycles
Sample denaturation Primer annealing Primer extension	98°C/10 sec 55-65°C/30 sec 68°C/1 min per kbp	8 cycles
Final extension	68°C/10 min	-

Table 2.6 PCR cycle for site directed mutagenesis

A temperature gradient of 55-65°C was used to permit optimum primer annealing temperatures during the PCR reaction. Since the starting plasmids were isolated from *E. coli* DH5α, following PCR 2 U *Dpn*I was added to the mixture to digest the methylated parental DNA template strands. Following PCR purification (Qiagen PCR purification kit following the manufacturer's protocol), *E. coli* cells were transformed with the modified circular plasmids, at which point any nicks in the mutated strands would be repaired (see 2.6.2).

2.2.6 Extraction of DNA from agarose gels

To extract specific DNA bands from agarose gels, the QIAquick Gel Extraction Kit (Qiagen) was used following the manufacturer's protocol.

2.2.7 Restriction-ligation cloning

DNA was restricted using Roche, Promega or NEB restriction endonucleases according to the manufacturer's guidelines and the buffer solutions provided. For

samples that required double digestion using enzymes with incompatible restriction buffers, digestions were conducted sequentially, with the low salt buffer digestion being carried out first before the salt concentration was adjusted for the second endonuclease. All samples for digestion were incubated at 37°C for at least 3 h (unless stated otherwise). Following restriction digestion, samples were cleaned using a Qiagen PCR purification kit following the manufacturer's protocol.

Following restriction-digestion of plasmids (prior to PCR clean up) and before DNA ligation, 1 U Calf Intestinal Phosphatase (CiP) (Promega) was added for 1 h at 37°C to minimise any self-ligation.

The ligation of restriction-digested, CiP treated plasmids and digested insert was performed by mixing 0.5 µl T4 DNA ligase (Promega), 1x (final) T4 ligase buffer (Table 2.4), ~50 ng digested plasmid, ~35 ng digested DNA insert, and made up to a final volume of 10 µl using deionised water. All ligations were conducted at 15°C overnight or for 1 h at room temperature.

2.2.8 Restriction-ligation free cloning

For the creation of plasmid constructs without the use of restriction enzymes or DNA ligation, a PCR-based approach was employed. Primers were designed to have a 20-30 bp region specific to both the insert and the plasmid/vector backbone at the desired integration site. In the first round, the primers were used to amplify the insert, creating a "megaprimer" of the insert with vector-compatible overhangs at the ends. Following this PCR, the product was gel extracted to ensure high purity (see 2.2.5). This "megaprimer" was then used to prime the second round of PCR. By using the vector as template and amplifying all the way around the backbone, this second PCR created a product that contained the insert within the vector. Typical PCR reactions are highlighted in Table 2.7.

Following the second round of PCR, the reaction mixture was incubated with 2 U *Dpn*I for 1 h at 37°C to digest the methylated parental starting DNA templates. The digest was subsequently cleaned using a Qiagen PCR purification kit following the manufacturer's recommended protocol. *E. coli* DH5α was then transformed with the recombinant plasmids (see 2.6.2).

Round 1: Creation of "Megaprimer"	Temperature/Time	Number of cycles
Initial denaturation	94°C/2 min	-
Sample denaturation Primer annealing Primer extension	98°C/10 sec Lowest primer Tm/30 sec 72°C/1 min per kbp	5 cycles
Sample denaturation Primer annealing Primer extension	98°C/10 sec Lowest primer Tm/30 sec 68°C/1 min per kbp	25 cycles
Final extension	68°C/10 min	-
Round 2: Creation of vector	Temperature/Time	Number of cycles
Initial denaturation	94°C/2 min	-
Sample denaturation Primer annealing Primer extension	98°C/10 sec 55-65°C gradient /30 sec 72°C/1 min per kbp	8 cycles
Sample denaturation Primer annealing Primer extension	98°C/10 sec 55-65°C gradient /30 sec 68°C/1 min per kbp	8 cycles
Final extension	68°C/10 min	-

Table 2.7 PCR protocol for restriction-ligation free cloning

2.2.9 Plasmids constructed and acquired

Plasmid	Genotype	Source/Construction
pMUTIN-His	*bla His*	Laboratory Stock
pDMR001	*bla 3'spoIIIE-His erm*	This work. *EcoR*I/*BamH*I double digested PCR of the final Kb of SpoIIIE (oDMR01-02) ligated with *EcoR*I/*BamH*I pMUTIN-His
pDMR002	*bla spc amyE::P$_{xyl}$*	Koh and Murray, 2014
pDR111	*bla amyE::P$_{hyspanc}$ spc*	Gifted to lab from David Rudner
pDMR011	*bla amyE::(P$_{spoIIQ}$-dam) spc*	This work. *Sph*I/*Xho*I double digested PCR of the *E. coli dam* using oDMR129-30 ligated to oDMR176-77 PCR and *Sph*I/*Xho*I double digested pDR111 (reverse orients *dam* in the plasmid).
pUC19	*bla MCS-lacZ*	NEB
pSG1728	*bla amyE::(P$_{xyl}$ spc)*	Marston & Lewis, 1999.
pNS056	*bla pelB::(P$_{spoIIQ}$-cfp kan)*	Sullivan *et al.*, 2009
pDMR015	*bla lacZ::(dam fragment 01)*	*Dpn*I digested chDNA from strain DMR056 at T$_3$ of sporulation ligated with phosphatase treated *Sma*I cut pUC19
pDMR016	*bla lacZ::(dam fragment 02)*	*Dpn*I digested chDNA from strain DMR056 at T$_3$ of sporulation ligated with phosphatase treated *Sma*I cut pUC19
pDMR017	*bla lacZ::(dam fragment 03)*	*Dpn*I digested chDNA from strain DMR056 at T$_3$ of sporulation ligated with phosphatase treated *Sma*I cut pUC19
pDMR018	*bla lacZ::(dam fragment 04)*	*Dpn*I digested chDNA from strain DMR056 at T$_3$ of sporulation ligated with phosphatase treated *Sma*I cut pUC19
pDMR019	*bla lacZ::(dam fragment 05)*	*Dpn*I digested chDNA from strain DMR056 at T$_3$ of sporulation ligated with phosphatase treated *Sma*I cut pUC19
pDMR020	*bla lacZ::(dam fragment 06)*	*Dpn*I digested chDNA from strain

		DMR056 at T_3 of sporulation ligated with phosphatase treated *Sma*I cut pUC19
pDMR021	*bla lacZ::(dam fragment 07)*	*Dpn*I digested chDNA from strain DMR056 at T_3 of sporulation ligated with phosphatase treated *Sma*I cut pUC19
pDMR022	*bla lacZ::(dam fragment 08)*	*Dpn*I digested chDNA from strain DMR056 at T_3 of sporulation ligated with phosphatase treated *Sma*I cut pUC19
pDMR023	*bla lacZ::(dam fragment 09)*	*Dpn*I digested chDNA from strain DMR056 at T_3 of sporulation ligated with phosphatase treated *Sma*I cut pUC19
pDMR024	*bla lacZ::(dam fragment 10)*	*Dpn*I digested chDNA from strain DMR056 at T_3 of sporulation ligated with phosphatase treated *Sma*I cut pUC19
pDMR025	*bla lacZ::(dam fragment blue)*	*Dpn*I digested chDNA from strain DMR056 at T_3 of sporulation ligated with phosphatase treated *Sma*I cut pUC19
pDMR027	*bla lacZ::(dam fragment 11)*	*Dpn*I digested chDNA from strain DMR056 at T_3 of sporulation ligated with phosphatase treated *Sma*I cut pUC19
pDMR028	*bla lacZ::(dam fragment 12)*	*Dpn*I digested chDNA from strain DMR056 at T_3 of sporulation ligated with phosphatase treated *Sma*I cut pUC19
pDMR029	*bla lacZ::(dam fragment 13)*	*Dpn*I digested chDNA from strain DMR056 at T_3 of sporulation ligated with phosphatase treated *Sma*I cut pUC19
pDMR030	*bla lacZ::(dam fragment 14)*	*Dpn*I digested chDNA from strain DMR056 at T_3 of sporulation ligated with phosphatase treated *Sma*I cut pUC19
pDMR031	*bla lacZ::(dam fragment 15)*	*Dpn*I digested chDNA from strain DMR056 at T_3 of sporulation ligated with phosphatase treated *Sma*I cut pUC19
pDMR032	*bla lacZ::(dam fragment blue 02)*	*Dpn*I digested chDNA from strain DMR056 at T_3 of sporulation ligated with

		phosphatase treated *Sma*I cut pUC19
pDMR033	*bla lacZ::(dam fragment 16)*	*Dpn*I digested chDNA from strain DMR056 at T_3 of sporulation ligated with phosphatase treated *Sma*I cut pUC19
pDMR034	*bla lacZ::(dam fragment 17)*	*Dpn*I digested chDNA from strain DMR056 at T_3 of sporulation ligated with phosphatase treated *Sma*I cut pUC19
pDMR035	*bla lacZ::(dam fragment 18)*	*Dpn*I digested chDNA from strain DMR056 at T_3 of sporulation ligated with phosphatase treated *Sma*I cut pUC19
pDMR036	*bla lacZ::(dam fragment 19)*	*Dpn*I digested chDNA from strain DMR056 at T_3 of sporulation ligated with phosphatase treated *Sma*I cut pUC19
pDMR037	*bla lacZ::(dam fragment 20)*	*Dpn*I digested chDNA from strain DMR056 at T_3 of sporulation ligated with phosphatase treated *Sma*I cut pUC19
pDMR038	*bla lacZ::(dam fragment blue 03)*	*Dpn*I digested chDNA from strain DMR056 at T_3 of sporulation ligated with phosphatase treated *Sma*I cut pUC19
pDMR039	*bla lacZ::(MCS)*	*Sma*I digested, phosphatase treated pUC19 plasmid re-ligated overnight. White colony 1
pDMR040	*bla lacZ::(MCS)*	*Sma*I digested, phosphatase treated pUC19 plasmid re-ligated overnight. White colony 2
pDMR041	*bla lacZ::(MCS)*	*Sma*I digested, phosphatase treated pUC19 plasmid re-ligated overnight. Blue colony.
pDMR042	*bla lacZ::(MCS)*	Non-digested chDNA from DMR056 at T_3 sporulation ligated with *Sma*I cut CiP treated pUC19. White colony 1
pDMR043	*bla lacZ::(MCS)*	Non-digested chDNA from DMR056 at T_3 sporulation ligated with *Sma*I cut CiP treated pUC19. White colony 2

pDMR044	*bla lacZ::(MCS)*	Non-digested chDNA from DMR056 at T_3 sporulation ligated with *Sma*I cut CiP treated pUC19. Blue colony 1
pDMR045	*bla lacZ::(dam fragment 21)*	*Dpn*I digested chDNA from strain DMR056 at T_3 of sporulation ligated with phosphatase treated *Sma*I cut pUC19
pDMR046	*bla lacZ::(dam fragment 22)*	*Dpn*I digested chDNA from strain DMR056 at T_3 of sporulation ligated with phosphatase treated *Sma*I cut pUC19
pDMR047	*bla lacZ::(dam fragment 23)*	*Dpn*I digested chDNA from strain DMR056 at T_3 of sporulation ligated with phosphatase treated *Sma*I cut pUC19
pDMR048	*bla lacZ::(dam fragment 24)*	*Dpn*I digested chDNA from strain DMR056 at T_3 of sporulation ligated with phosphatase treated *Sma*I cut pUC19
pDMR049	*bla lacZ::(dam fragment 25)*	*Sma*I digested, phosphatase treated pUC19 plasmid re-ligated overnight. Blue colony.
pDMR050	*bla lacZ::(dam fragment 26)*	*Dpn*I digested chDNA from strain DMR056 at T_3 of sporulation ligated with phosphatase treated *Sma*I cut pUC19
pDMR051	*bla lacZ::(dam fragment 27)*	*Dpn*I digested chDNA from strain DMR056 at T_3 of sporulation ligated with phosphatase treated *Sma*I cut pUC19
pDMR052	*bla lacZ::(dam fragment 28)*	*Sma*I digested, phosphatase treated pUC19 plasmid re-ligated overnight. Blue colony.
pDMR053	*bla lacZ::(dam fragment 29)*	*Sma*I digested, phosphatase treated pUC19 plasmid re-ligated overnight. Blue colony.
pDMR054	*bla lacZ::(dam fragment 30)*	*Sma*I digested, phosphatase treated pUC19 plasmid re-ligated overnight. Blue colony.
pDMR055	*bla lacZ::(dam fragment 31)*	*Dpn*I digested chDNA from strain

		DMR056 at T_3 of sporulation ligated with phosphatase treated *Sma*I cut pUC19
pDMR056	*bla lacZ::(dam fragment 32)*	*Dpn*I digested chDNA from strain DMR056 at T_3 of sporulation ligated with phosphatase treated *Sma*I cut pUC19
pDMR057	*bla lacZ::(dam fragment 33)*	*Dpn*I digested chDNA from strain DMR056 at T_3 of sporulation ligated with phosphatase treated *Sma*I cut pUC19
pDMR058	*bla lacZ::(dam fragment 34)*	*Sma*I digested, phosphatase treated pUC19 plasmid re-ligated overnight. Blue colony.
pDMR059	*bla lacZ::(dam fragment 35)*	*Dpn*I digested chDNA from strain DMR056 at T_3 of sporulation ligated with phosphatase treated *Sma*I cut pUC19
pDMR060	*bla lacZ::(dam fragment 36)*	*Dpn*I digested chDNA from strain DMR056 at T_3 of sporulation ligated with phosphatase treated *Sma*I cut pUC19
pDMR061	*bla lacZ::(dam fragment 37)*	*Dpn*I digested chDNA from strain DMR056 at T_3 of sporulation ligated with phosphatase treated *Sma*I cut pUC19
pDMR062	*bla lacZ::(dam fragment 38)*	*Dpn*I digested chDNA from strain DMR056 at T_3 of sporulation ligated with phosphatase treated *Sma*I cut pUC19
pDMR063	*bla lacZ::(dam fragment 39)*	*Dpn*I digested chDNA from strain DMR056 at T_3 of sporulation ligated with phosphatase treated *Sma*I cut pUC19
pDMR064	*bla lacZ::(dam fragment 40)*	*Dpn*I digested chDNA from strain DMR056 at T_3 of sporulation ligated with phosphatase treated *Sma*I cut pUC19

Table 2.8 Plasmids used in this study.

2.3 Transformation of *B. subtilis*

2.3.1. Standard transformation

Single colonies of *B. subtilis* were inoculated into SMM medium (Table 2.2) and incubated at 37^oC overnight. Cultures were then diluted 20x into 10 ml fresh SMM media and grown at 37^oC for 3 h before adding 10 ml SMM starvation medium (Table 2) and incubating at 37^oC for a further 2 h to allow *B. subtilis* to become competent. An appropriate amount (~50-500 ng) of DNA was added to 400 μl cells prior to incubation at 37^oC for 40 min and plating onto selective nutrient agar plates.

2.3.2. Pretransformation medium/transformation medium (PTM/TM) method

Occasionally, transformation was conducted by the PTM/TM method using a culture of *B. subtilis* cells from a fresh plate. In this case, *B. subtilis* was heavily inoculated into 5 ml pre-transformation medium (PTM) (Table 2.2). Cultures were grown at 37^oC until stationary phase was reached (OD_{600} ~3.0), and cells were competent. 100 μl culture was mixed with 1 ml transformation media (TM) (Table 2.2) and up to 1 μg/ml DNA. The mixture was then incubated at 37^oC for 1 h to allow DNA uptake prior to serial dilution and plating on selective agar.

2.4 *B. subtilis* DNA manipulations

2.4.1. Chromosomal DNA extraction

For cloning, PCR, sequencing and cell transformation, a clean preparation of DNA was extracted from *B. subtilis* using a Promega Wizard purification kit. Briefly, colonies of *B. subtilis* were grown in 5 ml LB media (Table 2.2) to an OD_{600} of 3.0. Cells were harvested by centrifugation (Hettich Universal 320) at 9000 rpm for 3 min and re-suspended in 100 μl lysis buffer A (Table 2.4) followed by incubation at 37^oC with 850 rpm shaking (Eppendorf Thermomixer Compact) for 35 min. 500 μl Nuclei Lysis Solution (Promega) was then added to lysates, followed by heating at 85^oC for 5 min. Once samples had cooled to room temperature, 200 μl Protein Precipitation Solution (Promega) was added prior to vigorous vortexing for 20 sec and then

incubation on ice for 10 min. Proteins were removed by centrifugation at 13,000 rpm for 10 min in a benchtop centrifuge (Thermo) and DNA then precipitated from the cleared supernatants by adding an equal volume of isopropanol followed by a 70% ethanol wash. Harvested DNA was dissolved in Qiagen EB buffer or sterile nuclease-free water.

2.4.2. Chromosomal DNA extraction (Quick prep)

For transformation of *B. subtilis*, DNA was occasionally prepared using a quick method. Using a freshly grown plate to minimise any possible contamination with spores, a 5 ml culture of bacteria was inoculated and grown in LB medium for 3 h at 37°C or until a thick broth was generated to ensure adequate concentration of DNA following extraction. Following growth, 2.5 ml SSC (Table 2.4) was added to cells collected by centrifugation for 4 min at 5000 rpm (Hettich Universal 320). Pellets were re-suspended in 1 ml SSC-L (Table 2.4) and cells lysed by incubation at 37°C for 20 min. 1 ml 4 M NaCl was added to lysates, prior to sterile filtration through a 0.45 μm filter. The resulting flow-through containing chromosomal DNA was stored at -20°C. For transformation, a serial dilution of DNA was added to cells prior to plating on selective nutrient agar.

2.4.3 Nanodrop and qPCR quantitation of DNA

DNA concentration and purity analysis was conducted using the Nanodrop spectrophotometer (Thermo Fisher). Typically 1 μl DNA was loaded onto the machine, and readouts were given as ng/μl. Optimum purity was determined as a 260/280 of 1.8, and a 260/230 of 2.0.

qPCR was conducted to assess the relative difference in DNA at the origin verses the terminus following chromatin affinity purification. For the origin, primers were designed in the intragenic region between *dnaA* and *dnaN*. For the terminus, primers were designed within *yocG*. The DNA and primers were mixed with Rotor-Gene SYBR green reaction mix (Qiagen) for the PCR reaction. All qPCR was conducted in a Rotor-Gene Q machine (Qiagen). Using the C_T values generated during qPCR, and taking into account the relative dilution factors, % IP values were calculated.

2.4.5 DNA sequencing and PacBio SMRT methylation sequencing

For conventional sequencing to confirm the correct construction of a deletion or point mutation, samples were sequenced commercially by the University of Dundee DNA Sequencing Service using a primer based sequencing approach. Samples were sent in a total volume of 30 µl using sterile deionised water, which contained 3.2 pmole of sequencing primer, and 500 ng primer or 50-100 ng purified PCR product to be sequenced.

For PacBio SMRT sequencing, samples were submitted to the University of Maryland DNA sequencing facility using the supplied pre-submission guidelines. DNA samples were purified using the Promega Wizard protocol (2.4.1), but additional wash steps were included to ensure greater sample purity, as recommended.

2.5. Sporulation of *B. subtilis*

2.5.1. Sporulation re-suspension method

Single colonies were inoculated into 3 ml hydrolysed casein (CH) medium (as described by Wu & Errington, 1998) (Table 2.2) and grown overnight at 30°C with shaking. To avoid overgrowth, a series of 1:10 serial dilutions were made. Overnight cultures (OD_{600}=1.0-2.0) were diluted to OD_{600}=0.1 in 10 ml fresh CH medium and incubated at 37°C with shaking. Upon OD_{600}=0.7-0.8, cultures were centrifuged in a Hettich Universal 320 at 9000 rpm for 3 mins prior to re-suspension in the pre-centrifugation volume (10 ml) of A+B sporulation salts (Table 2.2). This marked T_{0h} of sporulation. Cultures were then sporulated for various lengths of time prior to analysis (see individual Figures for details).

2.5.2. Determining sporulation efficiency

To determine sporulation efficiencies, cultures of *B. subtilis* were re-suspended in A+B sporulation salts (see 2.5.1). Following sporulation for 9 hours at 37°C, cultures were split and incubated +/- 95°C for 15 min. Heating does not affect spores, whereas all non-sporulating cells are killed. Following serial dilution, both

heated and non-heated cells were plated on nutrient agar. The sporulation efficiency was then determined as the fraction of colonies on heated versus non-heated plates per ml of starting culture.

For mutants that display significant lysis during ongoing sporulation (e.g. *minD*, *comN*), which would artificially increase the sporulation efficiency at T_{9h}, an aliquot of culture was spotted onto a 1.2% agar pad and imaged by microscopy at either T_{5h} or T_{6h}, at which point phase-bright spores would have developed inside the mother cell. The sporulation efficiency was then determined as the percentage of cells containing an internal phase-bright spore. At least 500 cells per sample were counted.

2.6 *E. coli* methods

2.6.1. Preparation of competent *E. coli*

To prepare competent cells of *E. coli*, a single colony from a fresh plate was inoculated into 5 ml LB (Table 2.2) medium and grown for 3 h at 37°C. The culture was then diluted into 100 ml LB medium and grown until OD_{600}=0.6. Cells were incubated on ice for 15 min prior to centrifugation at 4000 rpm (Hettich Universal 320) for 7 min at 4°C. Pellets were re-suspended gently into 0.1 M $CaCl_2$ and incubated on ice for a further 15 min. Following a second centrifugation (4000 rpm for 7 min at 4°C), cell pellets were gently re-suspended in 0.1 M $CaCl_2$/15 % glycerol. Stocks were aliquoted into Eppendorf tubes, incubated on ice for 1 h and frozen at -80°C until use.

2.6.2. Transformation of *E. coli*

Competent cells were thawed on ice and once defrosted, were gently mixed with DNA and incubated on ice for 1 h before being subjected to heat-shock at 42°C for 2 min and incubation on ice for 90 sec. Finally, 3.5x volume of LB medium was added and mixtures incubated at 37°C for 40 min before being plated on selective nutrient agar.

2.6.3. Plasmid isolation from *E. coli*

Plasmids were isolated using the Qiagen Miniprep kit following manufacturer's guidelines.

2.7 Protein methods

2.7.1. SDS-Polyacrylamide gel electrophoresis (SDS-PAGE)

For the examination of cellular proteins, in general, overnight cultures of cells were diluted to OD_{600}=0.1 and allowed to grow until OD_{600}=0.5-1.0. For sporulation experiments, cells were allowed to sporulate until an appropriate time point (see 2.5.1 and individual Figures for details). Cells were harvested and lysed using either lysozyme (300 µg/ml final) or sonication (400 A for 10 sec intervals) following re-suspension into Western blotting lysis buffer (Table 2.4). Following removal of cell debris by centrifugation, lysates were incubated with LDS-loading dye (Invitrogen) and 50 mM DTT at 65°C (or temperatures indicated) for 5 min to reduce disulphide bonds. Samples were loaded into NuPAGE 4-12% Bis-Tris gels (Invitrogen) in 1x MOPS buffer (Invitrogen) and separated at 150-180 V. Gels were then either subjected to Western blotting (2.7.3) or were silver stained (2.7.4).

2.7.2. Chromatin affinity purification (ChAP) of His-tagged proteins

10 ml *B. subtilis* cultures were grown in CH sporulation medium overnight at 30°C and then diluted to OD_{600}=0.1 in 200 ml CH media (Table 2.2) and grown at 37°C until OD_{600}=0.75. Following centrifugation using a Beckman Coulter Avanti J-26 XP centrifuge and a JSP F500 rotor, pellets were re-suspended in 200 ml A+B sporulation salts (Table 2.2). At this point, 100 ml cells were removed as the T_{0h} samples, and cross-linked with formaldehyde (Sigma) (1% final) at room temperature for 5 min. To quench the formaldehyde, glycine (150 mM final) was added prior to centrifugation. The harvested cells were rapidly frozen in liquid nitrogen and stored at -80°C. Remaining cells were allowed to sporulate to specific time-points (see Results) prior to crosslinking, quenching and cell harvesting (as above).

All cell pellets were lysed together by resuspension in 1 ml UT buffer (Table 2.4) and sonication on ice. Lysis was monitored by microscopy. Cell debris was

removed by centrifugation at 6000 rpm (Hettich Universal 320) for 20 min. Following removal of a 200 µl sample as the input control, samples were mixed with 50 µl MagneHis beads (Promega) and mixed (head-over-tail) overnight at 4°C. Beads (potentially containing the His-tagged protein-DNA complex) were pelleted using a magnetic rack, the supernatant was removed and beads samples re-suspended into UT buffer. This wash procedure was repeated up to seven times. His-tagged protein-DNA complexes were then eluted from the beads using UT-EB (Table 2.4). Eluted samples were then reverse cross-linked by heating (either 65°C overnight or 90°C for 1 h, see Results for details) and analysed (see individual results for details).

2.7.3. Western blotting

Following separation by SDS-PAGE (see 2.7.1), proteins were transferred to Hybond-P PVDF membranes (GE Healthcare, activated using 100% methanol) using semi-dry transfer (Hoefer Scientific Instruments) with Blotting buffer B (Table 2.4) at 75 mA for 1 h. Following transfer, membranes were immersed in blocking buffer (Table 2.4) to prevent the non-specific binding of proteins to the membrane for 1 h at room temperature or overnight at 4°C. Membranes were probed with primary antibodies against the protein of interest (see Figures for dilutions) in blocking buffer for 1.5 h. The membrane was washed 3x 15 min in PBS-T (0.1% Tween in PBS) followed by incubation in blocking buffer containing an appropriate concentration of horseradish peroxidase-linked secondary antibody (see Results for details). Membrane was again washed 3x 15 min in PBS-T, rinsed with Pierce ECL Plus Western Blotting Substrate chemiluminescence substrate (ThermoFisher) and the specific protein band visualised using the ImageQuant LAS digital imaging equipment (GE-Healthcare).

2.7.4 Silver Staining

Silver staining was conducted using the Silver Stain Plus kit (Bio-Rad) following manufacturers protocols.

2.8 Microscopy

2.8.1. General Microscopy

B. subtilis cells were visualised during a variety of growth conditions (see main text and Figures for details). In general, vegetative cells were imaged following a 1:100 dilution of overnight cultures and at least 2 cell doublings at 37^oC. Sporulating cultures were imaged at appropriate time's post-re-suspension in sporulation salts (see 2.5.1 and Figures for details). 0.5 µl of cells were spotted onto 1.2 % agarose slides and a 0.13-0.17 mm coverslip (VWR) was applied. Membranes were visualised by the addition of 0.5 µg/ml FM5-95 (Molecular Probes) to the agarose pad. Nucleoids were stained using DAPI (16 µg/ml). All images were captured using a Nikon Ti equipped with a Nikon Plan Apo 100x/1.40 Oil objective. The filters used were Modified Magnetron ET sets (Chroma). Images were acquired using Metamorph or FRAP-AI (Molecular Devices) and analysed using ImageJ (NIH, http://rsb.info.nih.gov/ij).

For GFP-MinD and mCherry-ComN co-localisation experiments, cells were immobilised on 1.5 % agarose slides prior to visualisation on a Nikon Eclipse Ti microscope fitted with a Nikon CFP APO TIRF x100/1.49 oil objective and 488 nm and 561 nm lasers, as well as an Andor Xion X3 EMCCD camera (Kloosterman et al., 2016). Images were captured using Nikon NIS elements 4.0.

2.8.2. CellASIC ONIX time-lapse microfluidic imaging

To gain an insight into origin dynamics in a variety of origin segregation and/or capture mutants, a microfluidics time-lapse approach was employed using the CellASIC ONIX system (Merck Millipore). There are three main advantages to this system. Firstly, cells are trapped in the chamber based upon their width, which ensures that the cells reside in one plane, minimising any potential out of focus drifting throughout the experiment. Secondly, the constant perfusion of the sample with up to five independent media wells allows rapid media switching (for example, addition of an inducer or compound), where appropriate. Finally, up to four chambers containing different cell samples can be imaged simultaneously. This allows a variety of mutants to be tested together in otherwise identical conditions.

However, the media and flow rates had to be optimised for sporulation. This is because when sporulation is conducted in a flask, traces of the rich growth medium are retained upon re-suspension of the cells in sporulation salts. These traces of nutrients were found to be important to promote sporulation, likely by preventing the rapid de-energisationof the cells (possibly via the loss of membrane potential) if no rich media was present (Ling Juan Wu and Henrik Strahl, personal communications), which prevents growth and sporulation. Using the constant perfusion of media in the ONIX system at the required flow rate for *B. subtilis*, any rich media traces would be lost in less than 5 mins. To overcome this, the A+B sporulation salts were supplemented with CH, which was then phased out over time as the cells entered sporulation. After trialling many combinations of media (see Chapter 4 for details), the optimised condition was found to be A+B sporulation salts supplemented with 0.57 % CH media for the first 1 h in the ONIX plate, prior to long term perfusion with pure A+B sporulation media.

Cells were imaged in B04A microfluidic plates (ONIX, CellASIC). Cells were grown overnight in either LB (for vegetative experiments) or CH (for sporulation experiments) media at 30°C. The following morning, cultures were diluted to OD_{600}=0.1 and grown at 37°C in flasks until OD_{600}=0.4-0.7. For sporulation experiments, cells were re-suspended in sporulation salts (see 2.5.1) and grown for a further 10 mins- 1 h (see Figures for details) at 30°C.

Cells were loaded into microfluidic chambers at 4 psi for 15 sec. The loading channel was then washed for 30 sec at 3 psi. Media supply was maintained at 2 psi and the temperature maintained at 32°C for growth and sporulation in the chamber. Images were captured every 1-5 mins (see Figures for details) using a Nikon Ti microscope equipped with a Nikon Plan Apo x100/1.40 oil objective and FRAP-AI software (Molecular Devices). Images were processed using ImageJ (NIH).

2.8.3 Polydopamine coating of coverslips

To minimise the binding of the hydrophobic FM5-95 membrane dye to the plastic coverslip causing high background signal, coverslips were coated with hydrophilic polydopamine. In general, coverslips were prepared as described in (Te Winkel *et al.*, 2016). In brief, a large droplet of polydopamine solution (2 mg/ml

polydopamine in 5 mM Tris-HCl, pH 8.5) was added to the central two thirds of a coverslip and incubated for 30 min at room temperature. Following aspiration of excess polydopamine solution, samples were rinsed in de-ionised water and dried at 37°C in a dust-free dish for a further 30 min. Coated coverslips were incubated in a cool, dry and dark environment until use.

2.8.4 Origin trapping assay

To study the ability for cells to trap the arm or origin regions of the chromosome, strains harbouring copies of *cfp* and *yfp* under the control of the P_{spoIIQ} promoter were used. Strains under investigation (containing the fluorescent proteins, *spoIIIE36* and the chromosome trapping mutation under investigation, see individual Results for details) were induced to sporulate using the re-suspension method (Section 2.5.1) for 4 hours. Following this, 0.5 µl of cells was spotted onto a microscope slide containing a 1.5 % agarose pad and a 0.13-0.17 mm coverslip (VWR) was applied. Membranes were visualised by adding 0.5 µg/ml of FM5-95 membrane dye (Molecular Probes) to the molten agarose. Cells were then imaged using a Nikon Ti microscope fitted with a Nikon Plan Apo x100/1.40 Ph3 Oil objective. Using Metamorph (Molecular Devices), the following wavelengths were captured: Brightfield (100 ms exposure), cfp (narrow wavelength, 1000 ms exposure), yfp (1000 ms exposure) and mCherry (500 ms exposure). Using ImageJ (NIH), cells were scored as containing either Cfp and Yfp expression, only Cfp expression, only Yfp expression, or no fluorescent signal expression in prespores. To avoid bias, cells for analysis were initially selected based upon the presence of asymmetric septa only (all other signals turned off in Metamorph during this process).

Chapter 3

Identifying the region of the prespore chromosome that is bisected following asymmetric cell division during sporulation

3.1 Introduction

Increasing evidence suggests that the orientation and organisation of chromosomes within bacteria are important for efficient DNA segregation (Chapter 1.4). However, many details pertaining to the underlying mechanisms, particularly during sporulation, remain unclear. Sporulation is a characteristic feature of *B. subtilis* in which, following the completion of DNA replication, chromosomes re-organise into an axial filament structure that is anchored at both cell poles (Bylund *et al.*, 1993; Ben-Yehuda *et al.*, 2003b; Wu and Errington, 2003) and the usually mid-cell divisome re-locates to a highly asymmetric site (Lewis *et al.*, 1994; Levin and Losick, 1996; Ben-Yehuda and Losick, 2002). It follows that the chromosome destined for the smaller prespore compartment becomes bisected by the division septum. Studies have revealed that the intersection is not random but converges on a region of the chromosome ~500-700Kb from o*riC* (Wu *et al.*, 1995; Wu and Errington, 1998). A hexameric membrane protein called SpoIIIE functions as a DNA translocase at the leading edge of the constricting septum to pump the trapped chromosome into the prespore (Wu and Errington, 1994; Wu and Errington, 1998; Massey *et al.*, 2006).

A mutant of the translocase (called SpoIIIE36, which carries a V429M mutation) is able to bind DNA normally, allowing the subsequent normal activation of prespore and mother cell specific sigma-factors, but SpoIIIE36 cannot translocate the bound DNA into the prespore (Wu and Errington, 1994; Besprozvannaya *et al.*, 2014). As such, SpoIIIE36 can be used to trap the bisected chromosome and has been used over time to identify a range of chromosome organisation mutants (*minD, divIVA, comN, soj, spo0J*) (Ireton *et al.*, 1994; Errington *et al.*, 2005; Kloosterman *et al.*, 2016). A key advantage of using SpoIIIE36 is it fixes the DNA at the point of septation. This means that in a given space of time, each prespore-segregating

chromosome becomes trapped at exactly the same point to generate what is essentially a synchronised population for this event.

The aims of this chapter were to:

1. Physically isolate cross-linked SpoIIIE36-DNA complexes and to develop a chromatin affinity purification-sequencing (ChAP-Seq) assay to sequence the co-purifying DNA. The ultimate goal was to identify sequences at the boundary between the mother cell and prespore.
2. Initiate a novel DNA methylation-based approach for the same ultimate goal. In theory, by specifically expressing *E. coli* deoxyadenosine methylase (Dam) in the prespore during sporulation, only the DNA located there would become methylated at GATC sequences. Sequencing of methylated (as opposed to non-methylated) fragments of DNA should therefore reveal the prespore content only.

For both, the initial aim was to validate the novel methodology using cells carrying just the SpoIIIE36 translocase. It should then be possible to extend the most successful approach to strains carrying mutations in genes causing various chromosome organisation defects.

3.2 Results

3.2.1 Generating a His-tagged SpoIIIE and SpoIIIE36

To isolate chromosomal DNA in the vicinity of the SpoIIIE translocase, a multiple (6x) histidine (His) tag was added to SpoIIIE and SpoIIIE36 (hereafter SpoIIIE/36) at the C-terminal end. When expressed and cross-linked to DNA, the His-tag should allow purification by chromatin affinity purification (ChAP) using nickel (Ni)-coated magnetic beads. Samples could then be prepared for sequence analysis of the linked DNA following a work scheme that is summarised in Figure 3.1.
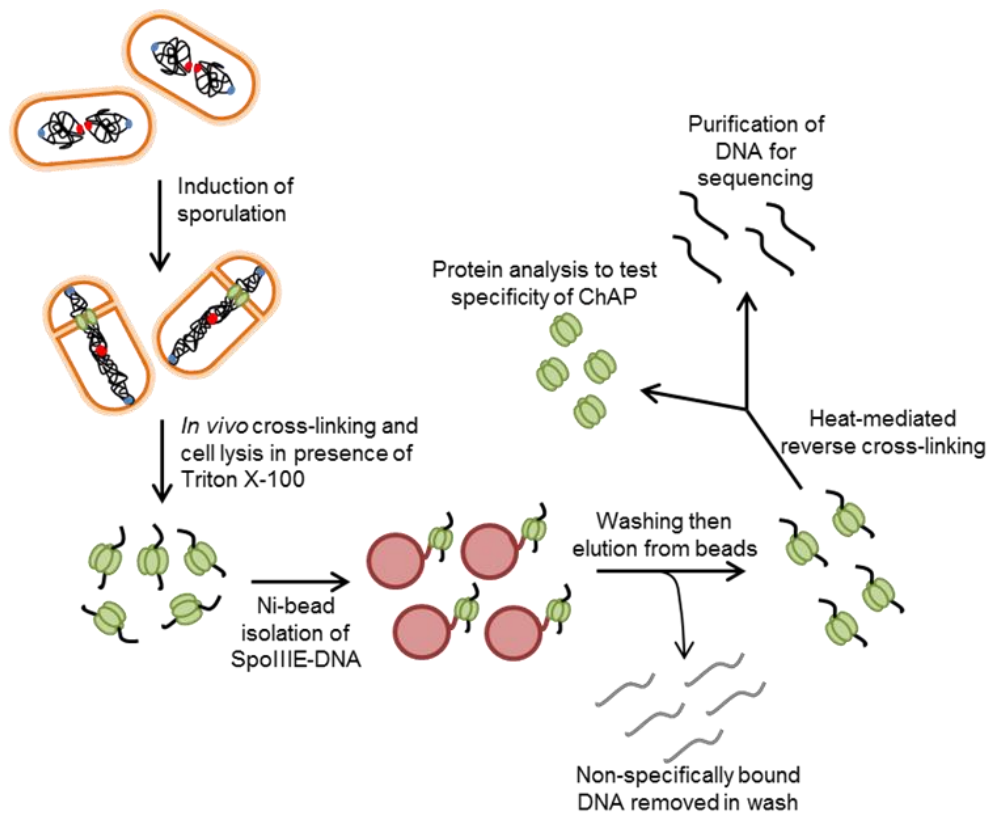
Figure 3.1. General workflow for isolating DNA in the vicinity of the asymmetric septum during sporulation

Black lines = chromosomal DNA; Green = SpoIIIE36-His; Dark red circles = Ni-beads; Grey lines = non-specific DNA.

SpoIIIE/36 proteins were expressed with a 6x histidine (His)-tag at their C-termini. The C-terminus was chosen in preference to the N-terminus where it might have interfered with the four N-terminal transmembrane spans (Besprozvannaya *et al.*, 2014). The presence of expressed His-tagged SpoIIIE (IIIE-H) and His-tagged SpoIIIE36 (IIIE36-H) was verified by the presence of expected sized bands in Western blotting using antiserum against both SpoIIIE and His (Figure 3.2) and DNA sequencing. The His tag did not appear to abolish the function of SpoIIIE, as demonstrated by the abundant spores visible for the SpoIIIE-H expressing strain in samples taken 9 h after induction of sporulation by the re-suspension method (Sterlini and Mandelstam, 1969) (data not shown).
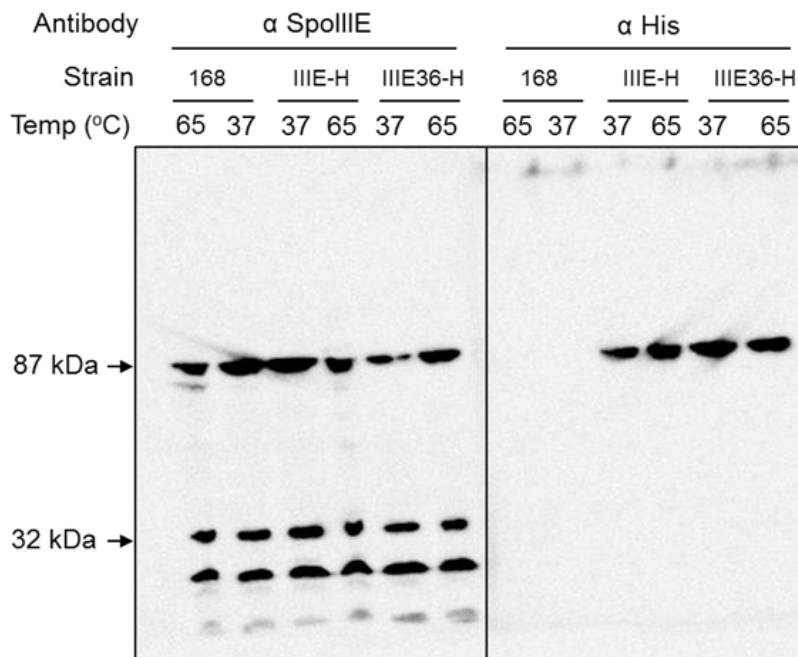
Figure 3.2 Detection of SpoIIIE and SpoIIIE36 +/- the His-tag.
Western blot of non-crosslinked lysate samples of vegetative cells probed with anti-SpoIIIE antiserum (left panel, 1:6667 dilution) or anti-His antibodies (right panel, 1:2000 dilution) following SDS-PAGE. - tag = untagged control; IIIE-H = SpoIIIE-His; IIIE36-H = SpoIIIE36-His. Temp refers to the 10 min heat denaturation condition used in sample preparation for SDS-PAGE. Number on left = molecular mass of full length SpoIIIE, based on gel size markers. – tag = 168CA; IIIE-H = DMR004; IIIE36-H = DMR006.

3.2.2 Isolation of non-crosslinked SpoIIIE from Ni-beads

It was important to demonstrate that SpoIIIE/36-His could be isolated and detected in whole cell lysates using nickel (Ni)-bead affinity chromatography (under denaturing conditions) in the absence of formaldehyde crosslinking. It was reasoned that if SpoIIIE could not be visualised in this way, then later experiments using sporulating samples to isolate and analyse SpoIIIE-associated DNA following crosslinking would become extremely challenging. As shown in Figure 3.3A (lanes 1-3) SpoIIIE was indeed detectable in whole cell lysates as a band of ~87 kDa. Here vegetatively growing cells were used as SpoIIIE is expressed constitutively during both vegetative growth and sporulation. Following incubation with Ni-beads and elution of bound proteins with imidazole, SpoIIIE was detected exclusively in the His-tagged samples (Figure 3.3A, compare lanes 5-6 with lane 4). A doublet was observed on elution, which presumably resulted from partial degradation of the N- or C-terminus of SpoIIIE36-His during binding and elution from the Ni-beads. However,

since both bands in the doublet reacted to the anti-His tag antiserum (Figure 3.3B), this suggested that degradation did not occur at the C-terminus. A silver stain of total eluate from the nickel matrix also suggested that isolation was relatively clean (Figure 3.3C).
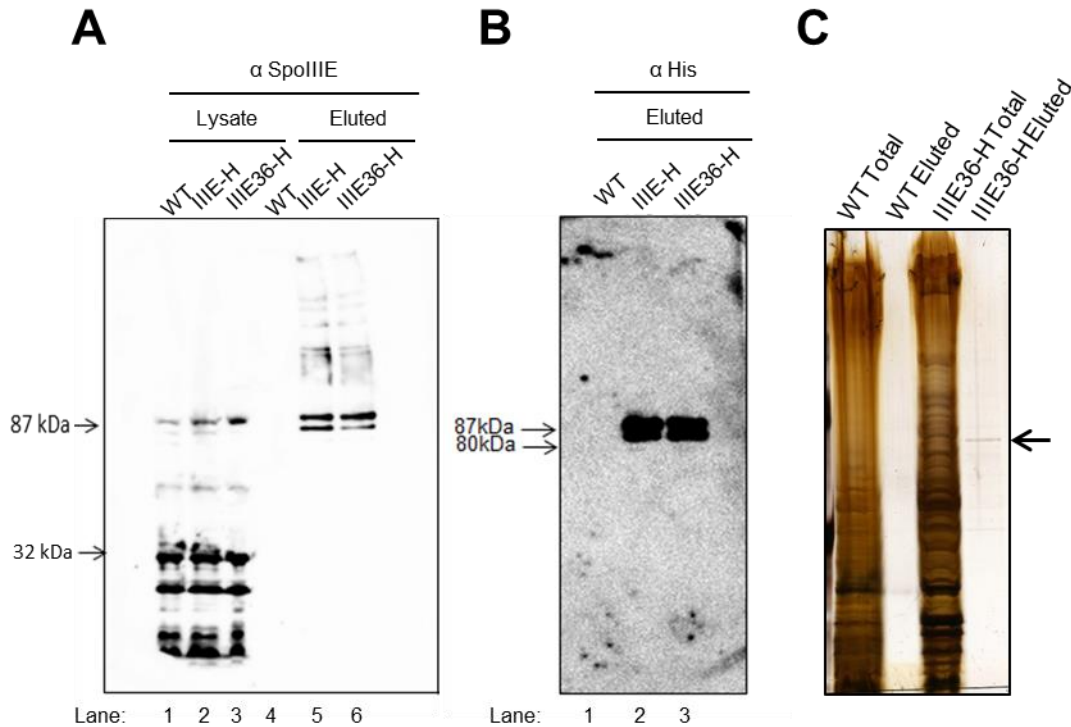
Figure 3.3 Distribution of SpoIIIE-His proteins following elution from Ni-beads. Eluates corresponding to 30ml of culture per lane were loaded for SDS-PAGE and Western blotting. Samples were probed with anti-SpoIIIE antibodies (A, 1:6666) or anti-His antibodies (B, 1:2000). Silver stained gel of the total lysates and eluted SpoIIIE36-H (C). Lysate represents pre-Ni bead samples, while Eluted represents Ni-bound material. Samples heated at 65°C for 10 min prior to loading onto the SDS-PAGE gel. Arrow in C indicates position of SpoIIIE based on MW markers. WT = 168CA; IIIE-H = DMR004; IIIE36-H = DMR006

It was important to check that the His tag did not compromise SpoIIIE function during sporulation and also to establish a suitable time point for addition of the formaldehyde cross-linker. Figure 3.4A shows that asymmetric septa were formed by T_3 in strains +/- the His tag, while Figure 3.4B demonstrated the presence of the SpoIIIE36 protein during sporulation. Since later morphological changes of sporulation might alter the resistance of prespores/cells to lysis by sonication or positioning of SpoIIIE, T_3 was chosen for cross-linking in subsequent ChAP experiments.
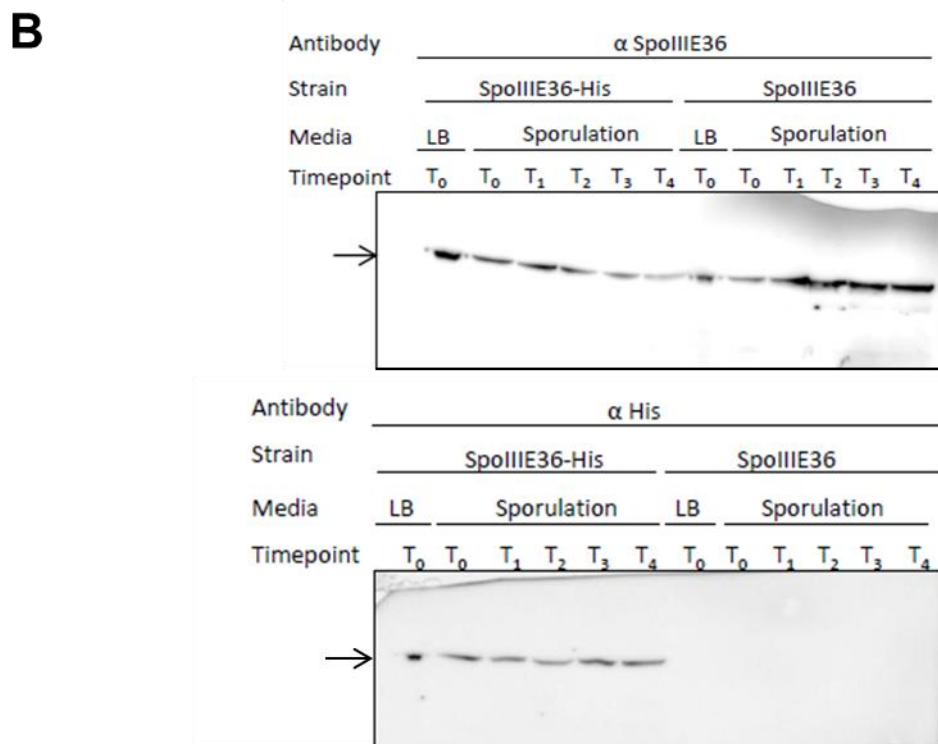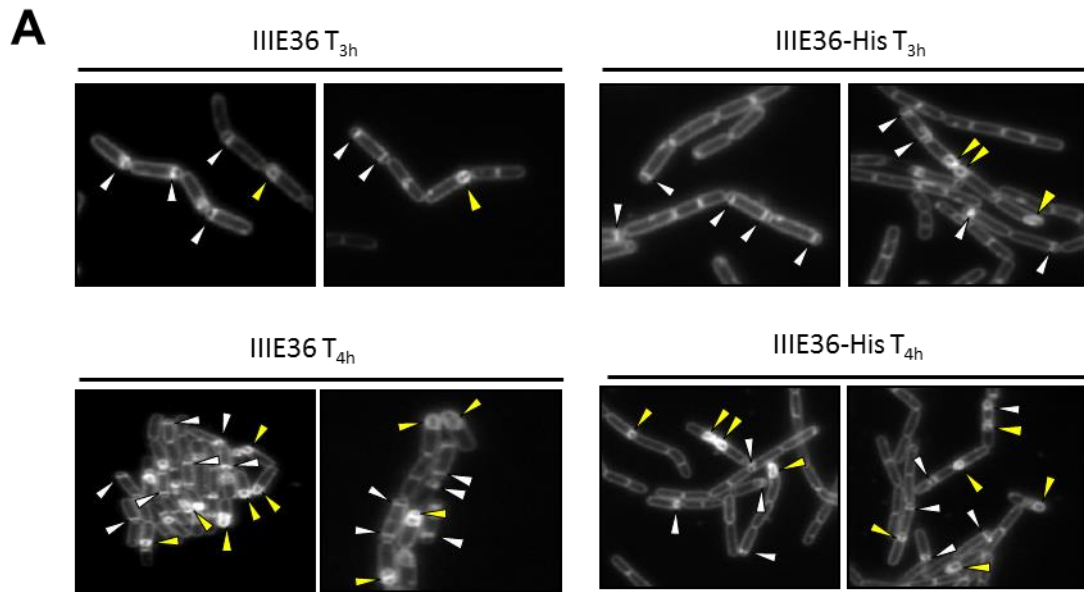
Figure 3.4 Detection of frequent asymmetric septa at T_3 of sporulation Western blotting time course of SpoIIIE36 +/- His

Cells were stained using a membrane dye (FM5-95) and imaged 3 h (top panels) and 4 h (bottom panels) after induction of sporulation to visualise the presence of asymmetric septa (white arrowheads) and engulfed prespores (yellow arrowheads) (A). Untagged *spoIIIE36* strain = IIIE36; SpoIIIE36-His = IIIE-His. Lysates were probed with anti-SpoIIIE antiserum (top panel, 1:6666) and anti-His antiserum (bottom panel, 1:2000) following SDS-PAGE and Western blotting (B). LB indicates a sample of vegetatively growing cells. T_0-T_4 indicates hours in sporulation medium. Arrows indicate the mobility expected for ~87 kDa SpoIIIE protein. IIIE36 = spoIIIE36; IIIE36-H = DMR006.

To test whether SpoIIIE36 could be detected following crosslinking using the membrane-permeable crosslinker formaldehyde, cells were induced to sporulate and in some samples formaldehyde was added (1% final) to crosslink neighbouring molecules. However, SpoIIIE36-H was only detected in samples that had *not* been subjected to the crosslinking and the reverse crosslinking steps (65°C overnight), and was absent from samples that have been reverse crosslinked at 65°C overnight (Figure 3.5).
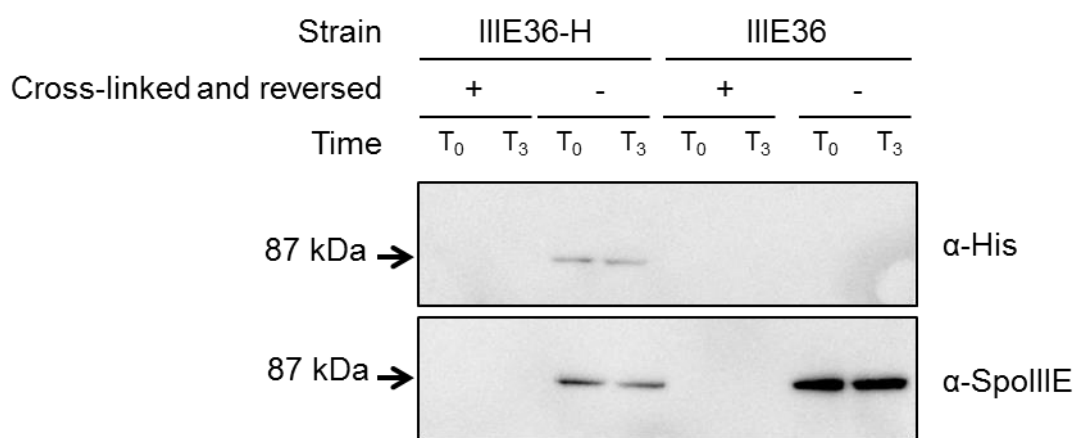
Figure 3.5 Western blot of SpoIIIE and SpoIIIE-His following formaldehyde cross-linking and reversal.
SDS-PAGE and Western blotting for the His-tag (top panel, anti-His antiserum; 1:2000) and SpoIIIE36 (bottom panel, anti-SpoIIIE antiserum; 1:6666). Sporulating strains: SpoIIIE36-His = IIIE36H; untagged SpoIIIE36 = IIIE36. T_0 and T_3 represent cells at 0 h and 3 h post-sporulation induction, respectively. Microscopy on samples prior to crosslinking confirmed the efficient induction of sporulation (not shown). Antiserum used for blotting indicated to the right of each panel. IIIE36-H = DMR006; IIIE36 = spoIIIE36.

To check whether SpoIIIE36 was lost at the crosslinking or reverse crosslinking step, various temperatures were tested, with and without the earlier addition of formaldehyde (Figure 3.6). SpoIIIE36 was only detected when samples were neither heated nor cross-linked (Figure 3.6, left panel). Thus, heating alone was sufficient to prevent detection of SpoIIIE36 (Figure 3.6, middle panel). In contrast, the

control protein FtsZ was readily detected after heating for 20 h (Figure 3.6, right panel). Therefore, the SpoIIIE36-His protein appears to be relatively thermolabile.
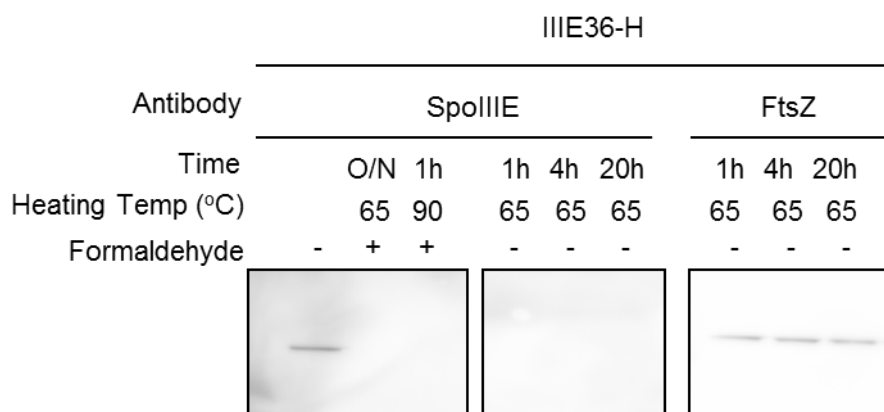
Figure 3.6 Comparison of SpoIIIE36 and FtsZ detection after heat treatments. SDS-PAGE and Western blotting against proteins from strain IIIE36-H (expressing SpoIIIE36-His). Probing was conducted with anti-SpoIIIE antiserum (left and middle panels, 1:6666) and anti-FtsZ antiserum (right hand panel, 1:8000) following cell lysate incubations at the temperatures and times indicated. Crosslinking with formaldehyde is indicated by + symbol. The non-crosslinked sample (left panel) was never heated. Representative example of 3 separate experiments. IIIE36-H = DMR006.

It was not known at what stage SpoIIIE degradation (disappearance) occurred. Since the aim of the experiment was to collect chromosomal DNA bound to SpoIIIE, if loss of SpoIIIE occurred during the final heating step of reverse cross-linking (Figures 3.5 and 3.6), after elution from the Ni-beads (Figure 3.1), SpoIIIE-associated DNA might still be present in the eluates and could be used for sequencing to identify the DNA fragments. To check the presence of DNA, the reverse-crosslinked samples were fractionated using the Promega Wizard purification protocol (See 2.4.1) and the purified products were resolved on a 3% agarose gel. Unfortunately, while this revealed the presence of ~50-500 bp DNA fragments in all reverse-crosslinked lysate preparations (Figure 3.7A, lanes 4-9) there was no detectable DNA from the Ni-bead eluates that had been subjected to the reverse crosslinking treatment (Figure 3.7A, lanes 2-3). To determine the step at which enrichment of the SpoIIIE36-His associated DNA was lost, bead run through and wash samples were also analysed by agarose gel electrophoresis. From Figure 3.7B, it appeared that DNA was never bound via SpoIIIE to the Ni-beads. As an alternative DNA quantification method, the DNA concentration in all samples was analysed by NanoDrop (Figure 3.7C).

Consistent with the gel data, very little DNA was found in the eluate, as compared to the debris and non-cross-linked samples. Furthermore, the 260/280 readings for these samples suggested that the DNA was of poor quality.

C

Sample	Average conc. (ng/µl)
DMR006 T_0 Elu	14.7
DMR006 T_3 Elu	5.7
DMR006 T_0 Pre-debris spin	872.5
DMR006 T_3 Pre-debris spin	525.8
DMR006 T_0 Post-debris spin	643.5
DMR006 T_3 Post-debris spin	349.9
DMR006 T_0 -F	154.5
DMR006 T_3 -F	194.7
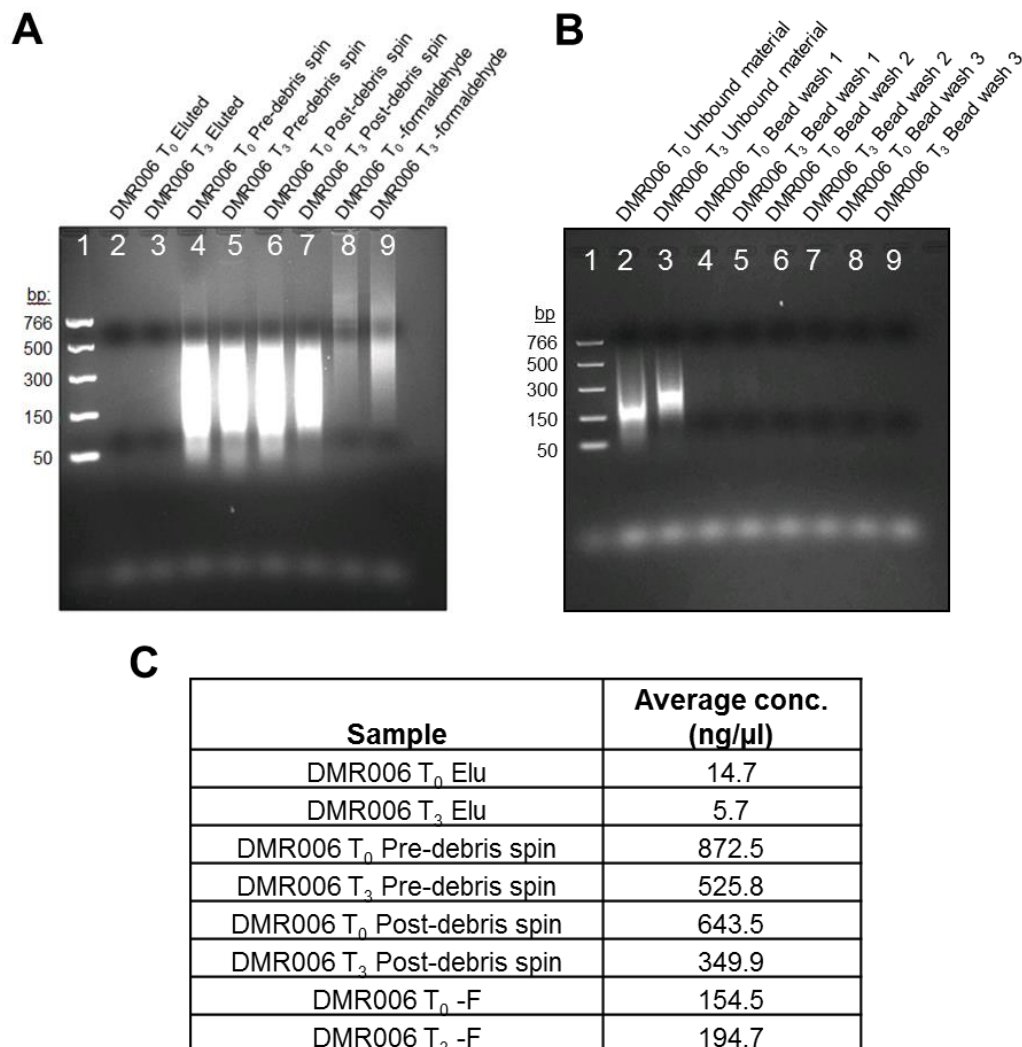
Figure 3.7 SpoIIIE-associated DNA is not detected following elution from Ni-beads. 3% agarose gel electrophoresis was used to resolve DNA from **A)** the final Ni-bead eluates (lanes 2-3); following initial cell lysis prior to removal of cell debris (whole cell lysate; lanes 4-5); and supernatants after removal of cell debris (lanes 6-7). DNA from non-crosslinked (-formaldehyde) whole cell lysates were run in lanes 8-9, and from **B)** 3% agarose gel electrophoresis of DNA from unbound run through (lanes 2-3); and the various wash fractions (lanes 4-9). In all cases for both gels, samples were heated at 65°C overnight to reverse formaldehyde cross-links before loading onto the gel. **C)** Average (n=3) DNA concentrations from NanoDrop calculation at the various purification stages. –F = no addition of formaldehyde.

To test whether the absence of significant concentrations of DNA in the eluates for SpoIIIE36 was due to technical error (e.g. buffer pH, bead integrity or sample handling etc.) or because of the inherent biological complexity of the SpoIIIE36-containing septal region, ChAP was conducted against an alternative His-tagged protein Spo0J-His, using exactly the same affinity purification protocol. Since Spo0J binds at *parS* sites clustered around *oriC*, the alternative output of qPCR (rather than agarose gel) was used to determine the relative amounts of DNA in the eluted sample at a specific *parS* site compared to a non-specific binding site (near the *ter*, 180° from *oriC*). This was done in a Spo0J-His strain and in a non-tagged strain (168^{CA}). qPCR revealed that Spo0J was 40-fold more enriched at *parS* relative to *ter* in the same Spo0J-His strain, compared to a ~2-fold enrichment at *parS* relative to *ter* in the untagged 168^{CA} strain (Figure 3.8).
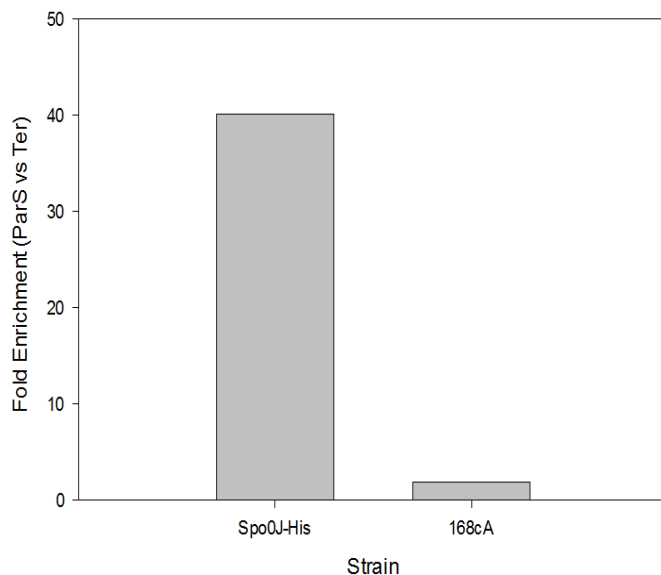
Figure 3.8 ChAP reveals a 40-fold enrichment of Spo0J-His at *parS* sites.

Following ChAP, using the same batch of Ni-beads, buffers and protocol as in earlier experiments, purified DNA was subject to qPCR. Specific primers were designed to bind at *parS* site 4 within *oriC*. Non-specific primers were placed within the terminus region of the chromosome. Triplicate samples were analysed in QIAGEN qPCR machine. n=1. Spo0J-His = DMR025.

These data showed that the ChAP enrichment protocol worked for Spo0J-His. The absence of high quality DNA enriched SpoIIIE36-DNA complexes in column eluates using what was otherwise a successful protocol led us to abandon this approach.

3.2.4 Using methylation to identify prespore localised DNA

As an alternative means of precisely probing the segment of DNA in the prespore in the *spoIIIE36* mutant background we tried to label the prespore DNA by expressing an ectopic DNA methylase under strict prespore-specific σ^F control (using the P_{spoIIQ} promoter) (Figure 3.9A) (Sullivan *et al.*, 2009; Kloosterman *et al.*, 2016). *E. coli* Dam methylase has been extensively studied (Horton *et al.*, 2005; Horton *et al.*, 2006; Liebert *et al.*, 2007; Xiao and Moore, 2011) and it has a small sequence recognition pattern (GATC), and was therefore selected as the methylase. Following asymmetric septation, σ^F is specifically activated in the prespore, which would in turn activate the ectopic P_{spoIIQ}-*dam,* leading to GATC methylation on DNA sequences resident in the prespore. Following purification of the chromosomal DNA, the methylation status of the DNA can be interrogated (either by sequencing or *Dpn*I digestion) to determine precisely which sequences originated in the prespore. Figure 3.9 illustrates the principles of this approach.
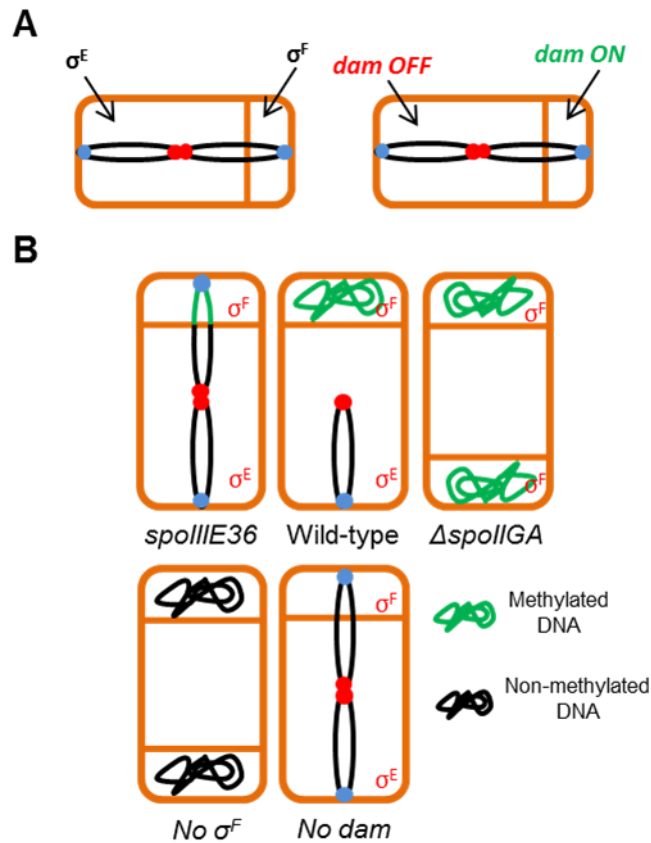
Figure 3.9 Utilisation of a methylase to label prespore DNA during sporulation.
Following asymmetric division, σ^F and σ^E are activated in the prespore and mother cell, respectively (A, left), and the σ^F-controlled *dam* methylase gene will be specifically activated in the prespore (A, right). Predicted prespore DNA methylation patterns in wild type and certain sporulation mutants (B). In the SpoIIIE36 trapping mutant (B, top left cell), only ~one third of the chromosome trapped in the prespore would be methylated (green). However, complete methylation of the prespore chromosome would be expected in wild-type sporulating cells (B, top middle cell). In the disporic mutant (*spoIIGA*), complete methylation of all cellular DNA would be predicted (B, top right cell). No methylation would be expected in the absence of either the prespore promoter (σ^F) or the *dam* gene (B, bottom left and right cells, respectively). Blue spots = origin regions; red spots = terminus regions.

Following the isolation of potential recombinant plasmids in *E. coli*, restriction digests confirmed the presence of the P_{spoIIQ}-*dam* insert (Figure 3.10). DNA sequencing of the plasmid from colony 6 (Figure 3.10) confirmed the successful construction of a P_{spoIIQ}-*dam p*lasmid (pDMR011) for integration into the *amyE* locus on the *B. subtilis* genome (data not shown).
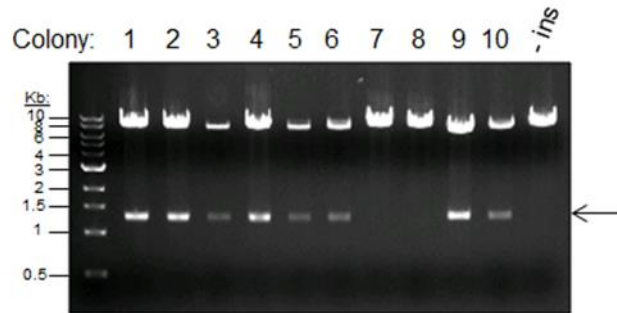
Figure 3.10 A P_{spoIIQ}-*dam* construct was cloned successfully into pDR111.
Following *Eco*RV digestion of plasmids isolated from a selection of transformants (one
*Eco*RV site is present in the *dam* gene, one in the pDR111 vector backbone), 1% agarose
gel electrophoresis was conducted to establish the presence/absence of a 1.2kbp insert,
diagnostic of successful insertion of *dam* into pDR111 vector. Insert was seen in colonies 1-
6, 9-10. – ins = empty vector control. Expected insert size = 1.2 Kbp (arrow).

Following transformation, growth curves of wild-type and known sporulation
mutants carrying plasmid pDMR011 (see Figure 3.9) were conducted to assess
whether the presence of the *dam* gene in *B. subtilis* had any effect on cell growth.
Figure 3.11 showed there was no detectable difference in doubling time of any of the
strains, irrespective of the presence or absence of *dam.*
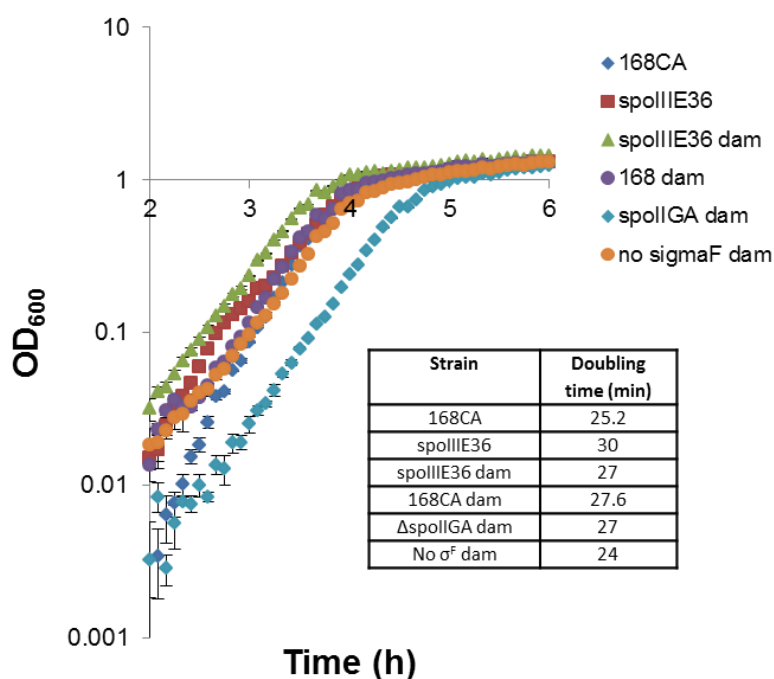
Figure 3.11. Growth curves of parent and *dam* methylase strains.
Each line shows the average of 3 separate growth curves, with error bars represented as standard deviations. Cells were grown in LB and incubated at 37°C. *spoIIIE36 dam* = DMR056; 168CA *dam* = DMR058; *ΔspoIIGA dam* = DMR060; no σ^F *dam* = DMR062.

An advantage of Dam-mediated methylation is that the modified DNA becomes a substrate for cleavage by *Dpn*I. Bioinformatics analysis showed that there are ~18,000 potential *Dpn*I sites evenly spread across the *B. subtilis* genome. Given that in the *spoIIIE36* mutant it is estimated that ~one third of the chromosome is trapped in the prespore (Wu and Errington, 1998), there should be ~6000 *Dpn*I sites available for methylation by Dam.

3.2.5 *Dpn*I digestion suggests prespore specific methylation

To assess whether the methylase was appropriately expressed and active in prespores during sporulation, the strains illustrated in Figure 3.9 were induced to sporulate and then DNA samples were used to verify the expected methylation patterns (Figure 3.12). Although gel analysis is qualitative, these digests revealed the expected approximate correlations when DNA from samples taken at T_0 and T_3 were treated +/- *Dpn*I. In the trapping strain (DMR056), approximately 1/6 of the DNA at T_3

was *Dpn*I-sensitive (top left gel), compared with ~50-60% of wild type cells (DMR058, top middle gel) and 100% in the disporic *ΔspoIIGA* mutant (DMR060, top right gel). Some very slight high molecular weight (10 Kbp and above) smearing may have occurred in the strain lacking σ^F (made by deleting *spoIIAABC*, bottom left gel, DMR062). This may reflect leakage of the promoter or as a consequence of the deletion of *spoIIAB* (see discussion). There were no low molecular weight smears typical of *Dpn*I digestion in the control that completely lacked the *dam* gene, which only showed smearing in the loading wells as is typical when loading whole genomes
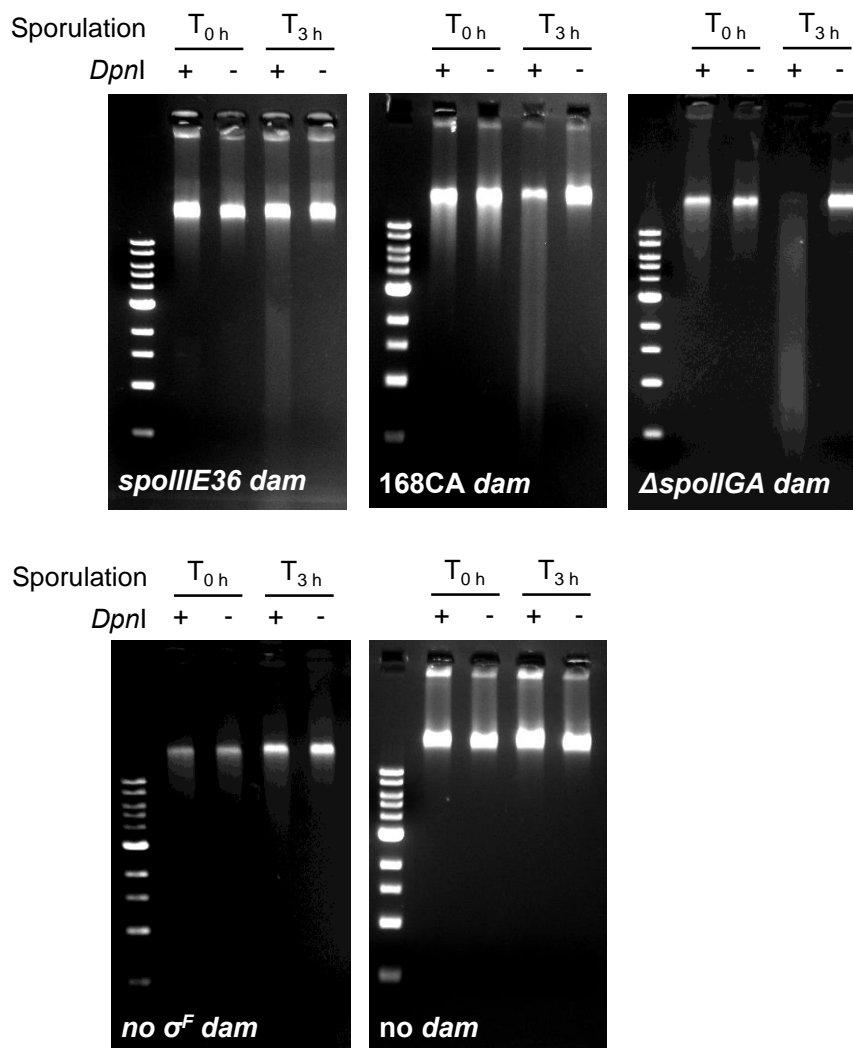
onto into agarose gels (bottom right gel).

Figure 3.12. ***Dpn*I digestion pattern of known sporulation mutants**.
spoIIIE36 dam (DMR056); 168CA *dam* (DMR058); *ΔspoIIGA dam* (DMR060); no σF *dam* (DMR062); no *dam* (168CA) strains were used. T0 h = no sporulation (sample taken upon sample resuspension in sporulation salts). T3 h = three hours into sporulation.

Encouraged by these data, the next step was to exploit a quantitative methylation detection and analysis protocol. For this, Pacific Biosciences Single-molecule, Real time (PacBio SMRT) sequencing was chosen since this approach has been used previously for the analysis of bacterial methylomes (Flusberg *et al.*, 2010; Beaulaurier *et al.*, 2015). PacBio SMRT should detect N^6-methyladenine motifs in GATC sequences directly during ongoing sequencing. It was hoped that this would allow a clearer definition of the boundary between methylated and non-methylated DNA on the chromosome, and by extension the boundary between the prespore and mother cell.

3.2.6 PacBio SMRT methylation sequencing

The principle of PacBio SMRT sequencing involves a slight time delay between fluorescent pulses when the polymerase encounters N^6-methyladenine (anticipated here in prespore methylated GATC motifs) (Figure 3.13A). It follows that changes in the interpulse duration (IPD) at each template position relative to a non-methylated or *in-silico* control template (Figure 3.13B) can be used to indicate the presence of modified adenines. High sequence coverage is required (>20x) to ensure that an increased IPD at a given site – suggesting methylation – is statistically significant above possible aberrations in the DNA sample that may cause stalling of the polymerase during the sequencing reaction (and a higher IPD). Figure 3.13C shows the ratio of the mean IPD at a given site in the modified sample that has at least 25x sequence coverage.
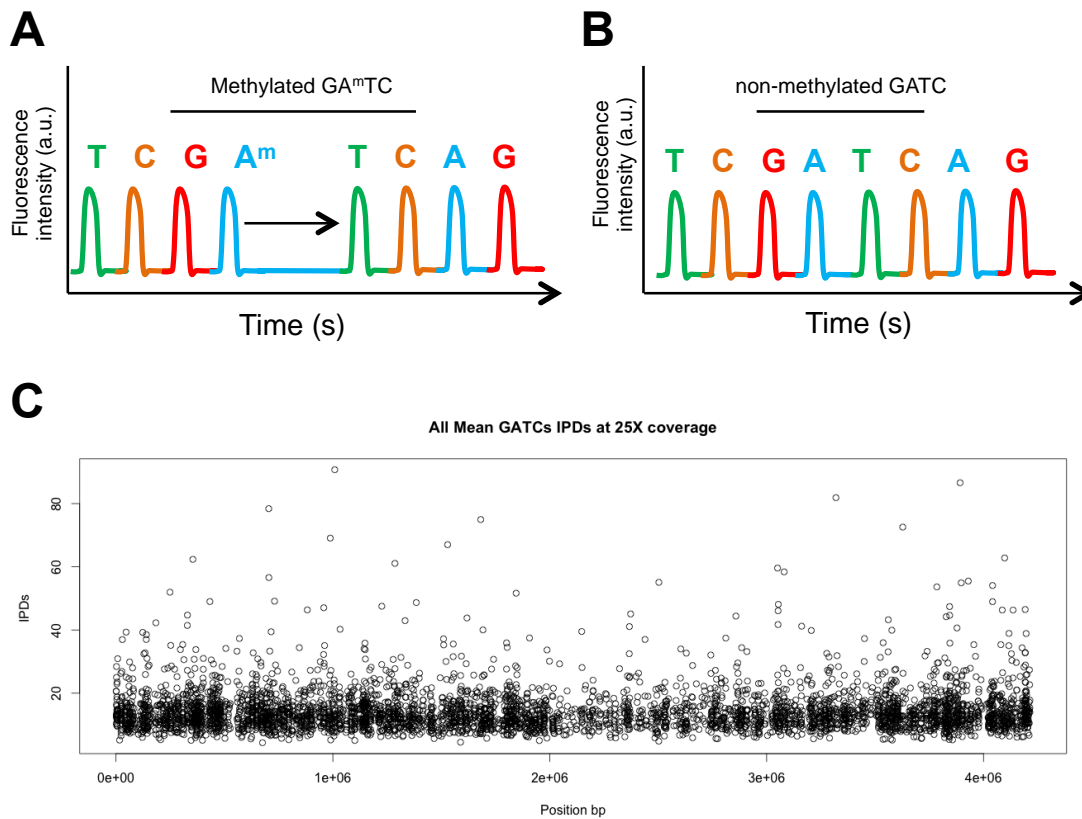
Figure 3.13. PacBio SMRT methylation sequencing of *spoIIIE36* sample.
Schematic representation of delayed insertion of nucleotides in the PacBio sequencing reaction caused by methylated GATC, leading to longer interpulse duration (IPD)(A).By contrast, there is no delay in nucleotide incorporation if no GATC methylation (no increased IPD) (B). Global view of all mean-IPD scores in GATC sequences across the genome in a T_3 sporulating sample of DMR056 (*trpC2 spoIIIE36 amyE::(P_{spoIIIQ}-dam spc)*) (C). Bioinformatic analysis conducted by Dr Robert Stones, Newcastle University FMS Bioinformatics Support Unit.

The SMRT methylation sequencing and analysis was carried out on 30 μg of the same DNA from the *spoIIIE36* sporulating cells as seen in Figure 3.12. Sequencing was performed using the commercial service offered by the University of Maryland DNA Sequencing Centre. Further expert refinement and bioinformatics to map the IPD ratios was kindly provided by Dr Robert Stones of the Newcastle University Faculty of Medical Sciences Bioinformatics Support Unit. Unfortunately, sequencing of the *spoIIIE36* sample (where only approximately 1/6th of the total cellular DNA could potentially be exposed to the methylase) revealed no significant bias in higher IPDs across the genome (Figure 3.13C). Lack of expected bias towards the origin in the prespore-specific methylation (Wu and Errington, 1998) was clearly different from the correlations of methylation obtained earlier (Figure 3.12).

92

However, there were a number of uncertainties with the methodology and the assumptions used at source to obtain the IPD scores given (see discussion).

As an alternative method to identify the *Dpn*I fragments, and also to confirm that the sample sequenced actually had methylated sites I tried blunt-end cloning of the DNA fragments from the *Dpn*I digest into *Sma*I-digested pUC19. The *Sma*I site lies in the *lacZ* α–complementing gene, so most inserts generate a white (rather than blue) colony phenotype upon transformation and selection of a suitable *E. coli* host strain on X-gal plates. The rationale for this approach was that the blunt ends generated from *Dpn*I digestions would allow the DNA fragments - representing methylated DNA – to be ligated to the linearized blunt ended vector. Plasmids were isolated from a random selection of 25 white colonies and sequenced (The University of Dundee DNA Sequencing and Services facility). The sequence reads were mapped to known GATC sites in the genome using CloneManager. Eleven of the 25 fragments mapped to within the proposed region that is initially captured in the prespore upon asymmetric cell division (Figure 3.14) (Wu and Errington, 1998), where methylated sequences were expected. However, 10 out of 25 sequences appeared to be in the region of the genome that does not enter the prespore (located in the mother cell) (Figure 3.14), with the remaining 4 plasmids returning non-mappable data (not shown).
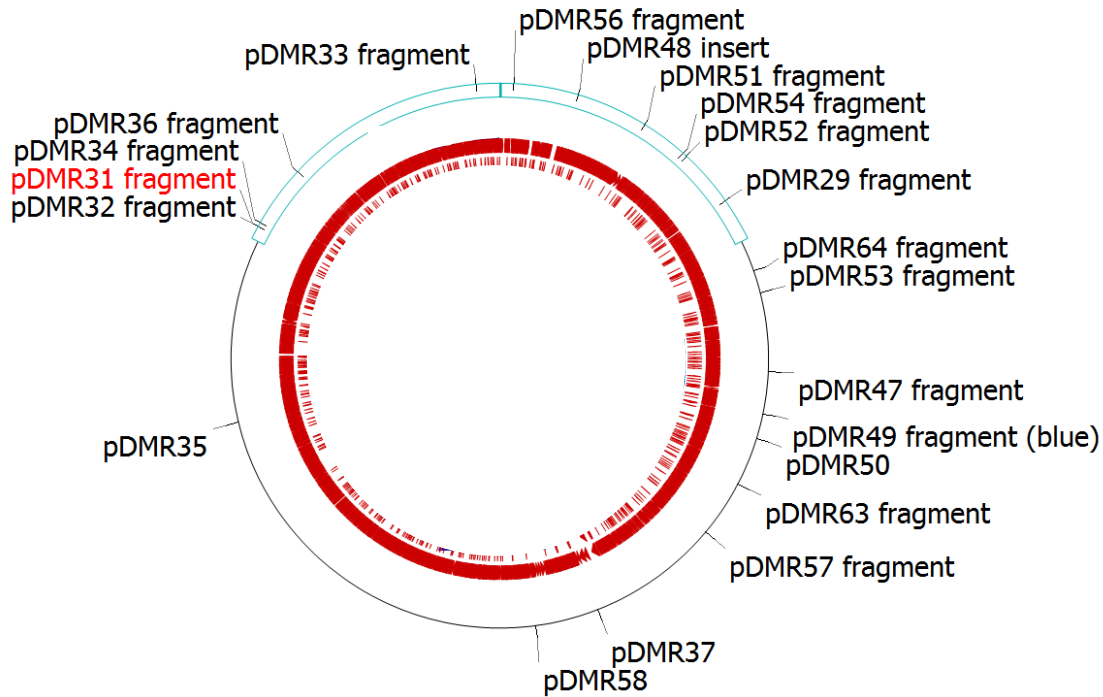
Figure 3.14. Locations of the *Dpn*I digested fragments on the *B. subtilis* genome. The expected prespore trapped region of the chromosome is indicated by the light blue box (top third of the chromosome). Operons are highlighted in red. Fragments are numbered based upon the plasmid isolated from white pUC19 transformants. pDMR31 is in red due to being selected in CloneManager.

Taking all these data with the PacBio sequencing results, it seemed unlikely that this approach would yield sufficient resolution to define the prespore-mother cell DNA boundary precisely.

3.3 Discussion

Although it was possible to express a tagged SpoIIIE and SpoIIIE36 without triggering conformational or functional instability (Figure 3.2), it wasn't possible to enrich DNA from cross-linked, affinity purified SpoIIIE36 (Figure 3.7). However, the initial stages of assay development were encouraging. The C-terminal tag of 6 histidines on SpoIIIE/SpoIIIE36 was sufficiently long to allow the protein to be isolated from detergent solubilised cell lysates using Ni-beads (Figure 3.3). Also, the tag did not appear to interfere with SpoIIIE function during sporulation (Figure 3.2B &

Figure 3.4). However, although a standard formaldehyde cross-linking protocol followed by affinity chromatography was successful for a His-tagged Spo0J and its associated DNA, with a 40-fold enrichment at *parS* verses non-*parS* sites seen (Figure 3.8), this was not possible with SpoIIIE36 (Figures 3.5, 3.6 and 3.7). For reasons discussed below it was concluded that isolation of SpoIIIE36-associated DNA presented a much more formidable challenge than for the Spo0J control.

The exact reason(s) for failure to isolate DNA associated with SpoIIIE36-H remain unclear, although there are some strong possibilities. To our knowledge, ChAP has not yet been successfully applied to a multi-spanning, DNA-binding integral membrane protein (David Sherratt, University of Oxford, personal communication). This may suggest the standard published protocols for soluble DNA-binding proteins are not suitable for SpoIIIE. Furthermore, SpoIIIE is not an abundant protein. Pumping both arms of the chromosome requires at least two SpoIIIE hexamers, and the most recent estimates suggest that each sporulating cell contains between just ~50 (Fiche *et al.*, 2013) and ~70 (Burton *et al.*, 2007) SpoIIIE monomers. However, and possibly more critical for ChAP is the fact that only two (Fiche et al., 2013) or four (Yen Shin *et al.*, 2015) sites on DNA (one on each arm of the chromosome) in each sporulating cell will ever interact with the SpoIIIE hexamer, to allow enrichment on Ni-beads. The approach used here therefore involved searching for limited DNA interactions with a scarce integral membrane protein. This contrasts with the Spo0J control which, following DNA binding as a dimer, spreads laterally and can bridge DNA to form a large soluble nucleoprotein complex over hundreds of Kbp (Murray *et al.*, 2006; Graham *et al.*, 2014).

Another difficulty in developing the ChAP assay in sporulating cells was the expected complexity of the division septum (Adams and Errington, 2009). The situation in sporulation is different to vegetative growth (where SpoIIIE can reside in the lateral membranes and cell pole as well as the divisome) (Wu, 2009). The divisome forms the septum and contains many integral membrane proteins and adaptors (Adams and Errington, 2009; den Blaauwen *et al.*, 2017). Isolation of a rare protein like SpoIIIE36-His from such a complex network could be exacerbated by non-specific formaldehyde cross-links with the numerous division site proteins.

Most formaldehyde cross-links that form between DNA and protein are believed to involve the formation of a –CH_2– methylene bridge between the amino group of a nucleoside and a nucleophilic nitrogen or sulphur of an amino acid side chain (Lu *et al.*, 2010). However, formaldehyde also induces protein-protein links by binding to reactive primary amines (lysine) and thiols (cysteine) to induce cross-linking via a methylene bridge with other nearby functional groups (Thavarajah *et al.*, 2012). Formaldehyde cross-linking of SpoIIIE to neighbouring DNA may therefore be complicated by continued covalent coupling to many other proteins in the vicinity, preventing the specific purification of SpoIIIE36-His:DNA. Furthermore, formaldehyde cross-linking is ~1000x less efficient at cross-linking duplex DNA (as in SpoIIIE-DNA binding), compared to single-stranded DNA or DNA that is rotated/bent (Von Hippel and Wong, 1971). A combination of these considerations may explain why, with there being so many competing crosslinking reactions, it wasn't possible to isolate DNA at SpoIIIE binding sites. It may be that the successful enrichment of His-tagged SpoIIIE/36 seen from vegetative cells (Figure 3.3) actually represented SpoIIIE proteins that had been resident as monomers in lateral membranes or at cell poles and not from the divisome. There was no evidence for DNA being enriched from cross-linked sporulating cells (Figure 3.7).

A further problem was the heat sensitivity of SpoIIIE. It was shown that prolonged heating (as opposed to 10 min of heating in gel sample preparation, Figure 3.2) at temperatures at or above 65°C triggered loss of detectable protein (Figure 3.6). It wasn't clear what the mechanism for this was, although it seemed likely that the protein denatured to aggregates at raised temperatures (Bert van den Berg, Newcastle University, personal communication). For example, it is well known that certain integral membrane proteins cannot be prepared for SDS-PAGE by boiling in SDS sample buffer because they aggregate and are unable to enter the gel (Sagne *et al.*, 1996). Some integral membrane proteins are therefore prepared for gel analysis by short, gentle heating at 37°C or 65°C, as was done here (Figure 3.2). If SpoIIIE was particularly heat sensitive when solubilised in detergent, then it could be that the very prolonged heating step (65°C overnight or 90°C for 1 h) required for reverse crosslinking after elution from the Ni matrix caused irreversible aggregation that prevented further analysis on gels.

In conclusion, although the ChAP approach for SpoIIIE was recognised early on to be extremely challenging and high-risk, we persevered with it for over a year because if successful, SpoIIIE36-His would have provided a highly-sensitive tool to study chromosome dynamics in wild-type and mutant cells over a relatively short time scale. However, this avenue of investigation was abandoned once it was shown that no pure DNA could be detected on agarose gels following ChAP (Figure 3.7; or by Nanodrop DNA determination).

As an alternative way to characterise the arrangement of DNA in the prespore I tried to develop a novel prespore specific methylation assay. Early attempts to clone the *Staphylococcus aureus sau3AI* methylase were unsuccessful due to gene toxicity to *E. coli* and plasmid rearrangements that occurred when *E. coli* was transformed during vector construction (data not shown). However, the *E. coli* Dam methylase (*dam*) gene, which has the same base recognition sequence as *Sau3A*I, turned out to be straightforward to manipulate. The gene was placed at the *amyE* locus, which is well known to be efficiently trapped in the prespore compartment (Wu and Errington, 1998; Kloosterman *et al.*, 2016) and under the control of the σ^F-dependent *spoIIQ* promoter that has been used frequently for prespore-specific expression previously (e.g. (Burton *et al.*, 2007; Sullivan *et al.*, 2009; Kloosterman *et al.*, 2016)). For several strains bearing the P_{spoIIQ}-*dam* construct, DNA isolated during sporulation became susceptible to *Dpn*I cleavage, as expected. Slight high molecular weight smearing (suggesting some DNA digestion) was unexpectedly seen in the strain lacking the σ^F (as compared to the strain lacking *dam*, compare Figure 3.12, bottom gels). As the $\Delta\sigma^F$ construct was made by knocking out *spoIIAABC*, it was possible that the lack of *spoIIAB* in this strain led the loss of tight regulation of the second prespore sigma factor, σ^G (which can also activate *spoIIQ*, in the prespore) and as a consequence, the partial activation of the P_{spoIIQ} promoter may explain the limited smearing (Rather *et al.*, 1990; Foulger and Errington, 1993) (Figure 3.12).

Since restriction enzyme digestions do not identify the fragmented sequences, a downstream assay for this was required. The current gold standard for determining methylation patterns is PacBio SMRT methylation sequencing. Owing to cost, only one sample of 30 µg methylated DNA from T_3 sporulating cells of the *spoIIIE36* trapping strain containing the *dam* gene was submitted to the Genomics Resource Centre in the University of Maryland (USA) for commercial PacBio SMRT methylation

sequencing. Due to the complexity of the raw data, genome assembly and the analysis of the PacBio sequencing was conducted in collaboration with Dr Robert Stones of the Bioinformatics Support Unit within Newcastle University (Figure 3.13C). It was reasoned that if every adenine at a particular GATC site was methylated, the mean IPD score at this site should be increased relative to the mean background IPD score at non-methylated sites.

Analysis of the PacBio data did not reveal a significant origin-region bias in long IPDs. Assuming prespore-specific methylation, the maximal proportion of methylated DNA in any extraction would be 16.5% (1/6th of total). However, the sporulation efficiency was unlikely to exceed 70%, so only 1/6 of 70% of total genomic DNA would be available for methylation (~11% of total DNA). It may also be the case that methylation is also inefficient. It follows that the actual incidence of prespore-specific methylation would be considerably less than 16.5% of the total.

Of course, it remains possible that methylation of the mother cell DNA was genuine, reflecting either methylase activity in cell extracts after lysis, or low-level expression from the supposed prespore-specific promoter of the *dam* copy in the chromosome of the mother cell. The first of these seemed unlikely. This is because the essential methyl donor, S-adenosyl methionine, would not function at the pH of the lysis buffer (Gareth Roberts, University of Edinburgh, personal communication). Regarding the second possibility, to our knowledge there is no report of σ^F activity in the mother cell. To cover this possibility if time had permitted, a 3' *ssrA* degradation tag would have been cloned onto the *dam* gene, along with the essential adaptor *ssrB*, regulated for expression specifically in the mother cell (using a σ^E-dependent promoter). Together, these would target any background level of mother cell Dam protein to be rapidly turned over by the ClpXP protease (Griffith and Grossman, 2008).

As a quick and inexpensive way to test whether the prespore-specific methylation was working, fragments from a *Dpn*I digested DNA sample were cloned into pUC19 and sequenced. Since, as discussed above, the prespore captured DNA in the *spoIIIE36* strain constitutes less than 1/6 of the DNA isolated, 55% of the sequenced fragments mapping to this region actually represents a ~6-fold enrichment over fragments from the mother cell localised DNA. However, a much larger sample of fragments, and fragments from samples without methylase, would

be needed to confirm the bias. It should be noted in addition, that in both the PacBio SMRT and pUC19-fragment cloning, there was lower number of reads/fragments between 180-270° of the chromosome. This may reflect DNA folding that prevents methylation of nucleotides since there is no obvious reduction of available GATC sequences in this region. Time did not permit any follow up of this potentially interesting observation.

Therefore, despite some early promise, it was concluded that many more control experiments and optimization of the methods would be needed before they could be used efficiently to identify the asymmetric septum boundary precisely. As a result it was decided to abandon this aim and investigate other aspects of chromosome dynamics during sporulation.

Chapter 4

Role and localisation of ComN and MinD in capturing the origin during sporulation

4.1 Introduction

Recently, a transposon mutagenesis screen was conducted to identify further factors required for correct origin placement at the cell pole in sporulating cells (Kloosterman *et al.*, 2016), thereby helping to advance our understanding of the mechanism of prespore chromosome segregation. The screen (Figure 4.1) was based on a strain in which a copy of *lacZ* (preceded by *lacO*) and *lacI* was placed on the chromosome, in "arm" (-418 Kbp) and "origin" (-79 Kbp) positions respectively. Both genes were under prespore control via the P_{spoIIQ} promoter. In a *spoIIIE36* background with no additional segregation mutation, both the arm and origin regions would be trapped and so expression of *lacZ* would be repressed by LacI. However, a transposon insertion that prevented segregation of the origin (and *lacI*) to the prespore pole, while at the same time successfully trapping the arm (and *lacZ*) within the prespore compartment, would be LacZ+ and thus be evident as a blue colony in the presence of the chromogenic substrate X-gal. Mutants that abolished sporulation or prevented trapping of any segments of the chromosome would give only white colonies. The screen provided a powerful means of identifying mutants defective specifically in trapping the origin region in the prespore.
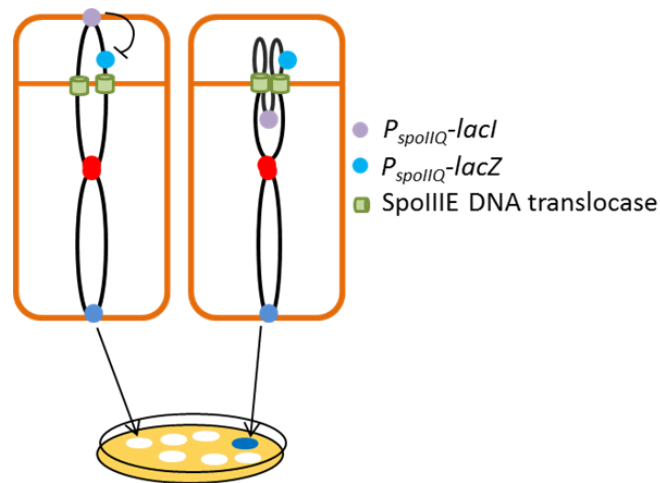
Figure 4.1 A genetic screen to identify novel proteins involved in capturing the origin within the prespore.

In wild-type cells (left cell) both the origin and arm are localised to the prespore allowing expressed LacI to repress the co-localised *lacZ* gene, generating white colonies in the presence of X-Gal. A transposon insertion mutant that specifically fails to localise the *lacI*-containing origin (right cell) will appear blue since *lacZ* will be expressed to produce functional β-galactosidase in the prespore.

From the Kloosterman screen of over 100,000 colonies, ~100 mutants were characterised further from which two surprising additional proteins, ComN and MinD, emerged as being implicated in origin capture during sporulation (Kloosterman *et al.*, 2016). It was already known that ComN was involved in the post-transcriptional regulation of competence through the specific accumulation of *comE* mRNA at the cell pole (Ogura and Tanaka, 2009; dos Santos *et al.*, 2012). However, ComN had not previously been linked to chromosome segregation. Several hits from the screen also suggested a role for MinD in origin placement at the pole. MinD was already known as the activator of MinC, the cell division inhibitor that controls mid-cell division placement (De Boer *et al.*, 1990; Marston and Errington, 1999; Bramkamp *et al.*, 2008; van Baarle and Bramkamp, 2010); also see Section 1.5). However, mutations in *minC* did not give blue colonies in the screen.

My role in this part of the project was to visually characterise the new proteins implicated in capturing the chromosome origin at the prespore cell pole. Specifically:

1. To confirm the localisation of polar complex proteins DivIVA, ComN and MinD at the cell pole using advanced imaging techniques.
2. To examine the functional hierarchy of these proteins.

3. To study the effects of *comN* and *minD* mutants on the dynamics of origin movement using time-lapse microscopy.

4.2 Results

4.2.1 Localisation of known and putative polar capture proteins

Initial experiments were focussed on establishing the localisation patterns of the newly identified proteins during sporulation. Functional *gfp* fusions under the control of their native promoters, available in the laboratory, were used for this analysis. The strains were induced to sporulate by the re-suspension method and imaged after 80 min (soon after asymmatric septa should appear) or later.

ComN-GFP was clearly visible at both the asymmetric septa and at the poles of those cells that were undergoing sporulation (Figure 4.2). Also, and consistent with previous work, ComN was present at mid-cell septa (Figure 4.2, red arrows) (dos Santos *et al.*, 2012).

| Brightfield | ComN-GFP | DAPI | ComN/DAPI |
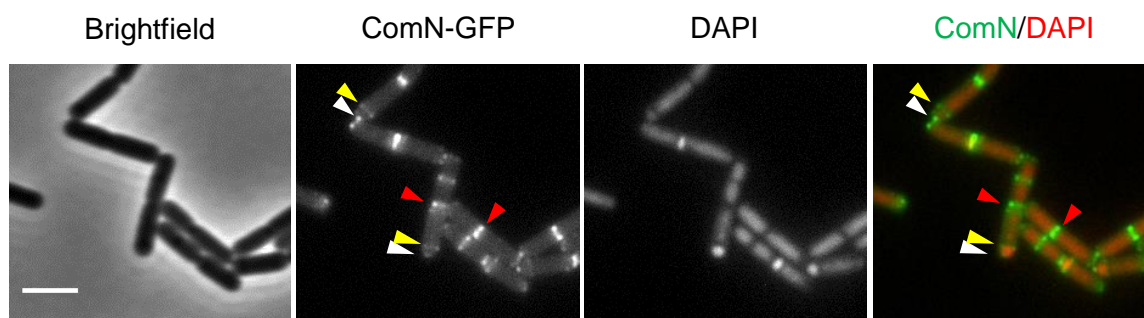
Figure 4.2 ComN-GFP localisation during sporulation.
Cells, after 80 min of sporulation, were spotted on 1 % agarose slides and visualised using a Nikon Ti microscope. Images are representative of 3 independent experiments. White arrow heads = poles. Yellow arrow heads = asymmetric septa. Red arrow heads = mid cell septa. Scale bar = 3 µm. ComN-GFP = DMR066.

Although it was already reported that MinD localises to the pole and septum in cells when expressed during vegetative growth using a xylose inducible (P_{xyl}) promoter located at the *amyE* locus (Marston *et al.*, 1998; Strahl and Hamoen, 2010), it was important to confirm this outcome using a GFP-MinD fusion expressed from the native locus using the native P_{minD} promoter. In these cells GFP-MinD showed a

strikingly similar localisation pattern to that observed for ComN, particularly during sporulation (Figure 4.3).
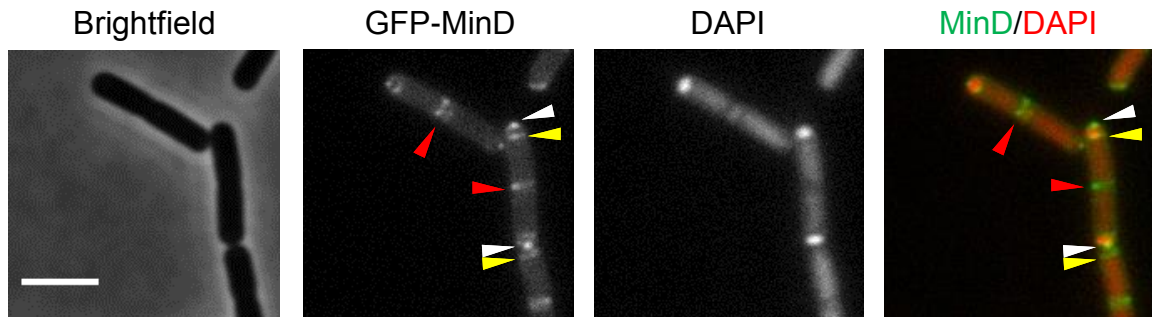
Figure 4.3 GFP-MinD localisation during sporulation.
Cells, after 80 min of sporulation, were incubated on 1 % agarose slides and visualised using a Nikon Ti microscope. Images are representative of 3 independent experiments. White arrow heads = poles. Yellow arrow heads = asymmetric septa. Red arrow heads = mid cell septa. Scale bar = 3 μm. GFP-MinD = DMR067.

Previous reports have shown that recruitment of MinD and ComN to division sites requires DivIVA (Bramkamp *et al.*, 2008; dos Santos *et al.*, 2012). It therefore made sense to also view DivIVA-msfGFP, a functional fluorescent fusion of DivIVA (Jahn *et al.*, 2015; Muller *et al.*, 2016), using the same conditions as used for ComN-GFP and GFP-MinD (Figure 4.4).

| Brightfield | DivIVA-msfGFP | Membrane | Merge |

T_0

T_{80}
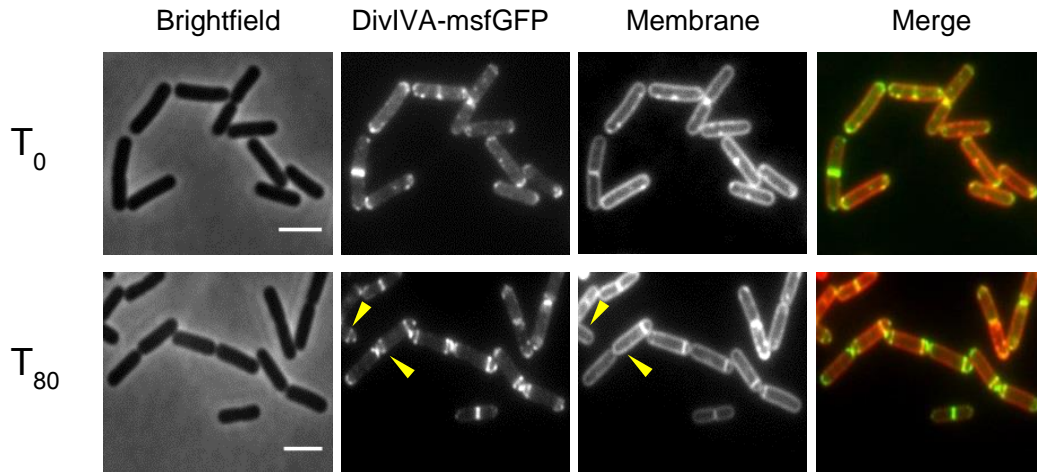
Figure 4.4 Localisation of DivIVA-msfGFP during sporulation.

Cells were spotted onto 1 % agarose containing 150 µg/ml FM5-95 membrane dye and visualised using a Nikon Ti microscope. Scale bar = 3 µm. Yellow arrow heads indicate sub-polar DivIVA signal in the absence of a septum (see Discussion). T represents minutes after re-suspension in sporulation medium. DivIVA-msfGFP = DMR113.

DivIVA-msGFP was evident at cell poles and division sites at both time points, as expected (Figure 4.4), suggesting that (at least during *this* differentiation process), DivIVA is retained at these sites for at least 80 min. Whether this is a static or dynamic process remains to be determined. This steady state level of DivIVA is required for the recruitment of all of the other known origin capture components (e.g. RacA, ComN, MinJ, MinD and Soj) (Ben-Yehuda *et al.*, 2003b; Wu and Errington, 2003; Errington *et al.*, 2005; Bramkamp *et al.*, 2008; Errington, 2010; van Baarle and Bramkamp, 2010; Kloosterman *et al.*, 2016).

One curious observation was the presence of DivIVA-msfGFP localisation in an asymmetric septum-like pattern in the absence of concomitant membrane staining (Figure 4.4, yellow arrows). Intriguingly, it seemed that this only occurred in cells that had already undergone asymmetric cell division at the opposite pole.

4.2.2 Hierarchy of ComN and MinD interactions in the chromosome origin capture pathway

MinD evidently has two separate cellular functions – control of mid-cell division placement and the newly identified role in capturing the origin at the cell pole during sporulation (Kloosterman *et al.*, 2016). For both functions, MinD is dependent upon MinJ and DivIVA (Bramkamp *et al.*, 2008; van Baarle and Bramkamp, 2010; Kloosterman *et al.*, 2016). Since Kloosterman *et al.* (2016) also revealed that ComN has a role in capturing the origin, and given the strikingly similar localisation pattern of the two proteins, it was important to determine whether ComN and MinD operated in a hierarchical or interdependent manner in origin capture. To test this, ComN-GFP and GFP-MinD were imaged in *ΔminD* and *ΔcomN* deletion backgrounds, respectively.
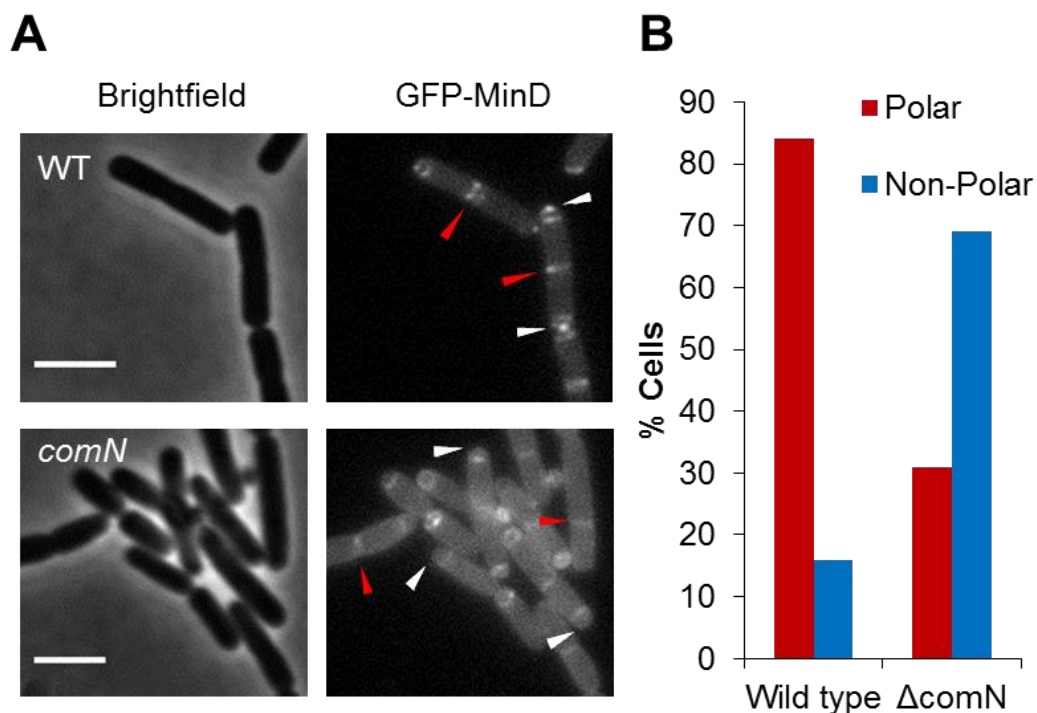
Figure 4.5 Polar localization of GFP-MinD is dependent on *comN*.
Images of wild-type (DMR067) and *comN* mutants (DMR070) containing a GFP-MinD fusion imaged after 80 minutes of sporulation (A). Cells were loaded onto 1 % agarose slides and imaged using a Nikon Ti microscope. White arrows = representative polar signal; red arrows = representative mid-cell signal. Scale bar = 3 μm. Images are representative of 3 independent experiments. The localisation patterns of GFP-MinD were scored as either polar or non-polar (B). At least 100 cells with asymmetric septa were counted.

Figure 4.5A shows that polar foci of GFP-MinD were greatly reduced in the presence of a *comN* deletion. Quantification of 100 prespores (Figure 4.5B) confirmed the marked reduction in prespores with a GFP-MinD signal at cell poles in the *comN* deletion strain when compared to wild-type cells. However, from the quantification, around 30% of cells *did* reveal a polar GFP-MinD signal in the *ΔcomN* mutant.

Close examination of images such as those in Figure 4.5A suggested that the loss of GFP-MinD foci at the cell pole might be accompanied by an increase in the GFP-signal intensity along the cell axis. Line scans of the GFP-MinD signal intensity along the length of the cell, starting at the prespore pole end of the cell (Figure 4.6A, C) revealed a clear reduction in the polar GFP-MinD signal for *ΔcomN* mutant cells (red line) compared to those of the wild-type (black line). Meanwhile, the GFP-MinD signal in *ΔcomN* at the asymmetric septum remained similar to that in wild type cells. As well as a decrease in detectable MinD at the cell pole, there was a reproducible suggestion that MinD signal intensity across the cell was slightly higher in the *ΔcomN* mutant. To further test this, GFP-MinD intensity plots of the cell width (indicated in Figure 4.6D) were measured in wild-type and *ΔcomN* mutant strains (Figure 4.6B). There was a slightly higher signal in the *ΔcomN* mutant but its significance was questionable.

Reciprocal experiments were then conducted to examine the localizaiton of ComN-GFP in wild-type and *ΔminD* mutant cells (Figure 4.7).
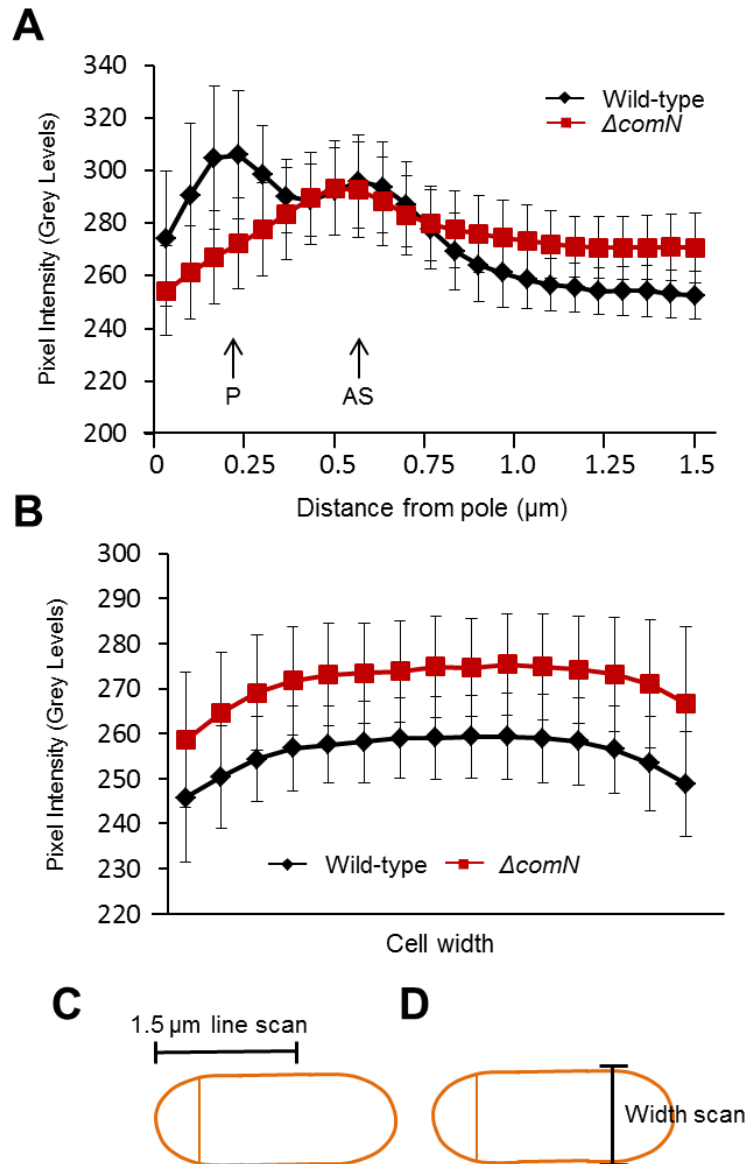
Figure 4.6 Line scans of GFP-MinD intensity.

Line scans of cell length (1.5 µm from cell pole, A) or cell total width (B) of cells containing asymmetric septa were measured using ImageJ. C-D represent cartoon schematics of the length (C) and width (D) measurements. P = cell pole. AS = asymmetric septum. For length measurements n= 25 cells, for width measurements n=50 cells.
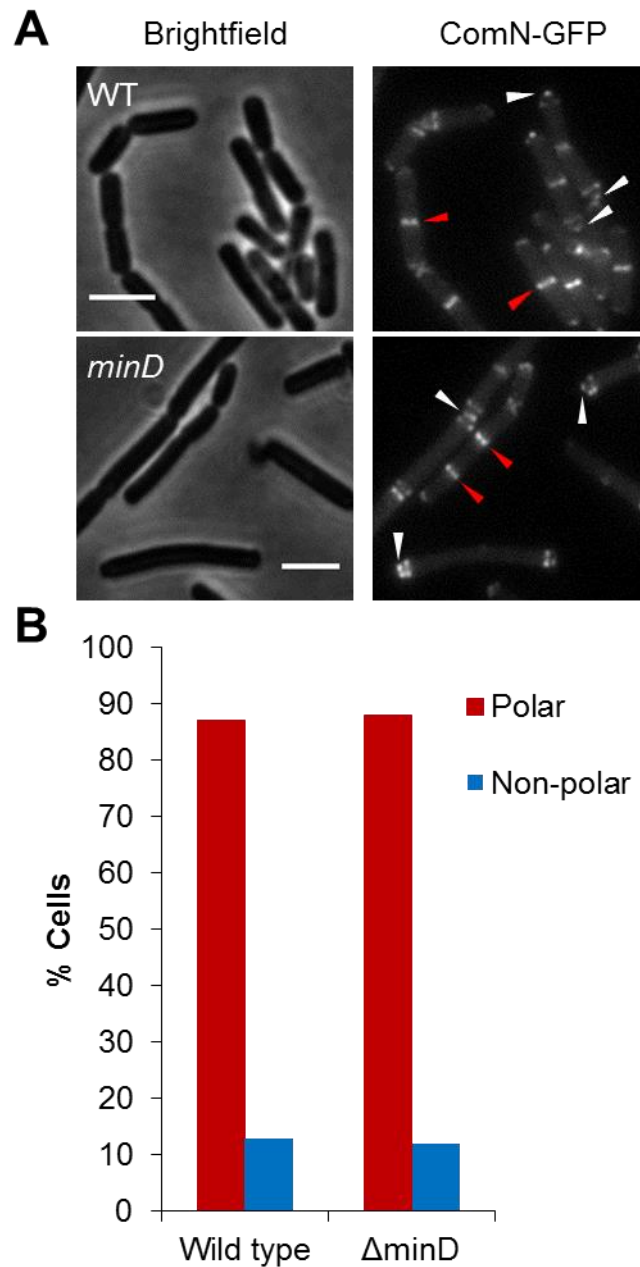
Figure 4.7 ComN-GFP localisation in wild-type and *ΔminD* backgrounds

Images of ComN-GFP in a wild-type background (DMR066) and a *ΔminD* mutant (TK313) (A). Cells at T_{80} of sporulation were loaded onto 1 % agarose slides and imaged on a Nikon Ti microscope. White arrows = representative polar signal; red arrows = representative mid-cell signal. Scale bar = 3 µm. Localisation patterns of ComN-GFP from >120 cells were scored as either polar or non-polar (B).

From the images (Figure 4.7A), it was clear that the ComN-GFP signal was present at the cell poles and asymmetric septa irrespective of the presence or absence of *minD* and this was confirmed by quantitation (Figure 4.7B). Taken together with previous results (Figure 4.5A-B) the deduced hierarchy of dependence for proteins at the cell pole during sporulation is DivIVA → ComN → MinD.

4.2.3 Co-localisation of polar capture proteins

ComN and MinD were identified as important proteins involved in origin capture at the cell pole (Kloosterman *et al.*, 2016) in sporulating cells, with a clear hierarchical dependency (Section 4.2.2). The above results highlighted the possible importance of the polar foci of ComN and MinD in chromosome capture. If correct, then the proteins are expected to co-localise. To test this, a strain harbouring both mCherry-ComN and GFP-MinD was created. The whereabouts of the two fusion proteins was then determined during vegetative growth and sporulation. As shown in Figure 4.8 the proteins appeared to co-localise at septa (yellow arrows) and at the pole (white arrows), with polar spots being particularly important in sporulating cells (since this is the sight of origin anchoring). This further supported the notion that ComN and MinD could function in the same capture machinery at the cell pole.
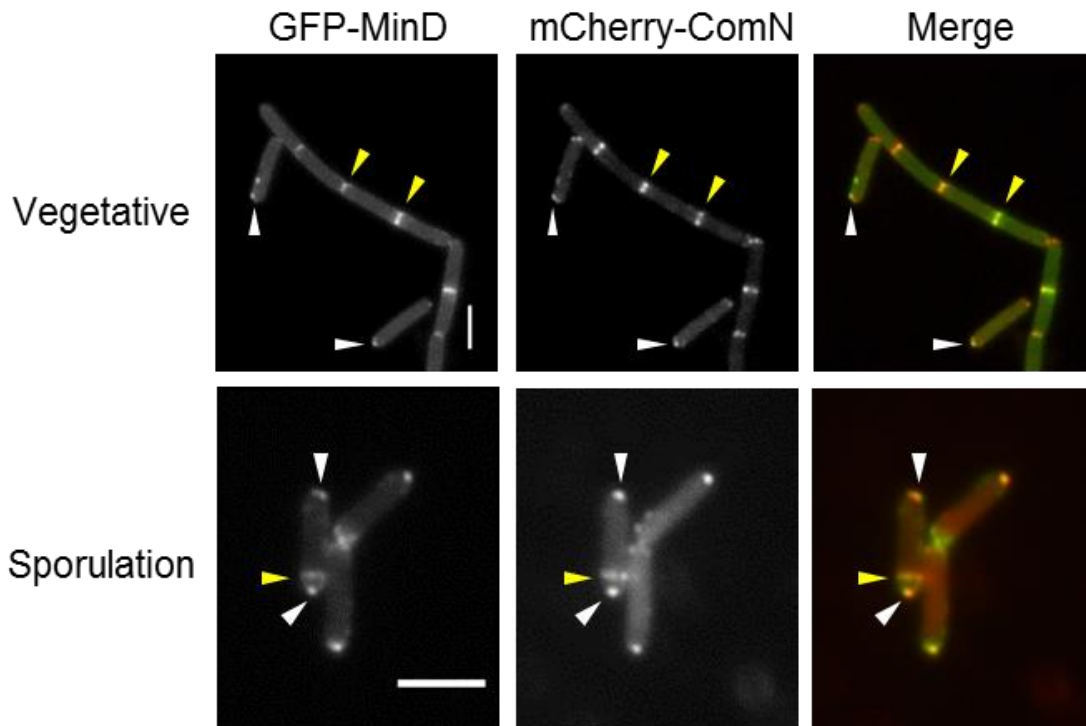
Figure 4.8 Co-localisation of mCherry-ComN and GFP-MinD.

Cells during vegetative growth (top panels) were imaged using a Nikon Ti microscope, as before. After 80 min of sporulation (bottom panels), samples were imaged using Nikon Ti microscope equipped with APO TIRF lasers. White arrow heads = representative cell poles; yellow arrowheads = representative vegetative (top panels) or asymmetric (bottom) septa. Scale bar = 3 μm. Strain = DMR111.

4.2.4 Do two distinct complexes anchor the chromosome to the pole?

From recruitment dependency (4.2.2), co-localisation (4.2.3), and positive bacterial two-hybrid interactions (Kloosterman *et al.*, 2016), it seemed that pole-localised ComN and MinD proteins co-operate in a chromosome capture system. Previous work has shown that there are probably two distinct systems involved in prespore chromosome capture, which operate synergistically (Wu and Errington, 2003).

It was therefore important to establish how *ΔcomN* and *ΔminD* mutations affected sporulation frequency. It was also important to consider redundancy in origin capture. It is known that RacA is directly recruited by DivIVA and binds to the chromosome through *ram* sites, tethering the origin-proximal region of the left chromosome arm to the cell pole (Ben-Yehuda *et al.*, 2003b; Wu and Errington, 2003). To determine the dependence and significance of the ComN-MinD system on

the established RacA-DNA binding pathway, sporulation efficiencies in at least 650 cells of both single ($\Delta racA$, $\Delta minD$ and $\Delta comN$) and $\Delta racA$ $\Delta comN$ double mutant backgrounds were examined. This double mutant was chosen because ComN appears to act "upstream" of MinD. To rule out any sporulation defect caused by minicell production in the $\Delta minD$, a $\Delta minC$ mutant, which makes minicells but has been previously shown not to affect origin capture (Kloosterman *et al.*, 2016), was also included (Figure 4.9).

Strain	Genotype	% sporulation efficiency at T_{5h}	% sporulation efficiency at T_{6h}
168CA	trpC2	27.5	73.7
DMR075	trpC2 ΔcomN::zeo	17.7	74.5
DMR114	trpC2 minCD::(minC⁺ ΔminD Ωerm)	19.1	64
TK144	trpC2 ΔminC::kan	23.7	69.4
DMR119	trpC2 ΔracA::erm	18.4	53.8
DMR124	trpC2 ΔracA::erm ΔcomN::zeo	8.7	8.1

Figure 4.9 Sporulation frequency of origin trapping mutants.
In all cases, > 650 cells were counted under microscope. % efficiency is the percentage of phase bright spore containing cells of the counted cells.

The data shown in Figure 4.9 revealed a slight delay in the formation of phase bright spores at $\sim T_{5h}$ in the known origin trapping mutants: $\Delta racA$, $\Delta comN$ and $\Delta minD$, with sporulation efficiencies just below 20%. However, by T_{6h}, with the exception of $\Delta racA$ (which showed a modest reduction) there was no marked difference in sporulation efficiency between wild-type (168CA) and the $\Delta minD$ or $\Delta comN$ mutants. A likely explanation for this is given in the Discussion below. As expected, $\Delta minC$ had no effect on sporulation efficiency, confirming that the formation of minicells does not prevent sporulation. Interestingly, however, the $\Delta racA$ $\Delta comN$ double mutant was severely defective in spore formation, suggesting that the functionality of these proteins in polar capture of DNA (and consequently sporulation) could occur via two redundant pathways. This scenario is potentially similar to the Δsoj $\Delta racA$ mutants that have been shown to be severely defective in spore formation (Errington *et al.*, 2005).

It seemed likely that the "arm-in but origin-out" sporulation phenotype exhibited by the mutants described above – permanently trapped in this initial capture orientation by the translocation deficient allele SpoIIIE36 - reflected a change in the dynamics of origin movement in those cells. This change could be mediated by at least two effects. First, lack of any mechanism to anchor the origin at the pole may cause random fluctuations of the chromosome through Brownian motion, leading to either incorrectly or correctly positioned origins in the polar region (Figure 4.10). Alternatively, the 'origin-out, arm-in' phenotype may arise due to a complete failure to extract the origin from a hypothetical fixed quarter-cell vegetative position (Figure 4.10)
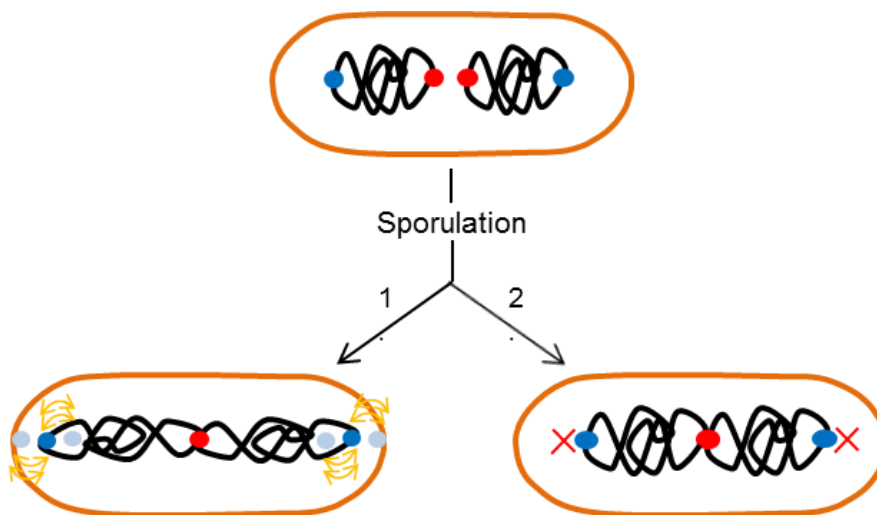
Figure 4.10 Possible origin dynamics in trapping mutants.

Upon initiation of sporulation, origins may fail to anchor (1) allowing more free movement near to the pole. Alternatively, origins may never move from quarter cell positions (2). Yellow arrows = increased origin movement as fluctuations; red crosses = no origin movement. *oriC* = blue, *ter* = red.

It was therefore considered pertinent to visualise movement of the origin in live cells over time, in both wild-type and in origin trapping mutants. The commercial plate-based CellASIC ONIX microfluidics platform (Millipore) was selected, as it has a number of advantages that we could exploit. First, cells are captured in the oxygen-permeable imaging chamber of the plate based on cell depth (width), thereby restricting bacterial growth to a single focal plane (Figure 4.11A), which reduces the potential for out-of-focus drift. Secondly, a constant flow of nutrients and/or media to the entire cell population enable uniform conditions over many hours. Thirdly, the 5 inlets to the chamber allow media or solutions to be switched during the experiment (Figure 4.11A) (crucial for the induction of sporulation through nutrient switching). Although these features made the case for CellASIC ONIX microfluidics platform compelling, it should be noted that this system had never before to our knowledge been adapted for sporulation. It was therefore anticipated that considerable effort may be required to optimise conditions for use.

A

Media wells

Imaging chambers

Cell inlet chamber

Media in Up to 5 types

Inlets
1
2
3
4
5

To outlet 7

4.5 μm
0.7 μm
0.9 μm
1.1 μm

6-Tier trap

Cell Inlet 8

Cell Outlet 6

Cell chamber

Objective
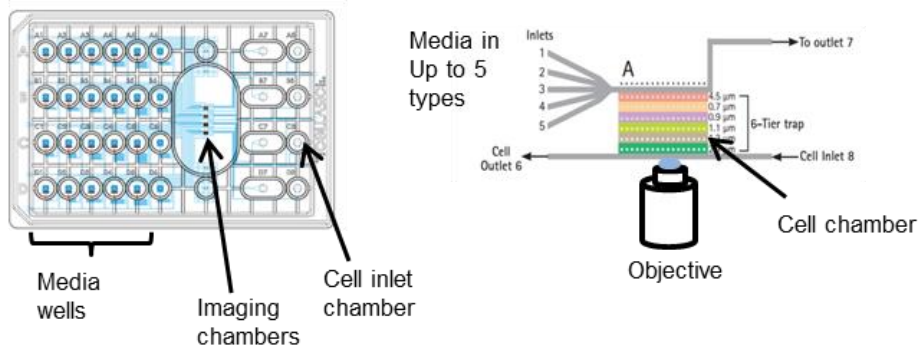
B

WALP23-GFP
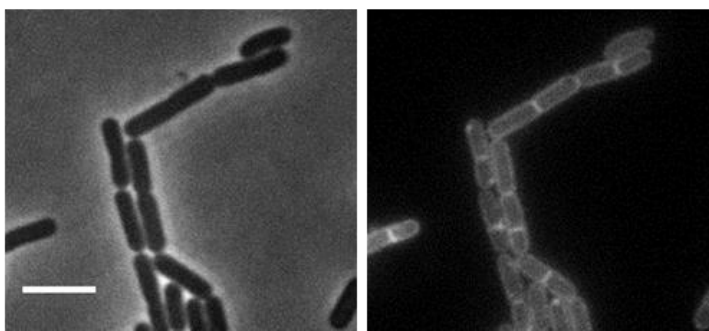
Figure 4.11 WALP23 peptide specifically labels cell membranes.

The CellASIC ONIX microfluidics plate can image up to 4 independent strains simultaneously (A, right), with live cells trapped in the cell chamber based upon cell width (A, left). *B. subtilis* strain DMR131 expressing WALP23-GFP imaged on a Nikon Ti microscope (B). Scale bar = 3 μm. Left panel = brightfield; right panel = GFP.

parS-binding Spo0J-GFP was selected as a marker for origin movement, for several reasons: the fusion is bright, it forms a large nucleoprotein complex at the origin proximal region (Lin and Grossman, 1998; Murray *et al.*, 2006; Graham *et al.*, 2014), and, since it is a native complex, this particular fusion avoids the possibility of affecting DNA replication (e.g. through roadblocks, as have been observed for FROS systems) (Teleman *et al.*, 1998; Graumann and Losick, 2001). The fusion is also sufficiently bright for frequent image acquisition over the long time scales required (every 1.5-3 min for >5h). Indeed, smaller and more functional *lacO* arrays have been developed (Sullivan *et al.*, 2009; Wang *et al.*, 2014a), but under our conditions these required exposures that led to photobleaching before significant numbers of cells had undergone asymmetric division (data not shown).

Another important consideration was to have an efficient way to label the membrane in order to identify the cell outline and timing of asymmetric division. Dyes such as FM5-95 are frequently used to label cell membranes for microscopy. However, it was not possible to use these hydrophobic dyes in the ONIX plates since they bind to the plastic and glass surfaces of the imaging chamber (data not shown). As a result, WALP23, an artificial transmembrane domain fused to either GFP or mCherry was selected for use (Figure 4.11B), which was recently used to successfully label the membranes of *B. subtilis in vivo* (Scheinpflug et al., 2017). WALP peptides are comprised of repeating units of alanine and leucine (flanked by tryptophan) that span the lipid bilayer (Weiss *et al.*, 2003; Siegel *et al.*, 2006). Specifically, WALP23 contains 23 amino acid residues (Matalon *et al.*, 2013).

Initial experiments focussed on optimising sporulation conditions, by measuring the emergence of phase bright spores within the chamber. Cells were loaded into the ONIX plate following re-suspension in sporulation medium (marking T_0 of sporulation). Sporulation medium was then continuously supplied to the cells and the temperature was maintained at $32^{\circ}C$ in all experiments. Figure 4.12 shows that no phase bright spores were evident even after 12 h, and that many cells lysed, with some limited re-growth after between 8 and 12 h.
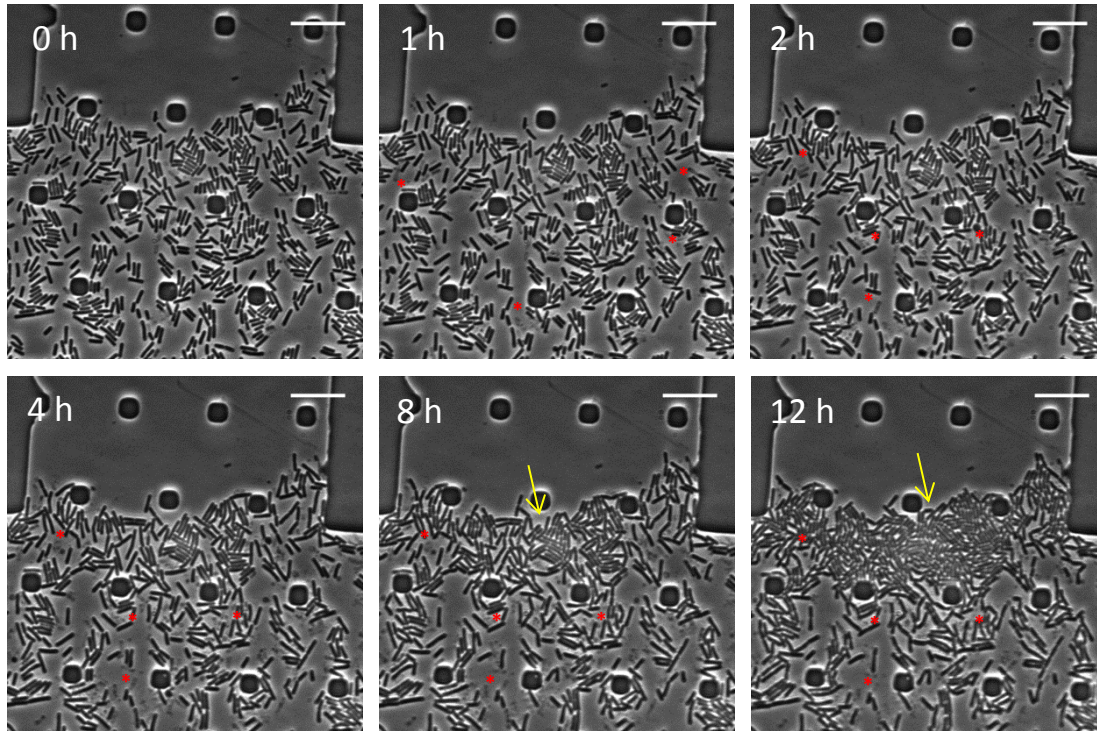
Figure 4.12 Sporulation of *B. subtilis* in the CellASIC ONIX chamber.
Cells of strain DMR145 were re-suspended in sporulation salts and loaded into chamber
(See 2.8.2). Sporulation medium was supplied to the cells at 2 psi continuously. Red
asterisks indicate sites of cell lysis. Yellow arrow indicates slight re-growth. Scale bars = 10
µm. Temperature = 32°C.

One possible reason for extensive lysis and the lack of phase bright spores is
that cells had suddenly lost membrane potential and become de-energised through
the loss of trace amounts of rich medium in a process that can lead to cell lysis
(Henrik Strahl, Newcastle University, personal communication; see below). It has
long been known in the laboratory that the presence of a small amount of rich CH
medium when the cells are re-suspended in the starvation (sporulation) medium
enhances sporulation efficiency. In the ONIX plate, the continuous perfusion of
medium under pressure would rapidly remove (in less than 10 min at the flow rate
used) all traces of the rich medium present at the time-lapse start point. To optimise
the amount and the delivery method of the CH medium, a wide range of different CH
supplements and protocols of delivery (i.e. concentration gradients or dilutions of
spent medium) were tested in attempts to increase the frequency of sporulation.
Table 4.1 summarises the results in assay development.

Condition	AS septa visible	Phase Bright spores	Cell lysis	Cell growth
A+B sporulation media only, cells loaded immediately after re-suspension	-	-	+ + +	+ +
A+B spent media (filter sterilised from T75 min culture), 0 % CH supplement	-	-	+	+ +
A+B sporulation salts supplemented with 0.3 % CH for the entire time lapse, cells loaded immediately after re-suspension	-	-	+ + +	+ +
A+B sporulation salts supplemented with 0.3 % CH for the entire time lapse, cells loaded 45 min after re-suspension	-	-	+ +	-
A+B sporulation salts supplemented with 0.3 % CH for the entire time lapse, cells loaded 1 h after re-suspension	-	-	+ +	-
A+B sporulation salts supplemented with 0.8 % CH for the first hour in the plate, cells loaded immediately after re-suspension	-	-	_	+ + +
A+B sporulation salts supplemented with 0.57 % CH for the first hour in the plate, cells loaded immediately after re-suspension	+ +	+ +	+	+
A+B sporulation salts supplemented with 0.57 % CH for the first hour in the plate, cells loaded 1 h after re-suspension	+ + +	+ + +	+	+

Table 4.1 Conditions tested to optimise sporulation in the ONIX chamber.
In all cases, images were acquired every 3 min for 12 h. Both brightfield and mCherry channels were imaged to visualise cells and membranes, respectively. AS = asymmetric; - = none detected after 12 h; + = low frequency (<5 % population); + + = moderate frequency (5-25% population); + + + = high frequency (>25%). Each condition was tested in at least two independent ONIX experiments. Temperature = 32°C.

From Table 4.1 it is clear that a supplement of CH medium in the A+B sporulation salts solution was required to obtain significant asymmetric septa and phase bright spores. However, if the amount of CH supplement was too high (0.8 %) or provided over too long a period, the frequency of phase bright spore formation was decreased. From all of the conditions tested, the optimal condition was for cells to

grow in flask for 1 h following re-suspension in A+B sporulation medium, supplemented with 0.57% CH medium for the first hour in the ONIX chamber.

To further assess the ability of cells to enter sporulation using the optimised conditions (Table 4.1), a strain containing a P_{spoIIA}-mCherry (where P_{spoIIA} is an early sporulation promoter) was viewed in the chamber and seen to increase in signal intensity over time without obvious cell lysis (Figure 4.13). A similar approach has been used previously to identify cells entering sporulation (Veening *et al.*, 2009).
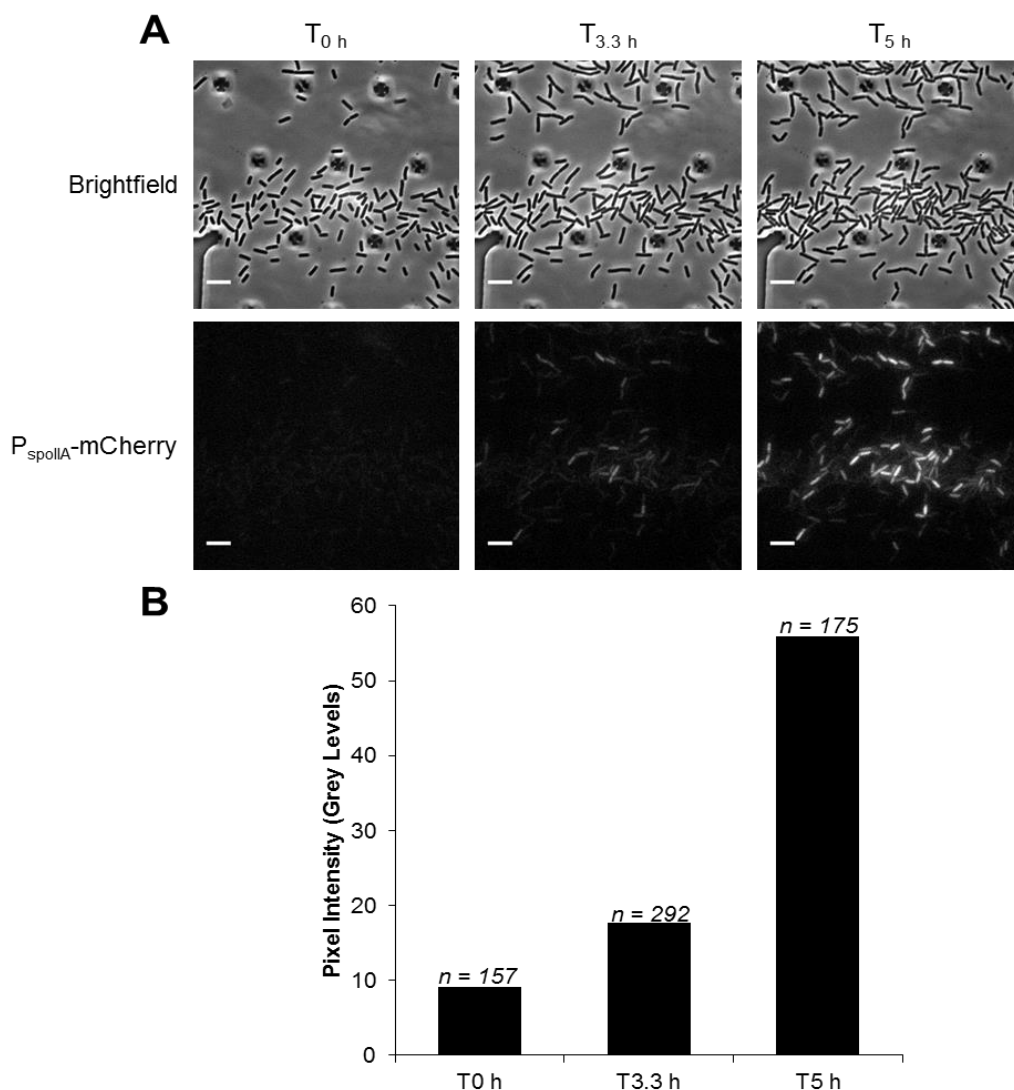
Figure 4.13 Activation of P_{spoIIA}-*mcherry* in the ONIX chamber.

T = hours following loading into ONIX plate (A). The mCherry signal intensity of n-cells (shown above each bar) was measured and averaged for each time point (B). Cells were randomly selected from the imaging field. Images were acquired every 3 min. Scale bar = 5 µm. Strain used = DMR081).

Satisfied that sporulation could be induced efficiently in the ONIX chamber the system could now be used to investigate origin dynamics in the mutants.

The relative cellular position of the origin marker (Spo0J-GFP) was imaged by time-lapse microscopy every three minutes. Kymographs provide a convenient way to illustrate the movement of objects in time lapse image series (see Figure 4.14), which in all subsequent experiments in this chapter were normalised so that they began 1 h prior to the formation of the asymmetric septum (displayed in red).
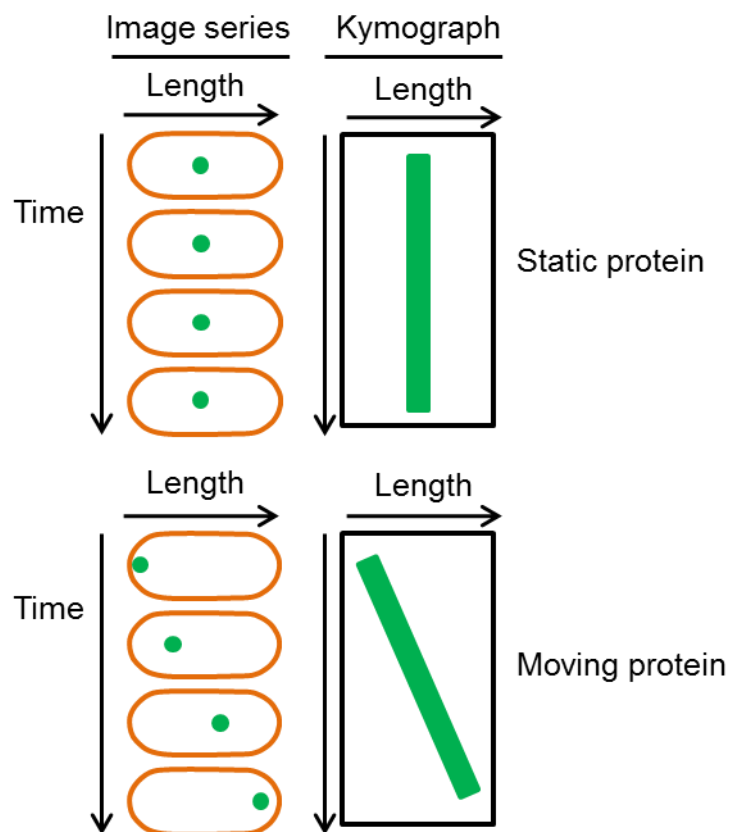
Figure 4.14 Kymographs display protein movement during time lapse microscopy. If a protein (green spot) remains static in multiple frames, the kympgraph profile would appear as a verticle line (top). By contrast, if the protein moves (e.g. left to right), the kymograph plot will display as a non-vertical profile (bottom).

Figure 4.15 shows representative kymographs of origin dynamics in wild type and *ΔcomN* cells. Using Spo0J-GFP, it is clear that following rapid movement to the cell poles, origins become highly constrained in wild type cells (Figure 4.15A, green

vertical lines), consistent with them being anchored to the cell pole. Anchoring appeared to occur at least 30 min prior to asymmetric septation, which was detected by the bright red transverse fluorescent band and vertical red line in the kymograph. Origins then remained closely apposed to the cell pole in both the prespore and the mother cell for up to 100 minutes following asymmetric division. In the *ΔcomN* mutant, however, origin movement was more irregular, with more fluctuations in position between frames and less processivity of movement towards the pole (Figure 4.15B, C). In the majority of examined cells (6 of 10), the origin failed to be captured in the prespore (Figure 4.15B). In the remaining cells, the origin was either captured, or was rapidly translocated into the prespore immediately prior to asymmetric cell division (Figure 4.15C, yellow arrow).

A

60 min 72 min 84 min 102 min 126 min 152 min 167 min 182 min

Spo0J-GFP   Membrane   Merge

1 h

3 h

Wild type

B

90 min 117 min 126 min 138 min 156 min 168 min 186 min 270 min

Spo0J-GFP   Membrane   Merge

1.5 h

3.5 h

ΔcomN origin-out

C

273 min 297 min 324 min 348 min 357 min 372 min 399 min 428 min

Spo0J-GFP   Membrane   Merge

4 h

6 h

ΔcomN origin-in
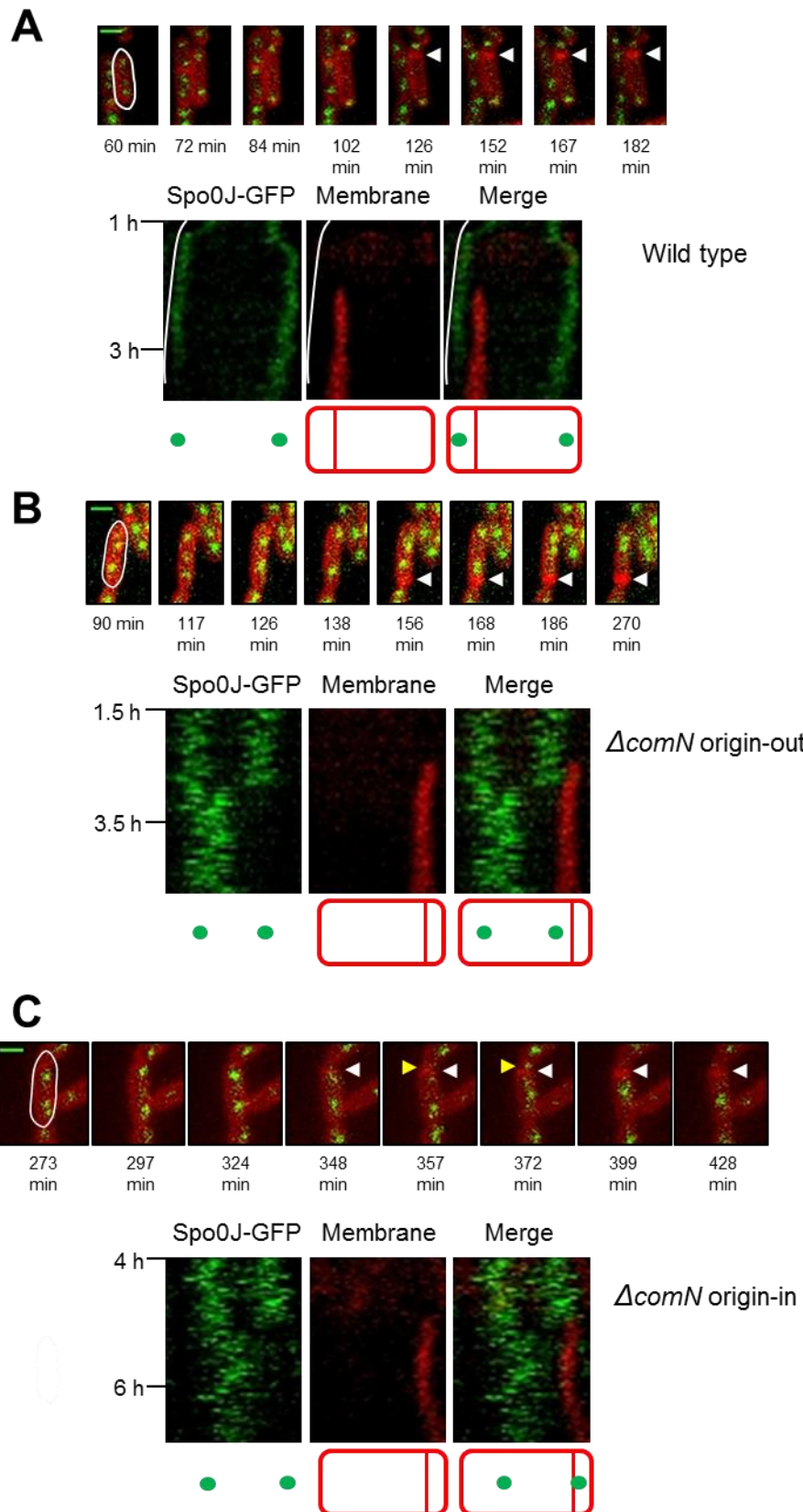
Figure 4.15 *ΔcomN* mutant displays increased origin movement in time lapse microscopy.

In all cases, top panels show stills of cells during time lapse, followed by representative kymograph plots with a schematic of the final frame below. Wild type (A) ΔcomN with origin trapped out (B) and ΔcomN with origin within prespore (C). Scale bar = 1 μm. White arrow = site of asymmetric septation. Yellow arrow = translocation into prespore. The white line around the cell in still number 1 represents the analysed cell in each instance. Temperature = 32°C. Wild type = DMR145; *ΔcomN* = DMR147.

Similar experiments were conducted with a *ΔracA* mutant (Figure 4.16). Again, origins were seen to segregate smoothly and rapidly to cell poles in wild type cells, after which they were anchored in 8 of 10 analysed cases (Figure 4.16A). This was not the case in the *ΔracA* mutant, where increased fluctuation in origin movement was seen, along with a concomitant decrease in the frequency of origin trapping in the prespore (Figure 4.16B, 6 of 11 cells). Occasionally, the origin was resident in the prespore area (Figure 4,16C, 5 of 11 cells) upon which it was constrained and sporulation was able to progress. Taken together, these results suggest that the origin region exhibited increased fluctuation and decreased processivity in both *ΔracA* and *ΔcomN* mutants.

A

60 min   78 min   90 min   108 min   135 min   162 min

Spo0J-GFP   Membrane   Merge

1 h

3 h

Wild type
8/10 cells

B

234 min   255 min   279 min   394 min   354 min   381 min

Spo0J-GFP   Membrane   Merge

3.9 h

5.9 h
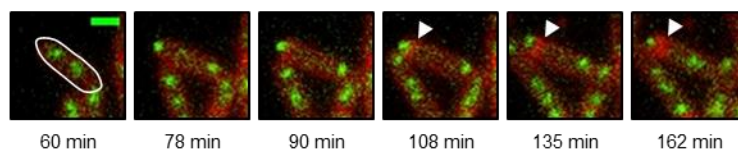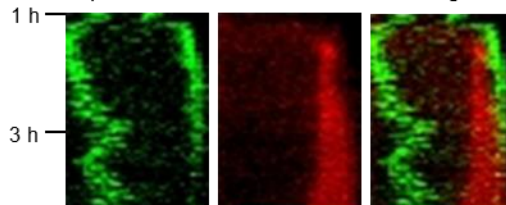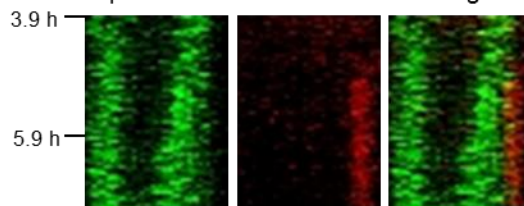
ΔracA origin-out

6/11 cells

C

234 min   279 min   285 min   297 min   315 min   369 min

Spo0J-GFP   Membrane   Merge

3.7 h

5.7 h
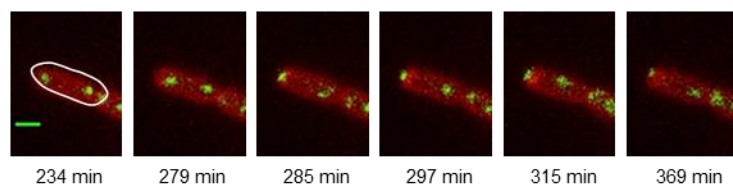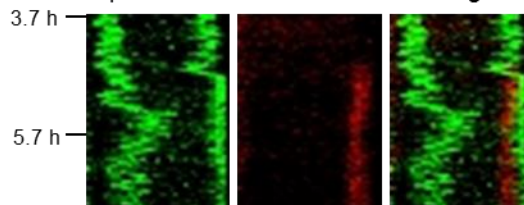
ΔracA origin-in

5/11 cells

Figure 4.16 Increased dynamics of the *ΔracA* mutant.

In all cases, top panels show stills of cells during time lapse, followed by representative kymograph plots with a schematic of the final frame below. Wild type (A); *ΔracA* with origin trapped out (B) and *ΔracA* with origin within prespore (C). Scale bar = 1 µm. White arrow = site of asymmetric septation. The white line around the cell in still number 1 represents the analysed cell in each instance. Temperature = 32°C. Wild type = DMR145; *ΔracA* = DMR146.

4.3. Discussion

From genetic screening, Kloosterman *et al.,* 2016 were able to identify two novel factors, ComN and MinD, involved in capturing the origin region at the cell pole during sporulation. Both proteins were known to have different established roles in vegetative growth that were distinct from chromosome capture (Section 4.1).

Initial experiments were focussed on establishing the localisation of ComN-GFP and GFP-MinD in the early stages of sporulation (Figure 4.2 and 4.3). As expected, these proteins were found to localise to both the asymmetric septa and cell poles in both sporulating and non-sporulating cells. The polar localisation is consistent with a direct role in origin capture. Evidence suggests that the localisation of both of these proteins at the cell pole is dependent upon the major polar hub protein DivIVA, which binds negatively curved membranes in bacteria (Bramkamp *et al.*, 2008; Lenarcic *et al.*, 2009; dos Santos *et al.*, 2012; Strahl and Hamoen, 2012). As a result, the localisation of DivIVA-msfGFP was also examined (Figure 4.4). I confirmed that DivIVA was localised at cell poles and septa during sporulation, as expected. Curiously, DivIVA also occasionally localised to what appeared to be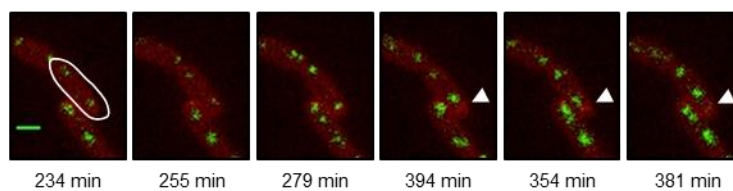 a second asymmetric site at $T_{80 \text{ min}}$ with no corresponding sign of cell division in the membrane stain (Figure 4.4, yellow arrows). The precise biological function of this DivIVA localisation is likely to be a by-product of divisome re-localisation to opposite cell poles during early sporulation (Ben-Yehuda and Losick, 2002), and different developmental rates of the two septa. A similar localisation pattern has also been reported for the septum-located SpoIIE protein (Wu *et al.*, 1998). It has been reported that SpoIIDMP is critical for preventing a second division event at the prespore distal pole, (Lewis *et al.*, 1994; Eichenberger *et al.*, 2001), however the initial Z-ring assembly at this site would lead to slight negative membrane curvature and recruitment of DivIVA prior to such inhibition.

Since *comN* and *minD* mutants exhibited a similar trapping phenotype (Kloosterman *et al.*, 2016), the clear co-localisation of GFP-MinD and mCherry-ComN signals during both vegetative growth and sporulation (Figure 4.8) was indicative of a possible functional relationship between these two factors. Critically for origin capture, co-localisation was observed at the cell poles (Figure 4.8) (Kloosterman *et al.*, 2016).

Some of the polar complex hierarchy had been previously established (Bramkamp *et al.*, 2008; dos Santos *et al.*, 2012). A logical next step was therefore to determine whether a functional hierarchy existed between the two newly implicated capture proteins. To test this, GFP-MinD and ComN-GFP were imaged in *ΔcomN* and *ΔminD* backgrounds, respectively (Figures 4.5 and 4.7). From single cell quantification of GFP-MinD in *ΔcomN*, polar signal was seen in ~30% of cells. This could be explained by the fact that MinD can also be recruited to the pole by DivIVA-MinJ in the Min-pathway. Indeed, the results shown in Figure 4.5 are in agreement with single cell characterisation of the *ΔminD* origin trapping defect performed by Kloosterman *et al*, 2016. It is possible therefore that the success of origin capture is correlated to the precise way MinD is recruited to the pole

There also appeared to be an increase in the background GFP-MinD signal intensity across the cell length compared to the wild-type (Figure 4.6A), possibly reflecting the absence of concentrated MinD at the pole. Although there was a slight elevation in GFP signal at the septum, this difference could be ascribed to the presence of double membranes. This is in contrast to the cell pole with its single membrane, where only background GFP-MinD signal was seen in the *ΔcomN* strain, suggesting no specific enrichment.

A *ΔminD* mutant exhibits a severe minicell phenotype (de Boer *et al.*, 1989; Marston *et al.*, 1998). Since GFP-MinD appeared absent at the cell pole in most of the *ΔcomN* mutant cells, this begged the question as to why there was no significant minicell phenotype in a *comN* deletion? One answer is that ComN is not the only recruiter of MinD. In fact, as is known, MinJ can recruit MinD to the pole in *B. subtilis* as well as in other organisms such as *Listeria monocytogenes* (Bramkamp *et al.*, 2008; Kaval *et al.*, 2014), as part of the "Min-system" for preventing misplacement of the divisome at the cell pole (Figure 4.17, below). Since there was no detectable GFP-MinD in a significant proportion of cells in the *ΔcomN* mutant (Figure 4.5), this result suggested that the amount of MinD required for chromosome capture is different and critically, is higher, than that for division site placement. By contrast, there was no effect on polar ComN recruitment in the presence or absence of MinD (Figure 4.7), suggesting ComN acts upstream of MinD (generating a hierarchy of DivIVA-ComN/MinJ-MinD).

ComN-mediated recruitment of MinD may lead to sufficient protein at the pole for successful origin capture. Higher levels of MinD may be critical for the recruitment of further chromosome segregation factors, such as Soj (Errington *et al.*, 2005; Murray and Errington, 2008), as compared to the levels required for the recruitment of MinC (Figure 4.17, below). It remains to be established whether the ComN-recruited MinD and MinJ-recruited MinD are held in different conformations or activities (sufficient for chromosome capture or division site placement, respectively). Taken together, it appears that the higher levels of MinD required for chromosome capture (as compared to divisome placement) are mediated by two distinct proteins: ComN and MinJ, respectively.

To establish whether the single and double (*ΔcomN ΔracA*) mutants displayed any sporulation defects, efficiencies of phase bright spore formation determined via microscopic imaging was used to assess sporulation efficiency for the mutants. This approach was chosen over the plating of heat-resistant spores after 9 hours of sporulation because the *ΔminD* mutant appeared to display significant lysis after about 6-7 hours, which could artificially raise the sporulation efficiency of this mutant. From Figure 4.9 it is clear that the single mutants were not severely defective in phase bright spore formation at $T_{6\,h}$. There was possibly a slight delay at $T_{5\,h}$, but the nevertheless respectable levels of sporulation may be because of the continued function of the SpoIIIE DNA pump present in the asymmetric septum. Origin out and arm in localisation coupled to SpoIIIE pumping may cause a delay in spore formation, but not its abolition. A *ΔminC* mutant (which does not affect origin anchoring) was also included to confirm that minicell formation did not adversely affect sporulation efficiency. Strikingly, the *ΔracA ΔcomN* double mutant was severely defective in sporulation. Kloosterman *et al.,* 2016 previously demonstrated that *ΔcomN* and *ΔminD* mutants are defective in capturing the origin region, whereas *ΔracA* is critical in capturing the arm-proximal region. This, combined with the limited sporulation defects in the single mutants but severe defects in the double mutant (*ΔcomN ΔracA*), are consistent with the notion that there are two genetically separable systems that operate to anchor the chromosome to the cell pole (Wu and Errington, 2003),which we term the RacA capture pathway and the *parS* capture pathway (Figure 4.17).

RacA capture pathway **parS capture pathway**

RacA interacts directly with **DivIVA** and the *ram* sites just left of *oriC*

A polar complex of proteins target the origin, which have the hierarchy of recruitment :
DivIVA>**ComN**-**MinJ**>**MinD**>**Soj**/**Spo0J**-*parS*
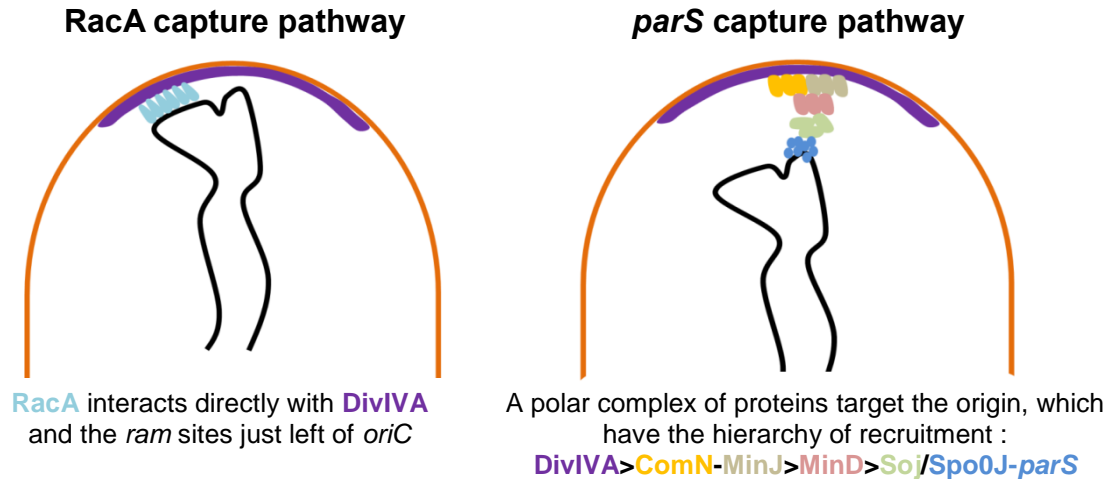
Figure 4.17 Two pathways anchor the origin at the cell pole during sporulation.
The RacA pathway (left) anchors the origin proximal arm region to the cell pole directly through interactions with *ram* sites on the DNA. The *parS* capture pathway (right) involves a hierarchical complex of proteins that recruit and retain the origin (*parS*) region at the pole.

The *parS* pathway involves the newly identified factors ComN and MinD, as well as the previously established proteins involved in polar chromosome segregation: Soj (which is recruited to the pole by MinD) and Spo0J, which binds the origin region via *parS* sites (Lin and Grossman, 1998; Wu and Errington, 2003; Errington *et al.*, 2005; Murray and Errington, 2008).

To further characterise the chromosome capture defects in the RacA and *parS* pathways, single cell time lapse microscopy of origin movement was developed using the CellASIC ONIX microfluidics system. Initial experiments focussed on developing an optimised protocol for sporulation (Table 4.1). This was necessary because during normal re-suspension experiments, the presence of traces of rich CH medium that is left in the flask appears to be crucial for efficient sporulation, probably to enable the now severely nutrient-limited cells to maintain energy until a commitment to sporulation is made. If cells are re-suspended without these trace nutrients, widespread cell death may occur due to the loss of membrane potential caused by the sudden and sharp decrease in nutrients, which triggers protein mis-localisation, cell division, growth and viability defects (Strahl and Hamoen, 2010). The optimal condition for sporulation in the chamber involved allowing cells to adapt to the nutrient down-shift in the flask for 1 h, followed by supplementation with 0.57% rich

medium in the flask for the first hour. This was the first demonstration of sporulation within the CellASIC ONIX microfluidic chambers. It was subsequently highlighted that agarose pad-based time lapse approaches may influence sporulation through local changes in nutrient availability in the agarose proximal to the cells over long periods of time (Richard Losick, Harvard University, personal communication), a process largely mitigated in the constant-flow microfluidic based approaches, such as the ONIX used here.

The optimized ONIX system provided a powerful way to quantitatively analyse origin behaviour during sporulation. Origins were rapidly segregated and anchored to the cell pole in wild type cells (Figures 4.14A and 4.15A). By contrast, both mutants of *ΔcomN* (Figure 4.14B-C) and *ΔracA* (Figure 4.15B-C) clearly showed less anchoring to the cell pole. This was deduced from the increased fluctuations in GFP signal that was observed in the kymographs for these mutants. Despite this increased movement, origins were captured by (or subsequently pumped into) the prespore in only a proportion of the cells (~40-45%). As RacA and ComN operate in genetically separable systems (the RacA and *parS*, respectively), it is possible that in the mutants either the arm-proximal region (in *ΔracA*) or the origin region (in *ΔcomN*) are not tethered to the pole, leading to increased Brownian motion and concomitantly greater chances that the origin is incorrectly localised within the mother cell upon septum formation (as shown in Figure 4.10, option 1). It would be interesting to quantify the extent of the increased origin movement in the capture mutants. However, this would require optimising origin tracking, and measuring the distance of the origin to the cell pole in each frame. Due to time constraints, and given the amount of bioinformatic development required, this was not conducted in the project at this time.

Taken together, the results presented in this chapter have confirmed the presence of two capture systems for ensuring successful segregation of the chromosome to the cell pole during sporulation: the RacA- and *parS*-capture pathways (Figure 4.17). Furthermore, two newly identified proteins in the *parS* pathway (ComN and MinD) have been further characterised visually, with ComN being critical for the recruitment of MinD at the cell pole. Using a novel time-lapse microfluidics approach that was optimised for this project, null mutants of these proteins exhibited defects in chromosome anchoring. Since MinD is known to be important for the recruitment of Soj (Marston and Errington, 1999; Autret and

Errington, 2003; Murray and Errington, 2008), which in turn interacts with the Spo0J-DNA complex, understanding the precise role of these downstream proteins will be critical to furthering our understanding of the mechanism of polar chromosome segregation.

Chapter 5

The role of Soj in chromosome segregation during sporulation in *Bacillus subtilis*

5.1 Introduction

Soj (ParA), the focus of this chapter, has two known cellular roles in *B. subtilis*: controlling DNA replication initiation and chromosome segregation. Soj is a ParA ATPase family member, expressed from a conserved locus in the origin region of the chromosome in *B. subtilis*. This locus also contains the gene for Spo0J (ParB) as well as a *parS* sequence (Gerdes *et al.*, 2000; Livny *et al.*, 2007), which together make up the *B. subtilis* chromosomally encoded ParABS system. The *spo0J-soj* locus was first identified through mutations that block entry into sporulation (Ireton *et al.*, 1994; Sharpe and Errington, 1996).

In *B. subtilis* extensive work has established a role for Soj as one of the critical regulators of DNA replication initiation (Murray and Errington, 2008; Scholefield *et al.*, 2012). Depending upon the nucleotide state of Soj, the protein can either activate or inhibit the master initiator of DNA replication, DnaA. Under conditions in which the ATP-dimeric form of Soj accumulates – either through deletion of the ATPase activator (Spo0J) or by a point mutation in Soj (D40A) that prevents ATP hydrolysis – DNA replication is stimulated (Ogura *et al.*, 2003; Lee and Grossman, 2006; Murray and Errington, 2008). On the other hand, mutant alleles of monomeric Soj (G12V) that prevent ATP-monomers dimerising, act to inhibit DnaA activity and, as a result, inhibit DNA replication. More specifically, monomeric Soj (or Soj^{G12V}) can directly bind to the AAA+ domain of DnaA, and this interaction prevents DnaA helix formation on the DNA in the initial stages of DNA replication initiation (Scholefield *et al.*, 2012). These studies highlighted the important role of Soj/Spo0J in DNA replication; Spo0J drives dimeric ATP-Soj to the monomeric form, switching Soj from an activator to an inhibitor of DNA replication *in vivo* (Scholefield *et al.*, 2011).

In *B. subtilis*, Soj and Spo0J have also been implicated in the accurate segregation of the chromosome, since *Δsoj* mutants exhibit an origin segregation

defect when analysed in vegetative cells using single cell microscopy (Wang *et al.*, 2014a). The segregation phenotype was more severe in *Δsmc Δsoj* double mutants (Lee and Grossman, 2006). Other work concerning the role of Soj in chromosome segregation has been investigated in studies of sporulation. Although a *Δsoj* strain was shown to have a minor defect in the formation of heat-resistant spores (Ireton *et al.*, 1994), subsequent studies have revealed that Soj plays an important role, alongside the sporulation specific protein RacA, in capturing and/or moving the segregating origins at opposite cell poles during axial filament formation (Wu and Errington, 2003; Sullivan *et al.*, 2009; Duan *et al.*, 2016; Kloosterman *et al.*, 2016).

Chapter 4 described aspects of the operation of two genetically separable polar origin capturing complexes – the RacA and *parS*-systems (Kloosterman *et al.*, 2016). As described earlier (Chapter 1), the first of these involves direct anchoring of origin-proximal DNA by RacA, which binds directly to the DNA at RacA-binding motif (*ram*) sites, distributed to the left of *oriC* (Ben-Yehuda *et al.*, 2003b; Wu and Errington, 2003) (Wu and Errington, 2002). The second *parS*-capture system includes a set of proteins (MinJ, ComN, MinD and Soj) that ensure correct capturing of the origin region itself (as opposed to the *ram* sites) (Wu and Errington, 2003; Duan *et al.*, 2016; Kloosterman *et al.*, 2016). The recruitment of the factors involved in both of these systems at the cell poles is dependent upon the major polar hub protein DivIVA (Ben-Yehuda *et al.*, 2003b; Kloosterman *et al.*, 2016), which preferentially binds to membranes of negative curvature (Strahl *et al.*, 2015; Kloosterman *et al.*, 2016).

Despite being implicated as an important member of the *parS*-capture pathway, the precise mechanistic role of Soj in origin segregation and capturing at the cell pole remains unclear (e.g. is it involved in directly moving the origin, inhibiting origin movement or as the tip of the polar hub that binds *oriC*?). This is in part due to redundancy in polar origin capturing and the difficulty in directly observing Soj *in vivo*. As necessary steps in elucidating the mechanism of Soj action, the main aims of this chapter were to:

1. Perform and optimise protein localisation studies of Soj in the early stages of sporulation
2. Conduct real-time visualisation of origin segregation dynamics in a range of mutant backgrounds,

3. Study the effect of various *soj* ATPase mutations on origin and arm capturing in the prespore using the established chromosome trapping assays (Sullivan *et al.*, 2009; Wagner *et al.*, 2009; Kloosterman *et al.*, 2016)

5.2 Results

5.2.1. Localisation of Soj

To decipher the role of Soj in origin segregation and capture during sporulation, it was important to improve our understanding of its localisation dynamics. Early imaging of an inducible copy of Soj suggested that the protein was highly dynamic, being localised to cell poles as well as jumping between nucleoids within the cell (Marston and Errington, 1999; Autret and Errington, 2003). It was also shown that the localisation of Soj at the division site and cell poles was dependent upon MinD (and not MinC) (Autret and Errington, 2003). However later GFP-Soj constructs, expressed from the native locus using the native P_{soj} promoter, failed to reproduce the nucleoid jumping although they did confirm the dependency of MinD for Soj localisation at the cell pole (Murray and Errington, 2008). GFP-Soj was also seen as foci within the cytoplasm, co-localising with both Spo0J and DnaA at origin regions. These foci are compatible with the known role of Soj in DNA replication initiation (Murray and Errington, 2008).

Conflicting historical results from the same laboratory made it pertinent to re-test Soj localisation in our current experimental conditions using a fully native GFP-Soj fusion (Figure 5.1). These data show clear Soj accumulation at septa and as punctate cytoplasmic foci. This localisation pattern was strikingly reminiscent of that previously observed in the more recent studies (Murray and Errington, 2008). There was no visual evidence for rapid nucleoid jumping (data not shown).
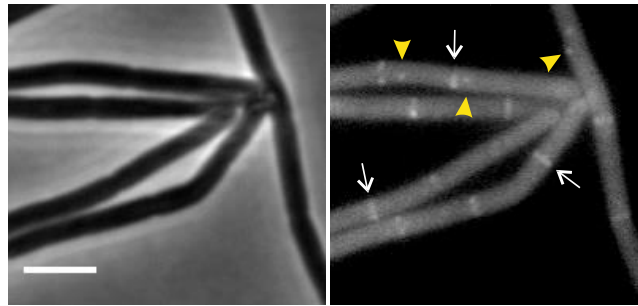
Figure 5.1 GFP-Soj localisation during vegetative growth.

Localisation of GFP-Soj (DMR065) was determined by epifluorescence microscopy. Cells were grown in CH medium at 37°C. White arrows = septal localisation; yellow arrowheads = cytoplasmic localisation. Scale bar = 3 µm.

Although Figure 5.1 was able to reproduce the previously observed localisation pattern of GFP-Soj (Murray and Errington, 2008), a very long GFP exposure time was required (5 sec) and signal intensity was low. In attempts to improve this, new fluorescent constructs of Soj were made using mNeonGreen (mNG). mNG (from *Branchiostoma lanceolatum*) was chosen as it is one of the brightest fluorescent proteins identified to date, is exclusively monomeric and is capable of rapid folding (<10 min) (Shaner *et al.*, 2013), potentially mitigating some of the problems encountered with the standard GFP. mNG fusions were therefore constructed to wild type Soj, the ATP-bound monomeric form (Soj(G12V)) and the empty monomer form (Soj(K16A)). All *soj* constructs bore the native P_{soj} promoter and were expressed from the native locus. Firstly, to confirm correct expression, Western blotting using anti-Soj antiserum was conducted (Figure 5.2).
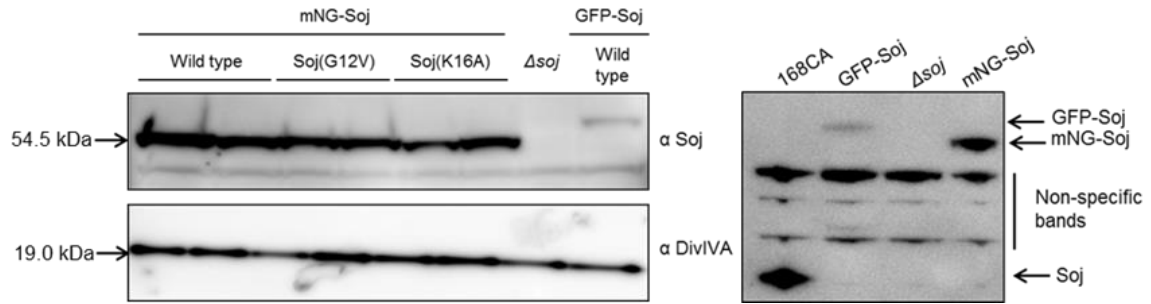
Figure 5.2 Construction of mNG-Soj fusion proteins.
(A) Two independent cell lysate samples expressing each fusion protein construct were Western blotted using anti-Soj antiserum (top panel, 1:5000). Bottom panel shows the same samples probed with anti-DivIVA (1:10,000) antiserum, as loading controls. Arrows indicate the anticipated MW of mNG-Soj or DivIVA. (B) Separate blot showing size of fusion proteins relative to native Soj. Arrows indicate expected size of products. Strains: mNG-Soj Wild type (DMR206); mNG-Soj(G12V) (DMR208); mNG-Soj(K16A) (DMR210); *Δsoj* = DMR065; GFP-Soj = DMR117.

The presence of bands of the expected size clearly demonstrated that all of the mNG-Soj constructs were present and expressed *in vivo* (Figure 5.2A), as was the original GFP-Soj. These bands were absent in the *Δsoj* strain. Interestingly, mNG-Soj seemed to be present at a higher level than GFP-Soj. Given the improved folding kinetics of mNG, it is possible that the latter fusion is more stable than the GFP equivalent, and that it more accurately represents native Soj expression levels. To test this, the wild type (168CA) as well as the mNG and GFP fusions were blotted (Figure 5.2B), which confirmed the higher expression of mNG-Soj compared to GFP-Soj. Some non-specific bands were seen in all cases. Next, the new mNG-Soj constructs were imaged in vegetative cells using optimised imaging settings and exposure times to assess whether the same or a different localisation pattern was observed using these new fusions (Figure 5.3).
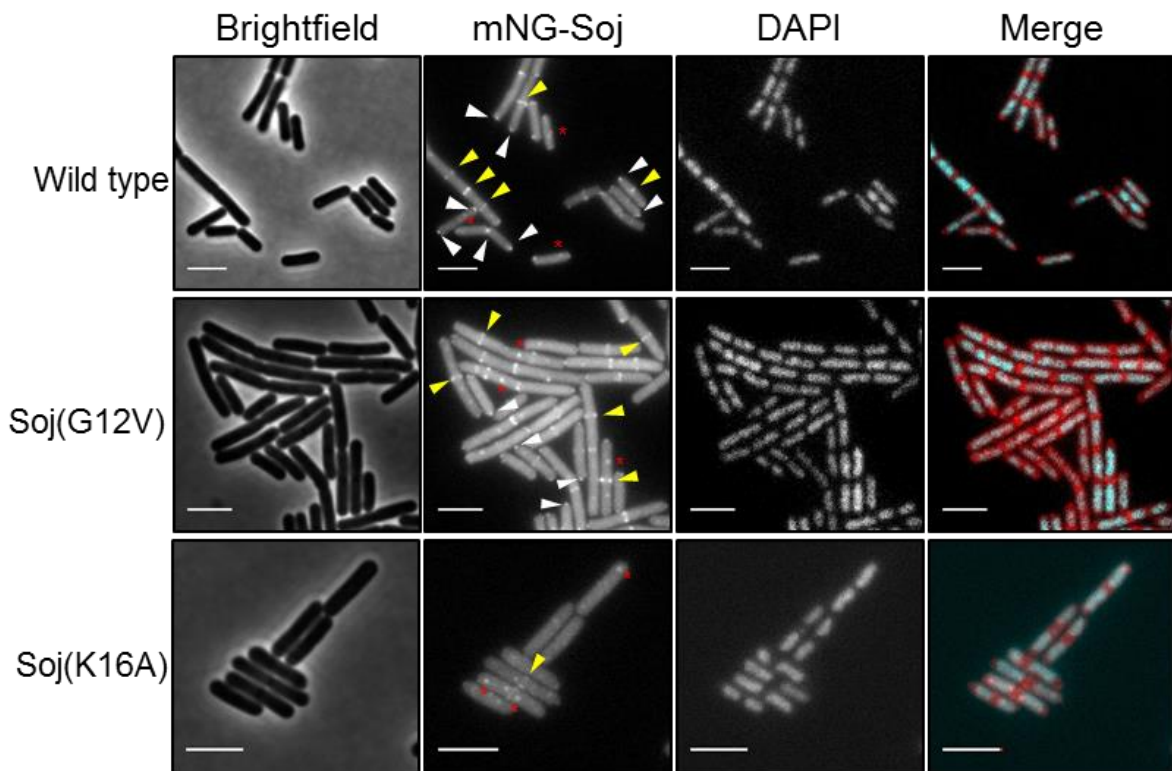
Figure 5.3 Localisation of mNG-Soj in vegetatively growing cells.
Wild type mNG-Soj (DMR206, top panels), mNG-Soj(G12V) (DMR208, middle panels) and mNG-Soj(K16A) (DMR210, bottom panels) were imaged using a Nikon Ti microscope. DAPI staining was used to visualise the nucleoids. White arrowheads = representative polar mNG-Soj foci; yellow arrowheads = representative septal mNG-Soj localisation and red asterisks = representative cytoplasmic mNG-Soj foci. Scale bars = 3 μm. Merge = mNG-Soj (red) and DAPI (blue). Images are representative of 3 independent experiments. BF exposure = 100 ms; GFP exposure = 4000 ms; DAPI exposure = 500 ms.

The new fusion construct showed improved signal intensity. In agreement with previous observations, the polar, septal and internal cytoplasmic foci were observed in wild type and Soj(G12V) strains using the mNG fluorophore (Figure 5.3) (Murray and Errington, 2008). With wild type and the two monomeric mutants, the cytoplasmic foci (red asterisks) also co-localised with nucleoids and were present at the leading edge of the chromosome (Figure 5.3), again in agreement with previous findings (Murray and Errington, 2008; Wang *et al.*, 2014a). It can therefore be concluded that the mNG-Soj constructs behaved as expected. One striking new observation, however, was the noticeable presence of mNG-Soj(K16A) at septa, albeit at a lower intensity than wild type or Soj(G12V). This showed that the enhanced mNG fluorescence is capable of revealing patterns previously undetectable, in this case with Soj(K16A), which was formerly presumed to be fully cytoplasmic (Murray and

Errington, 2008) (Figure 5.3, bottom panels, yellow arrow). To truly test functionality, the mNG-Soj fusions would need to be re-imaged in a Δ*spo0J* background.

Despite generating a more sensitive snapshot of the localisation of Soj, particularly Soj(K16A), the 488 nm (green) exposure was still longer than desirable (4 sec) since highly dynamic proteins such as Soj might display motion blur during image acquisition. The images described so far were generated using a fluorescent lamp-based excitation. Since laser-based excitation provides far greater power, the mNG constructs were next imaged using APO TIRF lasers (Figure 5.4).
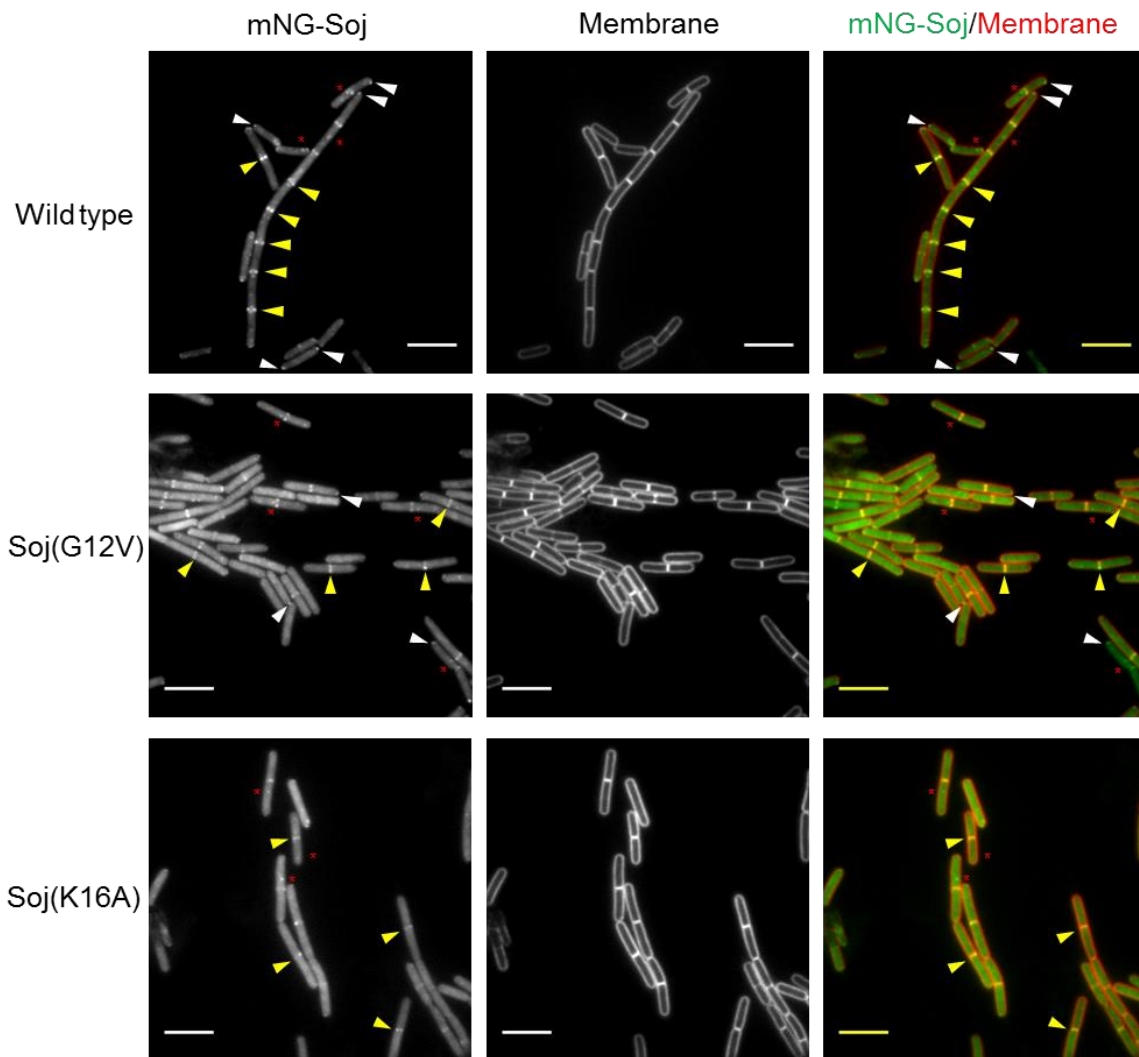
Figure 5.4 Localisation of mNG-Soj using APO-TIRF lasers.

mNG-Soj constructs of wild type Soj (DMR206, top panels), Soj(G12V) (DMR208, middle panels) and Soj(K16A) (DMR210, bottom panels) were imaged on 1 % agarose pads. Cells were incubated with FM5-95 membrane dye (100 µg/ml final concentration) for 5 min with shaking prior to spotting onto agarose pads. Coverslips were coated with 2 mg/ml polydopamine to minimise the hydrophobic FM5-95 binding non-specifically to the plastic coverslips. White arrow heads = polar mNG-Soj foci; yellow arrow heads = septal mNG-Soj; red asterisks = internal mNG-Soj foci. Scale bars = 5 µm. Exposure time = 1 sec.

Using laser-based epifluorescence microscopy and only a 1 sec exposure time (at 35% laser power to minimise cell damage) much sharper, well defined images were obtained (Figure 5.4). These strongly reinforced the previous observations that wild type mNG-Soj localised at septa, and as foci at cell poles and within the cytoplasm (Figure 5.4 top panels). This was also seen for the mutants (Figure 5.4, middle and lower panels), although it was noticeable that the mutants showed

increasingly lower signal to noise at poles and cytoplasmic foci, and greater cytoplasmic signals. It is possible that such observations were overlooked in earlier studies that utilised the weaker GFP reporter and less sensitive cameras.

Although Quisel *et al.,* 1999 investigated Soj localisation in stationary phase cells, to our knowledge; the localisation of Soj 80 minutes after re-suspension into sporulation medium has not been investigated. Since Soj is somehow involved in polar origin capture (as a member of the *parS* pathway), and its presence at septa and poles is dependent upon MinD (Marston and Errington, 1999; Autret and Errington, 2003; Murray and Errington, 2008), which is in turn dependent upon MinJ and ComN (Bramkamp *et al.*, 2008; Kloosterman *et al.*, 2016), the localisation of Soj is likely to be central in its role for origin segregation and capturing at the pole. As a result of the hierarchical protein localisation dependency (Chapter 4), it is reasonable to suppose that Soj may act at the interface between the polar capture complex and the DNA/Spo0J nucleoprotein complex.

Formation of the axial filament, in which sister replicated chromosomes extend along the entire length, provides a convenient visual marker for movement of the origins to the cell poles during the onset of sporulation (Figure 5.5).
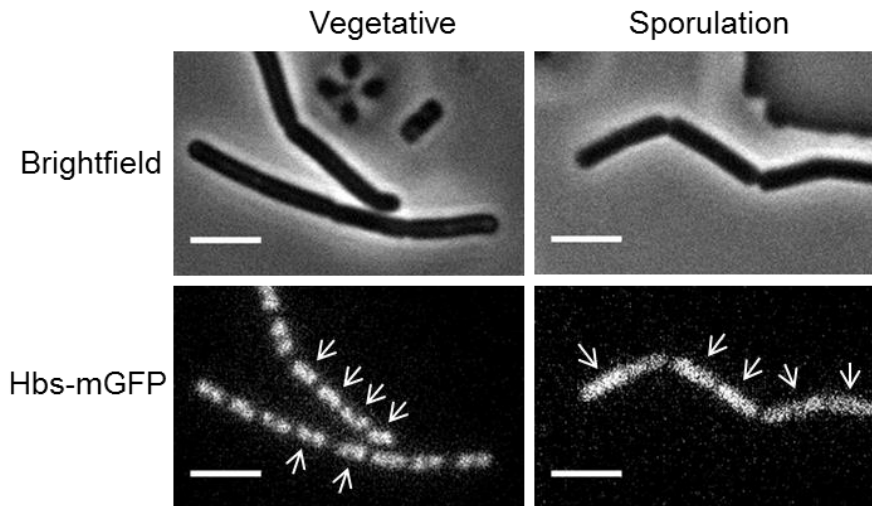
Figure 5.5 Axial filament formation as a marker for origin movement early in sporulation.

DNA was visualised using an mGFP fusion to the DNA binding protein Hbs (BWX2006). White arrows indicate compact vegetative nucleoids (bottom left panel) and elongated axial filaments (bottom right panel), respectively. Scale bars = 3 µm.

Hbs-GFP staining revealed condensed segregated nucleoids, in vegetatively growing cells (Figure 5.5, left panels). After sporulation was initiated, nucleoid staining revealed elongated structures, corresponding to the formation of axial filaments (Figure 5.5, rights panels).

Having established a pre-asymmetric division marker for sporulation, all mNG-Soj constructs (as before) could be co-imaged with a nucleoid marker to decipher the localisation of this protein during the critical origin moving and polar anchoring steps after the induction of sporulation (Figure 5.6).
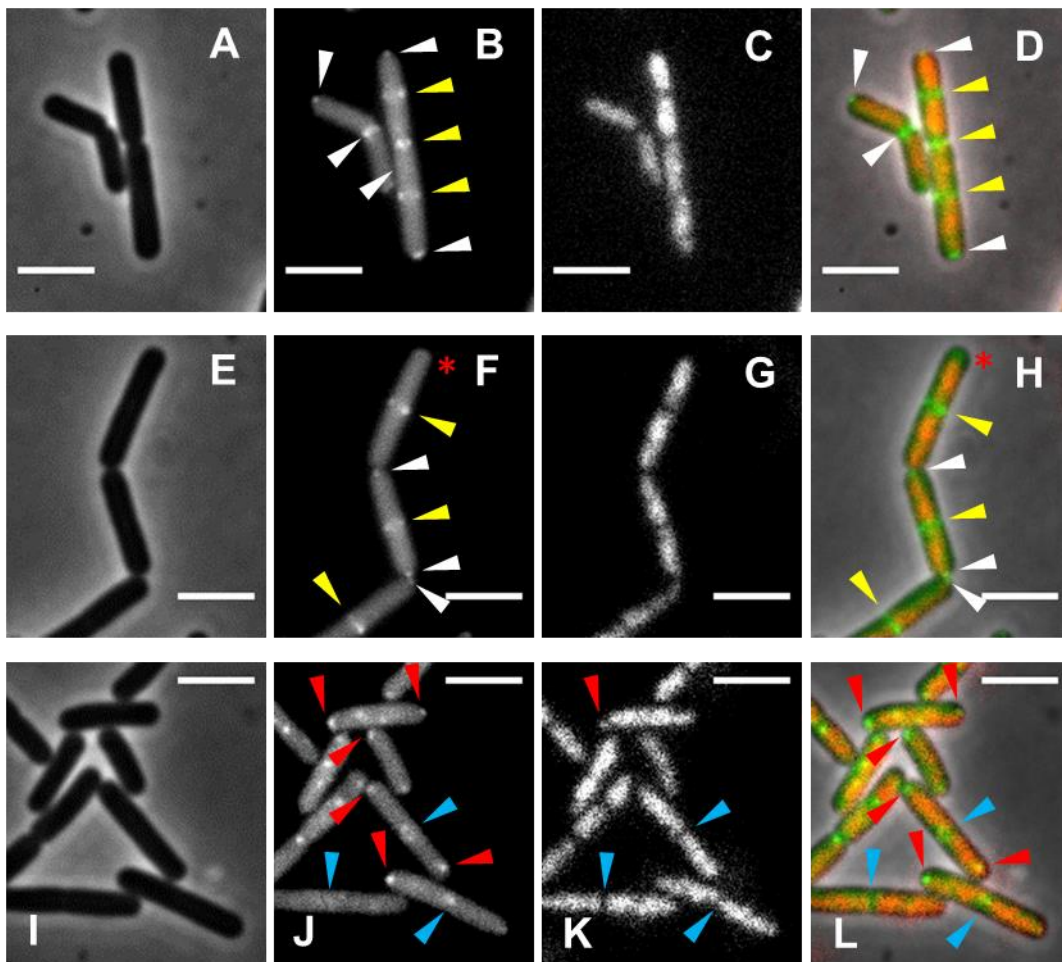
Figure 5.6 mNG-Soj localisation during sporulation

mNG-Soj wild type (A-D) (DMR206), G12V (E-H) (DMR208) and K16A (I-L) (DMR210) variants were imaged at $T_{80\ min}$ of sporulation. Panels A, E and I = Bright field; panels B, F and J = mNG; panels C, G and K = DAPI and panels D, H and L = merge (with mNG shown in green, DAPI in red and BF in grey). White arrows = polar mNG-Soj, yellow arrows = septal mNG-Soj, red arrows = internal mNG-Soj foci and blue arrows = division site but no detectable septal mNG-Soj. Scale bar = 3 µm.

In wild type cells, mNG-Soj was localised as discrete spots (cell poles) and bands (septa) (Figure 5.6A-D). A similar pattern was observed for the mNG-Soj(G12V) variant (Figure 5.6E-H); however, the signal intensity was generally lower in these cells. Furthermore, in some cells that appeared to be forming an axial filament there was a lack of detectable mNG-Soj(G12V) signal at the pole (Figure 5.6F, red asterisk). However, there was no detectable DNA in the pole region of this cell. Interestingly, bright polar foci of mNG-Soj(K16A) was observed in axial filament forming cells, which appeared to co-localise with the leading edge of the nucleoid, presumably at the origin (Figure 5.6J-L, red arrows). There was no detectable mNG-Soj(K16A) at septa (Figure 5.6I-L, blue arrows).

<u>5.2.2 Effect of *Δsoj* on origin movement and capture at the cell pole</u>

Using the origin trapping assay, Kloosterman *et al.*, 2016 established that around 40 % of cells failed to trap the origin marker in the prespore in *Δsoj* mutants, suggesting a potential role for Soj in capturing of the origin region. Furthermore, Wu and Errington, 2003 demonstrated that the entire origin region was excluded from the prespore in *Δsoj ΔracA* mutants. As these were end-point readouts, it was felt pertinent to test real time origin dynamics in these mutant backgrounds for the first time.
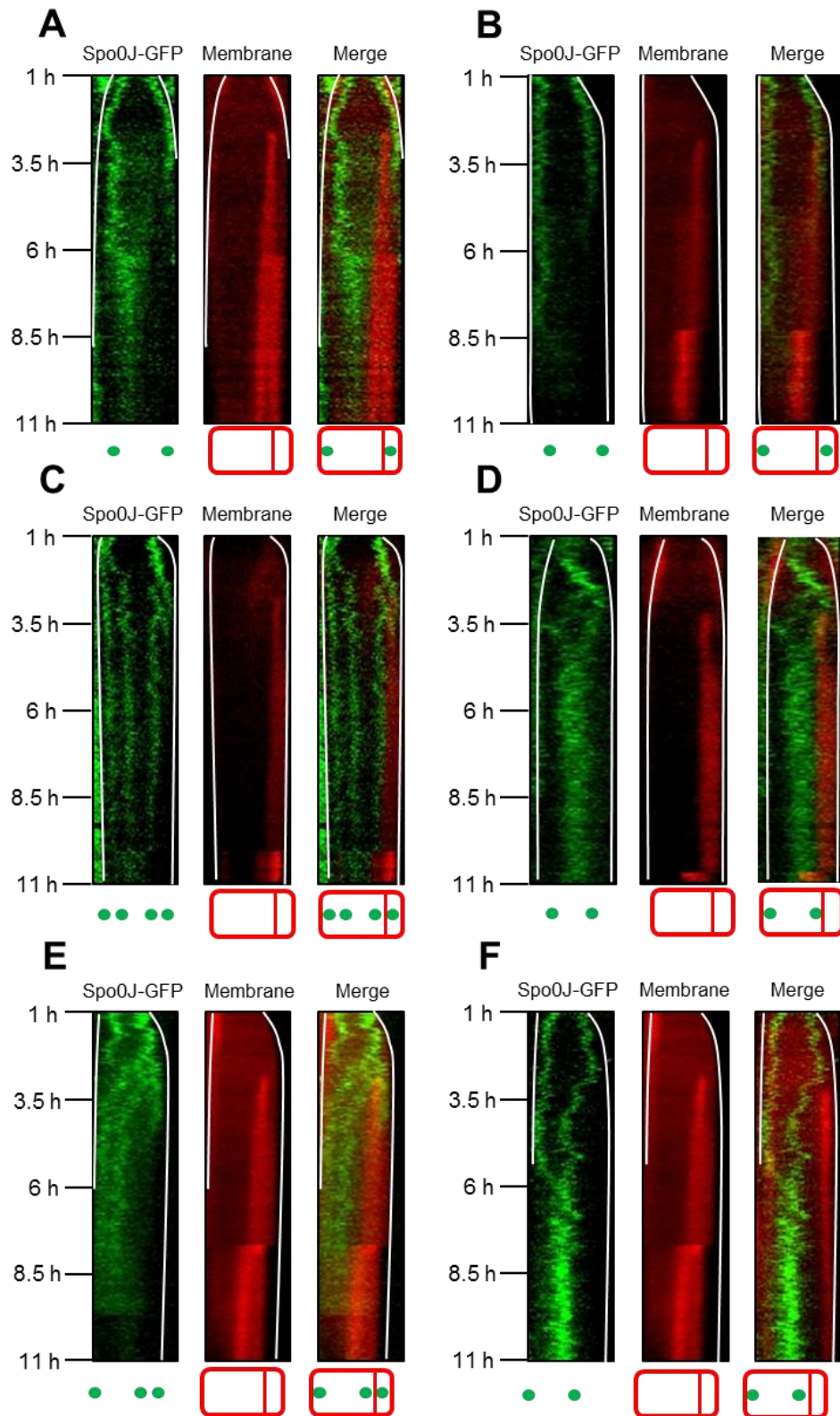
Figure 5.7 Origin dynamics in *Δsoj* and *Δsoj ΔracA* mutants.

Kymograph plots of origin (spo0J-GFP) dynamics in wild type (A); *Δsoj* (origin in prespore) (B); *Δsoj* (origin duplication) (C); *Δsoj* (origin out of prespore) (D); *Δsoj ΔracA* (origin duplication) (E) and *Δsoj ΔracA* (origin out of prespore) mutants (F). Images were acquired every 3 mins. White lines represent cell poles. Schematic under each cell represents the final frame. Abrupt brightening / broadening of the asymmetric septum signal corresponds to the

beginning of prespore engulfment. Strains: Wild type = DMR145; *Δsoj* = DMR159; *Δsoj ΔracA* = DMR173.

From the ONIX microfluidics, which as before utilised Spo0J-GFP as a marker for the origin (Chapter 4), origins in the wild type were seen to anchor to opposite cell poles prior to asymmetric septation, as expected (Figure 5.7A). Over the time course of imaging (10 h) prespores also became engulfed, as evidenced by the expanding membrane signal in the asymmetric septum and loss of the Spo0J-GFP signal in the prespore. A variety of phenotypes were observed in the *Δsoj* mutant. Some cells sufficiently segregated their origins such that the prespore origin was captured (Figure 5.7B). This was the most commonly observed pattern (5/10 cells) analysed cases). Despite capture, the origin may not have been as tightly anchored to the cell pole as in wild type, because the origin signal did not tightly overlap the cell membrane at the pole in this cell (indicated by the white lines, compare prespore origin in Figures 5.7A and B). A rarer phenotype was origin duplication (Figure 5.7C; 2/10 cells). This was unexpected because once sporulation initiates, initiation of DNA replication is normally inhibited through the action of the DnaA inhibitor, SirA (Jameson *et al.*, 2014). Previous studies with vegetative cells lacking Soj showed an over-initiation of DNA replication, probably due to the loss of DnaA regulation in this mutant (Murray and Errington, 2008). Possible reasons for the origin duplication seen here are discussed in section 5.3. Finally, a proportion of *Δsoj* cells (3/10 cells) exhibited both origins outside the prespore (as represented by Figure 5.7D).

The *Δsoj ΔracA* strain also exhibited both origin duplication and capture defects (Figure 5.7E-F). Furthermore, the origin region tended to be some distance from the cell pole (compare green signal not apposed to the cell pole (white line) in E-F), suggesting a complete failure of *ori* anchoring in these cells. These data support the origin trapping defects and previous results determined with these mutants (Wu and Errington, 2003; Kloosterman *et al.*, 2016), but reveal intriguing dynamics and positioning both before and after septum formation.

5.2.3 Effects of the Soj(G12V) substitution on chromosome dynamics during sporulation

Given that Soj is an ATPase, the ability of this protein to undergo a complete ATPase cycle, i.e. the ability to bind ATP, dimerise and hydrolyse ATP, might be critical for its function. Indeed, this is integral to the current model for chromosome segregation by the ParABS system in *C. cresentus* (Lim *et al.*, 2014). Biochemical data suggest that Soj(G12V) is proficient in ATP-binding but is unable to homodimerise, since the larger valine residue leads to steric hindrance in the dimerization interface (Leonard *et al.*, 2005; Murray and Errington, 2008; Scholefield *et al.*, 2011). To assess the effects of the G12V substitution, the mutant was examined using both the chromosome trapping assay and the origin-based microfluidic ONIX time-lapse microscopy (Figure 5.8-9).
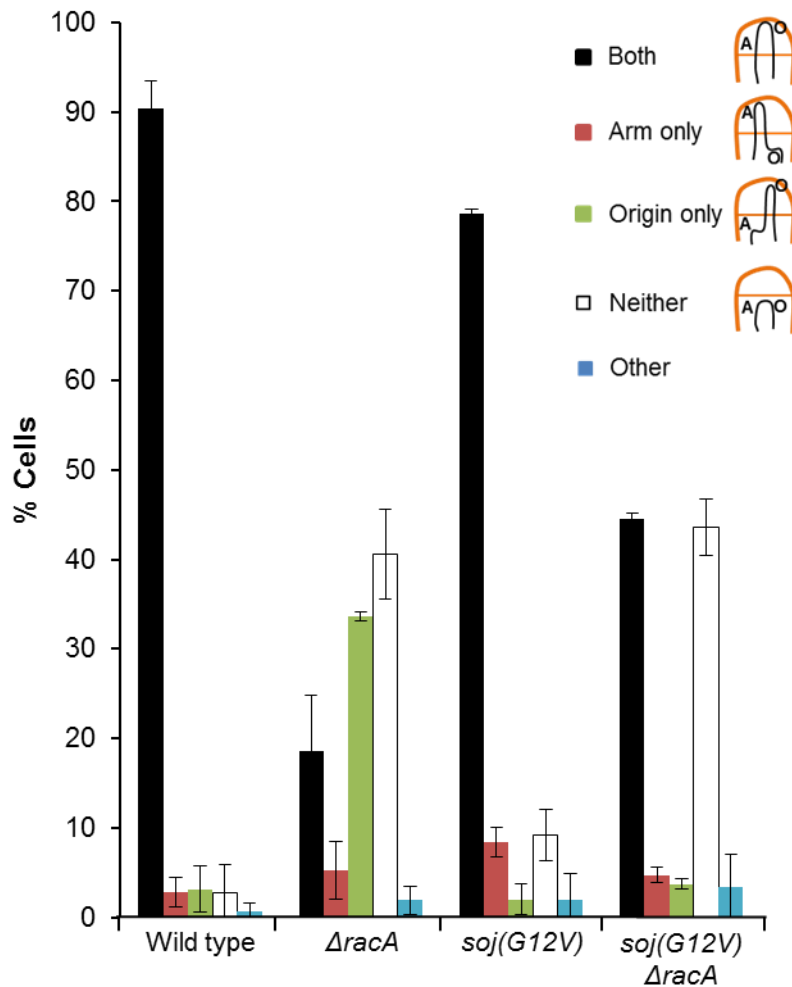
Figure 5.8 Soj(G12V) segregates and anchors the origin similarly to wild type.

Trapping assay to assess the prespore localisation of markers located at origin (-79 Kb from *oriC*) and arm (-418 Kb from *oriC*) regions. At least 100 cells were counted per repeat (n=3) for each mutant and average scores are shown. Error bars represent standard deviations. Images were acquired at T_{4h} of sporulation. Schematics show localisation of the origin (O) and arm (A) markers relative to the asymmetric septum and cell pole (orange). Other refers to signals not in the list (e.g. in both compartments). Strains: Wild type = DMR178; *ΔracA* = DMR190; *soj(G12V)* = DMR179; *soj(G12V) ΔracA* = DMR191.

The data from the origin trapping assays (Figure 5.8) report that the majority of wild type cells capture both the origin and arm regions in the prespore. Most surprisingly, however, the *soj(G12V)* mutant also trapped the origin and arm regions similarly to the wild type. Furthermore, the *ΔracA* single mutant either failed to trap both markers or captured only the origin. The latter was expected due to the presence of a functional *parS*-capture pathway in this strain. However, in the *ΔracA soj(G12V)* double mutant, the arm was trapped with the origin (labelled 'both') to a

higher level than in the *ΔracA* single mutant (with concomitantly fewer origin-only cells observed), while the proportion of cells that failed to trap either marker remained consistent. These data suggest that Soj(G12V) retains considerable activity for chromosome capture, and that the RacA and *parS* capture pathways provide similar contributions to polar origin trapping. Remarkably, it therefore appears that the ATP-bound monomeric Soj(G12V) mutant remains proficient in the origin capture pathway – perhaps even more proficient than wild type Soj.

To explore this further, origin movement was investigated in the *soj(G12V)* background (Figure 5.9).
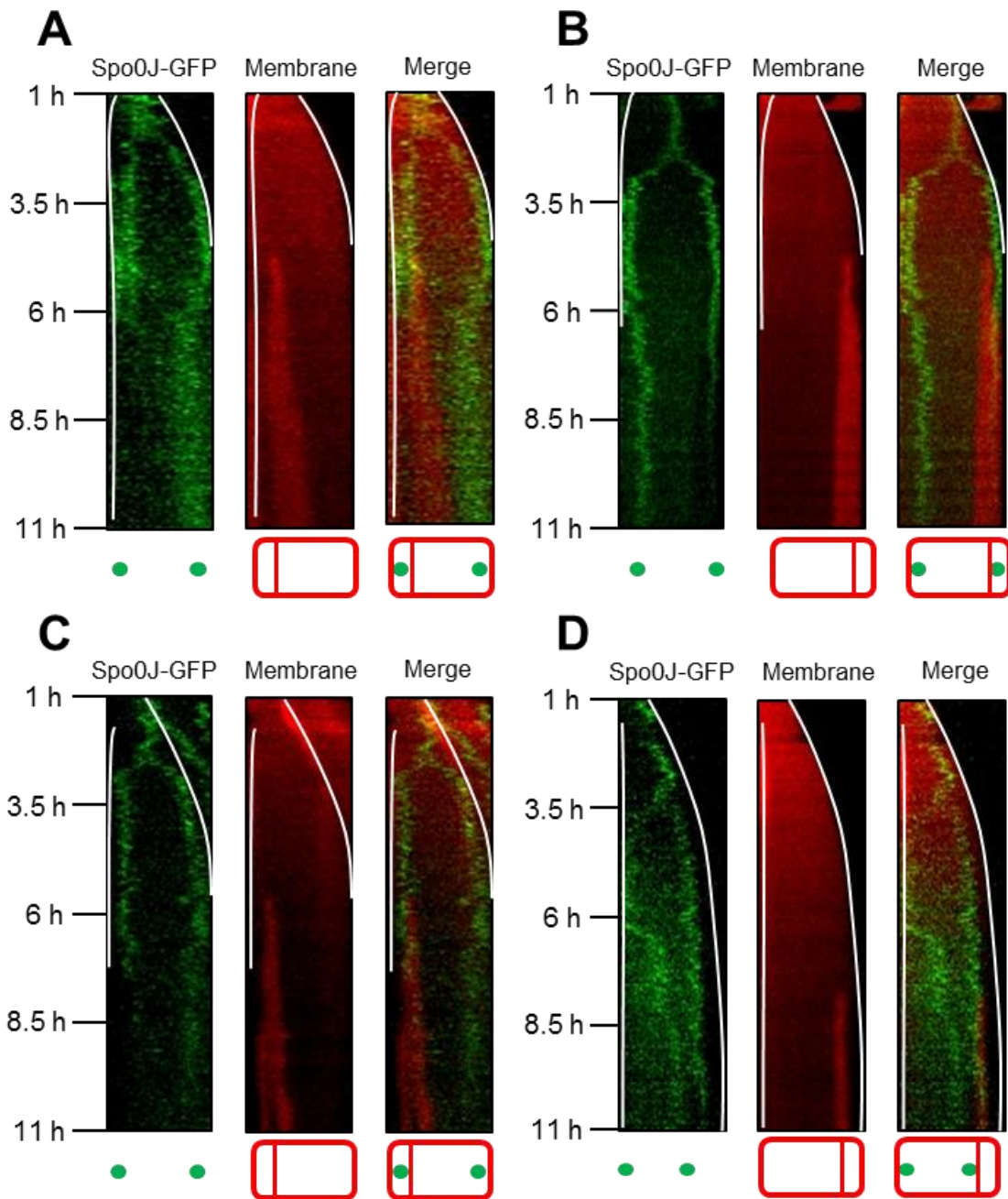
Figure 5.9 Kymograph plots of Soj(G12V) mutants. Representative kymograph plots of origin (Spo0J-GFP) movement in wild type (A); Soj(G12V) (B); Soj(G12V) *ΔracA* (origin captured in the prespore) (C); Soj(G12V) *ΔracA* (origin not captured in the prespore) (D). Time lapse microscopy was conducted using the ONIX microfluidics system and a schematic of the final frame is indicated below each plot. Images were acquired every 3 min. White lines represents the cell poles. Kymographs are representative of 6 analysed plots per mutant. Wild type = DMR145; Soj(G12V) = DMR157; Soj(G12V) *ΔracA* = DMR171.

Figure 5.9 confirmed that Soj(G12V) is functional for *ori* trapping and reminiscent of the wild type, since rapid segregation of the origins was followed by polar tethering for prolonged periods of time (up to 2 h) prior to asymmetric cell division (Figure 5.9A and B). However, in contrast to wild type, there appeared to be either one origin, or two linked origins, in Soj(G12V) for 1-2 h after the induction of sporulation (Figure 5.9B). This was followed by their rapid, non-random segregation to extreme cell poles in 33 min +/- 3 min (n= 5 analysed cells). Since time-lapse microscopy was conducted at low temperature (32°C), and segregation to poles occurred in approximately 30 minutes, it remains to be determined precisely *when* DNA replication initiated. It may be that origin movement occurred concomitantly with DNA replication fork progression, or that replication had already initiated prior to origin segregation. In the latter scenario, how the origins would remain linked, and the cue for their rapid segregation, is unknown.

Like the *soj(G12V)* mutant, *soj(G12V) ΔracA* double mutants appeared to enter sporulation with only a single origin visible. However, capture was less efficient, with some succeeding (Figure 5.9C) and others failing (Figure 5.9D) with equal frequencies (n=8 cells). In cells that succeeded, there was directed movement (~30 min +/- 3 min) but polar retention was less efficient (Figure 5.9C). This was expected due to the absence of RacA in these cells. Although the captured/non-captured ratio was consistent with observed trapping frequencies (Figure 5.8), since only 8 cells per mutant were analysed it remains to be determined whether this was a truly equivalent measurement to the trapping assay. Overall however, these observations strongly support the view that Soj(G12V) can act to move the origin, or that wild-type Soj holds *ori* in the vegetative quarter cell position until activated to segregate, which is then lost in the *soj(G12V)* mutant. Subsequently, RacA facilitates origin attachment to the poles.

5.2.4 Role of Soj(K16A) in chromosome dynamics during sporulation

Following the surprising finding that *soj(G12V)* mutants were proficient in rapid origin segregation and capture to the cell pole we examined another Soj ATPase mutant, *soj(K16A)*, in a similar manner (Figure 5.10). *In vitro* experiments have suggested that Soj(K16A) cannot bind ATP and the protein was only ever detected as a monomer (Murray and Errington, 2008; Scholefield *et al.*, 2011). This is because

the lysine at residue 16 is critical for nucleotide binding (Leonard *et al.*, 2005). As such, Soj(K16A) and Soj(G12V) are both monomeric and differ in the absence or presence of ATP, respectively.
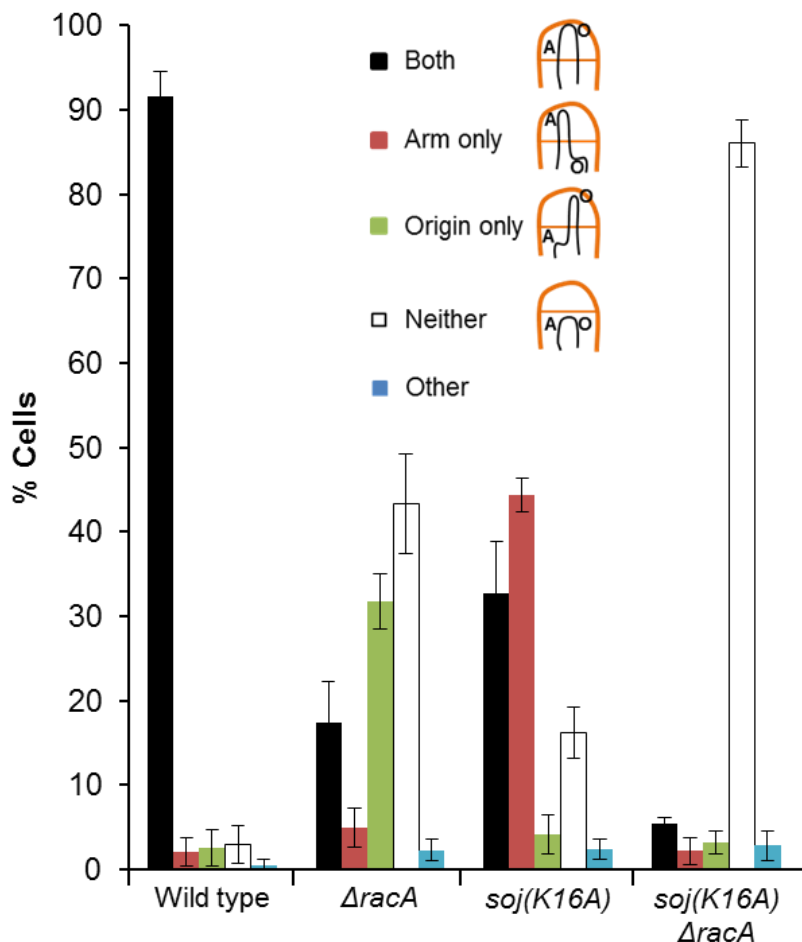
Figure 5.10 Soj(K16A) fails to capture origins in the prespore.

Trapping assay to assess the prespore localisation of markers located at origin and arm regions. At least 100 cells were counted per repeat (n=3) for each mutant and average scores are shown. Error bars represent standard deviations. Images were acquired at T_{4h} of sporulation. Schematics show localisation of the origin (O) and arm (A) markers relative to the asymmetric septum and cell pole (orange).). Other refers to signals not in the list (e.g. in both compartments). Strains: Wild type = DMR178; *soj(K16A)* = DMR181; *soj(K16A) ΔracA* = DMR192.

Unlike *soj(G12V)*, *soj(K16A)* mutants exhibited an origin trapping defect (Figure 5.10). A significant proportion of cells (compared to wild type) failed to capture both origin and arm markers in the prespore, but instead exhibited a prespore arm only localisation, with the origin residing in the mother cell (Figure 5.10). This "arm only" localisation pattern is strikingly similar to that seen in *ΔcomN*, *ΔminD* and *Δsoj* mutants (Kloosterman *et al.*, 2016). Since these are all members of the *parS*-capture pathway, and there is genetic redundancy between that pathway and RacA, it was hypothesised Soj(K16A) is not able to move and/or tether the origin to the pole, and that the observed arm-only trapping was due to the presence of DNA/*ram* site-RacA interactions on the origin-proximal arm region. To test this, a *soj(K16A) ΔracA* double mutant was examined (Figure 5.10). In this mutant, a large majority of cells failed to capture either marker in the prespore, consistent with the notion that Soj(K16A) is defective in the *parS*-capture pathway. Next, the dynamics of origin movement in the Soj(K16A) background was examined in the ONIX system (Figure 5.11).
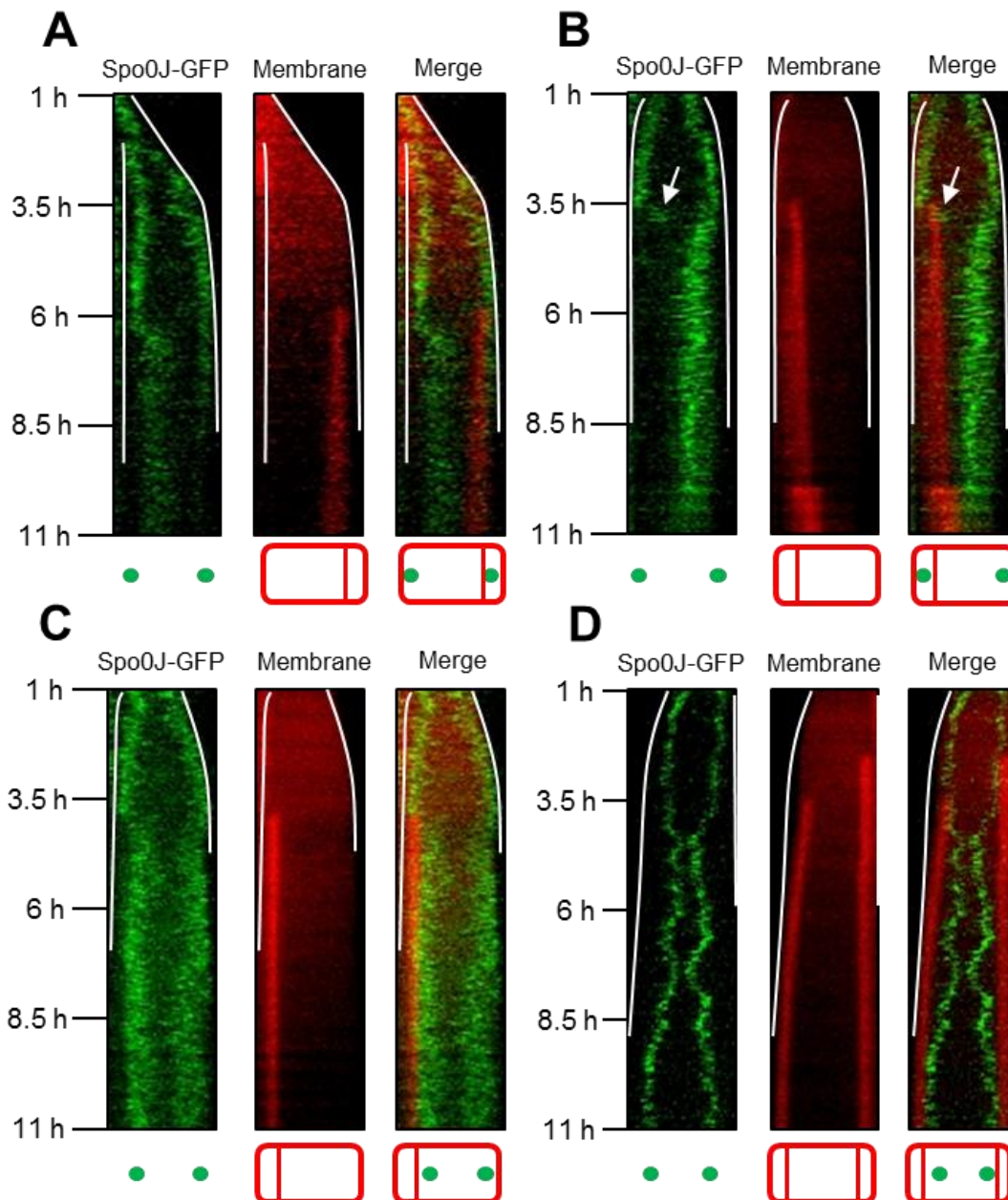
Figure 5.11 Kymographs of *soj(K16A)* and *soj(K16A) ΔracA* mutants.

Representative kymograph plots of origin (Spo0J-GFP) movement in wild type (A); Soj(K16A) (origin in the prespore) (B); Soj(K16A) (origin out of the prespore) (C) and Soj(K16A) *ΔracA* (D). Time lapse microscopy was conducted using the ONIX microfluidics system and a schematic of the final frame is indicated below each plot. Images were acquired every 3 min. White lines represents the cell poles. Kymographs are representative of 6 analysed plots per mutant. Wild type = DMR145; Soj(K16A) = DMR156; Soj(K16A) *ΔracA* = DMR174. White arrow indicates possible origin translocation into the prespore (see text for details.

The origin movement dynamics in the *soj(K16A)* strain exhibited two main patterns in the ONIX device (Figure 5.11). The first phenotype was a successful trapping of the origin within the prespore. Spo0J-GFP signal (origin) was present in the pole region and upon asymmetric septation was retained in the prespore. Occasionally, the origin focus moved close to the sporulation septum and then disappeared (Figure 5.11B, white arrow). It was assumed that DNA translocation directed by SpoIIIE protein resulted in translocation of the origin into the prespore, during which Spo0J protein would be stripped off (Marquis *et al.*, 2008). The origin must have been translocated because at least some of these cells went on to undergo prespore engulfment. The second phenotype observed was a failure to capture the origin, which persisted in the mother cell for many hours after asymmetric cell division (Figure 5.11C). In contrast, very little movement towards the cell poles was seen in the *soj(K16A) ΔracA* mutant, indicated by the narrow vertical lines of Spo0J-GFP signal (Figure 5.11D). In five of seven cells examined, they became disporic presumably because the σ^F-dependent *spoIIR* gene needs to be expressed in the first prespore compartment to prevent a second polar septum from being formed (Lewis *et al.*, 1998). Also, there always appears to be two origins in the *soj(K16A)* mutant cells at the beginning of the time lapse, possibly suggesting a lack of origin cohesion in these strains (Figure 5.11 B-D).

From Figures 5.8 to 5.11 three main conclusions can be drawn. Firstly, and most strikingly, the *soj(G12V)* mutation alone can directly or indirectly facilitate movement of the origin in the absence of its homo-dimerization, DNA binding and ATP hydrolysing activity. Secondly, and as stated before, genetic redundancy in polar capturing via the *parS* system and RacA tethering is critical to maintain a level of sporulation function. Finally, in considering Soj function in isolation of RacA, these data suggest that it is the binding of ATP that appears to be the critical determinant for function, rather than the ability to hydrolyse ATP for the accomplishment of origin movement during sporulation. These conclusions raise immediate questions as to how Soj(G12V) can facilitate DNA movement to the pole, and what is the identity of the Soj-interactor in the polar complex?

5.2.5 MinD is critical for successful origin capturing in the *soj(G12V)* mutant

The above results suggested that the G12V and K16A forms of Soj were on and off, respectively, for the putative *parS*-based segregation system. By combining these mutants with other mutations in the *parS*-pathway, it was hoped that we could determine whether Soj acted upstream or downstream of other factors. Since the presence of MinD is critical for polar and septum localisation of Soj in vegetative cells (Marston and Errington, 1999; Autret and Errington, 2003; Murray and Errington, 2008), and MinD has been identified as a component of the *parS*-capture complex at the cell pole (Kloosterman *et al.*, 2016), we hypothesised that MinD could be the critical interactor of Soj/Soj(G12V) at the cell pole during chromosome segregation and polar anchoring. To test this, we analysed wild type Soj and Soj(G12V) in the presence and absence of various additional factors, including MinD, to establish whether Soj(G12V) (normally active in segregation) could be made to resemble the segregation defective Soj(K16A) (Figure 5.12).
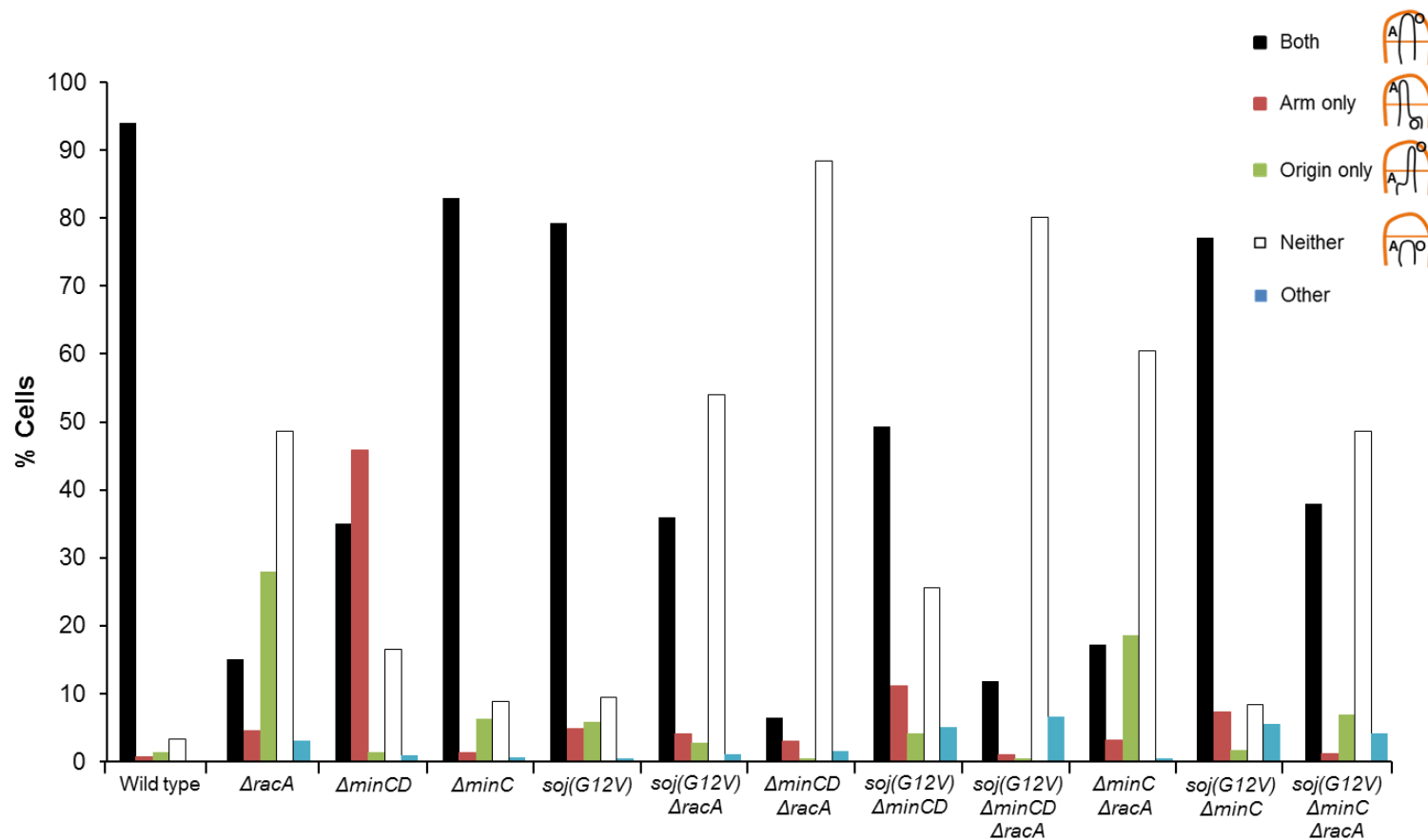
Figure 5.12 MinD or RacA is critical for Soj(G12V) function in prespore chromosome anchoring.

Trapping assay to assess the prespore localisation of markers located at origin and arm regions. At least 250 cells were counted for each mutant and average scores are shown. Images were acquired at T_{4h} of sporulation. Schematics show localisation of the origin (O) and arm (A) markers relative to the asymmetric septum and cell pole (orange). Other refers to signals not in the list (e.g. in both compartments). Strains: Wild type = DMR213; *ΔracA* = DMR215; *ΔminCD* = DMR217; *ΔminC* = DMR218; *soj(G12V)* = DMR214; *soj(G12V) ΔracA* = DMR216; *ΔracA ΔminCD* = DMR221; *soj(G12V) ΔminCD* = DMR219; *soj(G12V) ΔminCD ΔracA* = DMR223; *ΔracA ΔminC* = DMR222; *soj(G12V) ΔminC ΔracA* = DMR224.

Figure 5.12 firstly showed that wild type cells trapped both the arm and origin marker in the prespore in almost every analysed cell. Furthermore, both the *ΔracA* and *ΔminCD* mutants exhibited a trapping phenotype, with a significant increase in cells that isolated only the origin or the arm in the prespore respectively, as previously reported (Kloosterman *et al.*, 2016). A *ΔminC* mutant was also separately tested as a control and, as expected, there was no significant trapping phenotype, confirming in this assay that MinC by itself does not contribute. This particular test also confirmed that the formation of minicells (produced equivalently in *ΔminC* and *ΔminCD* mutants; (Bramkamp *et al.*, 2008)) does not in itself disrupt anchoring of the origin region at the cell pole.

Consistent with Section 5.2.3, *soj(G12V)* and *soj(G12V) ΔracA* cells exhibited a near wild type, or an all-or-nothing trapping phenotype, respectively. Knockouts of both the RacA and *parS* systems (*ΔracA ΔminCD* mutant) displayed a severe anchoring and segregation phenotype, with the majority of cells failing to trap either marker in the prespore. This confirmed the critical role of these redundant polar capture systems during sporulation.

Unexpectedly, proper trapping (i.e. origin and arm together) was more frequent in the *soj(G12V) ΔminCD* mutant than in *ΔminCD* alone. This effect was reminiscent of the increased arm plus origin cells in *soj(G12V) ΔracA* versus the *ΔracA* (Figure 5.12 and 5.8). These results imply that Soj(G12V) improves trapping of both markers (origin and arm) in mutants of either pathway, provided that the redundant pathway is operational. However, when *soj(G12V)* was combined with both *ΔminCD* and *ΔracA* mutations, trapping was virtually abolished for both markers (Figure 5.12). Thus, trapping promoted by Soj(G12V) requires either RacA or MinD activity.

5.2.6 A possible novel Soj-Spo0J-DNA interaction promoting origin capture

Soj(G12V)-ATP is monomeric and there is no current evidence that it is able to bind DNA. However, this mutant was able to rapidly segregate and anchor the origins to the cell poles during sporulation (Sections 5.2.3 and 5.2.5). How therefore can this protein facilitate chromosome segregation? We hypothesise that it acts through Spo0J, which is resident on the DNA at the origin-localised *parS* sites (Murray *et al.*, 2006; Graham *et al.*, 2014). Spo0J(L5H) has been characterised as a DNA segregation-proficient but sporulation-defective mutant (Gruber and Errington, 2009).

Since the mutation lies in the critical ATPase activating peptide, this protein may no longer sufficiently interact with Soj, leading to a chromosome segregation defect irrespective of the ability of Soj (or mutant forms of Soj) to interact with MinD at the pole. If correct, both Soj mutants described in this chapter would be predicted to display a trapping defect when combined with Spo0J(L5H) (Figure 5.13).
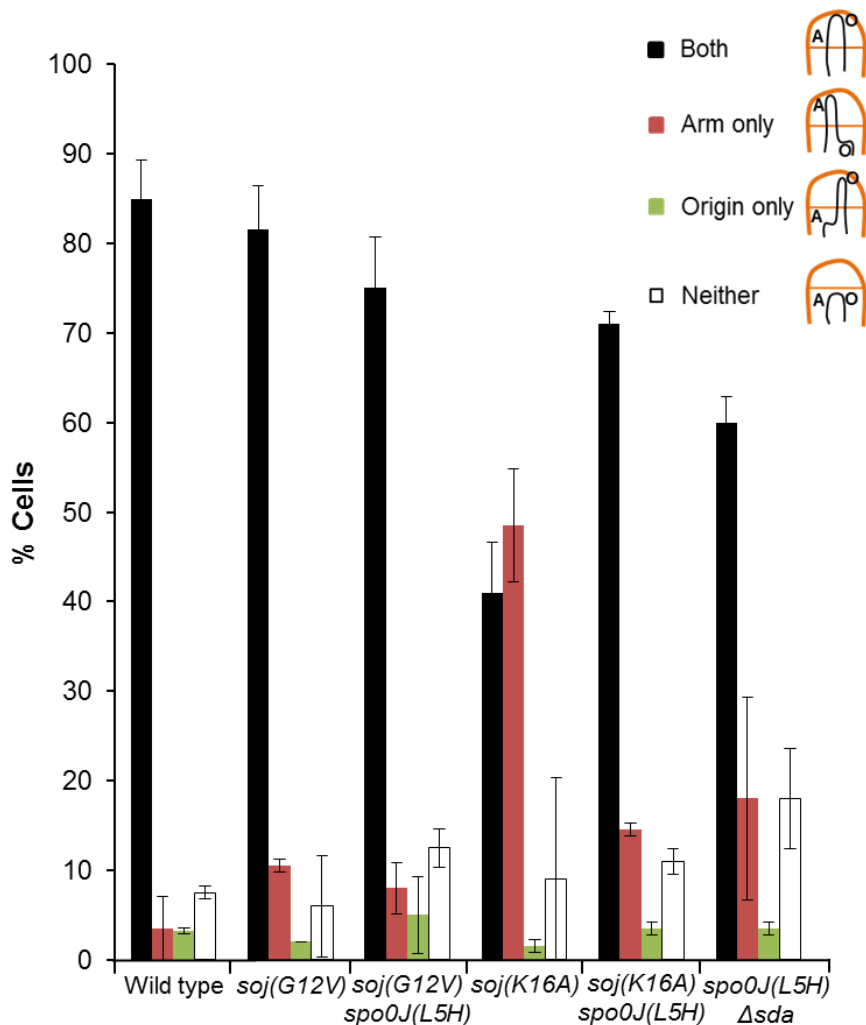
Figure 5.13 Spo0J(L5H) improves prespore trapping of DNA in *soj(K16A)*.
Trapping assay to assess the prespore localisation of markers located at origin and arm regions. At least 200 cells were counted for each mutant and average scores are shown. Scale bars represent standard deviations. Images were acquired at T_{4h} of sporulation. Schematics show localisation of the origin (O) and arm (A) markers relative to the asymmetric septum and cell pole (orange). Wild type = DMR178; *soj(G12V)* = DMR179; *soj(G12V) spo0J(L5H)* = DMR185; *soj(K16A)* = DMR181; *soj(K16A) spo0J(L5H)* = DMR184; *spo0J(L5H) Δsda* = TK244.

The *spo0J(L5H)* mutation, by itself, had a mild trapping defect, with a mixture of empty and arm-only cells. This strain also had an *sda* mutation, which was needed to enable sporulation (Murray and Errington, 2008). The G12V and K16A mutations both eliminate the need for the *sda* mutation since these mutants cannot form ATP-dimers. The data showed that the mutation impairing Spo0J interaction with Soj had almost no effect in the G12V background. Surprisingly, the mutation actually *improved* trapping in the K16A background. This result suggests that the K16A mutant protein interferes with trapping by interaction with Spo0J.

5.3 Discussion

Initial experiments were focussed on assessing the localisation of Soj during the cell cycle. Firstly, using a GFP-Soj construct, we confirmed the previously reported localisations of Soj to septa and as discrete foci within the cytoplasm (Figure 5.1) (Murray and Errington, 2008). New constructs of Soj were made using the brightest known fluorescent protein mNG in a bid to overcome known issues regarding low signal intensity of GFP-Soj and the long exposure times required for imaging. The mNG fluorophore has recently been used to successfully generate a *functional* mNG-FtsZ fusion, expressed from the *ftsZ* locus (Bisson-Filho *et al.*, 2017). Here, Western blotting demonstrated that full length mNG-Soj proteins, expressed from the native promoter, were more abundant at steady state than the original GFP-Soj construct (Figure 5.2). Since mNG folds more rapidly than GFP (Shaner *et al.*, 2013), these fusions may be more functional or more stable, with less turnover than the earlier GFP-Soj. The precise nature of the non-specific bands seen in Figure 5.2B was not explored here, but since they were present in all samples (including the *soj* knockout) and both blots, we moved on to attempt to directly visualise the new fusions microscopically. Analysing mNG-Soj microscopically confirmed the expected localisation pattern in wild type and Soj(G12V), suggesting that mNG fusions retained functionality to at least the same extent as GFP-Soj (Figure 5.3). In fact, mNG-Soj(K16A) was visualised at septa, as well as at the previously reported cytoplasmic foci (Figure 5.3). A laser-based illumination approach to further increase the signal and lower the exposure time confirmed the localisation patterns of all Soj variants, but the cytoplasmic signal increased from wild type to Soj(G21V) to Soj(K16A), respectively (Figure 5.4). The relevance of this pattern is not clear at present, but could reflect increased cytoplasmic dynamics or less efficient recruitment of the monomeric Soj mutants to specific sites.

Using the formation of axial filaments as a pre-asymmetric division marker to identify sporulating cells (Figure 5.5), the mNG-Soj strains were visualised during sporulation (Figure 5.6). Both wild type and Soj(G12V) shared a similar localisation pattern, being observed at poles and septa, consistent with the previous vegetative localisation patterns (Figure 5.4) (Murray and Errington, 2008). Strikingly, mNG-Soj(K16A) appeared predominantly as internal foci at the leading edge of the axial filaments. Indeed, upon RacA-mediated anchoring, these Soj(K16A) foci would

reside in the polar region due to the constraint of the nucleoid, as was seen. Again, this is similar to the vegetative localisation pattern (Murray and Errington, 2008), and the lack of polar signal may reflect a loss of polar recruitment of Soj(K16A) during sporulation.

Next, the origin dynamics in the known capture mutants *Δsoj* and *Δsoj ΔracA* strains was examined (Figure 5.7) (Wu and Errington, 2003; Kloosterman *et al.*, 2016). As well as successful and defective capture of the origins, some cells in both *Δsoj* single and *Δsoj ΔracA* double mutants exhibited origin duplication despite the presence of two pre-existing origins 1.5 hours after the induction of sporulation (Figure 5.7). This phenomenon has been reported in vegetatively growing cells where in the absence of Soj, the initiator of DNA replication – DnaA, is no longer inhibited (Murray and Errington, 2008). However, this result was somewhat unexpected during sporulation due to the existence of Spo0A- and SirA-mediated control mechanisms that regulate chromosome copy number and enforce diploidy in sporulating cells (Wagner *et al.*, 2009; Boonstra *et al.*, 2013; Jameson *et al.*, 2014). It may be possible that in the cells exhibiting origin duplication, DNA replication was initiated prior to the commitment to sporulation. An alternative explanation could be that the DNA replication inhibition mechanisms were not functional in the cells with duplicated origins, although this is unlikely.

One difficulty with the analysis of origin movement in live cells used throughout this work is its labour intensity. In order to reliably quantify origin dynamics in a population, extensive bioinformatics and imaging analysis work would be required to develop novel workflows to measure each spot (origin) placement within the cell and its distance from the cell pole for every frame. Lack of time and specific expertise in this area meant that automated image analyses could not be developed here. It follows that small numbers (< 10) of sporulating cells had to be randomly selected based on the formation of asymmetric septa and analysed in each instance. It therefore remains to be seen just how frequently the *Δsoj* origins duplicated following sporulation induction in a large population.

In attempts to probe how Soj facilitates chromosome segregation more precisely, monomeric versions of Soj were created that either could (G12V), or could not (K16A), bind ATP. To our surprise, *soj(G12V)* mutants highly resembled wild type cells in origin trapping assays. Even upon deletion of *racA*, Soj(G12V) retained

considerable arm and origin capture ability, suggesting that the *parS* pathway – of which Soj is a member – was still functional (possibly even more so than in a *racA* single mutant) (Figure 5.8). Examining *soj(G12V)* mutants in the ONIX device revealed that cells entered sporulation with only one visible origin. It was not clear whether this was truly one origin, or two interconnected origins that rapidly segregated to opposite cells poles prior to asymmetric cell division (Figure 5.9B). The latter may suggest a temporary origin segregation defect in these cells. To explore this further had time permitted, the experiment would have been repeated in a *soj(G12V)* strain that harboured both Spo0J-GFP and a marker of the DNA replisome, such as DnaN-mCherry. If replication and segregation occurred sequentially or concomitantly, then the appearance of DnaN-mCherry foci in this strain would occur prior to, or simultaneously with, the separation of the Spo0J-GFP labelled origins, respectively. Regardless of the precise timing of DNA replication, the results highlighted in Figures 5.8 and 5.9 reveal that the ability of Soj to dimerise and hydrolyse ATP is not required for origin movement to the cell pole during sporulation. To our knowledge, this is the first occasion that such movement occurs in the absence of Soj/ParA homodimer driven ATP-hydrolysis (Lim *et al.*, 2014; Brooks and Hwang, 2017).

In stark contrast to the results obtained with Soj(G12V), the empty monomer form of Soj (Soj(K16A)) was inefficient in segregating the DNA (Figures 5.10 and 5.11). In the presence of RacA, *soj(K16A)* did trap origins within the prespore in some cells (Figure 5.11B and C), although the dominant phenotype was arm-only capture (Figure 5.10). This may also account for the lower frequency of "both captured" phenotypes compared to the wild type, since it is likely that a RacA-mediated tethered arm and free origin lead to increased Brownian motion that allows the additional capturing of the origin region in a minority of cells. Significant failure to capture any marker or display any directed polar movement in the Soj(K16A) *racA* mutant confirmed that Soj(K16A) is non-functional for chromosome capture (Figures 5.10 and 5.11D). It would have been interesting to repeat the ONIX experiments with an arm marker (at *ram* sites) in *soj(K16A)* to establish whether the occasional origin trapping was due to arm tethering and Brownian motion of the *parS* region.

Taken together, the results with the monomeric Soj mutants revealed that the only requirement for sufficient origin segregation is the presence of ATP. It remains to be determined whether the Soj(G12V) mutant is active in driving chromosome

segregation, or whether it is the presence of ATP that promotes interactions in a particular orientation that is critical for chromosome capturing and movement. This interaction would be absent or non-productive with the empty Soj(K16A) monomer.

Since Soj is a member of the *parS* polar capture pathway, attempts were made to identify members of this pathway that cause the Soj(G12V) capture proficient mutant to resemble the Soj(K16A) capture defective mutant. Since MinD recruits Soj to the cell pole and division sites during vegetative growth (Marston and Errington, 1999; Autret and Errington, 2003; Murray and Errington, 2008), this was the obvious candidate. As predicted, a *soj(G12V) ΔracA ΔminCD* mutant was severely defective in origin trapping, exhibiting a defect at a similar level to *soj(K16A) ΔracA* (Figures 5.10 and 5.12). These data suggested that MinD is the critical polar component required for Soj function in chromosome capture. Since MinD is a ParA ATPase like Soj, one hypothesis is that the ATP bound monomer of Soj (in either wild type or Soj(G12V) mutants) is able to hetero-dimerise with MinD-ATP monomers at the cell pole. This is not unprecedented, since Soj monomers are already known to interact with the AAA+ DnaA (Scholefield *et al.*, 2012). A polar-localised MinD-Soj heterodimer may promote an alternate interaction with Spo0J that enables the formation of a Soj-Spo0J-DNA complex. Furthermore, MinD itself, or Spo0J-DNA, may act as a Soj-ATP/MinD-ATP nucleotide exchange factor. If correct, this hypothesis could explain how Soj(G12V) retains functionality, and how this non-DNA binding Soj mutant can facilitate capture of the DNA at the pole (Figure 5.14).
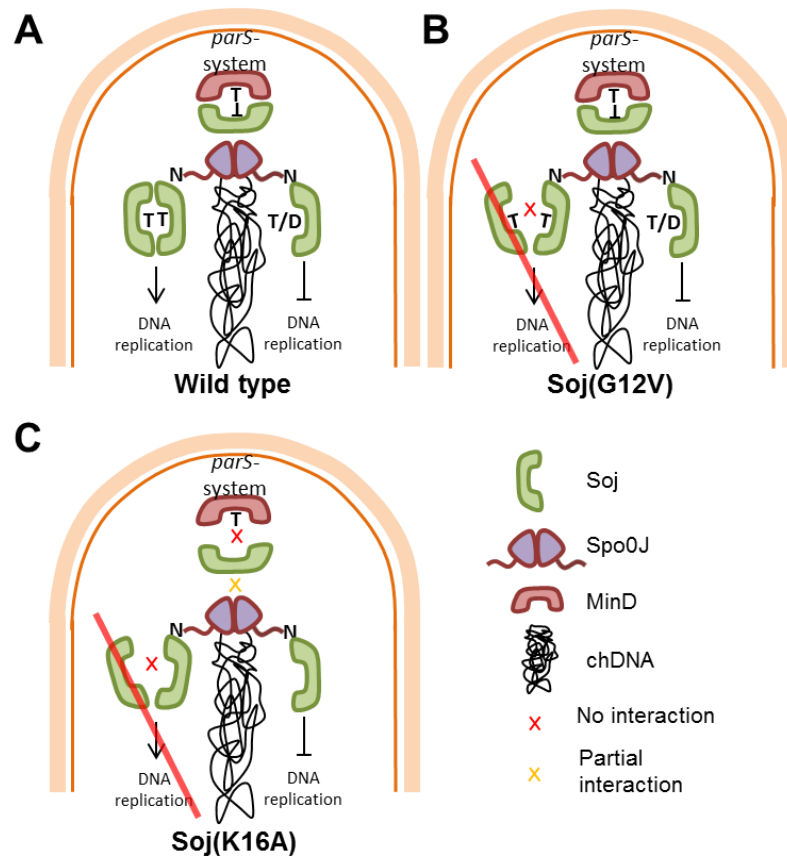
Figure 5.14 Model for Soj function in polar chromosome anchoring during sporulation
The schematic shows the various polar and cytoplasmic localisations of Soj (green). A) In wild type cells, a Soj-ATP-MinD-ATP heterodimer is critical in orienting Soj for interaction with Spo0J-DNA, thereby tethering DNA to the pole. Cytoplasmic Soj interactions with the Spo0J N-terminus coordinate DNA replication. B) In Soj(G12V), the polar Soj-MinD heterodimer is maintained. Since Soj(G12V) cannot homodimerise (blocked by 2 bulky V residues), ATPase stimulation by Spo0J is absent, but monomeric cytoplasmic Soj inhibits DNA replication. C) Soj(K16A) mutants can no longer heterodimerise at the pole (no polar localisation signal), losing the ability to anchor the chromosome. Cytoplasmic K16A can however interact with Spo0J in the N-terminus (inhibiting DNA replication).

Somewhat inconsistent with this model however, were several intriguing observations. While there was very little chromosome anchoring in the absence of both *racA* and *minD,* Soj(G12V) appeared to enhance the trapping of the origin *and* the arm in *ΔminD* cells. This unexpected outcome should not occur if a Soj-MinD heterodimer was critical (Figure 5.12). It should also be noted that Soj(G12V) also improved arm trapping in a *ΔracA* background, suggesting that origin capture was more efficient in a G12V mutant as long as one of the two capture pathways was operational (Figure 5.12). As a result, an alternative hypothesis could be proposed: that Soj may not be directly involved in a MinD complex to directly capture the origin,

but rather that it functions to compact the origin in the cytoplasm (Figure 5.15). This presumably occurs via Spo0J, and might reconcile earlier data (Marston and Errington, 1999) where Spo0J-GFP foci appeared less tight in *Δsoj* mutants compared to the wild type.
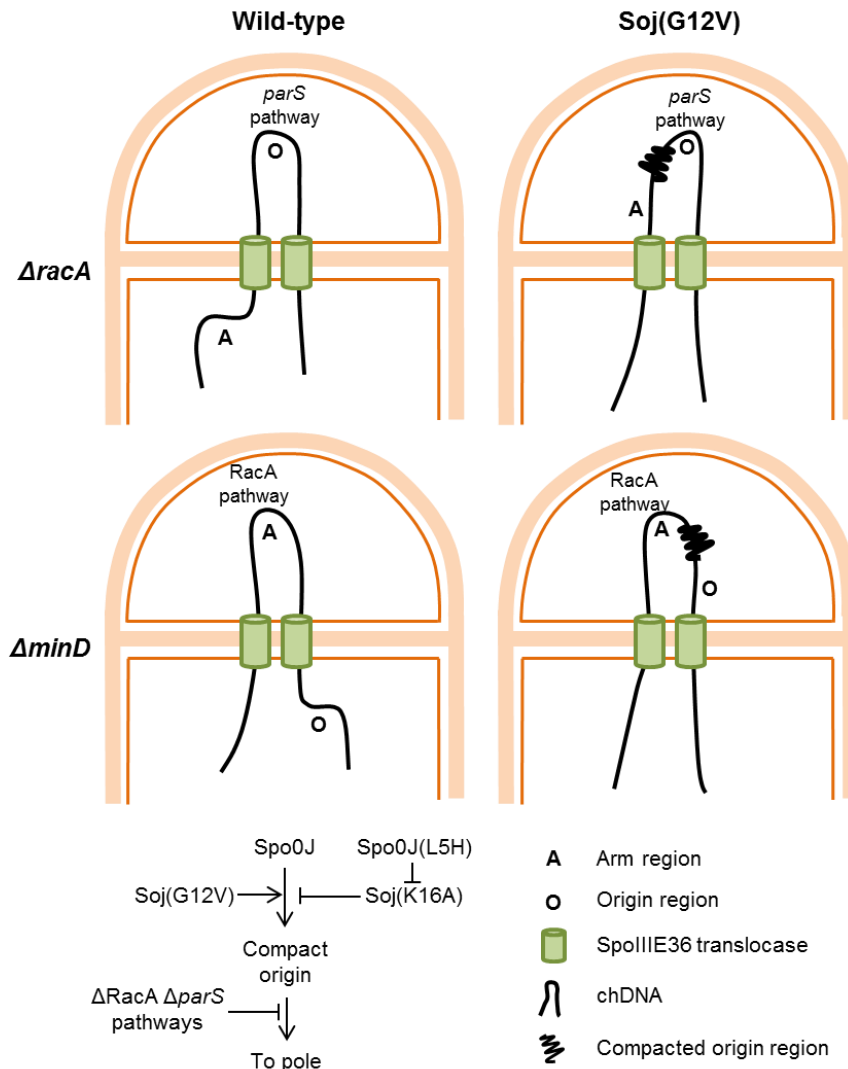
Figure 5.15 Compaction model for Soj function during polar anchoring of the origin
In wild type cells, either the origin (in the absence of the RacA pathway, top left cell) or the arm (in the absence of the *parS* pathway (e.g. *ΔminD*), bottom left cell) are present within the prespore. Due to the compaction of the origin in Soj(G12V) cells, both origin and arm cells are captured provided either of the two redundant capture pathways remains active (right hand cells). Schematic flowchart (bottom left) shows proposed hierarchy of compaction. See text for details.

This model states that Soj(G12V) is the compaction-proficient form of Soj. By contrast, Soj(K16A) is functionally deficient. It follows that in wild type cells, with the various Soj isoforms coexisting, compaction may be "intermediate" since it is limited by the available population of monomeric ATP-bound Soj (functionally equivalent to

G12V). However, in Soj(G12V) mutants, the whole complement of Soj is involved in origin compaction, facilitating Spo0J arrays and bridges (Murray *et al.*, 2006; Graham *et al.*, 2014) in bringing together this large nucleoprotein complex. Such compaction is proposed to bring the origin and arm markers more closely together, enhancing co-entrapment probability upon asymmetric division.

In this model, Soj(K16A) must operate as a negative regulator, where non-compacted origins lead to a non-functional *parS*-capture pathway (but in the presence of RacA, arm trapping can still occur, Figure 5.10). This is proposed because origin trapping is dramatically improved by introducing the *spo0J(L5H)* mutation that abolishes Soj-Spo0J interactions (Gruber and Errington, 2009) (Figure 5.13). As such, Soj(K16A) may prevent the Spo0J self-interactions required for origin compaction or interaction with polar components (e.g. MinD). However, Spo0J-GFP can clearly still form a focus in *soj(K16A)* mutants, since this was used to track origin movement in ONIX experiments (Figures 5.11). Whether this represents a less compacted origin region is unclear at this resolution, but may be a caveat for this model. While some progress has clearly been made in leading to these hypotheses, the precise molecular mechanism used by Soj in coordinating chromosome capture at the cell pole remains an outstanding question.

Taken together, the results presented in this chapter have revealed novel insights into the role of Soj in chromosome segregation and polar anchoring during sporulation in *B. subtilis*. To recap, these are:

- The two monomeric forms of Soj tested can be recruited to cell poles and division sites,
- The ATPase function and dimeric form of Soj is not required for movement of the origin into the prespore, but the presence of bound ATP is,
- That MinD is the key 'receptor' for Soj at the cell pole or that Soj(G12V) is the compaction-proficient isoform responsible for promoting origin region capture by MinD.

Chapter 6

Concluding Remarks and Future Directions

Studies in this thesis have focussed on the early stages of sporulation in *B. subtilis* where the chromosome forms a unique axial filament structure, origins become anchored to opposite cell poles and a highly asymmetric division event defines the small prespore and large mother cell (Errington, 2010; Tan and Ramamurthi, 2014).

At the outset, it was known that RacA, Soj and Spo0J were involved in anchoring the origin region to the cell pole upon axial filament formation (Wu and Errington, 2002; Ben-Yehuda *et al.*, 2003b; Wu and Errington, 2003; Ben-Yehuda *et al.*, 2005), to ensure specific genes are trapped in either compartment during the activation of alternate sigma factors. The bisection of the prespore chromosome is not random, but converges on a specific region of the genome between 500-700 Kbp from the origin such that approximately one third of the chromosome is trapped within the small compartment (Wu and Errington, 1998). It was also known that a range of mutants in chromosome organisation and polar origin anchoring led to incorrect localisation of the origin region in the mother cell (Errington *et al.*, 2005) (Errington laboratory, unpublished results). Understanding the organisation of the axial filament, and the way the origin is moved and retained at the cell pole is not only of great interest in understanding sporulation, but of broader significance since many of the factors are either bi-functional or implicated in similar (less genetically definable) processes during rapid vegetative growth. This thesis has therefore focussed on some of the outstanding questions regarding chromosome organisation in the axial filament and the factors involved in polar origin capture. These questions are encapsulated in the list of aims provided in Section 1.6. To avoid repetition of the earlier Discussion narratives, this section will principally concentrate on presenting future directions emerging from the work described herein.

The work described in Chapter 3 was aimed at precisely defining the regions of the prespore chromosome that were bisected by the closing asymmetric septum. Utilising the DNA binding-proficient but translocation-defective allele of SpoIIIE (SpoIIIE36), it was hypothesised that DNA immediately captured could be purified

166

and sequenced. The idea was to identify the trapped sequence (or region) at high resolution in wild type cells and existing chromosome organisation mutants (such as knockouts of *racA*, *comN*, *minD* and *soj*). However, despite intensive assay development and investigation, neither SpoIIIE nor associated DNA was enriched using our affinity purification protocol, even though this was successfully applied to the control (Spo0J). The logical progression of experiments described in Chapter 3 revealed that SpoIIIE was highly heat labile and difficult to extract from the membrane as a result of its rarity and propensity to aggregate. Furthermore, being part of a complex divisome, presumably crosslinked to multiple other integral membrane proteins, made the clean purification of sufficient quantities of SpoIIIE-DNA extremely challenging. To my knowledge, no published example currently exists showing successful ChAP-Seq of a rare multi-spanning membrane protein like SpoIIIE, suggesting in hindsight that the approach was inappropriate.

An alternative approach was to specifically identify prespore-localised DNA. By exploiting alternate sigma factor signalling, the *E. coli* DNA adenine methylase was specifically expressed in the *Bacillus* prespore, leading to methylation of resident DNA. Whilst initial qualitative gel analysis looked promising, no specific regions of methylation enrichment were detected when using the next generation PacBio SMRT methylation sequencing. Had time permitted, further assay development would have been conducted. For example, to mitigate any potential Dam expression in the mother cell (despite the supposed prespore specificity of the P_{spoIIQ} promoter), a *ssrA* degron tag fused to Dam, coupled with the specific mother cell expression of *ssrB*, would ensure that any low level expression in the mother cell would be rapidly targeted for degradation (Griffith and Grossman, 2008). Such an approach might reduce background methylation sufficiently to enable specific enrichment of prespore methylated DNA upon SMRT sequencing. Alternatively, extraction of Dam methylated DNA could have been performed in the presence of the specific Dam inhibitor, Sinefungin (Mashhoon *et al.*, 2006). A different approach to identify the prespore-mother cell boundary on the DNA would be to conduct Hi-C experiments to study the global organisation of the axial filament. This approach crosslinks nearby DNA together. Following purification and high throughput sequencing of crosslinked DNA, a map of interacting DNA pairs can be plotted against genome position in x and y (Le *et al.*, 2013; Marbouty *et al.*, 2015; Wang *et al.*, 2015; Marbouty and Koszul, 2017; Wang *et al.*, 2017). The presence of the asymmetric septum in sporulating

samples would lead to a blank readout at the point of septum bisection. Using subtractive deduction, it would be possible to then determine the boundary sequences. However, lack of time and specific bioinformatics expertise meant that this approach could not be pursued. Regrettably therefore, this part of the project was abandoned.

Axial filament formation is accompanied by the movement of the origin regions to opposite cell poles, and their capture/retention in these locations. In the absence of progress in understanding the precise organisation of axial filament formation, it was decided to refocus on aspects of the polar capture process instead. As a prelude to this, a genetic screen had been conducted in the laboratory that implicated two new factors in this pathway: ComN and MinD (Kloosterman *et al.*, 2016). While both proteins were already known to have roles in vegetative growth (Bramkamp *et al.*, 2008; dos Santos *et al.*, 2012), deletion of either gene leads to a failure of origin capture in the prespore during sporulation (Kloosterman *et al.*, 2016). My work in relation to these findings concerned further visual characterisation of these factors, aspects of which have been published (Kloosterman *et al.*, 2016) (Chapter 4). In summary, I established the hierarchy of polar protein localisation dependency, with ComN acting upstream of MinD. Both proteins co-localised, suggesting cooperation within the same capture pathway.

Wu and Errington, 2003 had previously implicated both RacA (which directly tethers the origin proximal arm region) and Soj-Spo0J (which promotes origin trapping) in polar chromosome anchoring, and shown that mutants doubly disrupted in the two putative pathways are severely defective in chromosome capture (Wu and Errington, 2003; Errington *et al.*, 2005). It was therefore likely that the newly discovered origin capturing roles for ComN and MinD lay within the Soj and Spo0J pathway rather than arm capturing RacA pathway (Kloosterman *et al.*, 2016). My data revealed that *comN racA* double mutants displayed severe sporulation defects (while single mutants had no significant effect), further supporting the notion that these factors operate in two redundant origin capture systems. We therefore named the two systems the RacA- and *parS*-capture pathways. Although this work showed that MinD was dependent upon ComN for significant polar localisation, it remains to be established whether there is any direct interaction between these two proteins *in vivo.* Therefore, future work could include reciprocal Co-IP of native ComN and MinD extracts followed by Western blotting, to probe any direct associations. Additionally,

the polar complex could be crosslinked *in vivo* (e.g. with DSP), affinity purified on appropriate immobilised antibody columns and subjected to tryptic digestion and mass spectrometric analysis. By establishing peptide-crosslinker-peptide interlinks, spatial organisation of the polar complex could be interrogated, and could possibly be ultimately solved using structural biology (Rappsilber, 2011; Leitner *et al.*, 2016).

Extensive effort was invested in developing a novel time lapse microscopy approach to directly study origin movement in the early stages of sporulation. This involved optimising re-suspension protocols in the commercially available CellASIC ONIX system using constant media perfusion and rapid switching to specifically control the flow of media over the cellular population for many hours. Application of the optimised imaging protocol to mutants of *comN* and *racA* revealed that origins were less anchored in these cells, as evidenced by increased fluctuations in real time that led to either origin capture or failure at a single cell level. Despite revealing novel insights into origin dynamics, further development of imaging analytics would be required to allow the scale-up of this approach. Such protocols could include establishing the spatial position of the origin and its distance from the cell pole in each imaging frame. Plotting this information graphically for each cell could then reveal origin dynamics in more detail. This would be readily applicable to large numbers of cells, but would require the development of novel algorithms and automated data capture and analysis.

Next, the precise role played by Soj in polar chromosome movement and/or origin anchoring at the cell pole was investigated (Chapter 5). To our surprise, both origin trapping assay data and ONIX microfluidics imaging revealed that near wild type levels of origin movement and trapping could occur with Soj trapped in the ATP-bound monomer form, Soj(G12V). This was not the case for the nucleotide-free monomer (Soj(K16A)). Soj(G12V) also appeared to improve the trapping of both the origin and the arm region in mutants of either the RacA- or *parS*-pathways. One hypothesis to explain these data is that the ATP-binding proficient Soj(G12V) is able to heterodimerise with MinD. It is already established that polar localisation of Soj is dependent upon MinD in vegetatively growing cells (Marston and Errington, 1999; Autret and Errington, 2003; Murray and Errington, 2008). It may follow that the replacement of the glycine to a bulkier valine only blocks dimerisation when both monomers contain the mutation. To test for Soj-MinD heterodimers, specific cysteine residues could be introduced into the likely dimerisation interface (based on the

recently published ParA-homodimer structure) (Zhang and Schumacher, 2017). Crosslinking of sporulating cells with the cysteine-specific BMOE reagent could then lock heterodimers together (Scholefield and Murray, 2013; Wilhelm *et al.*, 2015). Denaturing SDS-PAGE and Western blotting would probe for Soj-MinD sized bands. Alternatively, FLAG and/or His tagged crosslinked samples could be subjected to reciprocal Co-IP (i.e. IP against tagged MinD and blot for Soj, or vice versa).

An alternative model to explain these data is that the G12V mutant of Soj is actually involved in promoting compaction of the origin region, via Spo0J. This can explain how trapping of both origin and arm region actually improve in either *minD* or *racA* single mutants, respectively. By contrast Soj(K16A) inhibits Spo0J-mediated DNA compaction, since abolishing the interaction of Soj and Spo0J (via the Spo0J(L5H) mutation, (Gruber and Errington, 2009)) improved chromosome trapping in the Soj(K16A) background. To test this model, initial experiments would involve high resolution imaging of Spo0J foci in the various Soj ATPase mutants, which may show degrees of compaction in accordance with those previously observed by Marston and Errington, 1999. The origin (Spo0J-GFP foci) should appear compact in Soj(G12V) but not in the Soj(K16A) mutant. Furthermore, introduction of the Spo0J(L5H) into the *soj(K16A)* mutant should overcome the inhibition of compaction, leading to tight foci. An additional experiment would focus on the *parS* site at the -320 arm proximal region. By deleting this most distant origin-associated site, the trapping of the arm region around this site should be altered in the various compaction-proficient or deficient Soj backgrounds. This could be tested in the origin trapping assay using a *lacO*/LacI-GFP system inserted at this site (prespore localised signal would be expected in the tightly origin compacted Soj(G12V) or the Soj(K16A)-Spo0J(L5H) mutants, but not in the Soj(K16A) mutant).

Dissecting the functional role of Soj in chromosome dynamics during sporulation (and to some extent in vegetative growth) has been a long standing goal of the *B. subtilis* community since its implication in the process more than twenty years ago (Ireton *et al.*, 1994; Sharpe and Errington, 1996). It is now hoped that with the advent of sophisticated imaging and biochemical techniques, and the development of quantitative single cell assays, the insights already gained from this work and the experiments proposed herein may greatly facilitate this ultimate objective.

References

Abanes-De Mello, A., Sun, Y.L., Aung, S. and Pogliano, K. (2002) 'A cytoskeleton-like role for the bacterial cell wall during engulfment of the *Bacillus subtilis* forespore', *Genes Dev*, 16(24), pp. 3253-64.

Adams, D.W. and Errington, J. (2009) 'Bacterial cell division: Assembly, maintenance and disassembly of the Z ring', *Nat Rev Microbiol*, 7(9), pp. 642-653.

Adams, D.W., Wu, L.J. and Errington, J. (2015) 'Nucleoid occlusion protein Noc recruits DNA to the bacterial cell membrane', *EMBO J*, 34(4), pp. 491-501.

Anagnostopoulos, C. and Spizizen, J. (1961) 'Requirements for Transformation in *Bacillus Subtilis*', *J Bacteriol*, 81(5), pp. 741-6.

Autret, S. and Errington, J. (2003) 'A role for division-site-selection protein MinD in regulation of internucleoid jumping of Soj (ParA) protein in *Bacillus subtilis*', *Mol Microbiol*, 47(1), pp. 159-69.

Aylett, C.H., Wang, Q., Michie, K.A., Amos, L.A. and Lowe, J. (2010) 'Filament structure of bacterial tubulin homologue TubZ', *Proc Natl Acad Sci U S A*, 107(46), pp. 19766-71.

Barak, I. and Youngman, P. (1996) 'SpoIIE mutants of *Bacillus subtilis* comprise two distinct phenotypic classes consistent with a dual functional role for the SpoIIE protein', *J Bacteriol*, 178(16), pp. 4984-9.

Barilla, D., Rosenberg, M.F., Nobbmann, U. and Hayes, F. (2005) 'Bacterial DNA segregation dynamics mediated by the polymerizing protein ParF', *EMBO J*, 24(7), pp. 1453-64.

Bath, J., Wu, L.J., Errington, J. and Wang, J.C. (2000) 'Role of *Bacillus subtilis* SpoIIIE in DNA transport across the mother cell-prespore division septum', *Science*, 290(5493), pp. 995-7.

Baxter, J.C. and Funnell, B.E. (2014) 'Plasmid Partition Mechanisms', *Microbiol Spectr*, 2(6).

Beaulaurier, J., Zhang, X.S., Zhu, S., Sebra, R., Rosenbluh, C., Deikus, G., Shen, N., Munera, D., Waldor, M.K., Chess, A., Blaser, M.J., Schadt, E.E. and Fang, G. (2015) 'Single molecule-level detection and long read-based phasing of epigenetic variations in bacterial methylomes', *Nat Commun*, 6, p. 7438.

Becker, E., Herrera, N.C., Gunderson, F.Q., Derman, A.I., Dance, A.L., Sims, J., Larsen, R.A. and Pogliano, J. (2006) 'DNA segregation by the bacterial actin AlfA during *Bacillus subtilis* growth and development', *EMBO J*, 25(24), pp. 5919-31.

Becker, E.C. and Pogliano, K. (2007) 'Cell-specific SpoIIIE assembly and DNA translocation polarity are dictated by chromosome orientation', *Mol Microbiol*, 66(5), pp. 1066-79.

Ben-Yehuda, S., Fujita, M., Liu, X.S., Gorbatyuk, B., Skoko, D., Yan, J., Marko, J.F., Liu, J.S., Eichenberger, P., Rudner, D.Z. and Losick, R. (2005) 'Defining a centromere-like element in *Bacillus subtilis* by Identifying the binding sites for the chromosome-anchoring protein RacA', *Mol Cell*, 17(6), pp. 773-82.

Ben-Yehuda, S. and Losick, R. (2002) 'Asymmetric cell division in *B. subtilis* involves a spiral-like intermediate of the cytokinetic protein FtsZ', *Cell*, 109(2), pp. 257-266.

Ben-Yehuda, S., Rudner, D.Z. and Losick, R. (2003a) 'Assembly of the SpoIIIE DNA translocase depends on chromosome trapping in *Bacillus subtilis*', *Curr Biol*, 13(24), pp. 2196-200.

Ben-Yehuda, S., Rudner, D.Z. and Losick, R. (2003b) 'RacA, a bacterial protein that anchors chromosomes to the cell poles', *Science*, 299(5606), pp. 532-6.

Besprozvannaya, M., Pivorunas, V.L. and Burton, B.M. (2014) 'Mechanistic study of classical translocation-dead SpoIIIE36 reveals the functional importance of the hinge within the SpoIIIE motor', *J Bacteriol*.

Besprozvannaya, M., Pivorunas, V.L., Feldman, Z. and Burton, B.M. (2013) 'SpoIIIE protein achieves directional DNA translocation through allosteric regulation of ATPase activity by an accessory domain', *J Biol Chem*, 288(40), pp. 28962-74.

Bisson-Filho, A.W., Hsu, Y.P., Squyres, G.R., Kuru, E., Wu, F., Jukes, C., Sun, Y., Dekker, C., Holden, S., VanNieuwenhze, M.S., Brun, Y.V. and Garner, E.C. (2017)

'Treadmilling by FtsZ filaments drives peptidoglycan synthesis and bacterial cell division', *Science*, 355(6326), pp. 739-743.

Blaylock, B., Jiang, X., Rubio, A., Moran, C.P., Jr. and Pogliano, K. (2004) 'Zipper-like interaction between proteins in adjacent daughter cells mediates protein localization', *Genes Dev*, 18(23), pp. 2916-28.

Bonilla, C.Y. and Grossman, A.D. (2012) 'The primosomal protein DnaD inhibits cooperative DNA binding by the replication initiator DnaA in *Bacillus subtilis*', *J Bacteriol*, 194(18), pp. 5110-7.

Bonny, M., Fischer-Friedrich, E., Loose, M., Schwille, P. and Kruse, K. (2013) 'Membrane binding of MinE allows for a comprehensive description of Min-protein pattern formation', *PLoS Comput Biol*, 9(12), p. e1003347.

Boonstra, M., de Jong, I.G., Scholefield, G., Murray, H., Kuipers, O.P. and Veening, J.W. (2013) 'Spo0A regulates chromosome copy number during sporulation by directly binding to the origin of replication in *Bacillus subtilis*', *Mol Microbiol*, 87(4), pp. 925-938.

Bowman, G.R., Comolli, L.R., Zhu, J., Eckart, M., Koenig, M., Downing, K.H., Moerner, W.E., Earnest, T. and Shapiro, L. (2008) 'A polymeric protein anchors the chromosomal origin/ParB complex at a bacterial cell pole', *Cell*, 134(6), pp. 945-55.

Bramhill, D. and Kornberg, A. (1988a) 'Duplex opening by dnaA protein at novel sequences in initiation of replication at the origin of the *E. coli* chromosome', *Cell*, 52(5), pp. 743-55.

Bramhill, D. and Kornberg, A. (1988b) 'A model for initiation at origins of DNA replication', *Cell*, 54(7), pp. 915-8.

Bramkamp, M., Emmins, R., Weston, L., Donovan, C., Daniel, R.A. and Errington, J. (2008) 'A novel component of the division-site selection system of *Bacillus subtilis* and a new mode of action for the division inhibitor MinCD', *Mol Microbiol*, 70(6), pp. 1556-1569.

Broder, D.H. and Pogliano, K. (2006) 'Forespore engulfment mediated by a ratchet-like mechanism', *Cell*, 126(5), pp. 917-28.

Brooks, A.C. and Hwang, L.C. (2017) 'Reconstitutions of plasmid partition systems and their mechanisms', *Plasmid*, 91, pp. 37-41.

Bruand, C., Ehrlich, S.D. and Janniere, L. (1995) 'Primosome assembly site in *Bacillus subtilis*', *EMBO J*, 14(11), pp. 2642-50.

Burkholder, W.F., Kurtser, I. and Grossman, A.D. (2001) 'Replication initiation proteins regulate a developmental checkpoint in *Bacillus subtilis*', *Cell*, 104(2), pp. 269-279.

Burton, B. and Dubnau, D. (2010) 'Membrane-associated DNA transport machines', *Cold Spring Harb Perspect Biol*, 2(7), p. a000406.

Burton, B.M., Marquis, K.A., Sullivan, N.L., Rapoport, T.A. and Rudner, D.Z. (2007) 'The ATPase SpoIIIE transports DNA across fused septal membranes during sporulation in *Bacillus subtilis*', *Cell*, 131(7), pp. 1301-12.

Bylund, J.E., Haines, M.A., Piggot, P.J. and Higgins, M.L. (1993) 'Axial filament formation in *Bacillus subtilis*: induction of nucleoids of increasing length after addition of chloramphenicol to exponential-phase cultures approaching stationary phase', *J Bacteriol*, 175(7), pp. 1886-90.

Campbell, C.S. and Mullins, R.D. (2007) '*In vivo* visualization of type II plasmid segregation: bacterial actin filaments pushing plasmids', *J Cell Biol*, 179(5), pp. 1059-66.

Cano, R.J. and Borucki, M.K. (1995) 'Revival and identification of bacterial spores in 25- to 40-million-year-old Dominican amber', *Science*, 268(5213), pp. 1060-1064.

Carniol, K., Ben-Yehuda, S., King, N. and Losick, R. (2005) 'Genetic dissection of the sporulation protein SpoIIE and its role in asymmetric division in *Bacillus subtilis*', *J Bacteriol*, 187(10), pp. 3511-20.

Cattoni, D.I., Chara, O., Godefroy, C., Margeat, E., Trigueros, S., Milhiet, P.E. and Nollmann, M. (2013) 'SpoIIIE mechanism of directional translocation involves target search coupled to sequence-dependent motor stimulation', *EMBO Rep*, 14(5), pp. 473-9.

Cattoni, D.I., Thakur, S., Godefroy, C., Le Gall, A., Lai-Kee-Him, J., Milhiet, P.E., Bron, P. and Nollmann, M. (2014) 'Structure and DNA-binding properties of the *Bacillus subtilis* SpoIIIE DNA translocase revealed by single-molecule and electron microscopies', *Nucleic Acids Res*, 42(4), pp. 2624-36.

Chai, Y., Norman, T., Kolter, R. and Losick, R. (2011) 'Evidence that metabolism and chromosome copy number control mutually exclusive cell fates in *Bacillus subtilis*', *EMBO J*, 30(7), pp. 1402-13.

Chapman, J.W. and Piggot, P.J. (1987) 'Analysis of the inhibition of sporulation of *Bacillus subtilis* caused by increasing the number of copies of the *spo0F* gene', *J Gen Microbiol*, 133(8), pp. 2079-88.

Chastanet, A. and Losick, R. (2007) 'Engulfment during sporulation in *Bacillus subtilis* is governed by a multi-protein complex containing tandemly acting autolysins', *Mol Microbiol*, 64(1), pp. 139-52.

Cho, E., Ogasawara, N. and Ishikawa, S. (2008) 'The functional analysis of YabA, which interacts with DnaA and regulates initiation of chromosome replication in *Bacillus subtils*', *Genes Genet Syst*, 83(2), pp. 111-25.

de Boer, P.A.J., Crossley, R.E. and Rothfield, L.I. (1989) 'A division inhibitor and a topological specificity factor coded for by the minicell locus determine proper placement of the division septum in *E. coli*', *Cell*, 56(4), pp. 641-649.

De Boer, P.A.J., Crossley, R.E. and Rothfield, L.I. (1990) 'Central role for the *Escherichia coli minC* gene product in two different cell division-inhibition systems', *Proc Natl Acad Sci U S A*, 87(3), pp. 1129-1133.

Deakin, L.J., Clare, S., Fagan, R.P., Dawson, L.F., Pickard, D.J., West, M.R., Wren, B.W., Fairweather, N.F., Dougan, G. and Lawley, T.D. (2012) 'The *Clostridium difficile spo0A* gene is a persistence and transmission factor', *Infect Immun*, 80(8), pp. 2704-11.

den Blaauwen, T., Hamoen, L.W. and Levin, P.A. (2017) 'The divisome at 25: the road ahead', *Curr Opin Microbiol*, 36, pp. 85-94.

Derman, A.I., Becker, E.C., Truong, B.D., Fujioka, A., Tucey, T.M., Erb, M.L., Patterson, P.C. and Pogliano, J. (2009) 'Phylogenetic analysis identifies many

uncharacterized actin-like proteins (Alps) in bacteria: regulated polymerization, dynamic instability and treadmilling in Alp7A', *Mol Microbiol*, 73(4), pp. 534-52.

Derman, A.I., Nonejuie, P., Michel, B.C., Truong, B.D., Fujioka, A., Erb, M.L. and Pogliano, J. (2012) 'Alp7R regulates expression of the actin-like protein Alp7A in *Bacillus subtilis*', *J Bacteriol*, 194(10), pp. 2715-24.

Dervyn, E., Suski, C., Daniel, R., Bruand, C., Chapuis, J., Errington, J., Janniere, L. and Ehrlich, S.D. (2001) 'Two essential DNA polymerases at the bacterial replication fork', *Science*, 294(5547), pp. 1716-9.

Diez, V., Schujman, G.E., Gueiros-Filho, F.J. and de Mendoza, D. (2012) 'Vectorial signalling mechanism required for cell-cell communication during sporulation in *Bacillus subtilis*', *Mol Microbiol*, 83(2), pp. 261-74.

dos Santos, V.T., Bisson-Filho, A.W. and Gueiros-Filho, F.J. (2012) 'DivIVA-mediated polar localization of ComN, a posttranscriptional regulator of *Bacillus subtilis*', *J Bacteriol*, 194(14), pp. 3661-9.

Duan, Y., Huey, J.D. and Herman, J.K. (2016) 'The DnaA inhibitor SirA acts in the same pathway as Soj (ParA) to facilitate *oriC* segregation during *Bacillus subtilis* sporulation', *Mol Microbiol*, 102(3), pp. 530-544.

Duncan, L., Alper, S., Arigoni, F., Losick, R. and Stragier, P. (1995) 'Activation of cell-specific transcription by a serine phosphatase at the site of asymmetric division', *Science*, 270(5236), pp. 641-4.

Dunn, B.G., Jeffs, P. and Ma, N.H. (1978) 'The relationship between DNA replication and the induction of sporulation in *Bacillus subtilis*', *Microbiology*, 108, pp. 189-195.

Durre, P. (2014) 'Physiology and Sporulation in Clostridium', *Microbiol Spectr*, 2(4), pp. TBS-0010-2012.

Ebersbach, G., Briegel, A., Jensen, G.J. and Jacobs-Wagner, C. (2008) 'A self-associating protein critical for chromosome attachment, division, and polar organization in caulobacter', *Cell*, 134(6), pp. 956-68.

Ebersbach, G. and Gerdes, K. (2001) 'The double *par* locus of virulence factor pB171: DNA segregation is correlated with oscillation of ParA', *Proc Natl Acad Sci U S A*, 98(26), pp. 15078-83.

Ebersbach, G. and Gerdes, K. (2004) 'Bacterial mitosis: partitioning protein ParA oscillates in spiral-shaped structures and positions plasmids at mid-cell', *Mol Microbiol*, 52(2), pp. 385-98.

Ebersbach, G., Ringgaard, S., Moller-Jensen, J., Wang, Q., Sherratt, D.J. and Gerdes, K. (2006) 'Regular cellular distribution of plasmids by oscillating and filament-forming ParA ATPase of plasmid pB171', *Mol Microbiol*, 61(6), pp. 1428-42.

Edwards, D.H. and Errington, J. (1997) 'The *Bacillus subtilis* DivIVA protein targets to the division septum and controls the site specificity of cell division', *Mol Microbiol*, 24(5), pp. 905-15.

Eichenberger, P., Fawcett, P. and Losick, R. (2001) 'A three-protein inhibitor of polar septation during sporulation in *Bacillus subtilis*', *Mol Microbiol*, 42(5), pp. 1147-62.

Errington, J. (1993) '*Bacillus subtilis* sporulation: regulation of gene expression and control of morphogenesis', *Microbiol Rev*, 57(1), pp. 1-33.

Errington, J. (2003) 'Regulation of endospore formation in *Bacillus subtilis*', *Nat Rev Microbiol*, 1(2), pp. 117-126.

Errington, J. (2010) 'From spores to antibiotics via the cell cycle', *Microbiology*, 156(1), pp. 1-13.

Errington, J. and Illing, N. (1992) 'Establishment of cell-specific transcription during sporulation in *Bacillus subtilis*', *Mol Microbiol*, 6(6), pp. 689-95.

Errington, J., Murray, H. and Wu, L.J. (2005) 'Diversity and redundancy in bacterial chromosome segregation mechanisms', *Philos Trans R Soc Lond B Biol Sci*, 360(1455), pp. 497-505.

Errington, J. and Wu, L.J. (2017) 'Cell Cycle Machinery in *Bacillus subtilis*', *Subcell Biochem*, 84, pp. 67-101.

Erzberger, J.P., Mott, M.L. and Berger, J.M. (2006) 'Structural basis for ATP-dependent DnaA assembly and replication-origin remodeling', *Nat Struct Mol Biol*, 13(8), pp. 676-83.

Fang, L., Davey, M.J. and O'Donnell, M. (1999) 'Replisome assembly at *oriC*, the replication origin of *E. coli*, reveals an explanation for initiation sites outside an origin', *Mol Cell*, 4(4), pp. 541-53.

Feucht, A., Abbotts, L. and Errington, J. (2002) 'The cell differentiation protein SpoIIE contains a regulatory site that controls its phosphatase activity in response to asymmetric septation', *Mol Microbiol*, 45(4), pp. 1119-30.

Feucht, A., Magnin, T., Yudkin, M.D. and Errington, J. (1996) 'Bifunctional protein required for asymmetric cell division and cell-specific transcription in *Bacillus subtilis*', *Genes Dev*, 10(7), pp. 794-803.

Fiche, J.B., Cattoni, D.I., Diekmann, N., Langerak, J.M., Clerte, C., Royer, C.A., Margeat, E., Doan, T. and Nollmann, M. (2013) 'Recruitment, assembly, and molecular architecture of the SpoIIIE DNA pump revealed by superresolution microscopy', *PLoS Biol*, 11(5), p. e1001557.

Fink, G. and Löwe, J. (2015) 'Reconstitution of a prokaryotic minus end-tracking system using TubRC centromeric complexes and tubulin-like protein TubZ filaments', *Proc Natl Acad Sci U S A*, 112(15), pp. E1845-50.

Fleming, T.C., Shin, J.Y., Lee, S.H., Becker, E., Huang, K.C., Bustamante, C. and Pogliano, K. (2010) 'Dynamic SpoIIIE assembly mediates septal membrane fission during *Bacillus subtilis* sporulation', *Genes Dev*, 24(11), pp. 1160-72.

Flusberg, B.A., Webster, D.R., Lee, J.H., Travers, K.J., Olivares, E.C., Clark, T.A., Korlach, J. and Turner, S.W. (2010) 'Direct detection of DNA methylation during single-molecule, real-time sequencing', *Nat Methods*, 7(6), pp. 461-5.

Foulger, D. and Errington, J. (1993) 'Effects of new mutations in the *spoIIAB* gene of *Bacillus subtilis* on the regulation of sigma F and sigma G activities', *J Gen Microbiol*, 139(12), pp. 3197-203.

Fujikawa, N., Kurumizaka, H., Nureki, O., Terada, T., Shirouzu, M., Katayama, T. and Yokoyama, S. (2003) 'Structural basis of replication origin recognition by the DnaA protein', *Nucleic Acids Res*, 31(8), pp. 2077-86.

Fujita, M., Gonzalez-Pastor, J.E. and Losick, R. (2005) 'High- and low-threshold genes in the Spo0A regulon of *Bacillus subtilis*', *J Bacteriol*, 187(4), pp. 1357-68.

Fujita, M. and Losick, R. (2002) 'An investigation into the compartmentalization of the sporulation transcription factor sigmaE in *Bacillus subtilis*', *Mol Microbiol*, 43(1), pp. 27-38.

Fujita, M. and Losick, R. (2005) 'Evidence that entry into sporulation in *Bacillus subtilis* is governed by a gradual increase in the level and activity of the master regulator Spo0A', *Genes Dev*, 19(18), pp. 2236-44.

Fuller, R.S., Funnell, B.E. and Kornberg, A. (1984) 'The *dnaA* protein complex with the *E. coli* chromosomal replication origin (*oriC*) and other DNA sites', *Cell*, 38(3), pp. 889-900.

Galkin, V.E., Orlova, A., Rivera, C., Mullins, R.D. and Egelman, E.H. (2009) 'Structural polymorphism of the ParM filament and dynamic instability', *Structure*, 17(9), pp. 1253-64.

Gallego del Sol, F. and Marina, A. (2013) 'Structural basis of Rap phosphatase inhibition by Phr peptides', *PLoS Biol*, 11(3), p. e1001511.

Garner, E.C., Campbell, C.S. and Mullins, R.D. (2004) 'Dynamic instability in a DNA-segregating prokaryotic actin homolog', *Science*, 306(5698), pp. 1021-5.

Garner, E.C., Campbell, C.S., Weibel, D.B. and Mullins, R.D. (2007) 'Reconstitution of DNA segregation driven by assembly of a prokaryotic actin homolog', *Science*, 315(5816), pp. 1270-4.

Gerdes, K., Howard, M. and Szardenings, F. (2010) 'Pushing and pulling in prokaryotic DNA segregation', *Cell*, 141(6), pp. 927-42.

Gerdes, K., Moller-Jensen, J. and Bugge Jensen, R. (2000) 'Plasmid and chromosome partitioning: surprises from phylogeny', *Mol Microbiol*, 37(3), pp. 455-66.

Girinathan, B.P., Monot, M., Boyle, D., McAllister, K.N., Sorg, J.A., Dupuy, B. and Govind, R. (2017) 'Effect of *tcdR* Mutation on Sporulation in the Epidemic *Clostridium difficile* Strain R20291', *mSphere*, 2(1).

Glaser, P., Sharpe, M.E., Raether, B., Perego, M., Ohlsen, K. and Errington, J. (1997) 'Dynamic, mitotic-like behavior of a bacterial protein required for accurate chromosome partitioning', *Genes Dev*, 11(9), pp. 1160-8.

Graham, T.G., Wang, X., Song, D., Etson, C.M., van Oijen, A.M., Rudner, D.Z. and Loparo, J.J. (2014) 'ParB spreading requires DNA bridging', *Genes Dev*, 28(11), pp. 1228-38.

Graumann, P.L. and Losick, R. (2001) 'Coupling of asymmetric division to polar placement of replication origin regions in Bacillus subtilis', *J Bacteriol*, 183(13), pp. 4052-60.

Gregory, J.A., Becker, E.C. and Pogliano, K. (2008) 'Bacillus subtilis MinC destabilizes FtsZ-rings at new cell poles and contributes to the timing of cell division', *Genes Dev*, 22(24), pp. 3475-88.

Griffith, K.L. and Grossman, A.D. (2008) 'Inducible protein degradation in *Bacillus subtilis* using heterologous peptide tags and adaptor proteins to target substrates to the protease ClpXP', *Mol Microbiol*, 70(4), pp. 1012-25.

Grimshaw, C.E., Huang, S., Hanstein, C.G., Strauch, M.A., Burbulys, D., Wang, L., Hoch, J.A. and Whiteley, J.M. (1998) 'Synergistic kinetic interactions between components of the phosphorelay controlling sporulation in *Bacillus subtilis*', *Biochemistry*, 37(5), pp. 1365-75.

Gruber, S. (2017) 'Shaping chromosomes by DNA capture and release: gating the SMC rings', *Curr Opin Cell Biol*, 46, pp. 87-93.

Gruber, S. and Errington, J. (2009) 'Recruitment of condensin to replication origin regions by ParB/SpoOJ promotes chromosome segregation in *B. subtilis*', *Cell*, 137(4), pp. 685-96.

Gruber, S., Haering, C.H. and Nasmyth, K. (2003) 'Chromosomal cohesin forms a ring', *Cell*, 112(6), pp. 765-77.

Gruber, S., Veening, J.W., Bach, J., Blettinger, M., Bramkamp, M. and Errington, J. (2014) 'Interlinked sister chromosomes arise in the absence of condensin during fast replication in *B. subtilis*', *Curr Biol*, 24(3), pp. 293-298.

Gutierrez, J., Smith, R. and Pogliano, K. (2010) 'SpoIID-mediated peptidoglycan degradation is required throughout engulfment during *Bacillus subtilis* sporulation', *J Bacteriol*, 192(12), pp. 3174-86.

Hatano, T., Yamaichi, Y. and Niki, H. (2007) 'Oscillating focus of SopA associated with filamentous structure guides partitioning of F plasmid', *Mol Microbiol*, 64(5), pp. 1198-213.

Hayashi, M., Ogura, Y., Harry, E.J., Ogasawara, N. and Moriya, S. (2005) '*Bacillus subtilis* YabA is involved in determining the timing and synchrony of replication initiation', *FEMS Microbiol Lett*, 247(1), pp. 73-9.

Hayes, F. (2000) 'The partition system of multidrug resistance plasmid TP228 includes a novel protein that epitomizes an evolutionarily distinct subgroup of the ParA superfamily', *Mol Microbiol*, 37(3), pp. 528-41.

Hester, C.M. and Lutkenhaus, J. (2007) 'Soj (ParA) DNA binding is mediated by conserved arginines and is essential for plasmid segregation', *Proc Natl Acad Sci U S A*, 104(51), pp. 20326-31.

Hirano, T. (2016) 'Condensin-Based Chromosome Organization from Bacteria to Vertebrates', *Cell*, 164(5), pp. 847-57.

Hofmeister, A.E., Londono-Vallejo, A., Harry, E., Stragier, P. and Losick, R. (1995) 'Extracellular signal protein triggering the proteolytic activation of a developmental transcription factor in *B. subtilis*', *Cell*, 83(2), pp. 219-26.

Holmes, J.A., Follett, S.E., Wang, H., Meadows, C.P., Varga, K. and Bowman, G.R. (2016) '*Caulobacter* PopZ forms an intrinsically disordered hub in organizing bacterial cell poles', *Proc Natl Acad Sci U S A*, 113(44), pp. 12490-12495.

Horton, J.R., Liebert, K., Bekes, M., Jeltsch, A. and Cheng, X. (2006) 'Structure and substrate recognition of the *Escherichia coli* DNA adenine methyltransferase', *J Mol Biol*, 358(2), pp. 559-70.

Horton, J.R., Liebert, K., Hattman, S., Jeltsch, A. and Cheng, X. (2005) 'Transition from nonspecific to specific DNA interactions along the substrate-recognition pathway of dam methyltransferase', *Cell*, 121(3), pp. 349-61.

Hu, Z. and Lutkenhaus, J. (2001) 'Topological regulation of cell division in *E. coli*: Spatiotemporal oscillation of MinD requires stimulation of its ATPase by MinE and phospholipid', *Mol Cell*, 7(6), pp. 1337-1343.

Hwang, L.C., Vecchiarelli, A.G., Han, Y.W., Mizuuchi, M., Harada, Y., Funnell, B.E. and Mizuuchi, K. (2013) 'ParA-mediated plasmid partition driven by protein pattern self-organization', *EMBO J*, 32(9), pp. 1238-49.

Imamura, D., Kuwana, R., Kroos, L., Feig, M., Takamatsu, H. and Watabe, K. (2011) 'Substrate specificity of SpoIIGA, a signal-transducing aspartic protease in *Bacilli*', *J Biochem*, 149(6), pp. 665-71.

Imamura, D., Zhou, R., Feig, M. and Kroos, L. (2008) 'Evidence that the *Bacillus subtilis* SpoIIGA protein is a novel type of signal-transducing aspartic protease', *J Biol Chem*, 283(22), pp. 15287-99.

Ireton, K., Gunther, N.W.t. and Grossman, A.D. (1994) '*spo0J* is required for normal chromosome segregation as well as the initiation of sporulation in *Bacillus subtilis*', *J Bacteriol*, 176(17), pp. 5320-9.

Ishikawa, S., Core, L. and Perego, M. (2002) 'Biochemical characterization of aspartyl phosphate phosphatase interaction with a phosphorylated response regulator and its inhibition by a pentapeptide', *J Biol Chem*, 277(23), pp. 20483-9.

Jahn, N., Brantl, S. and Strahl, H. (2015) 'Against the mainstream: the membrane-associated type I toxin BsrG from *Bacillus subtilis* interferes with cell envelope biosynthesis without increasing membrane permeability', *Mol Microbiol*, 98(4), pp. 651-66.

Jameson, K.H., Rostami, N., Fogg, M.J., Turkenburg, J.P., Grahl, A., Murray, H. and Wilkinson, A.J. (2014) 'Structure and interactions of the *Bacillus subtilis* sporulation inhibitor of DNA replication, SirA, with domain I of DnaA', *Mol Microbiol*, 93(5), pp. 975-91.

Jameson, K.H. and Wilkinson, A.J. (2017) 'Control of Initiation of DNA Replication in *Bacillus subtilis* and *Escherichia coli*', *Genes (Basel)*, 8(1).

Jensen, R.B., Lurz, R. and Gerdes, K. (1998) 'Mechanism of DNA segregation in prokaryotes: replicon pairing by *parC* of plasmid R1', *Proc Natl Acad Sci U S A*, 95(15), pp. 8550-5.

Jensen, R.B. and Shapiro, L. (1999) 'The *Caulobacter crescentus smc* gene is required for cell cycle progression and chromosome segregation', *Proc Natl Acad Sci U S A*, 96(19), pp. 10661-6.

Jensen, R.B. and Shapiro, L. (2003) 'Cell-cycle-regulated expression and subcellular localization of the *Caulobacter crescentus* SMC chromosome structural protein', *J Bacteriol*, 185(10), pp. 3068-75.

Jiang, M., Shao, W., Perego, M. and Hoch, J.A. (2000) 'Multiple histidine kinases regulate entry into stationary phase and sporulation in *Bacillus subtilis*', *Mol Microbiol*, 38(3), pp. 535-42.

Jonas, R.M., Weaver, E.A., Kenney, T.J., Moran, C.P., Jr. and Haldenwang, W.G. (1988) 'The *Bacillus subtilis spoIIG* operon encodes both sigma E and a gene necessary for sigma E activation', *J Bacteriol*, 170(2), pp. 507-11.

Kamada, K., Su'etsugu, M., Takada, H., Miyata, M. and Hirano, T. (2017) 'Overall Shapes of the SMC-ScpAB Complex Are Determined by Balance between Constraint and Relaxation of Its Structural Parts', *Structure*, 25(4), pp. 603-616 e4.

Kaval, K.G., Rismondo, J. and Halbedel, S. (2014) 'A function of DivIVA in *Listeria monocytogenes* division site selection', *Mol Microbiol*, 94(3), pp. 637-54.

Kearns, D.B., Chu, F., Branda, S.S., Kolter, R. and Losick, R. (2005) 'A master regulator for biofilm formation by *Bacillus subtilis*', *Mol Microbiol*, 55(3), pp. 739-49.

Kloosterman, T.G., Lenarcic, R., Willis, C.R., Roberts, D.M., Hamoen, L.W., Errington, J. and Wu, L.J. (2016) 'Complex polar machinery required for proper chromosome segregation in vegetative and sporulating cells of *Bacillus subtilis*', *Mol Microbiol*, 101(2), pp. 333-50.

Kowalski, D. and Eddy, M.J. (1989) 'The DNA unwinding element: a novel, *cis*-acting component that facilitates opening of the *Escherichia coli* replication origin', *EMBO J*, 8(13), pp. 4335-44.

Kuzminov, A. (2014) 'The precarious prokaryotic chromosome', *J Bacteriol*, 196(10), pp. 1793-806.

Lam, H., Schofield, W.B. and Jacobs-Wagner, C. (2006) 'A landmark protein essential for establishing and perpetuating the polarity of a bacterial cell', *Cell*, 124(5), pp. 1011-23.

Larsen, R.A., Cusumano, C., Fujioka, A., Lim-Fong, G., Patterson, P. and Pogliano, J. (2007) 'Treadmilling of a prokaryotic tubulin-like protein, TubZ, required for plasmid stability in *Bacillus thuringiensis*', *Genes Dev*, 21(11), pp. 1340-52.

Le, T.B., Imakaev, M.V., Mirny, L.A. and Laub, M.T. (2013) 'High-resolution mapping of the spatial organization of a bacterial chromosome', *Science*, 342(6159), pp. 731-4.

LeDeaux, J.R., Yu, N. and Grossman, A.D. (1995) 'Different roles for KinA, KinB, and KinC in the initiation of sporulation in *Bacillus subtilis*', *J Bacteriol*, 177(3), pp. 861-3.

Lee, J.Y., Finkelstein, I.J., Arciszewska, L.K., Sherratt, D.J. and Greene, E.C. (2014) 'Single-Molecule Imaging of FtsK Translocation Reveals Mechanistic Features of Protein-Protein Collisions on DNA', *Mol Cell*.

Lee, P.S. and Grossman, A.D. (2006) 'The chromosome partitioning proteins Soj (ParA) and Spo0J (ParB) contribute to accurate chromosome partitioning, separation of replicated sister origins, and regulation of replication initiation in *Bacillus subtilis*', *Mol Microbiol*, 60(4), pp. 853-69.

Leitner, A., Faini, M., Stengel, F. and Aebersold, R. (2016) 'Crosslinking and Mass Spectrometry: An Integrated Technology to Understand the Structure and Function of Molecular Machines', *Trends Biochem Sci*, 41(1), pp. 20-32.

Lenarcic, R., Halbedel, S., Visser, L., Shaw, M., Wu, L.J., Errington, J., Marenduzzo, D. and Hamoen, L.W. (2009) 'Localisation of DivIVA by targeting to negatively curved membranes', *EMBO J*, 28(15), pp. 2272-82.

Leonard, T.A., Butler, P.J. and Lowe, J. (2004) 'Structural analysis of the chromosome segregation protein Spo0J from *Thermus thermophilus*', *Mol Microbiol*, 53(2), pp. 419-32.

Leonard, T.A., Butler, P.J. and Lowe, J. (2005) 'Bacterial chromosome segregation: structure and DNA binding of the Soj dimer--a conserved biological switch', *EMBO J*, 24(2), pp. 270-82.

Levin, P.A. and Losick, R. (1996) 'Transcription factor Spo0A switches the localization of the cell division protein FtsZ from a medial to a bipolar pattern in *Bacillus subtilis*', *Genes Dev*, 10(4), pp. 478-88.

Lewis, P.J., Partridge, S.R. and Errington, J. (1994) 'Sigma factors, asymmetry, and the determination of cell fate in *Bacillus subtilis*', *Proc Natl Acad Sci U S A*, 91(9), pp. 3849-53.

Lewis, P.J., Wu, L.J. and Errington, J. (1998) 'Establishment of prespore-specific gene expression in *Bacillus subtilis*: localization of SpoIIE phosphatase and initiation of compartment-specific proteolysis', *J Bacteriol*, 180(13), pp. 3276-84.

Liebert, K., Horton, J.R., Chahar, S., Orwick, M., Cheng, X. and Jeltsch, A. (2007) 'Two alternative conformations of S-adenosyl-L-homocysteine bound to *Escherichia coli* DNA adenine methyltransferase and the implication of conformational changes in regulating the catalytic cycle', *J Biol Chem*, 282(31), pp. 22848-55.

Lim, H.C., Surovtsev, I.V., Beltran, B.G., Huang, F., Bewersdorf, J. and Jacobs-Wagner, C. (2014) 'Evidence for a DNA-relay mechanism in ParABS-mediated chromosome segregation', *Elife*, 3, p. e02758.

Lin, D.C. and Grossman, A.D. (1998) 'Identification and characterization of a bacterial chromosome partitioning site', *Cell*, 92(5), pp. 675-85.

Lin, D.C., Levin, P.A. and Grossman, A.D. (1997) 'Bipolar localization of a chromosome partition protein in *Bacillus subtilis*', *Proc Natl Acad Sci U S A*, 94(9), pp. 4721-6.

Liu, N.J., Dutton, R.J. and Pogliano, K. (2006) 'Evidence that the SpoIIIE DNA translocase participates in membrane fusion during cytokinesis and engulfment', *Mol Microbiol*, 59(4), pp. 1097-113.

Livny, J., Yamaichi, Y. and Waldor, M.K. (2007) 'Distribution of centromere-like *parS* sites in bacteria: insights from comparative genomics', *J Bacteriol*, 189(23), pp. 8693-703.

Loose, M., Fischer-Friedrich, E., Ries, J., Kruse, K. and Schwille, P. (2008) 'Spatial regulators for bacterial cell division self-organize into surface waves *in vitro*', *Science*, 320(5877), pp. 789-792.

Lowe, J., Ellonen, A., Allen, M.D., Atkinson, C., Sherratt, D.J. and Grainge, I. (2008) 'Molecular mechanism of sequence-directed DNA loading and translocation by FtsK', *Mol Cell*, 31(4), pp. 498-509.

Lu, K., Ye, W., Zhou, L., Collins, L.B., Chen, X., Gold, A., Ball, L.M. and Swenberg, J.A. (2010) 'Structural characterization of formaldehyde-induced cross-links between amino acids and deoxynucleosides and their oligomers', *J Am Chem Soc*, 132(10), pp. 3388-99.

Lutkenhaus, J. (2007) 'Assembly dynamics of the bacterial MinCDE system and spatial regulation of the Z ring', *Annu Rev Biochem*, 76, pp. 539-62.

Magnin, T., Lord, M., Errington, J. and Yudkin, M.D. (1996) 'Establishing differential gene expression in sporulating *Bacillus subtilis*: phosphorylation of SpoIIAA (anti-anti-sigmaF) alters its conformation and prevents formation of a SpoIIAA/SpoIIAB/ADP complex', *Mol Microbiol*, 19(4), pp. 901-7.

Mandelstam, J. and Higgs, S.A. (1974) 'Induction of sporulation during synchronized chromosome replication in *Bacillus subtilis*', *J Bacteriol*, 120(1), pp. 38-42.

Marbouty, M. and Koszul, R. (2017) 'Generation and Analysis of Chromosomal Contact Maps of Bacteria', *Methods Mol Biol*, 1624, pp. 75-84.

Marbouty, M., Le Gall, A., Cattoni, D.I., Cournac, A., Koh, A., Fiche, J.B., Mozziconacci, J., Murray, H., Koszul, R. and Nollmann, M. (2015) 'Condensin- and Replication-Mediated Bacterial Chromosome Folding and Origin Condensation Revealed By Hi-C and Super-resolution Imaging', *Mol Cell*, 59, pp. 1-15.

Marquis, K.A., Burton, B.M., Nollmann, M., Ptacin, J.L., Bustamante, C., Ben-Yehuda, S. and Rudner, D.Z. (2008) 'SpoIIIE strips proteins off the DNA during chromosome translocation', *Genes Dev*, 22(13), pp. 1786-95.

Marston, A.L. and Errington, J. (1999) 'Dynamic movement of the ParA-like Soj protein of *B. subtilis* and its dual role in nucleoid organization and developmental regulation', *Mol Cell*, 4(5), pp. 673-82.

Marston, A.L., Thomaides, H.B., Edwards, D.H., Sharpe, M.E. and Errington, J. (1998) 'Polar localization of the MinD protein of *Bacillus subtilis* and its role in selection of the mid-cell division site', *Genes Dev*, 12(21), pp. 3419-3430.

Mashhoon, N., Pruss, C., Carroll, M., Johnson, P.H. and Reich, N.O. (2006) 'Selective inhibitors of bacterial DNA adenine methyltransferases', *J Biomol Screen*, 11(5), pp. 497-510.

Massey, T.H., Mercogliano, C.P., Yates, J., Sherratt, D.J. and Lowe, J. (2006) 'Double-stranded DNA translocation: structure and mechanism of hexameric FtsK', *Mol Cell*, 23(4), pp. 457-69.

Matalon, E., Kaminker, I., Zimmermann, H., Eisenstein, M., Shai, Y. and Goldfarb, D. (2013) 'Topology of the trans-membrane peptide WALP23 in model membranes under negative mismatch conditions', *J Phys Chem B*, 117(8), pp. 2280-93.

McKenney, P.T., Driks, A. and Eichenberger, P. (2013) 'The *Bacillus subtilis* endospore: Assembly and functions of the multilayered coat', *Nat Rev Microbiol*, 11(1), pp. 33-44.

Mera, P.E., Kalogeraki, V.S. and Shapiro, L. (2014) 'Replication initiator DnaA binds at the *Caulobacter* centromere and enables chromosome segregation', *Proc Natl Acad Sci U S A*, 111(45), pp. 16100-5.

Merrikh, H. and Grossman, A.D. (2011) 'Control of the replication initiator DnaA by an anti-cooperativity factor', *Mol Microbiol*, 82(2), pp. 434-46.

Messer, W., Blaesing, F., Majka, J., Nardmann, J., Schaper, S., Schmidt, A., Seitz, H., Speck, C., Tungler, D., Wegrzyn, G., Weigel, C., Welzeck, M. and Zakrzewska-Czerwinska, J. (1999) 'Functional domains of DnaA proteins', *Biochimie*, 81(8-9), pp. 819-25.

Meyer, P., Gutierrez, J., Pogliano, K. and Dworkin, J. (2010) 'Cell wall synthesis is necessary for membrane dynamics during sporulation of *Bacillus subtilis*', *Mol Microbiol*, 76(4), pp. 956-70.

Miller, A.K., Brown, E.E., Mercado, B.T. and Herman, J.K. (2015) 'A DNA-binding protein defines the precise region of chromosome capture during *Bacillus* sporulation', *Mol Microbiol*.

Millipore, M. 'CellASIC ONIX B04A-03 Microfluidic Bacteria Plates User Guide', *Merck Millipore CellASIC ONIX User Guide*, pp. 1-5.

Minnen, A., Burmann, F., Wilhelm, L., Anchimiuk, A., Diebold-Durand, M.L. and Gruber, S. (2016) 'Control of Smc Coiled Coil Architecture by the ATPase Heads Facilitates Targeting to Chromosomal ParB/*parS* and Release onto Flanking DNA', *Cell Rep*, 14(8), pp. 2003-16.

Mirouze, N., Parashar, V., Baker, M.D., Dubnau, D.A. and Neiditch, M.B. (2011) 'An atypical Phr peptide regulates the developmental switch protein RapH', *J Bacteriol*, 193(22), pp. 6197-206.

Mohl, D.A. and Gober, J.W. (1997) 'Cell cycle-dependent polar localization of chromosome partitioning proteins in *Caulobacter crescentus*', *Cell*, 88(5), pp. 675-84.

Molle, V., Fujita, M., Jensen, S.T., Eichenberger, P., González-Pastor, J.E., Liu, J.S. and Losick, R. (2003) 'The Spo0A regulon of *Bacillus subtilis*', *Mol Microbiol*, 50(5), pp. 1683-1701.

Møller-Jensen, J., Borch, J., Dam, M., Jensen, R.B., Roepstorff, P. and Gerdes, K. (2003) 'Bacterial mitosis: ParM of plasmid R1 moves plasmid DNA by an actin-like insertional polymerization mechanism', *Mol Cell*, 12(6), pp. 1477-87.

Morlot, C., Uehara, T., Marquis, K.A., Bernhardt, T.G. and Rudner, D.Z. (2010) 'A highly coordinated cell wall degradation machine governs spore morphogenesis in *Bacillus subtilis*', *Genes Dev*, 24(4), pp. 411-422.

Mott, M.L. and Berger, J.M. (2007) 'DNA replication initiation: mechanisms and regulation in bacteria', *Nat Rev Microbiol*, 5(5), pp. 343-54.

Mulder, E. and Woldringh, C.L. (1989) 'Actively replicating nucleoids influence positioning of division sites in *Escherichia coli* filaments forming cells lacking DNA', *J Bacteriol*, 171(8), pp. 4303-4314.

Muller, A., Wenzel, M., Strahl, H., Grein, F., Saaki, T.N., Kohl, B., Siersma, T., Bandow, J.E., Sahl, H.G., Schneider, T. and Hamoen, L.W. (2016) 'Daptomycin inhibits cell envelope synthesis by interfering with fluid membrane microdomains', *Proc Natl Acad Sci U S A*.

Murray, H. and Errington, J. (2008) 'Dynamic control of the DNA replication initiation protein DnaA by Soj/ParA', *Cell*, 135(1), pp. 74-84.

Murray, H., Ferreira, H. and Errington, J. (2006) 'The bacterial chromosome segregation protein Spo0J spreads along DNA from *parS* nucleation sites', *Mol Microbiol*, 61(5), pp. 1352-61.

Narula, J., Kuchina, A., Lee, D.Y., Fujita, M., Suel, G.M. and Igoshin, O.A. (2015) 'Chromosomal Arrangement of Phosphorelay Genes Couples Sporulation and DNA Replication', *Cell*, 162(2), pp. 328-37.

Newman, J.A., Rodrigues, C. and Lewis, R.J. (2013) 'Molecular basis of the activity of SinR protein, the master regulator of biofilm formation in *Bacillus subtilis*', *J Biol Chem*, 288(15), pp. 10766-78.

Ni, L.S., Xu, W.J., Kumaraswami, M. and Schumacher, M.A. (2010) 'Plasmid protein TubR uses a distinct mode of HTH-DNA binding and recruits the prokaryotic tubulin homolog TubZ to effect DNA partition', *Proc Natl Acad Sci U S A*, 107, pp. 11763-11768.

Nicholson, W.L., Munakata, N., Horneck, G., Melosh, H.J. and Setlow, P. (2000) 'Resistance of *Bacillus* endospores to extreme terrestrial and extraterrestrial environments', *Microbiol Mol Biol Rev*, 64(3), pp. 548-572.

Nishida, S., Fujimitsu, K., Sekimizu, K., Ohmura, T., Ueda, T. and Katayama, T. (2002) 'A nucleotide switch in the *Escherichia coli* DnaA protein initiates chromosomal replication: evidnece from a mutant DnaA protein defective in regulatory ATP hydrolysis *in vitro* and *in vivo*', *J Biol Chem*, 277(17), pp. 14986-95.

Noirot-Gross, M.-F., Dervyn, E., Wu, L.J., Mervelet, P., Errington, J., Ehrlich, S.D. and Noirot, P. (2002) 'An expanded view of bacterial DNA replication', *Proc Natl Acad Sci U S A*, 99, pp. 8342-8347.

Noirot-Gross, M.-F., Velten, M., Yoshimura, M., McGovern, S., Morimoto, T., Ehrlich, S.D., Ogasawara, N., Pollard, O. and Noirot, P. (2006) 'Functional dissection of YabA, a negative regulator of DNA replication initiation in *Bacillus subtilis*', *Proc Natl Acad Sci U S A*, 103(2368-2373).

Ogura, M. and Tanaka, T. (2009) 'The *Bacillus subtilis* late competence operon *comE* is transcriptionally regulated by *yutB* and under post-transcription initiation control by *comN* (*yrzD*)', *J Bacteriol*, 191(3), pp. 949-58.

Ogura, Y., Ogasawara, N., Harry, E.J. and Moriya, S. (2003) 'Increasing the ratio of Soj to Spo0J promotes replication initiation in *Bacillus subtilis*', *J Bacteriol*, 185(21), pp. 6316-24.

Ojkic, N., Lopez-Garrido, J., Pogliano, K. and Endres, R.G. (2016) 'Cell-wall remodeling drives engulfment during *Bacillus subtilis* sporulation', *Elife*, 5.

Parashar, V., Mirouze, N., Dubnau, D.A. and Neiditch, M.B. (2011) 'Structural basis of response regulator dephosphorylation by Rap phosphatases', *PLoS Biol*, 9(2), p. e1000589.

Park, K.T., Wu, W., Battaile, K.P., Lovell, S., Holyoak, T. and Lutkenhaus, J. (2011) 'The Min oscillator uses MinD-dependent conformational changes in MinE to spatially regulate cytokinesis', *Cell*, 146(3), pp. 396-407.

Park, K.T., Wu, W., Lovell, S. and Lutkenhaus, J. (2012) 'Mechanism of the asymmetric activation of the MinD ATPase by MinE', *Mol Microbiol*, 85(2), pp. 271-281.

Pease, P.J., Levy, O., Cost, G.J., Gore, J., Ptacin, J.L., Sherratt, D., Bustamante, C. and Cozzarelli, N.R. (2005) 'Sequence-directed DNA translocation by purified FtsK', *Science*, 307(5709), pp. 586-90.

Pedrido, M.E., de Ona, P., Ramirez, W., Lenini, C., Goni, A. and Grau, R. (2013) 'Spo0A links de novo fatty acid synthesis to sporulation and biofilm development in *Bacillus subtilis*', *Mol Microbiol*, 87(2), pp. 348-67.

Perego, M. (2013) 'Forty years in the making: understanding the molecular mechanism of peptide regulation in bacterial development', *PLoS Biol*, 11(3), p. e1001516.

Piggot, P.J. and Hilbert, D.W. (2004) 'Sporulation of *Bacillus subtilis*', *Curr Opin Microbiol*, 7(6), pp. 579-586.

Pogliano, K., Hofmeister, A.E. and Losick, R. (1997) 'Disappearance of the sigma E transcription factor from the forespore and the SpoIIE phosphatase from the mother cell contributes to establishment of cell-specific gene expression during sporulation in *Bacillus subtilis*', *J Bacteriol*, 179(10), pp. 3331-41.

Pohl, S. and Harwood, C.R. (2010) 'Heterologous protein secretion by *Bacillus* species from the cradle to the grave', *Adv Appl Microbiol*, 73, pp. 1-25.

Popp, D., Narita, A., Oda, T., Fujisawa, T., Matsuo, H., Nitanai, Y., Iwasa, M., Maeda, K., Onishi, H. and Maeda, Y. (2008) 'Molecular structure of the ParM polymer and the mechanism leading to its nucleotide-driven dynamic instability', *EMBO J*, 27(3), pp. 570-9.

Pottathil, M. and Lazazzera, B.A. (2003) 'The extracellular Phr peptide-Rap phosphatase signaling circuit of *Bacillus subtilis*', *Front Biosci*, 8, pp. d32-45.

Ptacin, J.L., Gahlmann, A., Bowman, G.R., Perez, A.M., von Diezmann, A.R., Eckart, M.R., Moerner, W.E. and Shapiro, L. (2014) 'Bacterial scaffold directs pole-specific centromere segregation', *Proc Natl Acad Sci U S A*, 111(19), pp. E2046-55.

Ptacin, J.L., Lee, S.F., Garner, E.C., Toro, E., Eckart, M., Comolli, L.R., Moerner, W.E. and Shapiro, L. (2010) 'A spindle-like apparatus guides bacterial chromosome segregation', *Nat Cell Biol*, 12(8), pp. 791-8.

Ptacin, J.L., Nollmann, M., Becker, E.C., Cozzarelli, N.R., Pogliano, K. and Bustamante, C. (2008) 'Sequence-directed DNA export guides chromosome translocation during sporulation in *Bacillus subtilis*', *Nat Struct Mol Biol*, 15(5), pp. 485-93.

Radnedge, L., Youngren, B., Davis, M. and Austin, S. (1998) 'Probing the structure of complex macromolecular interactions by homolog specificity scanning: the P1 and P7 plasmid partition systems', *EMBO J*, 17(20), pp. 6076-85.

Rahn-Lee, L., Gorbatyuk, B., Skovgaard, O. and Losick, R. (2009) 'The conserved sporulation protein YneE inhibits DNA replication in *Bacillus subtilis*', *J Bacteriol*, 191(11), pp. 3736-9.

Rahn-Lee, L., Merrikh, H., Grossman, A.D. and Losick, R. (2011) 'The sporulation protein SirA inhibits the binding of DnaA to the origin of replication by contacting a patch of clustered amino acids', *J Bacteriol*, 193(6), pp. 1302-7.

Rao, C.V., Glekas, G.D. and Ordal, G.W. (2008) 'The three adaptation systems of *Bacillus subtilis* chemotaxis', *Trends Microbiol*, 16(10), pp. 480-7.

Rappsilber, J. (2011) 'The beginning of a beautiful friendship: cross-linking/mass spectrometry and modelling of proteins and multi-protein complexes', *J Struct Biol*, 173(3), pp. 530-40.

Raskin, D.M. and De Boer, P.A.J. (1999) 'Rapid pole-to-pole oscillation of a protein required for directing division to the middle of *Escherichia coli*', *Proc Natl Acad Sci U S A*, 96(9), pp. 4971-4976.

Rather, P.N., Coppolecchia, R., DeGrazia, H. and Moran, C.P., Jr. (1990) 'Negative regulator of sigma G-controlled gene expression in stationary-phase *Bacillus subtilis*', *J Bacteriol*, 172(2), pp. 709-15.

Ravin, N.V., Rech, J. and Lane, D. (2003) 'Mapping of functional domains in F plasmid partition proteins reveals a bipartite SopB-recognition domain in SopA', *J Mol Biol*, 329(5), pp. 875-89.

Richardson, T.T., Harran, O. and Murray, H. (2016) 'The bacterial DnaA-trio replication origin element specifies single-stranded DNA initiator binding', *Nature*, 534(7607), pp. 412-6.

Ringgaard, S., van Zon, J., Howard, M. and Gerdes, K. (2009) 'Movement and equipositioning of plasmids by ParA filament disassembly', *Proc Natl Acad Sci U S A*, 106(46), pp. 19369-74.

Rivera, C.R., Kollman, J.M., Polka, J.K., Agard, D.A. and Mullins, R.D. (2011) 'Architecture and assembly of a divergent member of the ParM family of bacterial actin-like proteins', *J Biol Chem*, 286(16), pp. 14282-90.

Ruvolo, M.V., Mach, K.E. and Burkholder, W.F. (2006) 'Proteolysis of the replication checkpoint protein Sda is necessary for the efficient initiation of sporulation after transient replication stress in *Bacillus subtilis*', *Mol Microbiol*, 60(6), pp. 1490-508.

Ryter, A. (1965) '[Morphologic Study of the Sporulation of *Bacillus subtilis*]', *Ann Inst Pasteur (Paris)*, 108, pp. 40-60.

Sagne, C., Isambert, M.F., Henry, J.P. and Gasnier, B. (1996) 'SDS-resistant aggregation of membrane proteins: application to the purification of the vesicular monoamine transporter', *Biochem J*, 316 (Pt 3), pp. 825-31.

Schallmey, M., Singh, A. and Ward, O.P. (2004) 'Developments in the use of *Bacillus* species for industrial production', *Canadian Journal of Microbiology*, 50, p. doi: 10.1139.

Scheinpflug, K., Wenzel, M., Krylova, O., Bandow, J.E., Dathe, M. and Strahl, H. (2017) 'Antimicrobial peptide cWFW kills by combining lipid phase separation with autolysis', *Sci Rep*, 7, p. 44332.

Schofield, W.B., Lim, H.C. and Jacobs-Wagner, C. (2010) 'Cell cycle coordination and regulation of bacterial chromosome segregation dynamics by polarly localized proteins', *EMBO J*, 29(18), pp. 3068-81.

Scholefield, G., Errington, J. and Murray, H. (2012) 'Soj/ParA stalls DNA replication by inhibiting helix formation of the initiator protein DnaA', *EMBO J*, 31(6), pp. 1542-55.

Scholefield, G. and Murray, H. (2013) 'YabA and DnaD inhibit helix assembly of the DNA replication initiation protein DnaA', *Mol Microbiol*, 90(1), pp. 147-59.

Scholefield, G., Whiting, R., Errington, J. and Murray, H. (2011) 'Spo0J regulates the oligomeric state of Soj to trigger its switch from an activator to an inhibitor of DNA replication initiation', *Mol Microbiol*, 79(4), pp. 1089-100.

Schumacher, M.A., Glover, T.C., Brzoska, A.J., Jensen, S.O., Dunham, T.D., Skurray, R.A. and Firth, N. (2007) 'Segrosome structure revealed by a complex of ParR with centromere DNA', *Nature*, 450(7173), pp. 1268-71.

Schumacher, M.A., Lee, J. and Zeng, W. (2016) 'Molecular insights into DNA binding and anchoring by the *Bacillus subtilis* sporulation kinetochore-like RacA protein', *Nucleic Acids Res*, 44(11), pp. 5438-49.

Schwartz, M.A. and Shapiro, L. (2011) 'An SMC ATPase mutant disrupts chromosome segregation in *Caulobacter*', *Mol Microbiol*, 82(6), pp. 1359-74.

Sekimizu, K., Bramhill, D. and Kornberg, A. (1987) 'ATP activates dnaA protein in initiating replication of plasmids bearing the origin of the *E. coli* chromosome', *Cell*, 50(2), pp. 259-65.

Shaner, N.C., Lambert, G.G., Chammas, A., Ni, Y., Cranfill, P.J., Baird, M.A., Sell, B.R., Allen, J.R., Day, R.N., Israelsson, M., Davidson, M.W. and Wang, J. (2013) 'A bright monomeric green fluorescent protein derived from *Branchiostoma lanceolatum*', *Nat Methods*, 10(5), pp. 407-9.

Sharp, M.D. and Pogliano, K. (1999) 'An in vivo membrane fusion assay implicates SpoIIIE in the final stages of engulfment during Bacillus subtilis sporulation', *Proc Natl Acad Sci U S A*, 96(25), pp. 14553-8.

Sharpe, M.E. and Errington, J. (1996) 'The *Bacillus subtilis soj-spo0J* locus is required for a centromere-like function involved in prespore chromosome partitioning', *Mol Microbiol*, 21(3), pp. 501-9.

Shebelut, C.W., Guberman, J.M., van Teeffelen, S., Yakhnina, A.A. and Gitai, Z. (2010) '*Caulobacter* chromosome segregation is an ordered multistep process', *Proc Natl Acad Sci U S A*, 107(32), pp. 14194-8.

Siegel, D.P., Cherezov, V., Greathouse, D.V., Koeppe, R.E., 2nd, Killian, J.A. and Caffrey, M. (2006) 'Transmembrane peptides stabilize inverted cubic phases in a biphasic length-dependent manner: implications for protein-induced membrane fusion', *Biophys J*, 90(1), pp. 200-11.

Soh, Y.M., Burmann, F., Shin, H.C., Oda, T., Jin, K.S., Toseland, C.P., Kim, C., Lee, H., Kim, S.J., Kong, M.S., Durand-Diebold, M.L., Kim, Y.G., Kim, H.M., Lee, N.K., Sato, M., Oh, B.H. and Gruber, S. (2015) 'Molecular basis for SMC rod formation and its dissolution upon DNA binding', *Mol Cell*, 57(2), pp. 290-303.

Soufo, C.D., Soufo, H.J., Noirot-Gros, M.F., Steindorf, A., Noirot, P. and Graumann, P.L. (2008) 'Cell-cycle-dependent spatial sequestration of the DnaA replication initiator protein in *Bacillus subtilis*', *Dev Cell*, 15(6), pp. 935-41.

Soutourina, O. (2017) 'RNA-based control mechanisms in *Clostridium difficile*', *Curr Opin Micriobiol*, 36, pp. 62-68.

Spizizen, J. (1958) 'Transformation of Biochemically Deficient Strains of *Bacillus Subtilis* by Deoxyribonucleate', *Proc Natl Acad Sci U S A*, 44(10), pp. 1072-8.

Sterlini, J.M. and Mandelstam, J. (1969) 'Commitment to sporulation in *Bacillus subtilis* and its relationship to development of actinomycin resistance', *Biochem J*, 113(1), pp. 29-37.

Stragier, P., Bonamy, C. and Karmazyn-Campelli, C. (1988) 'Processing of a sporulation sigma factor in *Bacillus subtilis*: how morphological structure could control gene expression', *Cell*, 52(5), pp. 697-704.

Strahl, H. and Hamoen, L.W. (2010) 'Membrane potential is important for bacterial cell division', *Proc Natl Acad Sci U S A*, 107(27), pp. 12281-6.

Strahl, H. and Hamoen, L.W. (2012) 'Finding the corners in a cell', *Curr Opin Microbiol*, 15(6), pp. 731-6.

Strahl, H., Ronneau, S., Gonzalez, B.S., Klutsch, D., Schaffner-Barbero, C. and Hamoen, L.W. (2015) 'Transmembrane protein sorting driven by membrane curvature', *Nat Commun*, 6, p. 8728.

Sullivan, N.L., Marquis, K.A. and Rudner, D.Z. (2009) 'Recruitment of SMC by ParB-*parS* organizes the origin region and promotes efficient chromosome segregation', *Cell*, 137(4), pp. 697-707.

Surovtsev, I.V., Campos, M. and Jacobs-Wagner, C. (2016a) 'DNA-relay mechanism is sufficient to explain ParA-dependent intracellular transport and patterning of single and multiple cargos', *Proc Natl Acad Sci U S A*, 113(46), pp. E7268-E7276.

Surovtsev, I.V., Lim, H.C. and Jacobs-Wagner, C. (2016b) 'The Slow Mobility of the ParA Partitioning Protein Underlies Its Steady-State Patterning in *Caulobacter*', *Biophys J*, 110(12), pp. 2790-2799.

Swick, M.C., Koehler, T.M. and Driks, A. (2016) 'Surviving Between Hosts: Sporulation and Transmission', *Microbiol Spectr*, 4(4).

Tan, I.S. and Ramamurthi, K.S. (2014) 'Spore formation in *Bacillus subtilis*', *Environ Microbiol Rep*, 6(3), pp. 212-25.

Tanaka, T. (2010) 'Functional analysis of the stability determinant AlfB of pBET131, a miniplasmid derivative of *Bacillus subtilis* (*natto*) plasmid pLS32', *J Bacteriol*, 192(5), pp. 1221-30.

Tang, M., Bideshi, D.K., Park, H.W. and Federici, B.A. (2006) 'Minireplicon from pBtoxis of *Bacillus thuringiensis* subsp. *israelensis*', *Appl Environ Microbiol*, 72(11), pp. 6948-54.

Te Winkel, J.D., Gray, D.A., Seistrup, K.H., Hamoen, L.W. and Strahl, H. (2016) 'Analysis of Antimicrobial-Triggered Membrane Depolarization Using Voltage Sensitive Dyes', *Front Cell Dev Biol*, 4, p. 29.

Teleman, A.A., Graumann, P.L., Lin, D.C., Grossman, A.D. and Losick, R. (1998) 'Chromosome arrangement within a bacterium', *Curr Biol*, 8(20), pp. 1102-9.

Thanbichler, M. (2009) 'Spatial regulation in *Caulobacter crescentus*', *Curr Opin Microbiol*, 12(6), pp. 715-21.

Thavarajah, R., Mudimbaimannar, V.K., Elizabeth, J., Rao, U.K. and Ranganathan, K. (2012) 'Chemical and physical basics of routine formaldehyde fixation', *J Oral Maxillofac Pathol*, 16(3), pp. 400-5.

Thomaides, H.B., Freeman, M., El Karoui, M. and Errington, J. (2001) 'Division site selection protein DivIVA of *Bacillus subtilis* has a second distinct function in chromosome segregation during sporulation', *Genes Dev*, 15(13), pp. 1662-73.

Tinsley, E. and Khan, S.A. (2006) 'A novel FtsZ-like protein is involved in replication of the anthrax toxin-encoding pXO1 plasmid in *Bacillus anthracis*', *J Bacteriol*, 188(8), pp. 2829-35.

Tocheva, E.I., Lopez-Garrido, J., Hughes, H.V., Fredlund, J., Kuru, E., Vannieuwenhze, M.S., Brun, Y.V., Pogliano, K. and Jensen, G.J. (2013) 'Peptidoglycan transformations during *Bacillus subtilis* sporulation', *Mol Microbiol*, 88(4), pp. 673-86.

Toro, E., Hong, S.H., McAdams, H.H. and Shapiro, L. (2008) '*Caulobacter* requires a dedicated mechanism to initiate chromosome segregation', *Proc Natl Acad Sci U S A*, 105(40), pp. 15435-40.

van Baarle, S. and Bramkamp, M. (2010) 'The MinCDJ system in Bacillus subtilis prevents minicell formation by promoting divisome disassembly', *PLoS One*, 5(3), p. e9850.

van den Ent, F., Moller-Jensen, J., Amos, L.A., Gerdes, K. and Lowe, J. (2002) 'F-actin-like filaments formed by plasmid segregation protein ParM', *EMBO J*, 21(24), pp. 6935-43.

Vecchiarelli, A.G., Han, Y.W., Tan, X., Mizuuchi, M., Ghirlando, R., Biertumpfel, C., Funnell, B.E. and Mizuuchi, K. (2010) 'ATP control of dynamic P1 ParA-DNA interactions: a key role for the nucleoid in plasmid partition', *Mol Microbiol*, 78(1), pp. 78-91.

Vecchiarelli, A.G., Hwang, L.C. and Mizuuchi, K. (2013) 'Cell-free study of F plasmid partition provides evidence for cargo transport by a diffusion-ratchet mechanism', *Proc Natl Acad Sci U S A*, 110(15), pp. E1390-7.

Vecchiarelli, A.G., Neuman, K.C. and Mizuuchi, K. (2014) 'A propagating ATPase gradient drives transport of surface-confined cellular cargo', *Proc Natl Acad Sci U S A*, 111(13), pp. 4880-5.

Veening, J.W., Hamoen, L.W. and Kuipers, O.P. (2005) 'Phosphatases modulate the bistable sporulation gene expression pattern in *Bacillus subtilis*', *Mol Microbiol*, 56(6), pp. 1481-94.

Veening, J.W., Murray, H. and Errington, J. (2009) 'A mechanism for cell cycle regulation of sporulation initiation in *Bacillus subtilis*', *Genes Dev*, 23(16), pp. 1959-1970.

Veening, J.W., Stewart, E.J., Berngruber, T.W., Taddei, F., Kuipers, O.P. and Hamoen, L.W. (2008) 'Bet-hedging and epigenetic inheritance in bacterial cell development', *Proc Natl Acad Sci U S A*, 105(11), pp. 4393-8.

Viollier, P.H., Thanbichler, M., McGrath, P.T., West, L., Meewan, M., McAdams, H.H. and Shapiro, L. (2004) 'Rapid and sequential movement of individual chromosomal

loci to specific subcellular locations during bacterial DNA replication', *Proc Natl Acad Sci U S A*, 101(25), pp. 9257-62.

Vivian, J.P., Porter, C.J., Wilce, J.A. and Wilce, M.C. (2007) 'An asymmetric structure of the *Bacillus subtilis* replication terminator protein in complex with DNA', *J Mol Biol*, 370(3), pp. 481-91.

Vlamakis, H., Chai, Y., Beauregard, P., Losick, R. and Kolter, R. (2013) 'Sticking together: building a biofilm the *Bacillus subtilis* way', *Nat Rev Microbiol*, 11(3), pp. 157-68.

Von Hippel, P.H. and Wong, K.Y. (1971) 'Dynamic aspects of native DNA structure: kinetics of the formaldehyde reaction with calf thymus DNA', *J Mol Biol*, 61(3), pp. 587-613.

Vreeland, R.H., Rosenzweig, W.D. and Powers, D.W. (2000) 'Isolation of a 250 million-year-old halotolerant bacterium from a primary salt crystal', *Nature*, 407(6806), pp. 897-900.

Wagner-Herman, J.K., Bernard, R., Dunne, R., Bisson-Filho, A.W., Kumar, K., Nguyen, T., Mulcahy, L., Koullias, J., Gueiros-Filho, F.J. and Rudner, D.Z. (2012) 'RefZ facilitates the switch from medial to polar division during spore formation in *Bacillus subtilis*', *J Bacteriol*, 194(17), pp. 4608-4618.

Wagner, J.K., Marquis, K.A. and Rudner, D.Z. (2009) 'SirA enforces diploidy by inhibiting the replication initiator DnaA durina snore formation in *Bacillus subtilis*', *Mol Microbiol*, 73(5), pp. 963-974.

Wang, X., Brandao, H.B., Le, T.B., Laub, M.T. and Rudner, D.Z. (2017) '*Bacillus subtilis* SMC complexes juxtapose chromosome arms as they travel from origin to terminus', *Science*, 355(6324), pp. 524-527.

Wang, X., Le, T.B., Lajoie, B.R., Dekker, J., Laub, M.T. and Rudner, D.Z. (2015) 'Condensin promotes the juxtaposition of DNA flanking its loading site in *Bacillus subtilis*', *Genes Dev*, 29(15), pp. 1661-75.

Wang, X., Montero Llopis, P. and Rudner, D.Z. (2013) 'Organization and segregation of bacterial chromosomes', *Nat Rev Genet*, 14(3), pp. 191-203.

Wang, X., Montero Llopis, P. and Rudner, D.Z. (2014a) '*Bacillus subtilis* chromosome organization oscillates between two distinct patterns', *Proc Natl Acad Sci U S A*, 111(35), pp. 12877-82.

Wang, X., Tang, O.W., Riley, E.P. and Rudner, D.Z. (2014b) 'The SMC condensin complex is required for origin segregation in *Bacillus subtilis*', *Curr Biol*, 24(3), pp. 287-92.

Washington, T.A., Smith, J.L. and Grossman, A.D. (2017) 'Genetic networks controlled by the bacterial replication initiator and transcription factor DnaA in *Bacillus subtilis*', *Mol Microbiol*.

Weiss, T.M., van der Wel, P.C., Killian, J.A., Koeppe, R.E., 2nd., and Huang, H.W. (2003) 'Hydrophobic mismatch between helices and lipid bilayers', *Biophys J*, 84(1), pp. 379-85.

Wilhelm, L., Burmann, F., Minnen, A., Shin, H.C., Toseland, C.P., Oh, B.H. and Gruber, S. (2015) 'SMC condensin entraps chromosomal DNA by an ATP hydrolysis dependent loading mechanism in *Bacillus subtilis*', *eLife*, 4.

Woldringh, C.L., Mulder, E., Huls, P.G. and Vischer, N. (1991) 'Toporegulation of bacterial division according to the nucleoid occlusion model', *Res Microbiol*, 142(2-3), pp. 309-320.

Woldringh, C.L., Zaritsky, A. and Grover, N.B. (1994) 'Nucleoid partitioning and the division plane in *Escherichia coli*', *J Bacteriol*, 176(19), pp. 6030-6038.

Wu, L.J. (2009) 'It takes two DNA translocases to untangle chromosomes from the division septum', *Mol Microbiol*, 74(4), pp. 773-6.

Wu, L.J. and Errington, J. (1994) '*Bacillus subtilis* SpoIIIE protein required for DNA segregation during asymmetric cell division', *Science*, 264(5158), pp. 572-5.

Wu, L.J. and Errington, J. (1997) 'Septal localization of the SpoIIIE chromosome partitioning protein in *Bacillus subtilis*', *EMBO J*, 16(8), pp. 2161-9.

Wu, L.J. and Errington, J. (1998) 'Use of asymmetric cell division and *spoIIIE* mutants to probe chromosome orientation and organization in *Bacillus subtilis*', *Mol Microbiol*, 27(4), pp. 777-86.

Wu, L.J. and Errington, J. (2002) 'A large dispersed chromosomal region required for chromosome segregation in sporulating cells of *Bacillus subtilis*', *EMBO J*, 21(15), pp. 4001-11.

Wu, L.J. and Errington, J. (2003) 'RacA and the Soj-Spo0J system combine to effect polar chromosome segregation in sporulating *Bacillus subtilis*', *Mol Microbiol*, 49(6), pp. 1463-75.

Wu, L.J. and Errington, J. (2004) 'Coordination of cell division and chromosome segregation by a nucleoid occlusion protein in *Bacillus subtilis*', *Cell*, 117(7), pp. 915-925.

Wu, L.J., Feucht, A. and Errington, J. (1998) 'Prespore-specific gene expression in *Bacillus subtilis* is driven by sequestration of SpoIIE phosphatase to the prespore side of the asymmetric septum', *Genes Dev*, 12(9), pp. 1371-80.

Wu, L.J., Ishikawa, S., Kawai, Y., Oshima, T., Ogasawara, N. and Errington, J. (2009) 'Noc protein binds to specific DNA sequences to coordinate cell division with chromosome segregation', *EMBO Journal*, 28(13), pp. 1940-1952.

Wu, L.J., Lewis, P.J., Allmansberger, R., Hauser, P.M. and Errington, J. (1995) 'A conjugation-like mechanism for prespore chromosome partitioning during sporulation in *Bacillus subtilis*', *Genes Dev*, 9(11), pp. 1316-26.

Wu, M.Y., Zampini, M., Bussiek, M., Hoischen, C., Diekmann, S. and Hayes, F. (2011) 'Segrosome assembly at the pliable *parH* centromere', *Nucleic Acids Res*, 37, pp. 5082-5097.

Xiao, R. and Moore, D.D. (2011) 'DamIP: using mutant DNA adenine methyltransferase to study DNA-protein interactions *in vivo*', *Curr Protoc Mol Biol*, Chapter 21, p. Unit21 21.

Yen Shin, J., Lopez-Garrido, J., Lee, S.H., Diaz-Celis, C., Fleming, T., Bustamante, C. and Pogliano, K. (2015) 'Visualization and functional dissection of coaxial paired SpoIIIE channels across the sporulation septum', *Elife*, 4, p. e06474.

Zhang, H. and Schumacher, M.A. (2017) 'Structures of partition protein ParA with nonspecific DNA and ParB effector reveal molecular insights into principles governing Walker-box DNA segregation', *Genes Dev*, 31(5), pp. 481-492.

Zhang, W., Carneiro, M.J., Turner, I.J., Allen, S., Roberts, C.J. and Soultanas, P. (2005) 'The Bacillus subtilis DnaD and DnaB proteins exhibit different DNA remodelling activities', *J Mol Biol*, 351(1), pp. 66-75.

Zhao, C.R., De Boer, P.A.J. and Rothfield, L.I. (1995) 'Proper placement of the *Escherichia coli* division site requires two functions that are associated with different domains of the MinE protein', *Proc Natl Acad Sci U S A*, 92(10), pp. 4313-4317.

Zorman, S., Seitz, H., Sclavi, B. and Strick, T.R. (2012) 'Topological characterization of the DnaA-*oriC* complex using single-molecule nanomanipuation', *Nucleic Acids Res*, 40(15), pp. 7375-83.